Tomography and Dynamics of Western-Pacific Subduction Zones

Dapeng Zhao

Department of Geophysics, Tohoku University, Sendai 980-8578, Japan
e-mail: zhao@aob.gp.tohoku.ac.jp

Received July 4, 2011; **Revised** November 7, 2011; **Accepted** November 8, 2011; **Online published** January 31, 2012.

Citation: Zhao, D. (2012), Tomography and dynamics of Western-Pacific subduction zones, *Monogr. Environ. Earth Planets*, *1*, 1–70, doi:10.5047/meep.2012.00101.0001.

Abstract We review the significant recent results of multiscale seismic tomography of the Western-Pacific subduction zones and discuss their implications for seismotectonics, magmatism, and subduction dynamics, with an emphasis on the Japan Islands. Many important new findings are obtained due to technical advances in tomography, such as the handling of complex-shaped velocity discontinuities, the use of various later phases, the joint inversion of local and teleseismic data, tomographic imaging outside a seismic network, and P-wave anisotropy tomography. Prominent low-velocity (low-V) and high-attenuation (low-Q) zones are revealed in the crust and uppermost mantle beneath active arc and back-arc volcanoes and they extend to the deeper portion of the mantle wedge, indicating that the low-V/low-Q zones form the sources of arc magmatism and volcanism, and the arc magmatic system is related to deep processes such as convective circulation in the mantle wedge and dehydration reactions in the subducting slab. Seismic anisotropy seems to exist in all portions of the Northeast Japan subduction zone, including the upper and lower crust, the mantle wedge and the subducting Pacific slab. Multilayer anisotropies with different orientations may have caused the apparently weak shear-wave splitting observed so far, whereas recent results show a greater effect of crustal anisotropy than previously thought. Deep subduction of the Philippine Sea slab and deep dehydration of the Pacific slab are revealed beneath Southwest Japan. Significant structural heterogeneities are imaged in the source areas of large earthquakes in the crust, subducting slab and interplate megathrust zone, which may reflect fluids and/or magma originating from slab dehydration that affected the rupture nucleation of large earthquakes. These results suggest that large earthquakes do not strike anywhere, but in only anomalous areas that may be detected with geophysical methods. The occurrence of deep earthquakes under the Japan Sea and the East Asia margin may be related to a metastable olivine wedge in the subducting Pacific slab. The Pacific slab becomes stagnant in the mantle transition zone under East Asia, and a big mantle wedge (BMW) has formed above the stagnant slab. Convective circulations and fluid and magmatic processes in the BMW may have caused intraplate volcanism (e.g., Changbai and Wudalianchi), reactivation of the North China craton, large earthquakes, and other active tectonics in East Asia. Deep subduction and dehydration of continental plates (such as the Eurasian plate, Indian plate and Burma microplate) are also found, which have caused intraplate magmatism (e.g., Tengchong) and geothermal anomalies above the subducted continental plates. Under Kamchatka, the subducting Pacific slab shortens toward the north and terminates near the Aleutian-Kamchatka junction. The slab loss was induced by friction with the surrounding asthenosphere, as the Pacific plate rotated clockwise 30 Ma ago, and then it was enlarged by the slab-edge pinch-off by the asthenospheric flow. The stagnant slab finally collapses down to the bottom of the mantle, which may trigger upwelling of hot mantle materials from the lower mantle to the shallow mantle. Suggestions are also made for future directions of the seismological research of subduction zones.

Keywords: Seismic tomography, Subduction zones, Subducting slabs, Arc volcanoes, Mantle wedge, Forearc, Back-arc, Interplate megathrust zone, Earthquakes, Intraplate magmatism, Mantle transition zone.

1. Introduction

The study of subduction zones is of fundamental importance to Earth scientists because they constitute one of the key elements in plate tectonics and geodynamics. Subduction zones are convergent plate boundaries characterized geomorphologically by deep ocean trenches and island arcs or continental margins, seismically by the largest earthquakes ($M \geq 9.0$) on Earth and the landward dipping plane of deep earthquakes (the so-called Wadati-Benioff zone), tectonically by regional-scale crustal faulting and terrane movements, and magmatically by a linear belt of eruptive centers (the so-called volcanic front). Subduction and arc magmatism are fundamental processes in the evolution of the Earth. They play critical roles in the present day differentiation of the Earth's materials and are believed to be major sites of the generation of continental crust (Maruyama and Santosh, 2007). Subduction also plays a significant role in water and carbon cycles (Ohtani *et al.*, 2004).

doi:10.5047/meep.2012.00101.0001 ISSN: 2186-4853

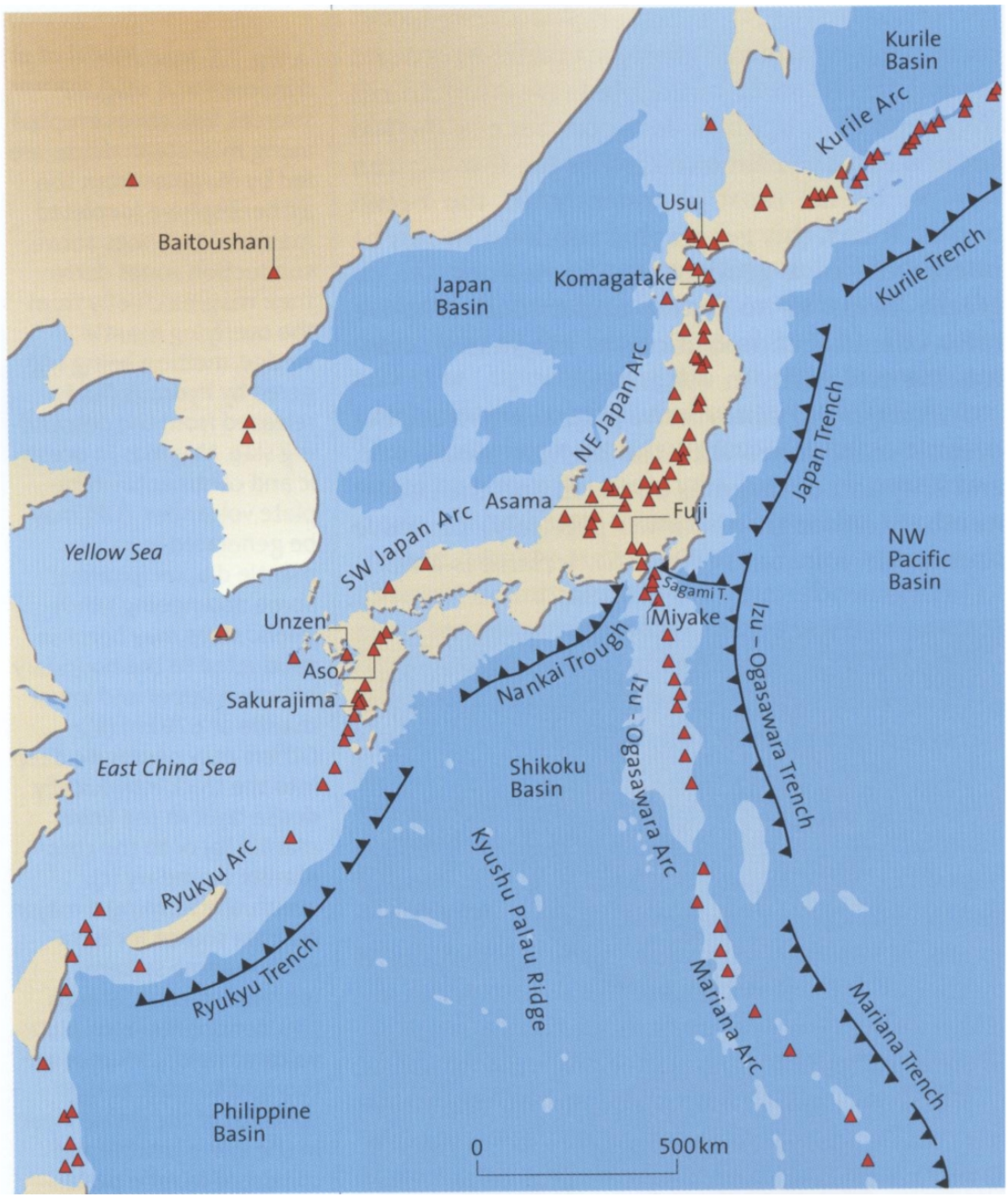

Fig. 1. Tectonic background in and around the Japan Islands. Red triangles denote active volcanoes. Black lines with teeth symbols show the oceanic trenches where the oceanic plates are subducting into the mantle. (From Schmincke, 2004.)

Seismic tomography is one of the most powerful tools for studying the structure and dynamics of subduction zones (Zhao, 2001a). It is a geophysical imaging method to determine three-dimensional (3-D) images of the Earth's interior by combining abundant information from a large number of crisscrossing seismic waves triggered by natural or artificial seismic sources. Tomographic imaging can provide crucial information for us to better understand seismotectonics, volcanism and dynamics of the Earth's interior. It signifies a revolution in Earth science (Dziewonski and Anderson, 1984). During the past three decades, seismic tomography has had a far-reaching and deep impact on the geological community and will continue to influence future developments in the Earth sciences (Zhao and Kayal, 2000). Tomographic studies can be classified in several ways. According to the seismic data used, there is body-wave tomography and surface-wave tomography; according to the scale of the study areas, there is global tomography and local/regional tomography; according to the depth range of the modeling space, there is crustal tomography, upper-mantle tomography, and whole-mantle tomography, etc. The pioneer studies of body-wave tomography were carried out by Aki and Lee (1976) and Aki *et al*. (1977) for local and regional scales, and Dziewonski *et al*. (1977) for the global scale. Surface-wave tomography was initiated by Nakanishi and Anderson (1982), and Woodhouse and Dziewonski (1984). Generally speaking,

doi:10.5047/meep.2012.00101.0001

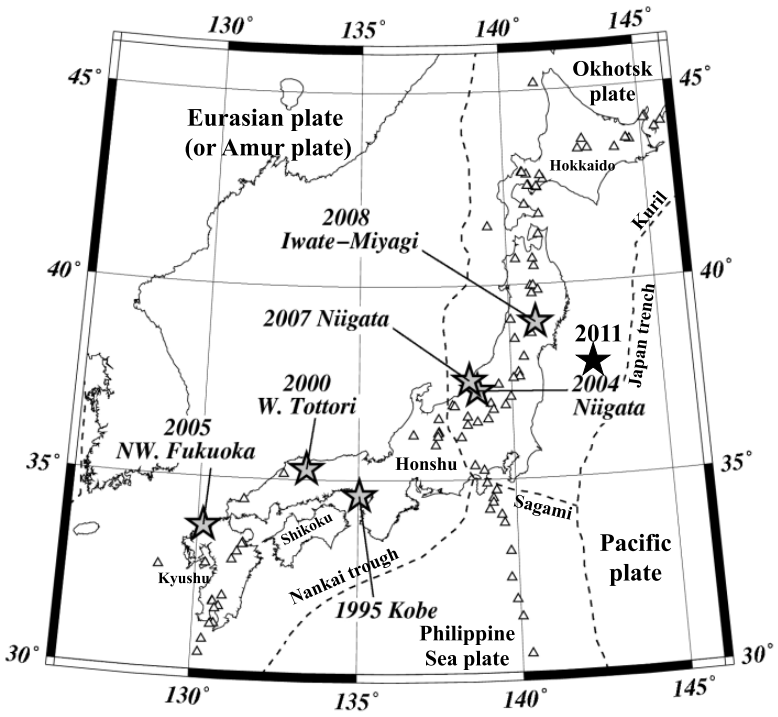

Fig. 2. Distribution of large crustal earthquakes (gray stars) which have occurred on the Japan Islands since 1995. The year of occurrence and the name of each earthquake are also shown. Dashed lines and open triangles denote plate boundaries and active volcanoes, respectively. The black star shows the mainshock epicenter of the great Tohoku-oki earthquake (M_w 9.0) that occurred on 11 March, 2011. (Modified from *Island Arc*, *19*, Zhao, D., M. Santosh, and A. Yamada, Dissecting large earthquakes in Japan: Role of arc magma and fluids, 4–16, Copyright 2010, with permission from John Wiley & Sons.)

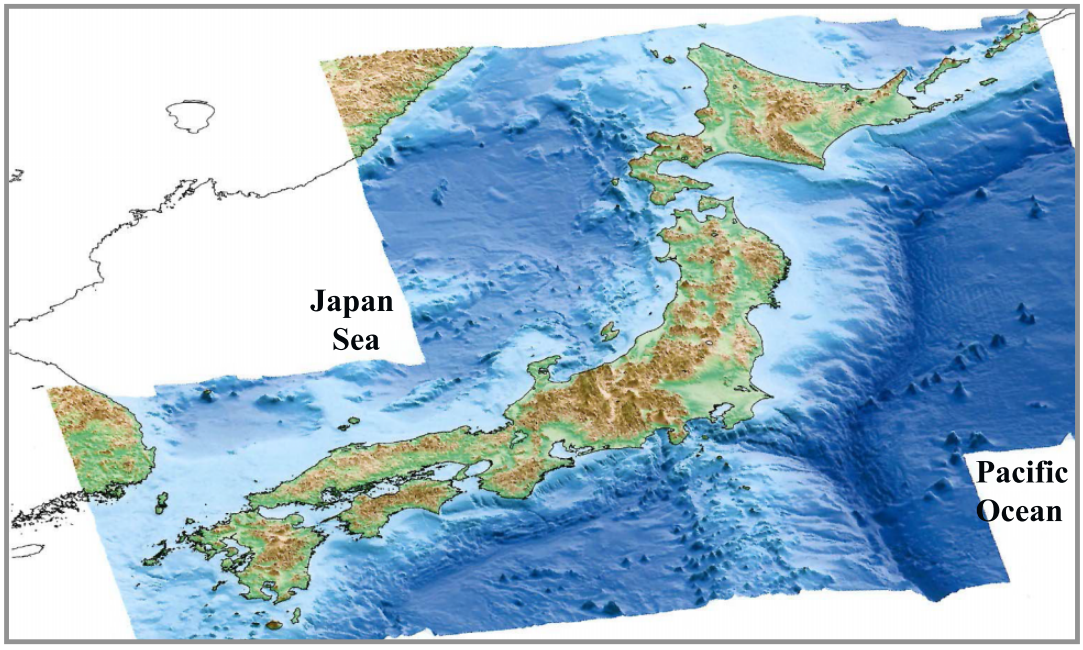

Fig. 3. Surface topography of the Japan Islands and bathymetry of the Japan Sea and Pacific Ocean. (From Yamamoto, 2002.)

surface-wave tomography has a lower spatial resolution because of the long-wavelength nature of surface waves, and so it is more appropriate for global and regional-scale studies (e.g., Tanimoto and Anderson, 1985; Kobayashi and Zhao, 2004; Yoshizawa *et al*., 2010). In contrast, body-wave tomography can have a much higher spatial resolution because of the short wavelengths of body waves, and it can be applied to studies from local to global scales (Zhao, 2009). Because of the sparse and uneven coverage of global seismic networks and natural earthquakes, global tomographic models

doi:10.5047/meep.2012.00101.0001

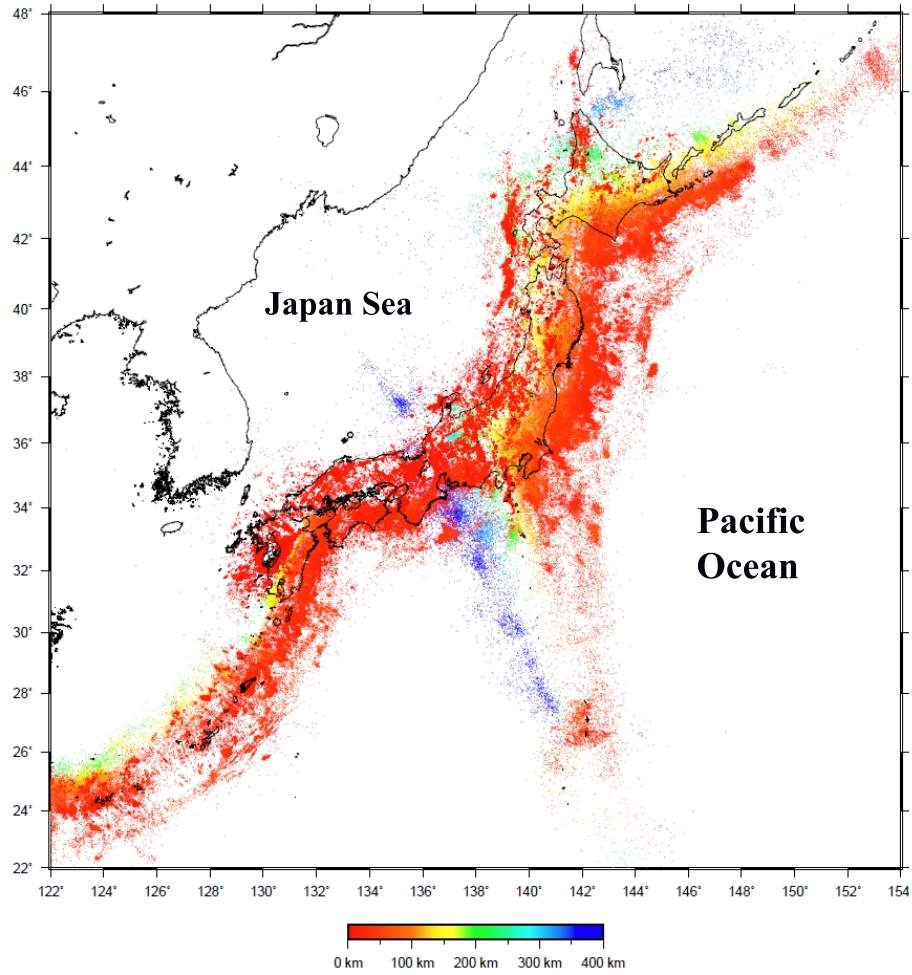

Fig. 4. Distribution of earthquakes in and around the Japan Islands during the period June 2006 to September 2010. The color shows the focal depth. The color scale is shown at the bottom.

still have a lower resolution (> a few hundred kilometers) for most parts of the Earth, but global models can provide information on the deep Earth structure. In contrast, local and regional tomographic models for some regions like Japan and California have a much higher resolution (5–30 km), thanks to the dense coverage of seismic stations and the high level of seismicity there, but these local-tomography models are limited to the crust and/or the upper mantle. Technical details of seismic tomography can be found in Aki and Lee (1976), Thurber (1983), Nolet (1987), Zhao (2001b, 2009), and Rawlinson *et al*. (2010), among many other reviews.

So far, multiscale (local, regional and global) approaches of seismic tomography have been adopted because of the limitation of seismic data now available in different areas and the difference in nature and features of each scientific target (Zhao, 2009). For example, local tomography has been used to determine high-resolution 3-D fine structure of the crust and uppermost mantle under volcanic areas and source zones of large earthquakes to detect structural heterogeneities that may be associated with earthquake nucleation and magma chambers; regional tomography has been used to image subducting slabs and mantle plumes down to the mantle transition zone or the uppermost lower mantle, while global tomography has been used to determine the large-scale whole-mantle structure to clarify the fate of subducting slabs, the origin of deep mantle plumes, and deep Earth dynamics (Zhao, 2009).

The Japan Islands are located in the western Pacific trench–arc–back-arc system, and form a typical subduction zone (Fig. 1). Many active arc and back-arc volcanoes exist in this region, and the arc volcanoes form a clear volcanic front that is parallel with the oceanic trenches in the western Pacific (Figs. 2, 3). The Pacific plate is subducting beneath Hokkaido and Northeast (NE) Japan (Tohoku) from the Kuril and Japan trenches at a rate of 7–10 cm/year. The Philippine Sea plate is subducting beneath the central and Southwest (SW) Japan from the Sagami and Nankai troughs at a rate of 4–5 cm/year. It is generally considered that Hokkaido and NE Japan belong to the Okhotsk plate, whereas SW Japan belongs to the Eurasian (or Amur) plate (e.g., Bird, 2003). Because of the strong interactions between the lithospheric plates in and around the Japan Islands, seismicity is very active there (Fig. 4). Every month, about 11,000 earthquakes ($M \geq \sim 1.5$) take place in and around Japan, which are recorded by the dense and high-sensitivity seismic networks on the Japan Islands (Fig. 5). The seismicity as shown

doi:10.5047/meep.2012.00101.0001

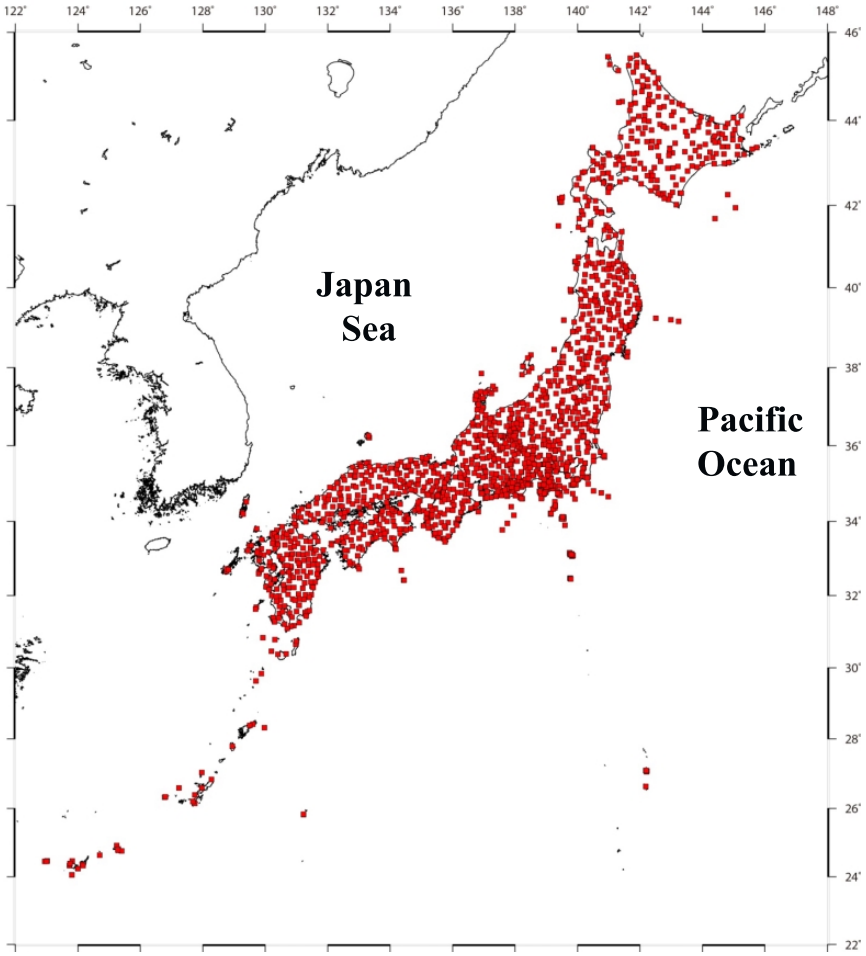

Fig. 5. Distribution of high-sensitivity seismic stations on the Japan Islands.

in Fig. 4 actually occurs every month in Japan, and the pattern of earthquake distribution is almost the same, except for some periods when many aftershocks occur following a great earthquake, such as the 11 March, 2011, Tohoku-oki earthquake (M_w 9.0). Because of the high level of seismicity and the availability of the dense and high-sensitivity seismic networks operated by the Japan Meteorological Agency (JMA), Japanese national universities, National Research Institute for Earth Science and Disaster Prevention (NIED), and other research institutions (Fig. 5), a great amount of high-quality seismic data has been accumulated and has been used to determine the 3-D seismic structure of the crust and upper mantle of the Japan subduction zone. These studies have been conducted continuously during the past thirty years since the advent of the seismic tomography method, making the Japan Islands the best-studied subduction zone in the world.

During the last decade, significant advances have been made in the multiscale tomographic imaging of subduction zones, which have shed new light on the arc and back-arc magmatism, the nucleation mechanism of various types of earthquakes, and subduction dynamics. In this monograph I review the recent results of multiscale tomographic imaging of the Western-Pacific subduction zones and discuss their geodynamic implications, with an emphasis on the Japanese region. I have attempted to make a complete and balanced review on this topic. However, a great amount of literature exists on this topic and space is limited here, hence I have drawn mainly on the studies which I have been involved in, or am relatively familiar with.

2. Advent of Subduction-zone Tomography

Seismic tomography was applied to study the 3-D velocity structure of subduction zones soon after the method was proposed by Aki and Lee (1976) and Aki *et al*. (1977). The first literature on subduction-zone tomography seems to be Hirahara (1977) who used arrival-time data recorded by the JMA seismic network, and those compiled by the International Seismological Center (ISC), to determine a 3-D P-wave velocity model down to 650-km depth beneath the Japan Islands. Although Hirahara adopted coarse cubic blocks, with a size of about 100 km, for tomographic inversion, he was able to detect the subducting Pacific slab that exhibits a higher P-velocity than the surrounding mantle. Later, many researchers applied the block inversion method (Aki and Lee, 1976) to local-earthquake arrival times to study the 3-D velocity structure in many local areas in Japan (e.g., Hirahara, 1981; Horie and Aki, 1982; Takanami, 1982; Miyamachi and Moriya, 1984; Hasemi *et al*., 1984;

doi:10.5047/meep.2012.00101.0001

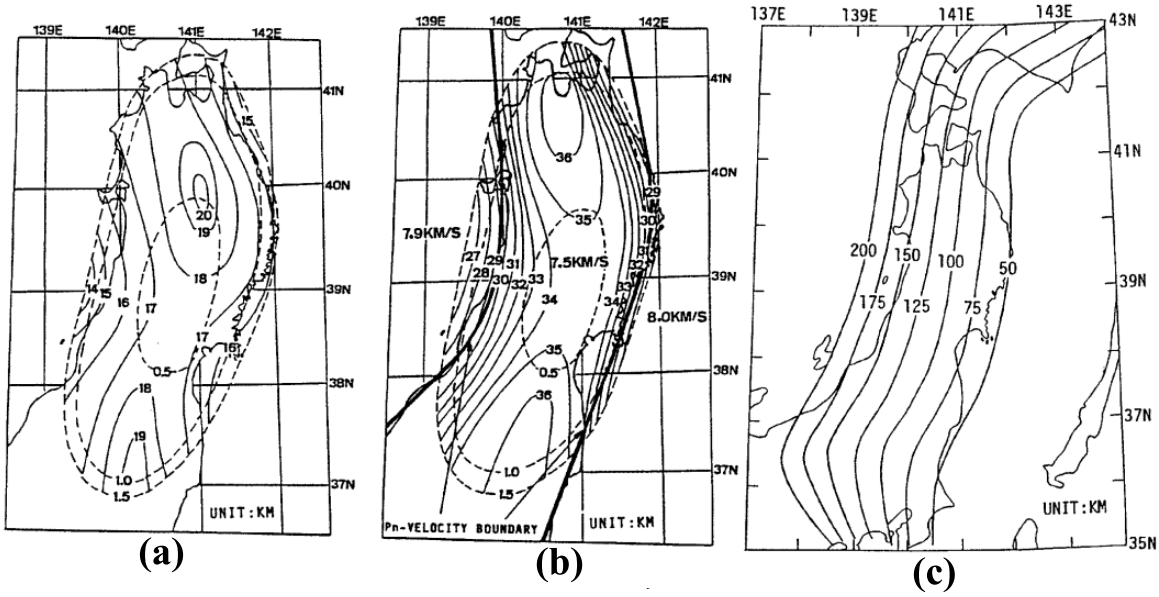

Fig. 6. Depth distributions of (a) the Conrad and (b) Moho discontinuities (Zhao *et al*., 1990) and (c) the upper boundary of the subducting Pacific slab (from Hasegawa *et al*., 1983). The dotted lines in (a) and (b) show the range of the estimated uncertainties (1.0 and 1.5 km). (Reprinted from *Tectonophysics*, *181*, Zhao, D., S. Horiuchi, and A. Hasegawa, 3-D seismic velocity structure of the crust and uppermost mantle in the northeastern Japan arc, 135–149, Copyright 1990, with permission from Elsevier.)

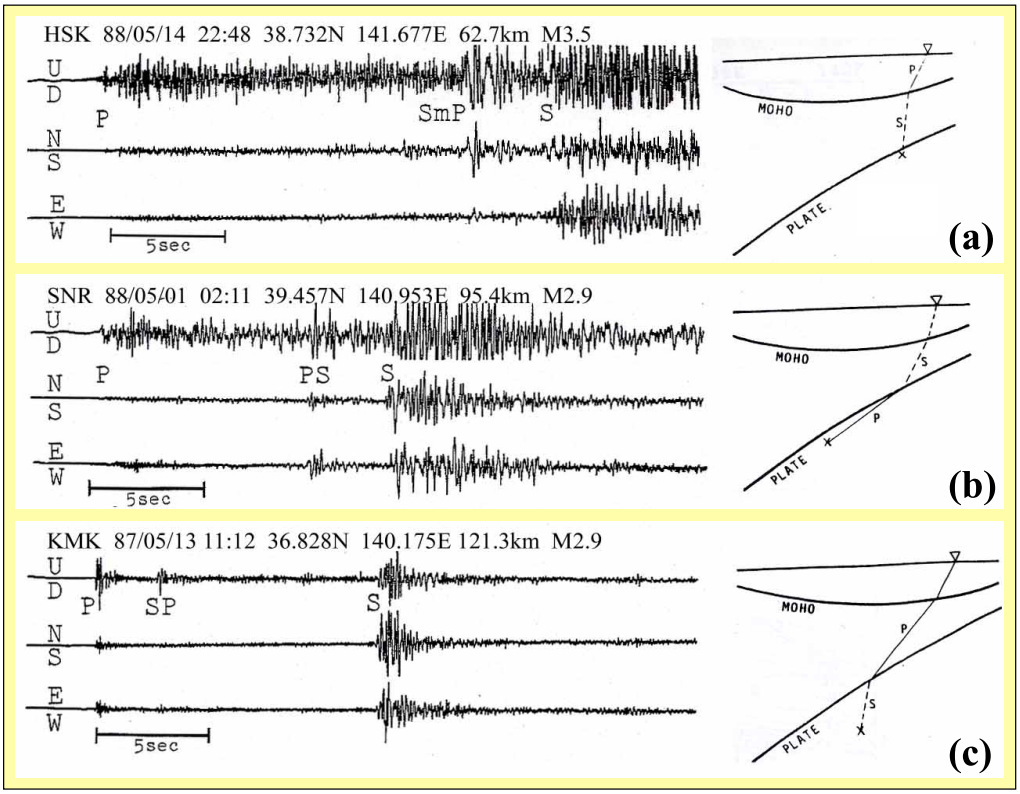

Fig. 7. Examples of (a) converted wave (*SmP*) at the Moho discontinuity and (b) *PS* and (c) *SP* converted waves at the upper boundary of the subducting Pacific slab (from Zhao *et al*., 1992b).

doi:10.5047/meep.2012.00101.0001

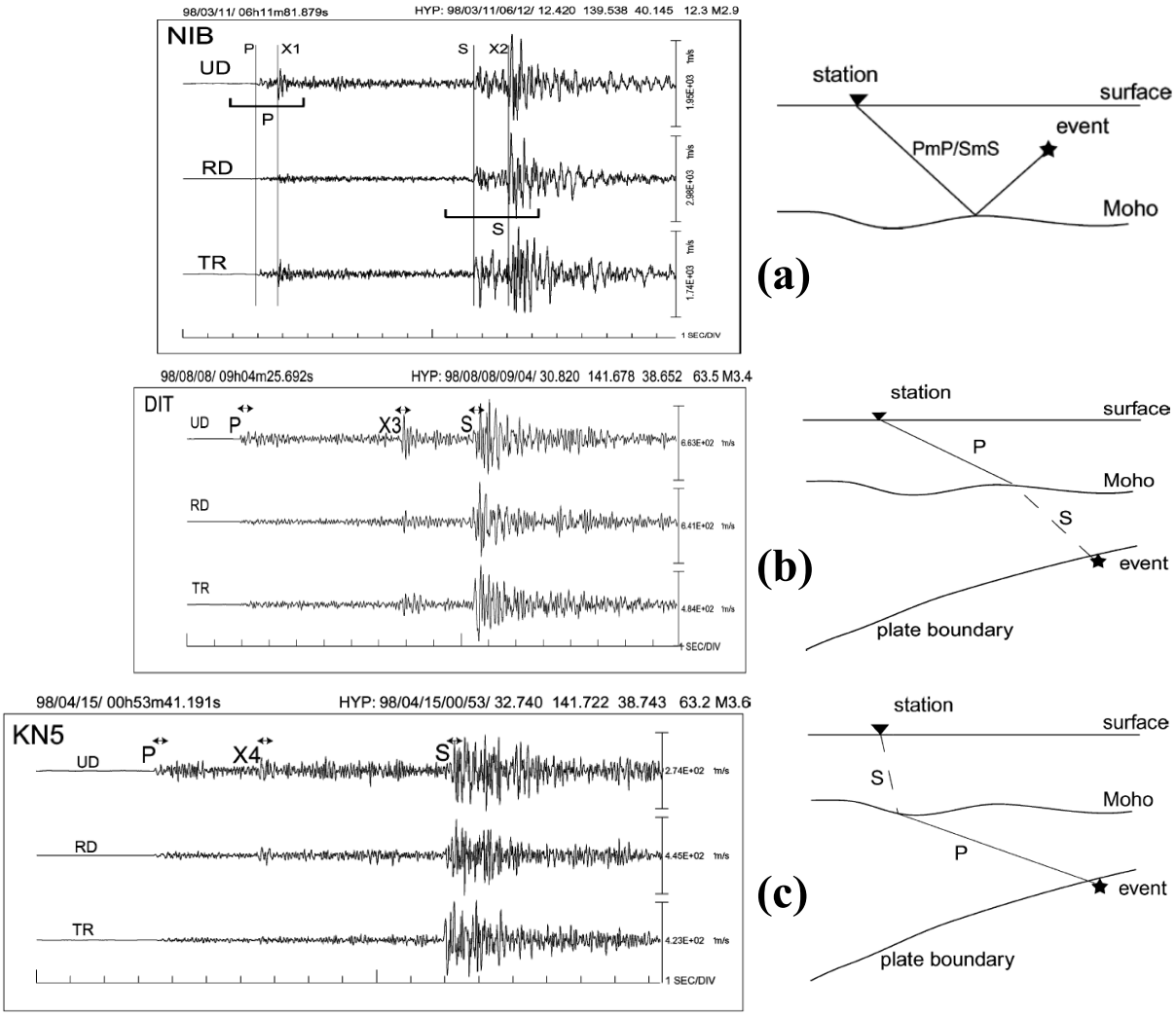

Fig. 8. Examples of (a) *P* and *S* reflected waves at the Moho discontinuity and (b) *S*-*P* and (c) *P*-*S* converted waves at the Moho discontinuity. (Reprinted from *Phys. Earth Planet. Inter.*, *130*, Nakajima, J., T. Matsuzawa, and A. Hasegawa, Moho depth variation in the central part of northeastern Japan estimated from reflected and converted waves, 31–47, Copyright 2002, with permission from Elsevier.)

Nakanishi, 1985; Obara *et al*., 1986; Ishida and Hasemi, 1988, among many others). These local tomography studies used arrival-time data from intermediate-depth earthquakes and obtained 3-D velocity models down to 200-km depth under the Japan land areas.

Horiuchi *et al*. (1982a, b) studied the 3-D crustal structure under central Tohoku using an approach different from the tomographic method. They divided the medium under study into three constant-velocity layers (corresponding to the upper crust, lower crust, and uppermost mantle) by the Conrad and Moho discontinuities, and adopted a power series of latitude and longitude to express the Conrad and Moho depth variations. By inverting the arrival-time data of local crustal earthquakes for the hypocentral parameters, the coefficients of the power series, and the station corrections (that account for the lateral velocity variations in the crust and uppermost mantle), they could estimate the Conrad and Moho geometries under central Tohoku. Later, their approach was applied to the whole Tohoku area as well as the entire Japan Islands, and the results show that the Conrad and Moho discontinuities exhibit significant lateral depth variations under Japan (Zhao *et al*., 1990, 1992a). Both Conrad and Moho are deeper under the land area but become shallower toward the Pacific Ocean and the Japan Sea (Fig. 6(a, b)), which are generally consistent with the results of active-source seismic experiments (e.g., Iwasaki *et al*., 2001).

Several prominent later phases have been detected from seismograms of local earthquakes that occurred beneath the Japan Islands, such as the *ScSp* converted wave at the upper boundary of the subducting Pacific and Philippine Sea slabs (Okada, 1971, 1979; Hasegawa *et al*., 1978; Nakanishi, 1980), *PS* and *SP* converted waves at the upper boundary of the Pacific slab from intermediate-depth earthquakes (Matsuzawa *et al*., 1986, 1990) (Fig. 7(b, c)), reflected *S* waves from the Pacific slab upper boundary (Obara, 1989), and converted and reflected waves from the Moho discontinuity (Zhao *et al*., 1992b; Nakajima *et al*., 2002) (Figs. 7(a), 8). The geometry of the subducting Pacific slab under NE Japan was estimated by using the distribution of intermediate-depth earthquakes (Hasegawa *et al*., 1983) and

doi:10.5047/meep.2012.00101.0001

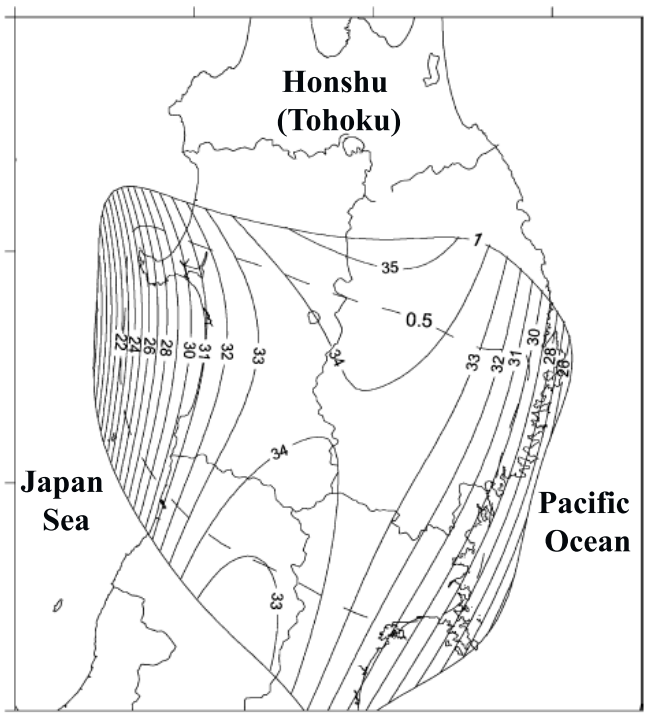

Fig. 9. Depth distribution of the Moho discontinuity estimated with reflected and converted waves. (Reprinted from *Phys. Earth Planet. Inter.*, *130*, Nakajima, J., T. Matsuzawa, and A. Hasegawa, Moho depth variation in the central part of northeastern Japan estimated from reflected and converted waves, 31–47, Copyright 2002, with permission from Elsevier.)

PS and *SP* converted waves at the slab boundary (Matsuzawa *et al*., 1986, 1990; Zhao *et al*., 1997a) (Fig. 6(c)). Nakajima *et al*. (2002) determined the Moho geometry under central Tohoku using the converted and reflected waves at the Moho, and their result (Fig. 9) is well consistent with the earlier results by Zhao *et al*. (1990, 1992a) (Fig. 6(b)). These later-phase studies indicate that the Moho, and the subducting slab boundary under Japan, are very sharp seismic discontinuities that exhibit complex geometries rather than simple planes (Figs. 6, 9).

In the late 1970s and the 1980s, almost all the local and regional tomographic studies were made by applying the block inversion method (Aki and Lee, 1976; Aki *et al*., 1977) or the grid inversion method (Thurber, 1983). However, the block inversion method cannot deal with the lateral depth variations of velocity discontinuities, and the grid inversion method does not even allow the existence of velocity discontinuities. The velocity must be continuous everywhere in the model, in both the lateral and vertical directions (Thurber, 1983).

To overcome the drawbacks of the block and grid inversion methods, Zhao (1991) and Zhao *et al*. (1992b) proposed a new approach for conducting tomographic inversion in the NE Japan subduction zone. In their modeling space (Fig. 10), they introduced three velocity discontinuities (the Conrad, Moho, and the Pacific slab upper boundary) that have curved geometries, and set up 3-D grid nodes to express the 3-D velocity variations. Velocity perturbations at the grid nodes from a starting velocity model are taken as unknown parameters, while the velocity perturbation at any point in the model is calculated by linearly interpolating the velocity perturbations at the eight grid nodes surrounding that point. The unknown velocity parameters and hypocentral parameters were determined by inverting the arrival-time data from both crustal and intermediate-depth earthquakes that occurred under the seismic network in Tohoku. The geometries of the Conrad, Moho and the slab upper boundary, determined from previous studies (Fig. 6), were adopted, and they were fixed in the inversion process. In the starting model for the tomographic inversion, the velocity in the subducting Pacific slab (90-km thick) was set to be 4–6% faster than in the normal mantle.

To calculate theoretical travel times and ray paths accurately and rapidly in the complex 3-D velocity model (Fig. 10), Zhao (1991) and Zhao *et al*. (1992b) developed a new 3-D ray tracing technique that combines the pseudo-bending scheme (Um and Thurber, 1987) and Snell's law iteratively. Their 3-D ray tracing technique can deal with not only first *P* and *S* wave arrivals, but also later phases of converted and reflected waves at the velocity discontinuities in the model (Zhao *et al*., 1992b).

The distinct feature of the boundary-grid tomographic method of Zhao (1991) and Zhao *et al*. (1992b) is that it can deal with complex-shaped velocity discontinuities in the model. Why are velocity discontinuities introduced into the model? There are at least three reasons for this. First, velocity discontinuities do exist beneath NE Japan, as demonstrated by the above-mentioned studies of the converted and reflected waves (Figs. 6–9). Second, theoretical travel times and ray paths can be computed more accurately when the ve-

doi:10.5047/meep.2012.00101.0001

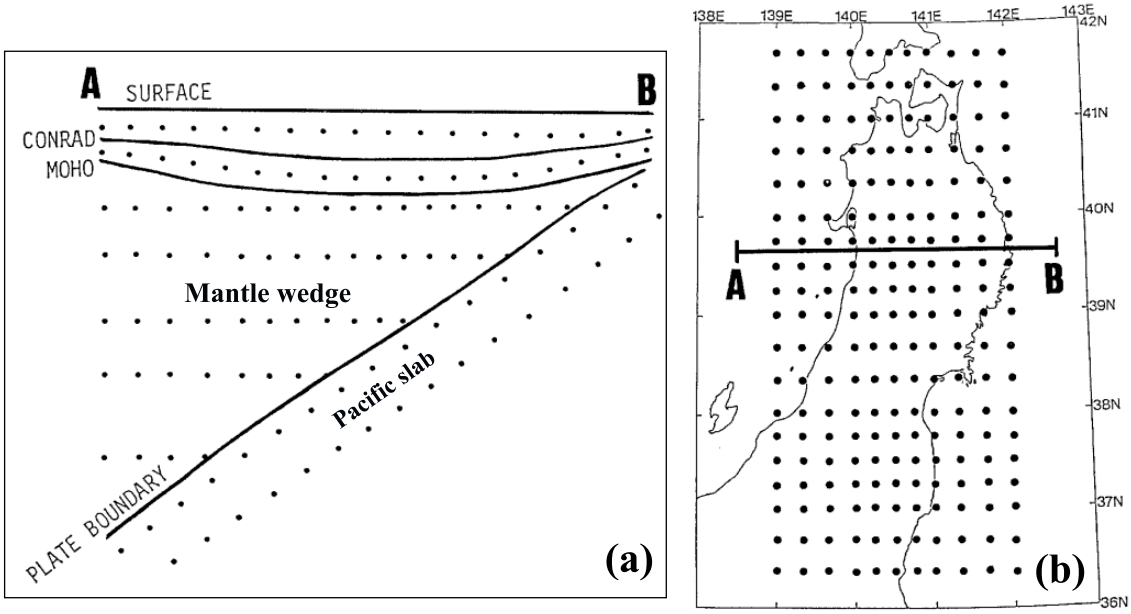

Fig. 10. (a) Vertical cross-section and (b) map view of the boundary-grid model parameterization (adopted by Zhao *et al*., 1992b) for tomographic inversion in NE Japan. Three velocity discontinuities (the Conrad, Moho and the upper boundary of the Pacific slab) are introduced into the model. Velocity perturbations at the 3-D grid nodes and hypocenter parameters are taken as unknown parameters which are determined by inverting arrival-time data.

locity discontinuities are considered in the model. The subducting Pacific slab is 85–90-km thick and it has a seismic velocity 4–6% higher than the normal mantle, and so the slab is the most significant velocity anomaly in the upper mantle under the entire Japan Island. If the slab is not considered in the starting velocity model, the theoretical travel times can be computed with an inaccuracy of one to several seconds (note that the picking error of the arrival-time data is only 0.1–0.2 s), and the errors in ray paths can be over 10–20 km for long rays (>300 km) from the intermediate-depth earthquakes in the Pacific slab. Third, once the velocity discontinuities are introduced into the model, the arrival-time data of converted and reflected waves at the discontinuities (Figs. 7, 8) can also be used in the earthquake location and velocity inversion. The later-phase data contain very important information on the Earth's structure, and so should be used in the tomographic study once they are detected from the seismograms. Many arrivals of the *PS* and *SP* converted waves at the slab upper boundary and the *SmP* converted waves at the Moho were actually used in the tomographic study of the NE Japan subduction zone (Zhao, 1991; Zhao *et al*., 1992b).

Figure 11 shows the tomographic images thus obtained (Zhao, 1991; Zhao *et al*., 1992b). The subducting Pacific slab, which has a P-wave velocity 4–6% higher than the normal mantle, is clearly imaged. The upper-plane earthquakes in the double seismic zone (Umino and Hasegawa, 1975; Hasegawa *et al*., 1978) are located near the upper boundary of the slab, while the lower-plane earthquakes of the double seismic zone occurred in the central part of the Pacific slab. Prominent low-velocity (low-V) zones are revealed in the crust and uppermost mantle beneath the active arc volcanoes, and low-V zones exist in the central part of the mantle wedge, subparallel with the subducting Pacific slab. Under the volcanic front, the low-V zone seems to be connected with the slab (Fig. 11(b)). This tomographic model (Fig. 11) explains several seismic observations well, such as the distribution of low-frequency microearthquakes, lower crust reflectors, and large crustal earthquakes, etc. (Zhao, 1991; Hasegawa and Zhao, 1994; Zhao *et al*., 1992b, 2000a).

Zhao (1991) also conducted a tomographic inversion using a simple 1-D starting velocity model; that is, the Pacific slab was not considered in the starting model. The results show that the subducting Pacific slab could be imaged well beneath the central part of the seismic network, where the ray path coverage is very good, but the slab was imaged very poorly under the edge portions of the study area, because of the poor path coverage there. Of course, the sharp upper boundary of the Pacific slab could not be imaged, even where the slab is clearly visible as a high-velocity (high-V) anomaly, because the tomographic image was obtained by the interpolation of velocities inverted at the grid nodes. To image the sharp upper boundary of the Pacific slab, a very dense grid (with a grid interval of ∼1 km?) has to be set up, but, of course, the velocities at the dense grid nodes cannot be obtained by tomographic inversion because of the limitations in the station spacing and the 3-D ray path coverage. Such a situation remains unchanged even now, despite the dense coverage of seismic stations available on the Japan Islands (Fig. 5) (e.g., Matsubara *et al*., 2008). In any case, the sharp velocity discontinuities have to be introduced into the model to obtain a high-resolution tomography of the Japan subduction zone, though it is generally preferred to adopt a simple 1-D velocity model as a starting model for tomographic inversions. This seems to be a very distinctive feature of subduction-

doi:10.5047/meep.2012.00101.0001

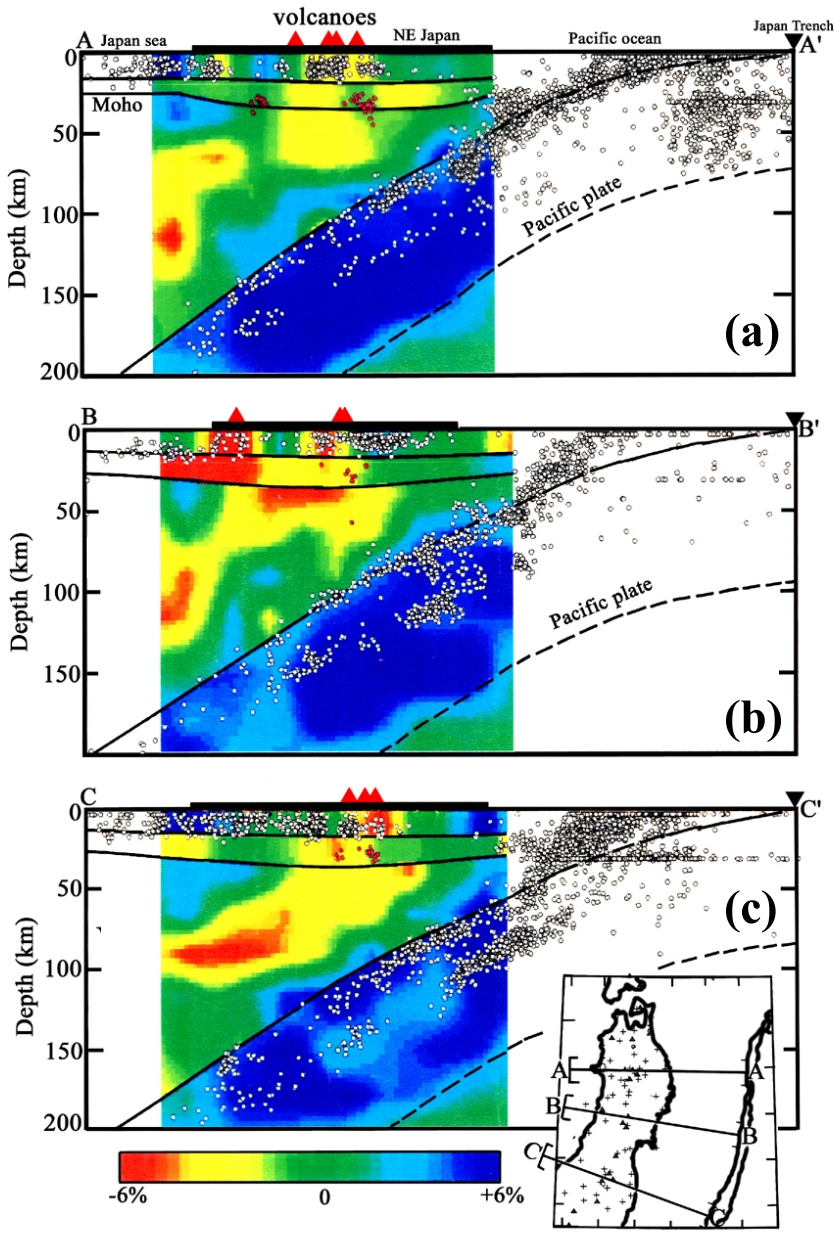

Fig. 11. Vertical cross sections of *P*-wave tomography beneath NE Japan from the Earth's surface to 200-km depth along the profiles shown on the inset map. Red and blue colors denote slow and fast velocities, respectively. The velocity perturbation scale is shown at the bottom. Open circles denote earthquakes that occurred within a 30-km width along each profile. Red dots show low-frequency microearthquakes that occurred around the Moho discontinuity, due to the magmatic and volcanic activity. Red triangles, active volcanoes; reverse triangle, location of the Japan Trench. The horizontal bar at the top of each cross-section shows the land area where seismic stations exist. The three thick curved lines denote the Conrad and Moho discontinuities and the upper boundary of the subducting Pacific slab. The dashed line shows the estimated lower boundary of the Pacific slab (from Zhao *et al*., 1992b).

zone tomography.

Note that Zhao (1991), and Zhao *et al*. (1992b), inverted for only the 3-D velocity variations, but fixed the geometries of the velocity discontinuities in the inversion process. If many more later-phase data are available, the geometries of velocity discontinuities can also be inverted. But one should be careful that only when a velocity discontinuity is found to actually exist in the study area, and its geometry is determined reliably, should it be introduced into the tomographic model, otherwise it should not be considered. For example, it has been recognized for a long time that the subducting Philippine Sea slab exists beneath SW Japan, and its upper boundary is found to be a sharp velocity discontinuity in some areas, from analyses of later-phase data, but its general geometry is still not very clear. Hence, the Philippine Sea slab has not been considered in the starting model for tomographic inversions up to the present (e.g., Zhao, 1991; Zhao and Hasegawa, 1993; Zhao *et al*., 2000b; Xia *et al*., 2008a).

Receiver-function analysis is an effective tool to map the

doi:10.5047/meep.2012.00101.0001

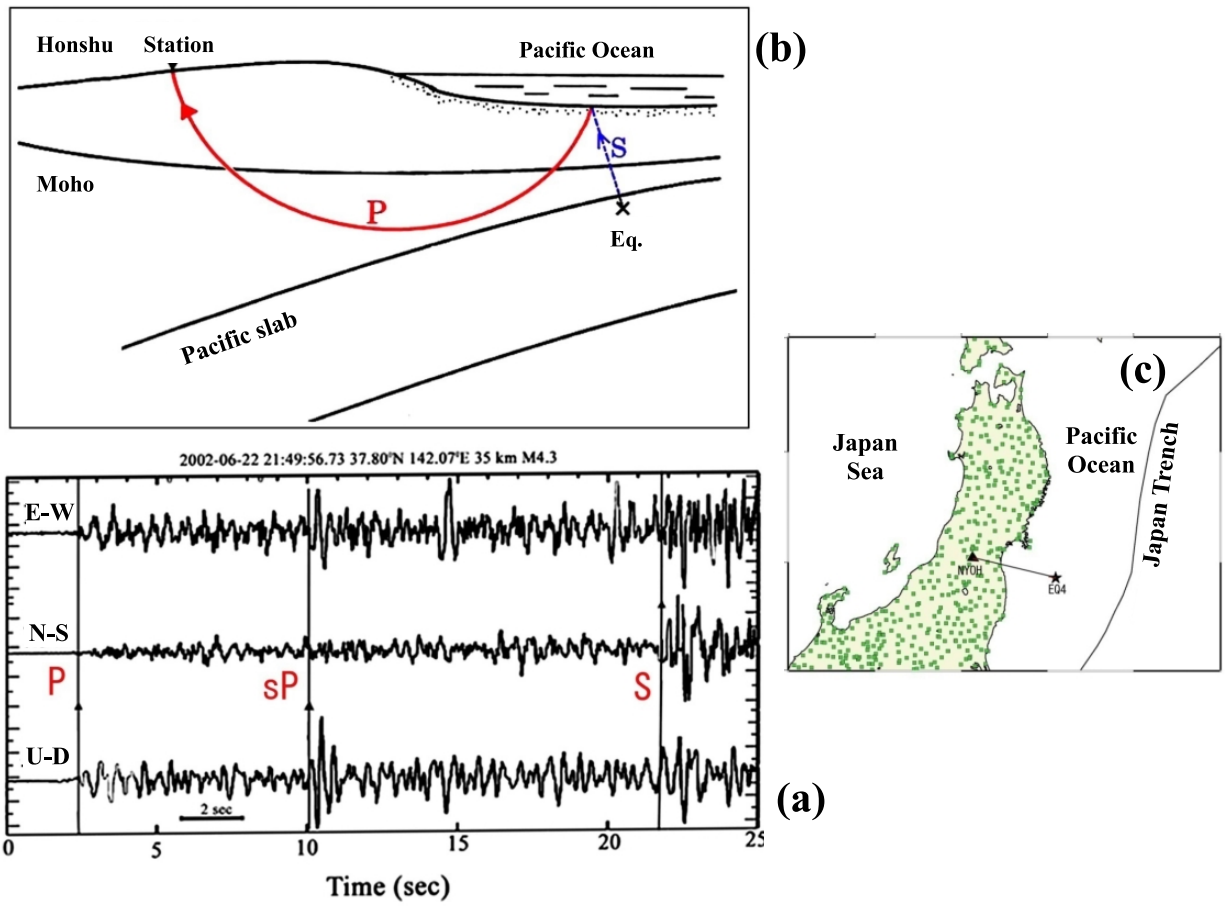

Fig. 12. An example of an *sP* depth phase from an event under the Pacific Ocean. The green squares on the inset map show the seismic stations of the Kiban seismic network. (Reprinted from *Tectonophysics*, *467*, Zhao, D., Z. Wang, N. Umino, and A. Hasegawa, Mapping the mantle wedge and interplate thrust zone of the northeast Japan arc, 89–106, Copyright 2009, with permission from Elsevier.)

Moho, 410- and 660-km discontinuities, as well as the subducting slab boundary (e.g., Ai *et al*., 2005; Shiomi *et al*., 2006; Kawakatsu and Watada, 2007; Tonegawa *et al*., 2008; Tian *et al*., 2010). A combination of receiver-function and tomography methods may enable us to estimate simultaneously velocity discontinuities and 3-D velocity variations (e.g., Hirahara, 2006).

The tomographic method (Zhao *et al*., 1992b) was later applied to a much better data set, recorded by many more seismic stations in Tohoku, which resulted in an improved 3-D *P* and *S* wave velocity model of the NE Japan subduction zone (Nakajima *et al*., 2001). However, the main features of the tomographic image remain the same as those in Fig. 11. The method has been also applied to several other subduction zones, leading to nice tomographic images in those regions, such as Alaska (Zhao *et al*., 1995), Taiwan (Ma *et al*., 1996; Chou *et al*., 2006, 2009), Tonga (Zhao *et al*., 1997b), Romania (Fan *et al*., 1998), Kamchatka (Gorbatov *et al*., 1999), and South America (Myers *et al*., 1998; Wagner *et al*., 2005), in addition to many other applications in various tectonic settings. The boundary-grid approach has been extended to conduct global tomography (Zhao, 2001c, 2004; Zhao and Lei, 2004) by considering the lateral depth variations of the Moho, 410- and 670-km discontinuities. Recently, Ballard *et al*. (2009) and Simmons *et al*. (2011) applied the 3-D ray tracing approach of Zhao *et al*. (1992b) for global-scale travel-time calculations and tomographic inversions.

In the same period of active tomographic studies of 3-D velocity structures, some researchers investigated the 3-D attenuation structure in subduction regions, mainly in the Japan Islands (e.g., Umino and Hasegawa, 1984; Furumura and Moriya, 1990; Sekiguchi, 1991; Tsumura *et al*., 2000; Salah and Zhao, 2003a). These studies show that the subducting Pacific slab exhibits very small attenuation with Q values of up to 1000 to 1500. In contrast, the mantle wedge and the crust beneath active volcanoes show very strong attenuation with Q values of 100 or smaller. Tsumura *et al*. (2000) determined a high-resolution (∼40 km) 3-D attenuation model under Tohoku that shows clearly the high-Q Pacific slab and low-Q anomalies in the crust and mantle wedge beneath active volcanoes. The general pattern of Q tomography is quite similar to that of velocity tomography in this region (Fig. 11). Roth *et al*. (2000) estimated a 3-D Q model of the Tonga-Fiji region and found that low-Q anomalies extend down to 400-km depth in the mantle wedge above the high-Q Tonga slab, in good agreement with the velocity images of Zhao *et al*. (1997b).

doi:10.5047/meep.2012.00101.0001

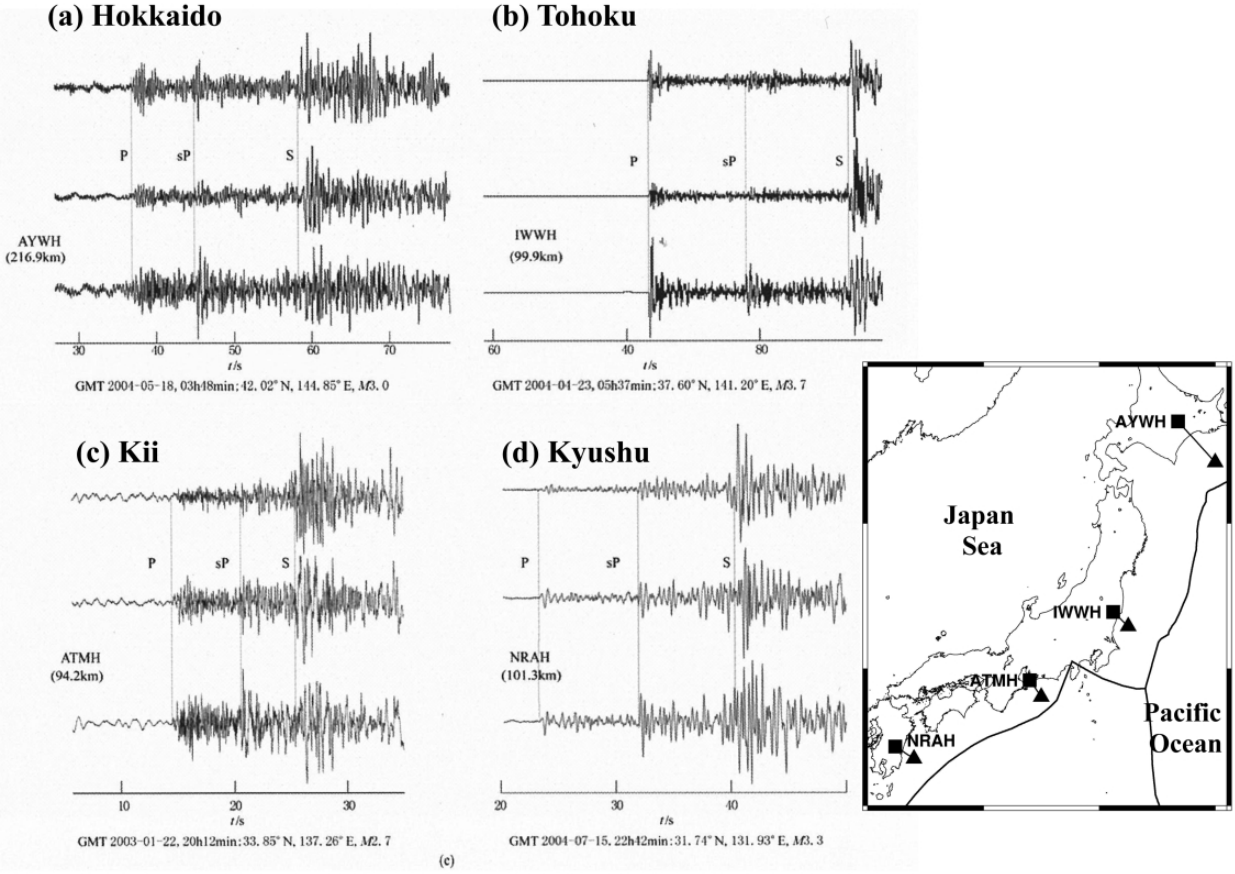

Fig. 13. Examples of 3-component seismograms showing *sP* depth phases from suboceanic events under the Pacific Ocean. (With kind permission from Springer Science+Business Media: *Earthq. Sci.*, Interplate coupling and seismotectonics under the fore-arc regions of Japan, *23*, 2010, 555–565, Wang, Z., figure 2.)

The attenuation structure of subduction zones has also been investigated by using seismic intensity data (e.g., Hashida, 1989). By May 1996, however, seismic intensity was usually measured on the basis of human perception and the movement of objects observed by experts without instruments. The estimated attenuation models show a similarity to those determined with precise seismological data such as seismic wave amplitudes and amplitude spectra. Although the 3-D Q models cannot achieve a resolution as high as that of velocity tomography, they can provide additional information on the physical properties of subduction zones. Hence, future efforts should be made to determine more accurate, high-resolution, models of seismic attenuation in subduction zone regions.

3. Tomographic Imaging outside a Seismic Network

Since the advent of travel-time tomography (Aki and Lee, 1976; Aki *et al.*, 1977), the method has been applied to determine the 3-D velocity structure directly beneath a seismic network, whereas the 3-D structure outside a seismic network could not be determined accurately. This is a serious limitation of the methodology. However, a series of studies in recent years has demonstrated that this limitation of travel-time tomography can be overcome in some cases, and the 3-D structure outside a seismic network can be determined as accurately as that beneath the network (Zhao *et al.*, 2002, 2007a).

Those earthquakes occurring in the crust and in the subducting Pacific and Philippine Sea slabs under Japan land areas have reliable hypocenter locations because they are located right beneath the dense seismic network (Fig. 5). In contrast, the earthquakes under the Pacific Ocean and the Japan Sea (Fig. 4) occur outside the seismic network and so have poor hypocenter locations, because only the first P and S wave arrival times are used in routine earthquake location by the seismic networks. Therefore, earlier tomographic studies could only determine a 3-D velocity model of the crust and upper mantle beneath Japanese land areas (e.g., Fig. 11), whereas a 3-D model under the surrounding oceanic regions was not determined. Because many large and small earthquakes occur beneath the Pacific Ocean and the Japan Sea (Fig. 4), it is very important to study the 3-D velocity structure under the adjacent oceanic areas so as to understand the mechanism of interplate earthquakes in the megathrust zone (such as the 2011 $M_{\rm w}$ 9.0 Tohoku-oki earthquake) and the interplate seismic coupling in the forearc region, as well as the back-arc magmatism and seismotectonics under the Japan Sea.

Determining hypocenters precisely is of fundamental im-

doi:10.5047/meep.2012.00101.0001

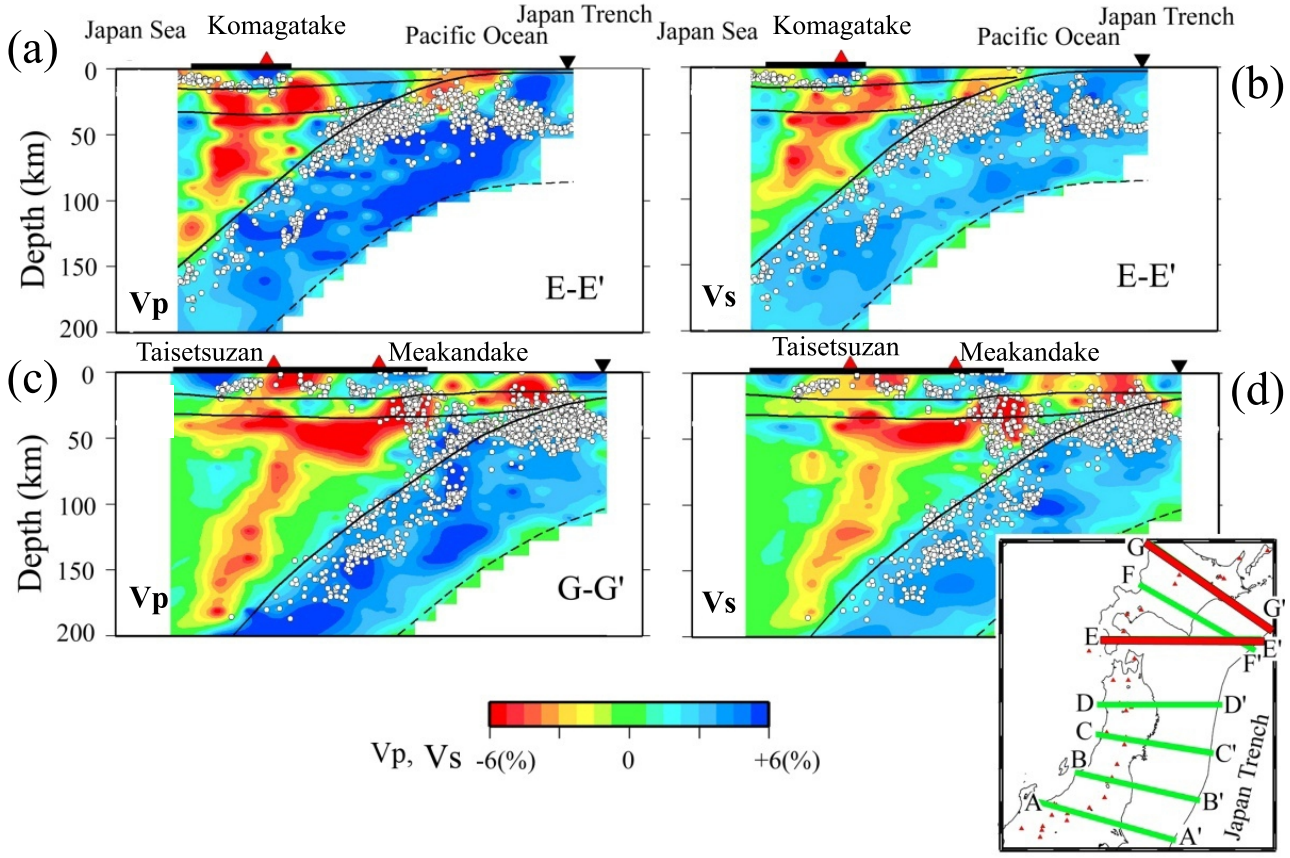

Fig. 14. Vertical cross-sections of (a, c) *P*- and (b, d) *S*-wave velocity images along the profiles E–E′ and G–G′ as shown on the inset map. Red and blue colors denote low and high velocities, respectively. The velocity perturbation scale (in %) is shown at the bottom. Red triangles denote active arc volcanoes. The inverted triangles show the location of the oceanic trench. Small white dots show earthquakes which occurred within a 15-km width from the profile. The three curved lines show the Conrad and Moho discontinuities and the upper boundary of the subducting Pacific slab. The dashed lines denote the estimated lower boundary of the Pacific slab. There is no vertical exaggeration of the cross-sections in this and following figures. The resolution of the tomographic images is 10–20 km in the vertical direction and 25–30 km in the horizontal direction. The uncertainty in the hypocenter locations is 1–4 km under the seismic network on the land area and 3–9 km under the Pacific Ocean. (Reprinted from *Phys. Earth Planet. Inter.*, *152*, Wang, Z., and D. Zhao, Seismic imaging of the entire arc of Tohoku and Hokkaido in Japan using P-wave, S-wave and sP depth-phase data, 144–162, Copyright 2005, with permission from Elsevier.)

portance in many disciplines of seismology, being necessary to estimate the rupture process on the fault plane, strong ground motions in the source area, and the crustal and upper-mantle structure, etc. Among the four hypocentral parameters (i.e., origin time, latitude, longitude, and focal depth), the focal depth is usually harder to determine in the case of events outside a seismic network. To locate earthquakes (in particular, suboceanic earthquakes) accurately, seismologists have traditionally used the so-called depth phases (e.g., *pP*, *sP*, etc.) in teleseismic distances of thousands of kilometers (e.g., Herrmann, 1976; Forsyth, 1982; Engdahl and Billington, 1986). Such depth phases are reflected waves from the surface (or seafloor) with bouncing points close to the epicenter (Fig. 12(b)), and so their travel times are very sensitive to the focal depth. Hence, the suboceanic earthquake hypocenters, in particular, their focal depths, can be well constrained by using *pP* or *sP* phase data. The use of a depth-phase datum in earthquake location is just like installing a new seismic station close to the epicenter (at the bouncing point on the Earth's surface or seafloor).

In order to locate precisely suboceanic earthquakes surrounding NE Japan, Umino and Hasegawa (1994) and Umino *et al*. (1995) detected *sP* depth phases, at a local distance (<300 km), from short-period seismograms of shallow earthquakes that occurred under the Japan Sea and the Pacific Ocean, recorded by the seismic network in Tohoku. Figures 12 and 13 show some examples of seismograms in which *sP* depth phases are clearly visible. It is found that suboceanic earthquakes could be located very accurately with the *sP* depth-phase data, and the location accuracy is comparable to that for the earthquakes under the seismic network in the Honshu land area (hypocenter uncertainty <3 km) (Umino and Hasegawa, 1994; Umino *et al*., 1995; Wang and Zhao, 2005; Gamage *et al*., 2009; Huang *et al*., 2010).

Zhao *et al*. (2002) first determined a 3-D *P*-wave velocity model under the Tohoku forearc region from the Japan Trench to the Pacific coast using a large number of *P*-wave arrival times of suboceanic earthquakes that were relocated precisely with the *sP* depth phase, and suggested that this

doi:10.5047/meep.2012.00101.0001

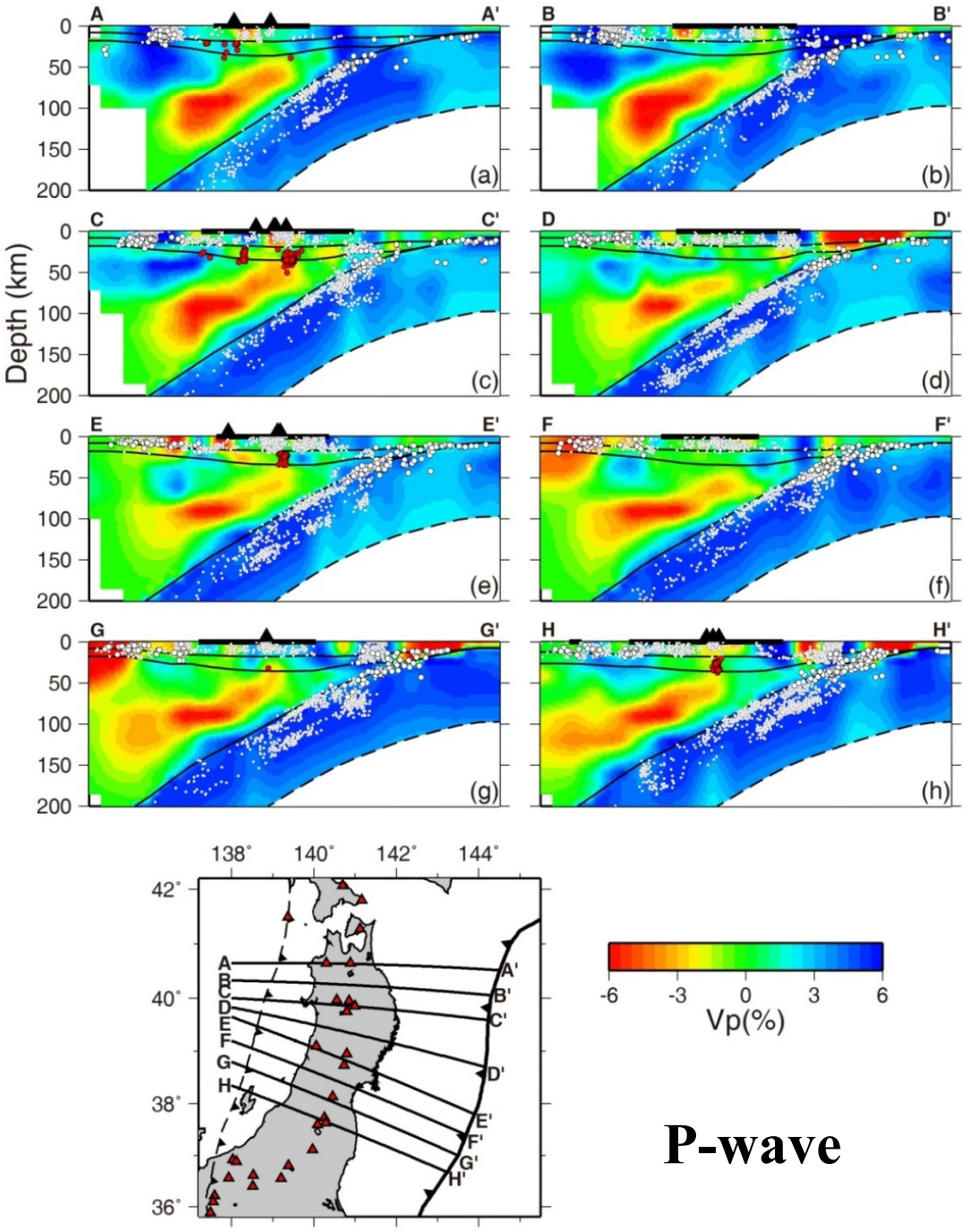

Fig. 15. The same as Fig. 14 but for *P*-wave tomography along the eight profiles in NE Japan. (Reprinted from *Geophys. J. Int.*, *184*, Huang, Z., D. Zhao, and L. Wang, Seismic heterogeneity and anisotropy of the Honshu arc from the Japan Trench to the Japan Sea, 1428–1444, Copyright 2011, with permission from John Wiley & Sons.)

approach is a reliable way of tomographic imaging outside a seismic network. Later, both *P* and *S* wave arrival times from the relocated suboceanic events, as well as earthquakes under the land area, were used to determine the 3-D *P* and *S* wave velocity and Poisson's ratio structures under the Hokkaido and Tohoku forearc areas (Mishra *et al*., 2003; Wang and Zhao, 2005, 2006a; Zhao *et al*., 2007a, 2009a) and the eastern margin of the Japan Sea (Huang *et al*., 2010) (Figs. 14–18). *sP* depth phases are also observed clearly from seismograms of suboceanic events in SW Japan (Fig. 13(c, d)), and so the 3-D velocity structure under the Kyushu forearc region was also studied (Wang and Zhao, 2006b) (Figs. 19, 21).

Recently, Huang *et al*. (2011a) determined a 3-D *P* and *S* wave velocity model of the NE Japan arc by inverting 310,749 *P* and 150,563 *S* wave arrival times from 4,655 local earthquakes which occurred in the crust and the subducting Pacific slab from the Japan Trench to the Japan Sea

doi:10.5047/meep.2012.00101.0001

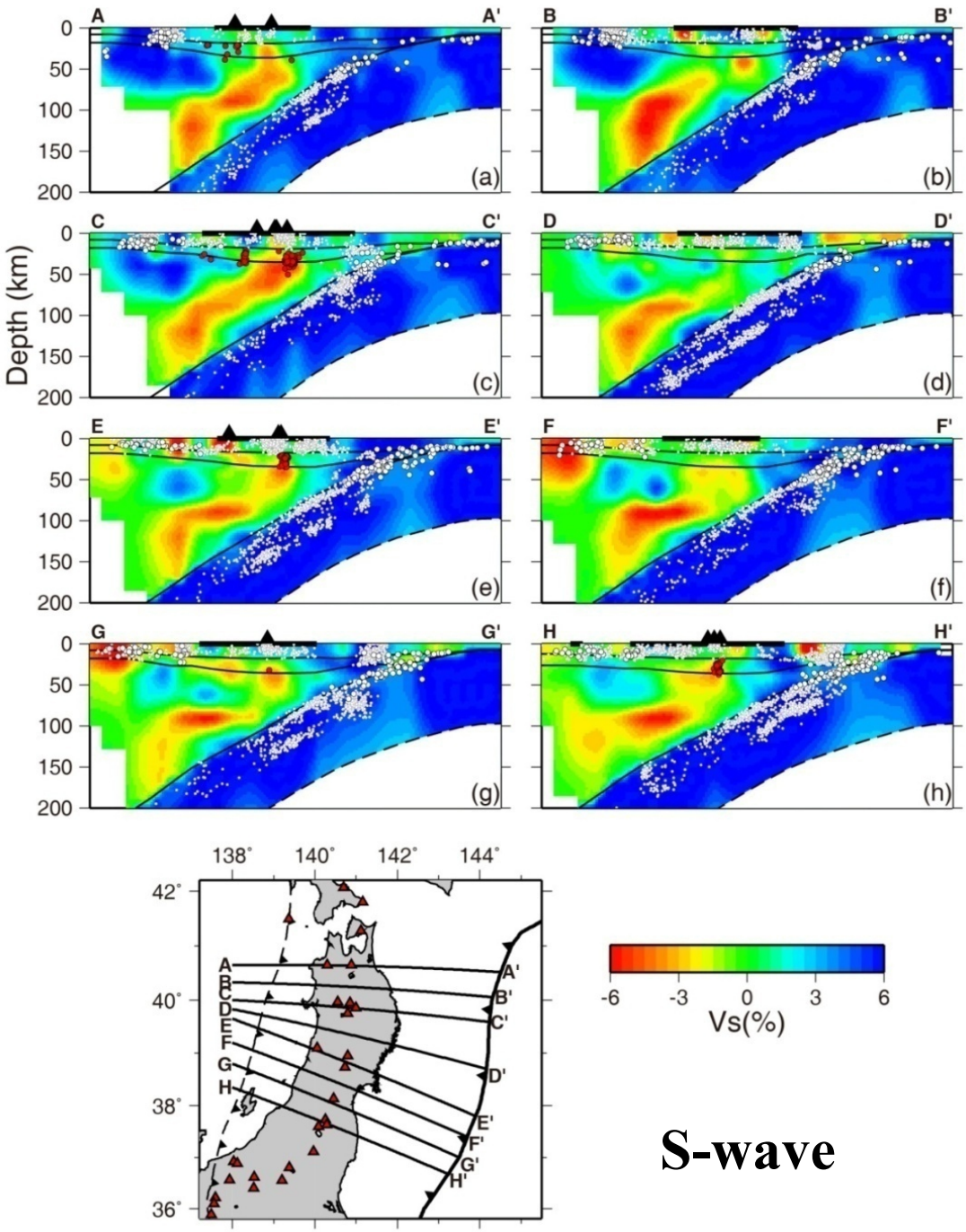

Fig. 16. The same as Fig. 15 but for *S*-wave tomography along the eight profiles in NE Japan. (Reprinted from *Geophys. J. Int.*, *184*, Huang, Z., D. Zhao, and L. Wang, Seismic heterogeneity and anisotropy of the Honshu arc from the Japan Trench to the Japan Sea, 1428–1444, Copyright 2011, with permission from John Wiley & Sons.)

(Figs. 15, 16). They relocated suboceanic events precisely using *P* and *S* arrival times, as well as *sP* depth-phase data, measured from the seismograms recorded by the seismic stations on the Tohoku land area, similar to previous studies (Umino *et al*., 1995; Mishra *et al*., 2003; Wang and Zhao, 2005; Gamage *et al*., 2009; Zhao *et al*., 2009a). The 3-D velocity model under the Pacific Ocean and the Japan Sea was determined reliably with a resolution of 30–40 km (Huang *et al*., 2011a). As compared with previous tomographic studies (e.g., Zhao *et al*., 2009a), Huang *et al*. (2011a) used many more suboceanic events that were relocated with *sP* depth phases, and the events used were distributed more densely and uniformly in the forearc, so they could determine the 3-D velocity model under the Pacific Ocean more reliably (Figs. 15–17).

Benefiting from the dense seismic networks on the Japan Islands, we can apply the approach of off-network tomography to broad regions surrounding the Japan Islands, such

doi:10.5047/meep.2012.00101.0001

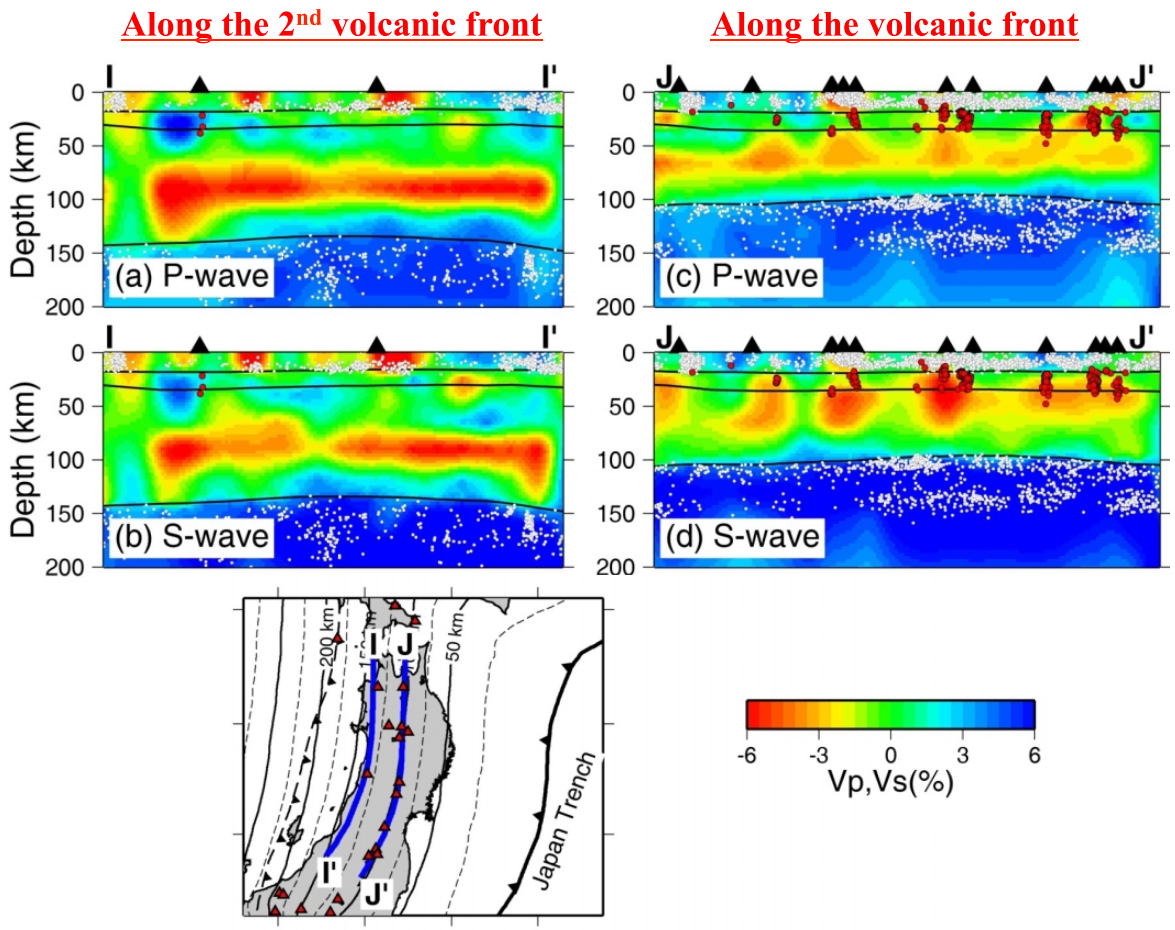

Fig. 17. Two vertical cross-sections of *P* and *S* wave tomography along the volcanic front and the Japan Sea coast as shown on the inset map. The other labeling is the same as that in Fig. 15. (Reprinted from *Geophys. J. Int.*, *184*, Huang, Z., D. Zhao, and L. Wang, Seismic heterogeneity and anisotropy of the Honshu arc from the Japan Trench to the Japan Sea, 1428–1444, Copyright 2011, with permission from John Wiley & Sons.)

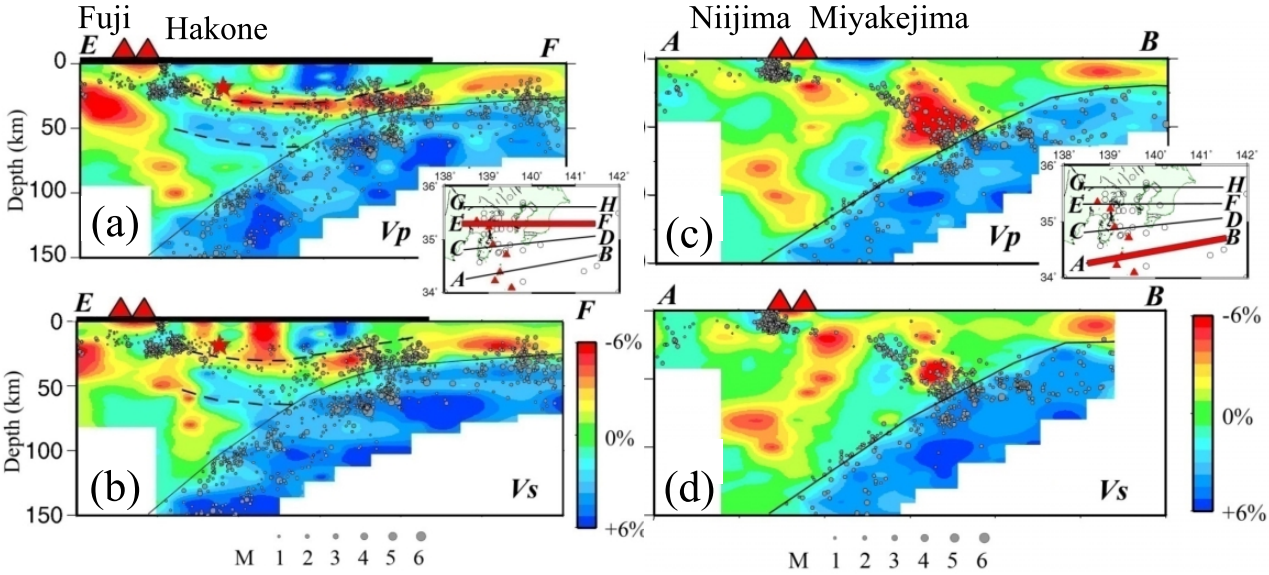

Fig. 18. Vertical cross-sections of (a, c) *P*- and (b, d) *S*-wave velocity images along the profiles E–F (a, b) and A–B (c, d) as shown on the inset maps of the Kanto District. The solid curved lines show the upper boundary of the subducting Pacific slab, while the dashed lines in (a, b) show the estimated upper and lower boundaries of the subducting Philippine Sea slab. The red star in (a, b) shows the hypocenter of the 1923 Kanto earthquake (*M* 7.9). Other labels are the same as those in Fig. 14. (Reprinted from *Earth Planet. Sci. Lett.*, *241*, Wang, Z., and D. Zhao, Suboceanic earthquake location and seismic structure in the Kanto district, central Japan, 789–803, Copyright 2006, with permission from Elsevier.)

doi:10.5047/meep.2012.00101.0001

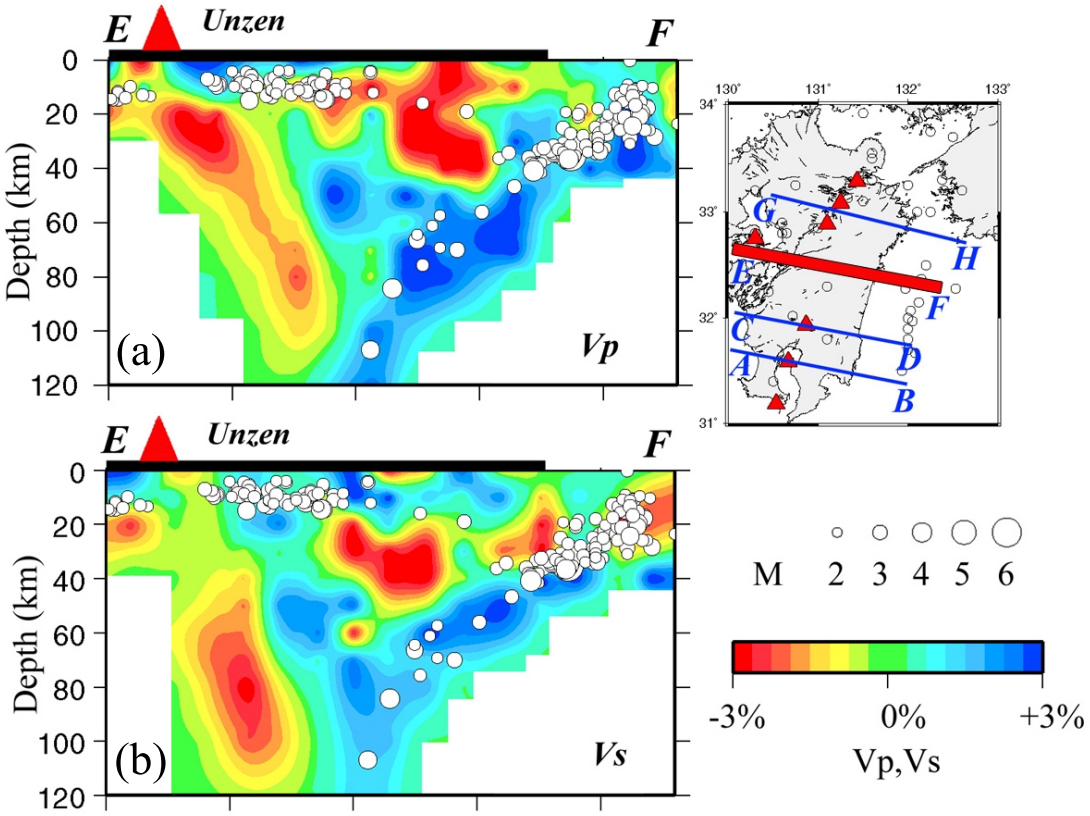

Fig. 19. The same as Fig. 14(a, b) but along profile E–F as shown on the inset map of Kyushu Island. (Reprinted from *Phys. Earth Planet. Inter.*, *157*, Wang, Z., and D. Zhao, Vp and Vs tomography of Kyushu, Japan: New insight into arc magmatism and forearc seismotectonics, 269–285, Copyright 2006, with permission from Elsevier.)

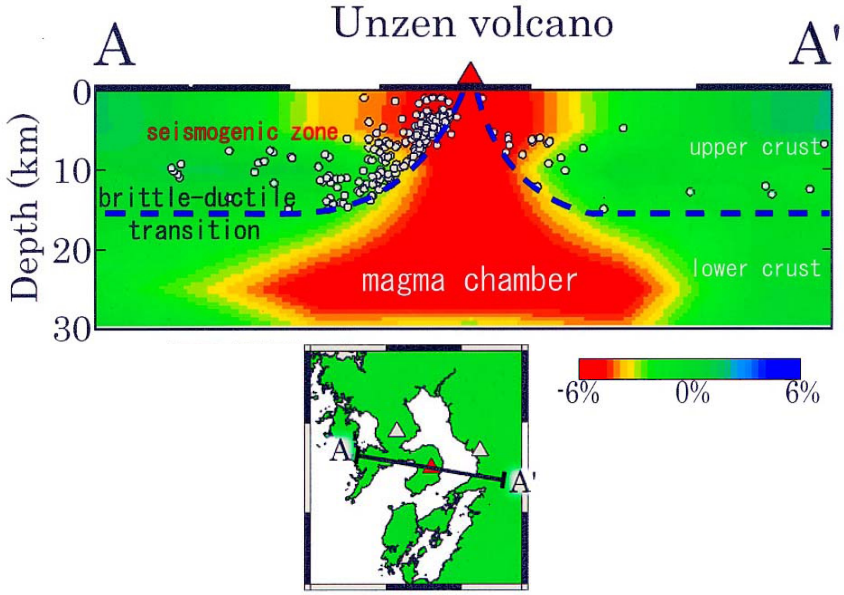

Fig. 20. A vertical cross-section of *P*-wave tomography along profile A–A′ as shown on the inset map (Zhao *et al.*, 2000b, 2002). Red denotes low velocity, while blue denotes high velocity. The color scale is shown at the bottom. The red triangle denotes the active Unzen volcano. (Reprinted from *Phys. Earth Planet. Inter.*, *132*, Zhao, D., O. P. Mishra, and R. Sanda, Influence of fluids and magma on earthquakes: seismological evidence, 249–267, Copyright 2002, with permission from Elsevier.)

doi:10.5047/meep.2012.00101.0001

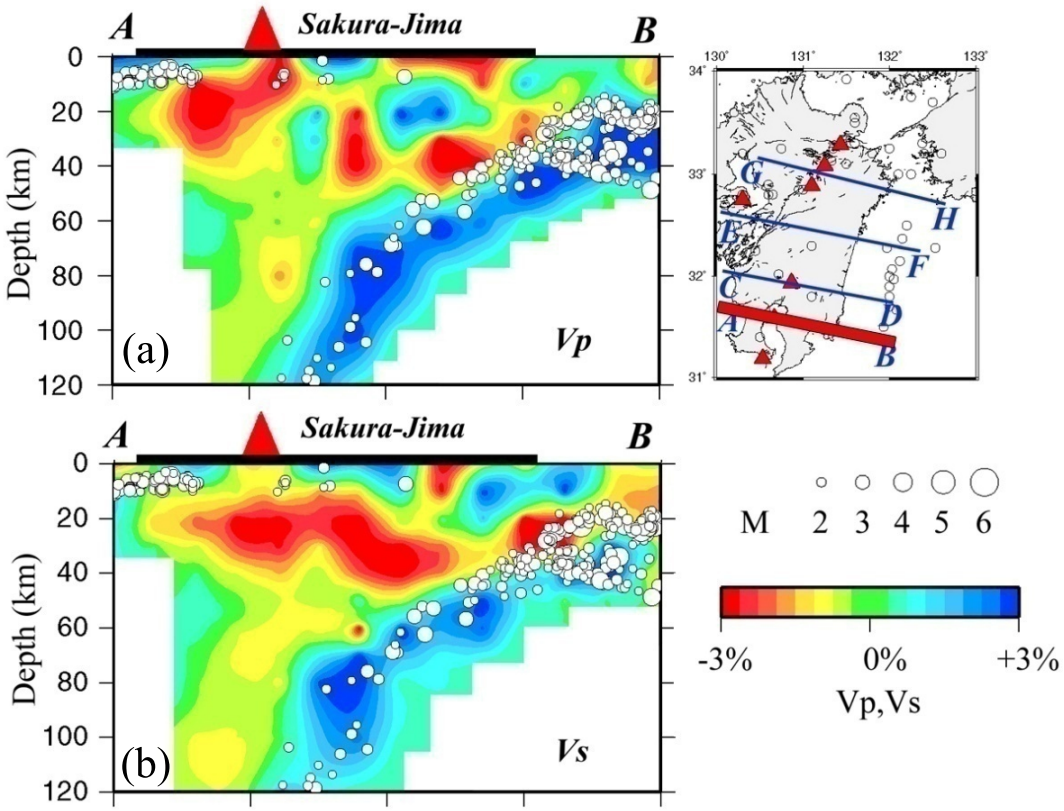

Fig. 21. The same as Fig. 19 but along profile A–B as shown on the inset map of Kyushu Island. (Reprinted from *Phys. Earth Planet. Inter.*, *157*, Wang, Z., and D. Zhao, Vp and Vs tomography of Kyushu, Japan: New insight into arc magmatism and forearc seismotectonics, 269–285, Copyright 2006, with permission from Elsevier.)

as the Kuril subduction zone north of Hokkaido, the Izu-Mariana region south of Kanto, and the Ryukyu subduction zone south of Kyushu. Thus, using the abundant waveform data recorded by Japanese seismic networks, we can study the 3-D structure and seismotectonics of broad regions in the Western Pacific, which greatly expands the scope and usage of the dense seismic networks of Japan.

The off-network tomography approach has important implications for the methodology of seismic tomography, and will find a wide range of applications (Zhao *et al*., 2007a). Most of the subduction zones in the world are located in island arcs or continental margins, and forearc regions are generally under oceans having intense seismicity but with no, or few, seismometers. Similar to the case of NE Japan, the forearc regions of most subduction zones are less studied. The use of this new approach will greatly advance our understanding of the structure and seismotectonics of forearc regions in the world.

Most deep earthquakes in subduction zones occur outside the existing seismic networks and they are usually hard to locate accurately. We can try to detect the depth phases to determine the precise hypocentral locations of intermediate-depth, and deep-focus, earthquakes so as to better understand the morphology of the Wadati-Benioff zone and the mechanism of deep earthquakes, though high-resolution tomographic images may not be determined in and around the deep slab because the ray path coverage from deep earthquakes alone may not be good enough.

In recent years, the structure and dynamics of the Tibetan Plateau have attracted much attention within the geoscience community, but the region is still poorly studied and tomographic images of it still have a lower resolution (e.g., Zheng *et al*., 2007; He *et al*., 2010). Seismicity in the Tibetan region is very active, but it is very difficult to install and maintain a permanent (even a portable) seismic network in this region because of its adverse natural conditions. Using the permanent seismic networks in the Sichuan and Yunnan provinces of Mainland China, however, a detailed tomographic image under the Tibetan Plateau can be obtained by applying the off-network tomography method (Zhao *et al*., 2007a).

Similarly, this approach can also be applied to many other regions of the world where a seismic network exists and earthquakes occur in and around the network. Thus, such costly seismic networks can be better exploited for studying seismotectonics and the Earth's structure. However, this approach of tomographic imaging is only applicable to regions having sufficient seismicity that is recorded by a nearby seismic network. For aseismic regions, it is not applicable.

4. Subducting Slabs and Arc Magmatism

4.1 Tomographic images

Figure 14 shows vertical cross-sections of P and S wave velocity (V_p, V_s) images under Hokkaido from the Kuril Trench to the Japan Sea coast (Wang and Zhao,

doi:10.5047/meep.2012.00101.0001

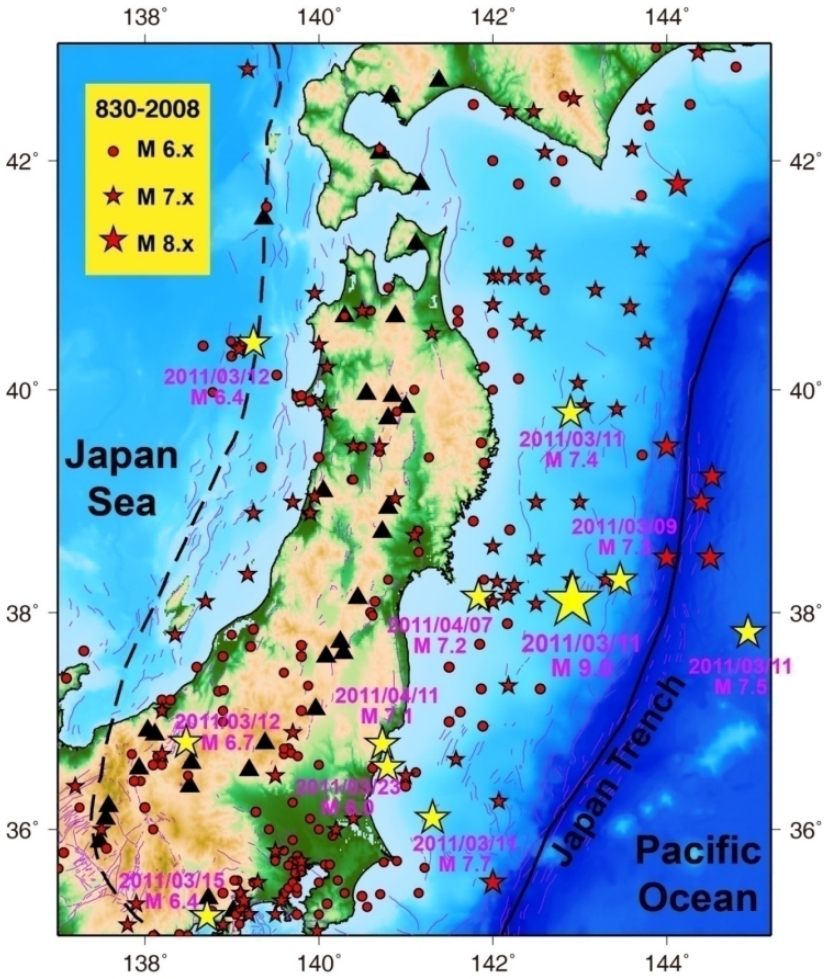

Fig. 22. Epicentral distribution of large earthquakes during the period 830 to 2008 (red dots and stars). The yellow stars show the large events that have occurred since March 2011. Black triangles denote the active arc volcanoes.

2005). The two profiles pass through three active volcanoes (Komagatake, Taisetsuzan, and Meakandake). The subducting Pacific slab is imaged clearly as a high-V zone with seismic velocities 4–6% higher than that of the average mantle. Intermediate-depth earthquakes occur actively in the subducting Pacific slab and they form a clear double seismic zone. Prominent low-V zones are visible in the crust and uppermost mantle beneath the active arc volcanoes, and they extend to a depth of 150–200 km in the central portion of the mantle wedge. The mantle-wedge low-V zone is roughly parallel with the subducting slab, and is close to, or connected with, the slab at some depth, e.g., at about 90-km depth in Fig. 14(b).

Similar seismic images of the crust and upper mantle are obtained under the NE Japan arc (Figs. 15, 16). The double-planed deep seismic zone in the Pacific slab under NE Japan is more clearly visible than that under Hokkaido. Normal crustal earthquakes occur in the upper crust down to about 20-km depths, but some earthquakes occur in the lower crust and uppermost mantle around the Moho discontinuity and they usually exhibit a lower frequency than that of the normal crustal earthquakes (Figs. 11, 15, 16). It is considered that these low-frequency microearthquakes are associated with the magmatic activity under the active arc volcanoes (Hasegawa and Yamamoto, 1994; Hasegawa and Zhao, 1994). The low-V zones also show high values of Poisson's ratio (Wang and Zhao, 2005). Figure 17 shows vertical cross-sections of V_p and V_s images along the volcanic front and the second volcanic front in NE Japan. Continuous low-V zones are visible in the central part of the mantle wedge under the second volcanic front along the Japan Sea coast, whereas intermittent low-V zones exist under each group of active volcanoes along the volcanic front.

Beneath the Kanto district, the Philippine Sea (PHS) slab is subducting from the Sagami trough and the Suruga trough (Ishida and Hasemi, 1988; Wang and Zhao, 2006a). The subducting Pacific slab is located beneath the PHS slab and the two slabs are interacting with each other (Ishida, 1992). This scenario is clearly imaged by seismic tomography (Fig. 18(a, b)). Subcrustal earthquakes are very abundant in the Kanto region because they occur in both the Pacific and PHS slabs. The Pacific slab is old (110–130 Ma) and so it is thick (about 85 km), whereas the PHS slab is young (20–30 Ma) and so it is thin (20–30 km) (Seno *et al*., 1993, 2001; Zhao *et al*., 2000b), as is clearly visible in the tomographic images (Fig. 18). A low-V layer exists atop the PHS slab (Fig. 18(a,

doi:10.5047/meep.2012.00101.0001

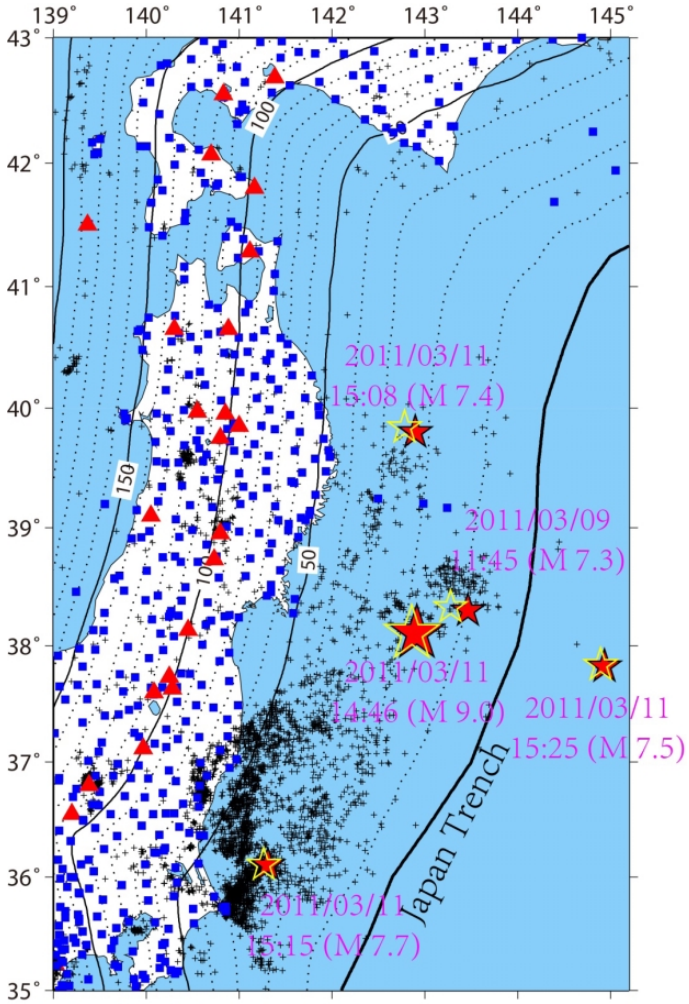

Fig. 23. Map showing the relocated epicentral locations (red stars) of the great 2011 Tohoku-oki earthquake (M_w 9.0) on 11 March, 2011, and its largest foreshock (M_{JMA} 7.3) on 9 March, 2011, and major aftershocks ($M_{JMA} > 7.0$) on 11 March, 2011. The open yellow stars show the epicenters determined by the Kiban seismic network (JMA Unified Catalogue). The blue squares show the Kiban network stations used to relocate the earthquakes. The red triangles show the active arc volcanoes. The solid and dotted contour lines show the depths to the upper boundary of the subducting Pacific slab. The thick solid line denotes the Japan Trench. The cross symbols show the relocated epicenters of the seismicity during 9–27 March, 2011. (From Zhao *et al*., 2011b.)

b)), which may represent the subducting oceanic crust and slab dehydration. The hypocenter of the 1923 Kanto earthquake (M 7.9) is located at the upper boundary of the PHS slab and was caused by underthrusting of the PHS slab beneath the overriding continental plate. In Hokkaido and NE Japan, the subducting Pacific slab is located approximately 100 km beneath the volcanic front (Figs. 14–16). However, under the Fuji and Hakone volcanoes in Kanto, the upper boundary of the Pacific slab is about 150-km deep (Fig. 18(a)). This westward displacement of the volcanic front is caused by the subduction of the PHS slab under Kanto (Iwamori, 2000). However, the mantle-wedge low-V zone is connected with the Pacific slab at about 100-km depth, and it seems that the magma ascending path is deflected toward the west by the PHS slab.

In the Izu-Bonin region south of Kanto, the Pacific plate is subducting beneath the PHS plate. The active arc volcanoes (Niijima, Miyakejima, etc.) are located about 110–120 km above the Pacific slab, and the mantle-wedge low-V zone is connected with the Pacific slab at that depth (Fig. 18(c, d)). However, the low-V zone is not straight but shows a winding image, suggesting that the upwelling magma is deflected by corner flow in the mantle wedge, just like a mantle plume under a hotspot volcano being deflected by the mantle convection (Zhao, 2001c, 2007; Zhao *et al*., 2006; Gupta *et al*., 2009a).

Beneath Kyushu Island, the PHS slab is subducting with a dipping angle of about 45 degrees, and several active volcanoes exist there (Fig. 19). A clear volcanic front is also formed. Low-V anomalies are clearly visible in the crust and mantle wedge under the volcanic front in Kyushu (Figs. 19, 21), similar to the images under the active volcanoes above the subducting Pacific slab. Unzen volcano is located about 100 km west of the volcanic front in Kyushu (Fig. 19). It is a very active volcano, and a recent eruption occurred in 1991–1995 killing tens of people. A prominent dipping low-V zone is visible in the crust and mantle wedge under Unzen, which connects Unzen at the surface and the PHS slab

doi:10.5047/meep.2012.00101.0001

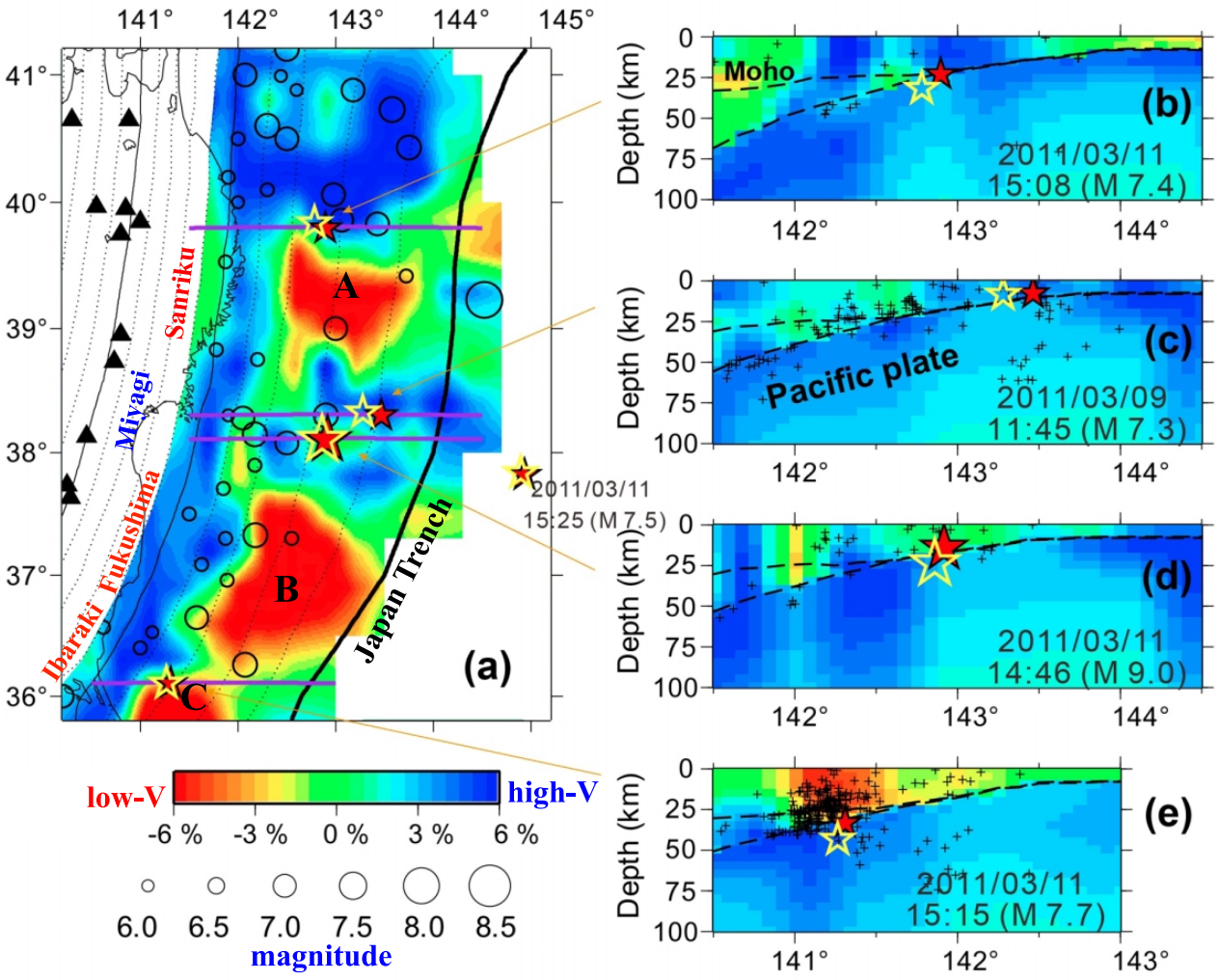

Fig. 24. (a) P-wave tomographic image in the megathrust zone directly above the upper boundary of the subducting Pacific slab. Red and blue show low and high velocities, respectively. The velocity perturbation (in %) scale is shown at the bottom. Three low-velocity anomalies exist (A) off Sanriku, (B) off Fukushima, and (C) off Ibaraki. Black triangles denote the active arc volcanoes. The open circles denote the large earthquakes ($M_{\rm JMA} \geq 6.0$) from 1900 to 2008, most of which were interplate earthquakes (see text for details). (b–e) East-west vertical cross-sections of P-wave tomography passing through the epicenters of the 2011 Tohoku-oki mainshock (d), foreshock (c), and two aftershocks (b, e). The color scale is the same as in (a). The two dashed lines in each cross-section represent the Moho discontinuity and the upper boundary of the subducting Pacific plate. The magnitude and origin time of the large earthquakes ($M_{\rm JMA} > 7.0$) are shown in each of the cross-sections. Cross symbols denote the relocated earthquakes during 9–27 March, 2011, within a 10-km width to each profile. (From Zhao *et al*., 2011b.)

at about 100-km depth, indicating that the Unzen magmatism is also related to the dehydration process of the PHS slab at about 100-km depth, though the volcano is located at the back-arc side (Fig. 19).

Figure 20 shows a high-resolution crustal tomography under Unzen volcano (Zhao *et al*., 2000b, 2002). A cone-shaped low-V zone is visible in the crust under Unzen, which may represent high-temperature anomalies containing a magma reservoir. The cutoff-depth of crustal seismicity shallows toward the crater of the volcano, which is in good agreement with the upper boundary of the low-V zone (Fig. 20). These features indicate a thinning of the brittle seismogenic layer beneath the volcano. Earlier studies suggested that there are large lateral variations in the temperature of the crust and in the cutoff-depth of crustal seismicity in volcanic areas (e.g., Ito, 1993; Zhao *et al*., 2000a, 2002). Figure 20 shows a nice example of these features.

Compared with the forearc areas above the Pacific slab, the forearc areas above the PHS slab exhibit more significant low-V anomalies (Figs. 19, 21). The low-V zones may reflect the subducting oceanic crust atop the PHS slab and the forearc mantle serpentinization resulting from fluids from the PHS slab dehydration (Zhao *et al*., 2000b; Wang and Zhao, 2006b; Xia *et al*., 2008a). The PHS slab is much younger and warmer than the Pacific slab and so its dehydration can take place at a shallow depth under the forearc area.

In Shikoku Island and the Chugoku District in western Honshu, there are no volcanoes as active as those in Hokkaido, NE Japan and Kyushu (Fig. 2). Only a few Quaternary volcanoes exist along the coastline of the Japan Sea, though some of them are potentially active (Kiyosugi *et al*., 2010; Zhao *et al*., 2011a). The reason for the absence of

doi:10.5047/meep.2012.00101.0001

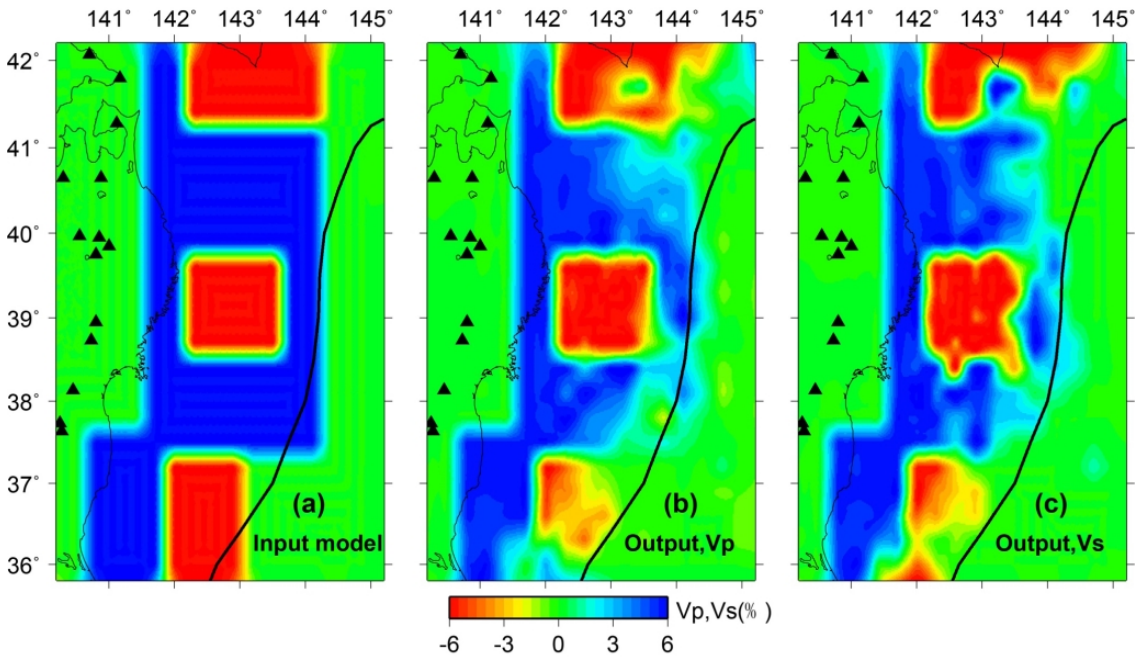

Fig. 25. Input model (a) and inverted results (b–c) of a synthetic test for the interplate thrust zone along the upper boundary of the subducting Pacific plate (from the online supporting material of Huang *et al*., 2011a). The velocity perturbation scale is shown at the bottom. Blue and red colors denote fast and slow velocities, respectively. The curved lines and triangles denote the Japan Trench and active arc volcanoes, respectively. (Reprinted from *Geophys. J. Int*., *184*, Huang, Z., D. Zhao, and L. Wang, Seismic heterogeneity and anisotropy of the Honshu arc from the Japan Trench to the Japan Sea, 1428–1444, Copyright 2011, with permission from John Wiley & Sons.)

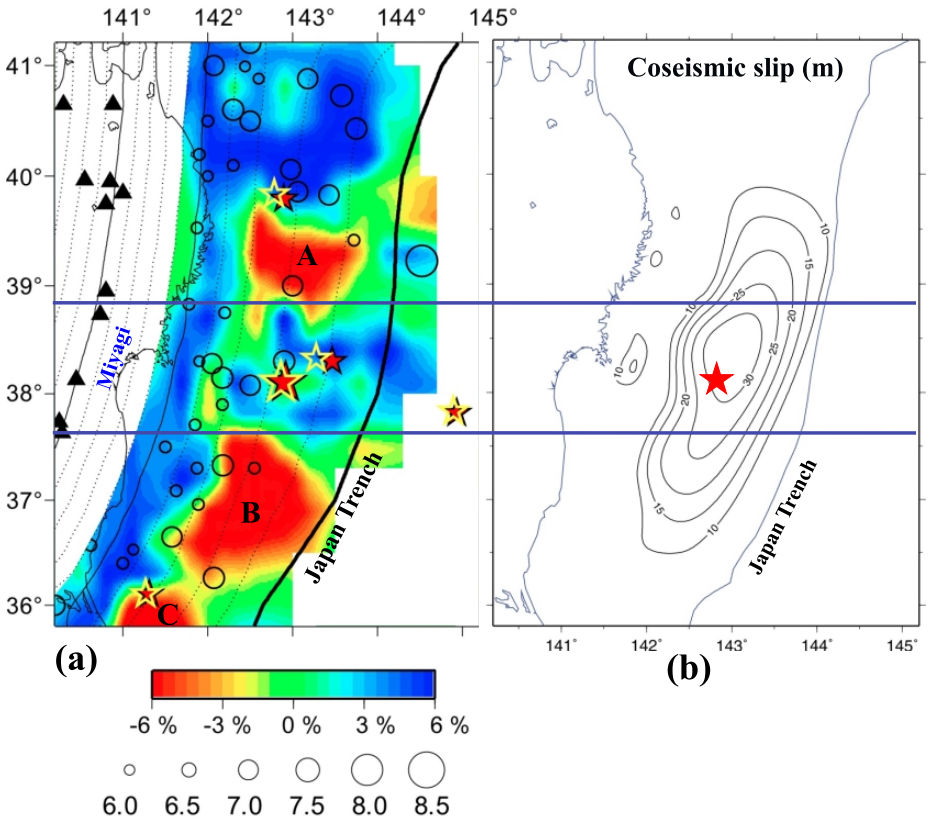

Fig. 26. Comparison of (a) *P*-wave tomography in the megathrust zone (the same as Fig. 24(a)) with (b) the coseismic slip distribution of the 2011 Tohoku-oki earthquake (M_w 9.0, red star) estimated from GPS observations (contour lines with an interval of 5 m) (Iinuma *et al*., 2011). The two blue lines show the north-south range of the off-Miyagi high-velocity zone in (a), where large coseismic slips (>25 m) took place (b). (From Zhao *et al*., 2011b.)

doi:10.5047/meep.2012.00101.0001

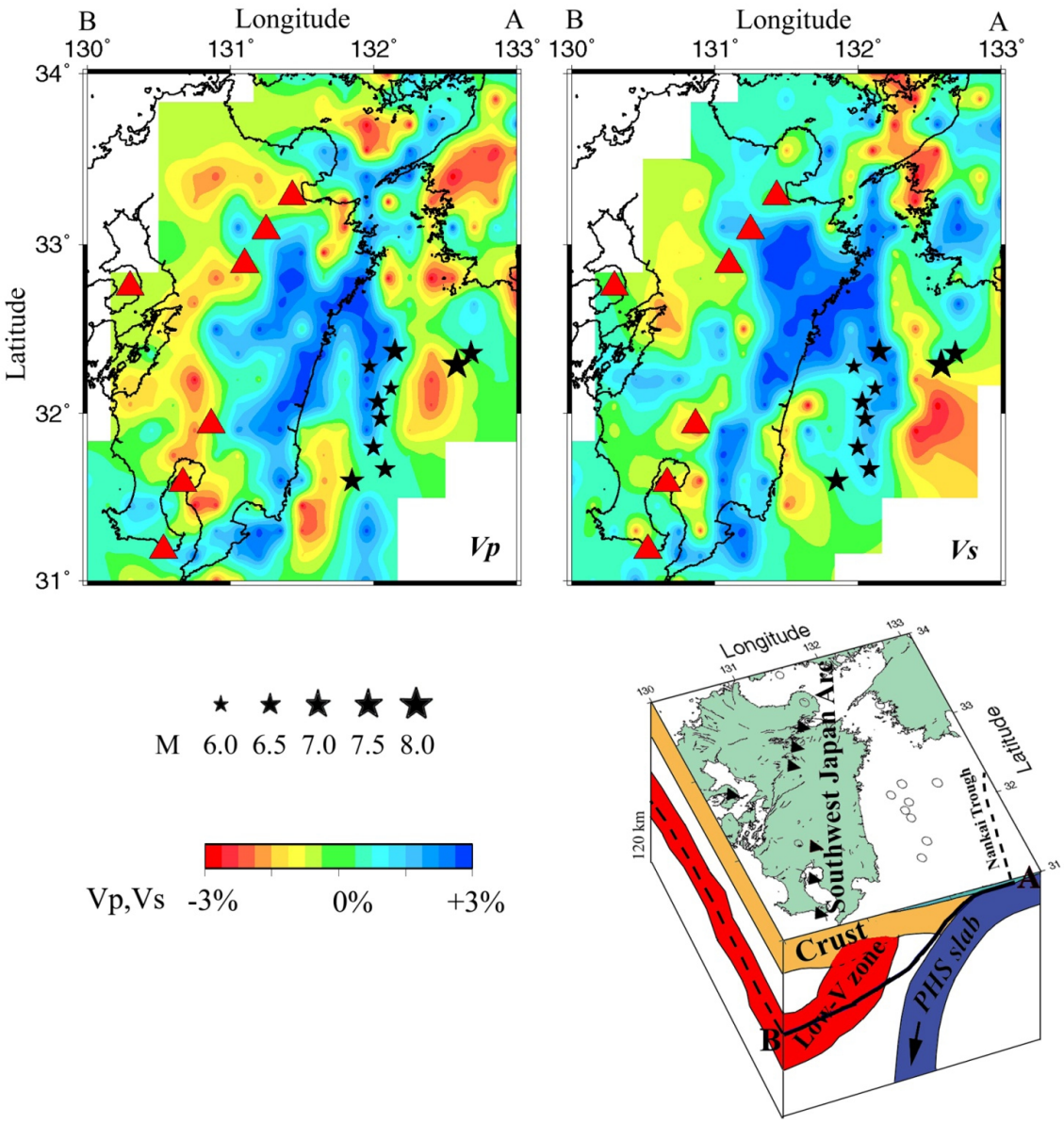

Fig. 27. Map views of *P* and *S* wave tomography along the profile as shown on the inset map. Beneath the forearc area under the Pacific Ocean, the profile is along the upper boundary of the subducting Philippine Sea plate, while under the Kyushu land the profile passes through the central part of the mantle wedge. Red and blue colors denote low and high velocities, respectively. The velocity perturbation scale is shown at the bottom. Red triangles show the active arc volcanoes. The black stars show the large interplate earthquakes during the period 1923 to 1998. (Reprinted from *Phys. Earth Planet. Inter.*, *157*, Wang, Z., and D. Zhao, Vp and Vs tomography of Kyushu, Japan: New insight into arc magmatism and forearc seismotectonics, 269–285, Copyright 2006, with permission from Elsevier.)

active volcanoes in the Shikoku and Chugoku areas seems to be that the PHS slab has a very small dipping angle under those areas and the slab is located directly beneath the crust under Shikoku. The PHS slab has a complicated geometry in and around the Kii Peninsula and it is still unclear whether the slab is continuous or disconnected (e.g., Ide *et al*., 2010). Thus, the mantle wedge above the PHS slab is not well developed enough to form a corner flow that can bring heat from the deeper mantle to generate arc magma, as described in the following section.

4.2 Slab dehydration and mantle wedge convection

Many geochemical, geophysical and numerical modeling studies have suggested that a significant amount of water is expelled from a subducting slab and contributes to melt generation in the hot portion of the mantle wedge (e.g., Tatsumi, 1989; Peacock, 1990; Zhao *et al*., 1992b; Hasegawa and Zhao, 1994; Iwamori and Zhao, 2000; Scambelluri and Philippot, 2001; Stern, 2002; Gerya, 2011). The introduction of water lowers the melting temperature of rocks, which can produce significant amounts of melt even in a relatively cool environment above a subducting slab. Water transport and melting have been often implemented in numerical models

doi:10.5047/meep.2012.00101.0001

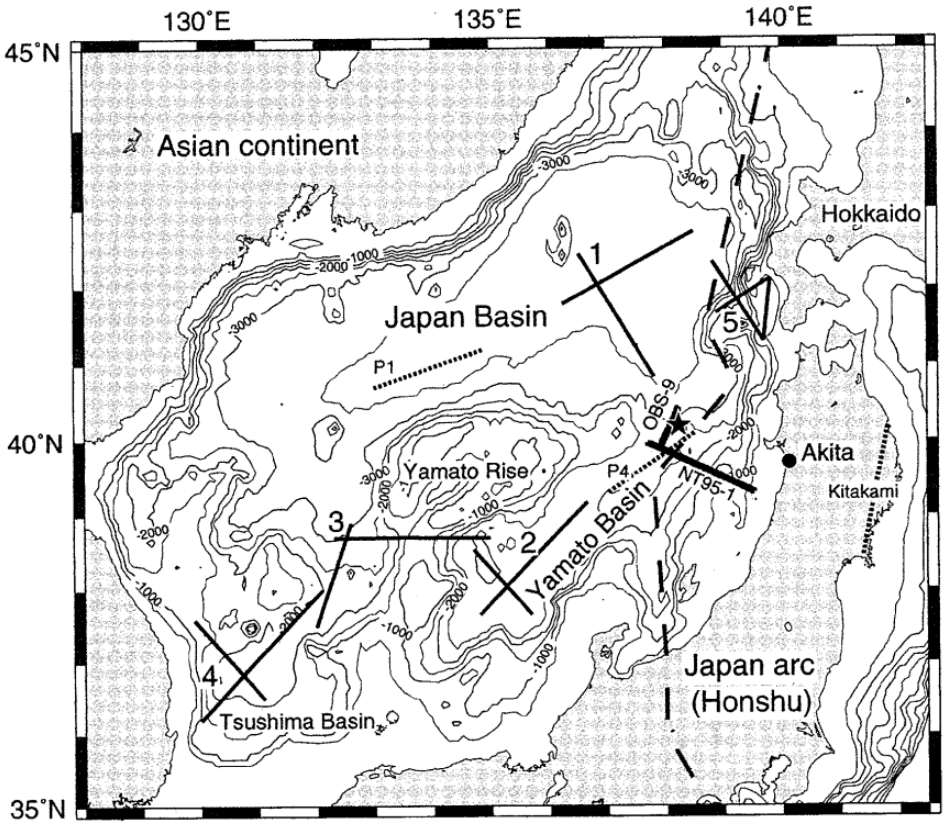

Fig. 28. Bathymetry and tectonic units in the Japan Sea. The solid and dotted straight lines show the profiles of seismic explosion experiments conducted by Japanese researchers. The bold dashed line shows the estimated Amur-Okhotsk plate boundary. (Reprinted from *Tectonophysics*, *306*, Nishizawa, A., and A. Asada, Deep crustal structure off Akita, eastern margin of the Japan Sea, deduced from ocean bottom seismographic measurements, 199–216, Copyright 1999, with permission from Elsevier.)

of subduction using kinematic, porous flow and water diffusion approaches (see a recent review by Gerya, 2011). van Keken *et al*. (2011) used a recent global compilation of the thermal structure of subduction zones to predict the metamorphic facies and H_2O content of subducting slabs. Their results show that mineralogically-bound water can pass efficiently through old and fast subduction zones such as in the Western Pacific, whereas hot subduction zones such as SW Japan and Cascadia see a nearly complete dehydration of the subducting slab. The top of the slab is sufficiently hot in all subduction zones, so that the upper crust (including sediments and volcanic rocks) is predicted to dehydrate significantly. The degree and depth of dehydration in the deeper crust and uppermost mantle are highly diverse and depend strongly on composition (gabbro versus peridotite) and local pressure and temperature conditions. The upper mantle dehydrates at intermediate depths in all but the coldest subduction zones. On average, about $1/3$ of the bound H_2O subducted globally in slabs reaches a depth of 240 km, carried principally, and roughly equally, in the gabbro and peridotite sections. The predicted global flux of H_2O to the deep mantle is smaller than previous estimates but still amounts to about one ocean mass over the age of the Earth. At this rate, the overall mantle H_2O content increases by 0.037 wt% (370 ppm) over the age of the Earth, which is qualitatively consistent with inferred H_2O concentrations in the Earth's mantle, assuming that secular cooling of the Earth has increased the efficiency of the volatile recycling over time (van Keken *et al*., 2011).

On the other hand, solid-state mantle wedge flow in subduction zones plays an important role in controlling the thermal structure and geodynamics of subduction zones (e.g., Wada *et al*., 2011). As the cold oceanic lithosphere subducts, it cools the overriding mantle wedge. The wedge flow, however, replenishes the wedge with hot mantle material, providing a thermal condition necessary for melt generation and arc magmatism. The hot mantle also heats up the top of the subducting slab and promotes slab dehydration, which is important to such processes as intraslab seismicity and volatile recycling (e.g., van Keken *et al*., 2011; Wada *et al*., 2011).

The low-V zones in the mantle wedge revealed by seismic tomography are caused by a combination of aqueous fluids from the slab dehydration and corner flow in the mantle wedge. Low-V zones are also visible in the crust and uppermost mantle under the forearc regions, which reflect the shallow dehydration of the subducting slabs. Low-V and high Poisson's ratio (high-PR) zones in the mantle wedge are visible in all the vertical cross-sections passing through active arc volcanoes (Figs. 14–19, 21). However, the amplitude of the anomalies seems larger in the cross-sections passing through the active arc volcanoes, while it is smaller in the cross-sections without volcanoes (Zhao *et al*., 2009a; Huang

doi:10.5047/meep.2012.00101.0001

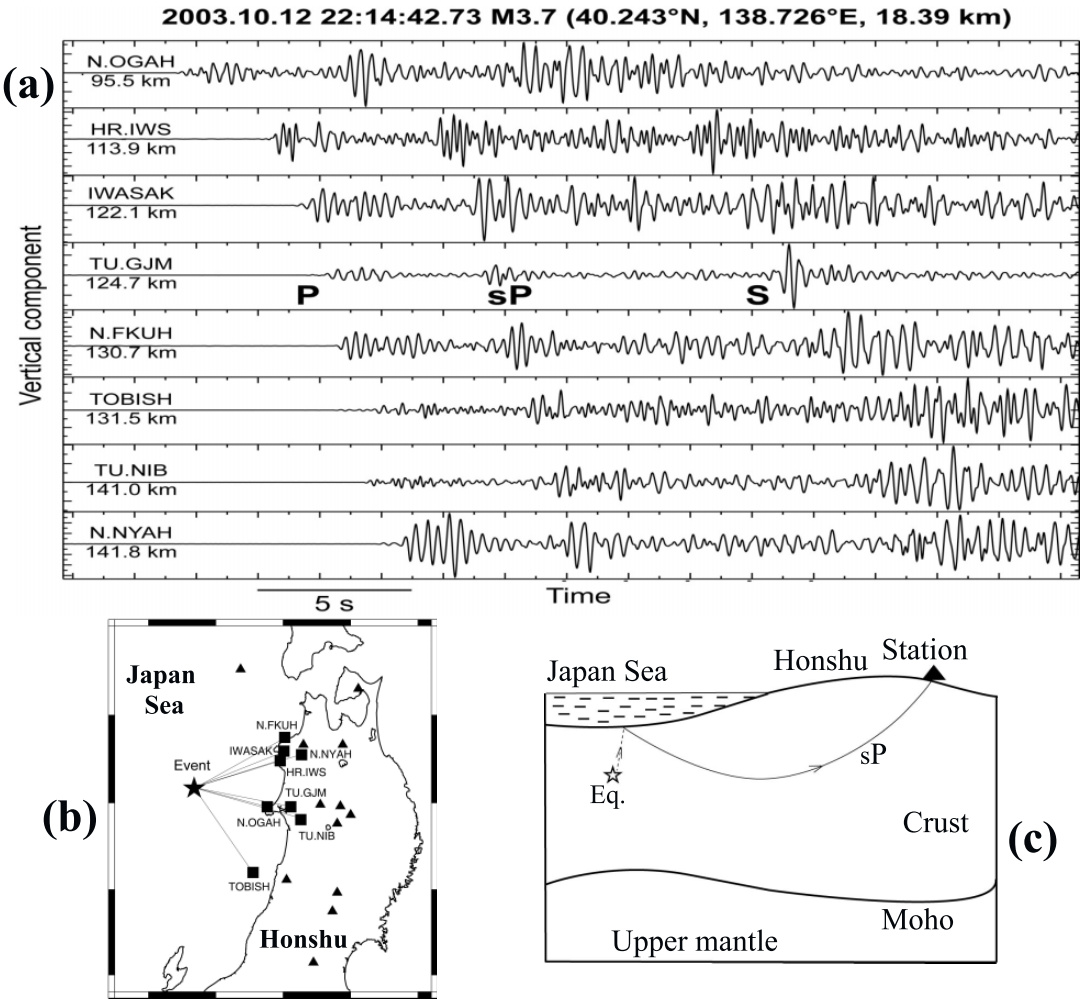

Fig. 29. (a) An example of vertical-component seismograms of a crustal earthquake that occurred beneath the Japan Sea. Hypocenter parameters of the earthquake are shown above the seismograms. The station codes and epicenter distances are shown on the left. Clear *sP* depth phases are visible at 5–6 s after the first *P*-wave arrivals. (b) A map showing the locations of the epicenter and seismic stations in (a). (c) A schematic diagram showing the ray path of the *sP* depth phase. (Reprinted from *Phys. Earth Planet. Inter.*, *188*, Zhao, D., Z. Huang, N. Umino, A. Hasegawa, and T. Yoshida, Seismic imaging of the Amur-Okhotsk plate boundary zone in the Japan Sea, 82–95, Copyright 2011, with permission from Elsevier.)

et al., 2011a). In addition, low-frequency microearthquakes occurring in the lower crust and uppermost mantle, which are good indicators of magmatic activity, are visible mainly in the cross-sections passing through the active volcanoes (Figs. 15–17). These features suggest along-arc variations of the low-V and high-*PR* zones in the mantle wedge, consistent with the hot-finger model proposed by Tamura *et al*. (2002). Because the low-V and high-*PR* zones are generally considered to reflect the magma-related hot and wet anomalies caused by slab dehydration and corner flow in the mantle wedge, the along-arc variations of the low-V and high-*PR* zones indicate a spatial variation in the amount of fluids released from the slab dehydration, as well as in the strength of mantle-wedge corner flow along the arc. It was proposed that the along-arc variation of the velocity anomalies under NE Japan is due to small-scale convection occurring in the mantle wedge, similar to that under the cooling oceanic lithosphere (Honda *et al*., 2002; Honda and Saito, 2003). Such a small-scale convection can take place because the viscosity in the mantle wedge can be reduced significantly by the water released from the subducting slab. Another possibility for the along-arc variation in seismic property is the diapiric ascent of metasomatized mantle (e.g., Hall and Kincaid, 2001; Gerya and Yuen, 2003). Several recent numerical-modeling studies have dealt explicitly with the seismic signature of diapirs in the mantle wedge (e.g., Gerya *et al*., 2006; Gorczyk *et al*., 2006; Gerya, 2011). The seismic structure predicted by these modeling studies is generally consistent with that observed by tomographic studies.

5. Forearc: Mechanism of Megathrust Earthquakes

One of the main purposes of local tomographic imaging is to detect any structural heterogeneity that may be related to seismogenesis, so as to understand the generating mechanism of large and small earthquakes. Most earthquakes in a subduction zone occur in and around the megathrust zone under the forearc region, where the subducting oceanic plate interacts with the overlying continental plate. Thus, once we determine the tomographic image under the forearc region,

doi:10.5047/meep.2012.00101.0001

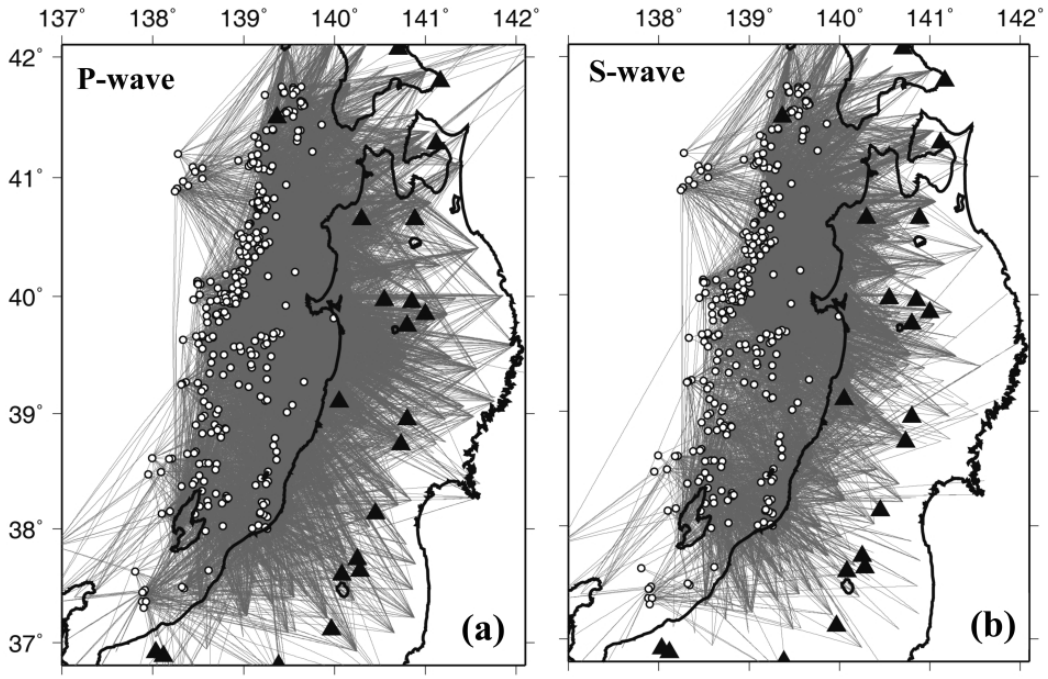

Fig. 30. Distribution of (a) *P*-wave and (b) *S*-wave ray paths (gray lines) from the 361 crustal earthquakes (open circles) in the eastern margin of the Japan Sea. Black triangles denote the active volcanoes. (Reprinted from *Phys. Earth Planet. Inter.*, *188*, Zhao, D., Z. Huang, N. Umino, A. Hasegawa, and T. Yoshida, Seismic imaging of the Amur-Okhotsk plate boundary zone in the Japan Sea, 82–95, Copyright 2011, with permission from Elsevier.)

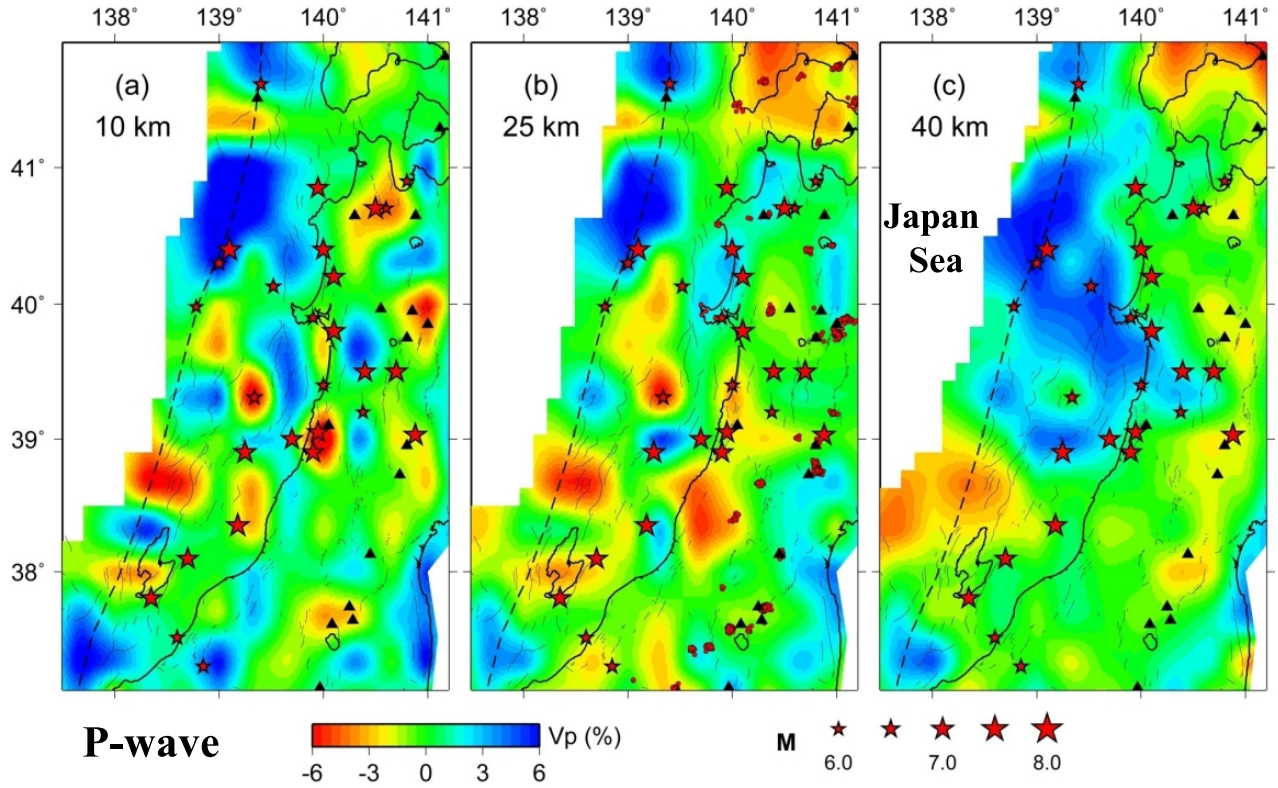

Fig. 31. *P*-wave velocity images at depths of (a) 10, (b) 25, and (c) 40 km. Red and blue colors denote low and high velocities, respectively. Red stars denote large crustal earthquakes ($M \geq 6.0$) that occurred during the period 830 to 2010 (Utsu, 1982; Usami, 2003). Black triangles denote active arc volcanoes. Low-frequency microearthquakes within 5 km of each depth are shown by red dots. The velocity perturbation scale and the earthquake magnitude scale are shown at the bottom. The dashed lines show the Amur-Okhotsk plate boundary. (Reprinted from *Phys. Earth Planet. Inter.*, *188*, Zhao, D., Z. Huang, N. Umino, A. Hasegawa, and T. Yoshida, Seismic imaging of the Amur-Okhotsk plate boundary zone in the Japan Sea, 82–95, Copyright 2011, with permission from Elsevier.)

doi:10.5047/meep.2012.00101.0001

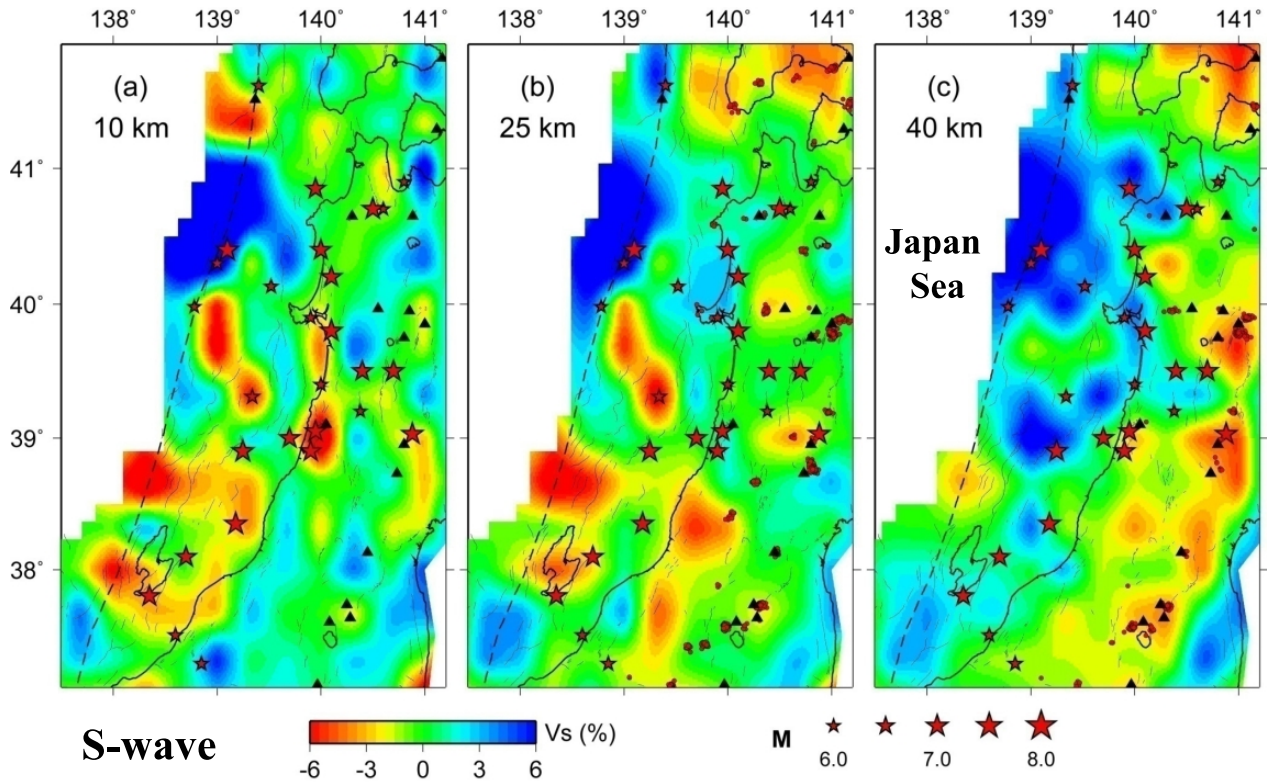

Fig. 32. The same as Fig. 31 but for *S*-wave velocity images. (Reprinted from *Phys. Earth Planet. Inter.*, *188*, Zhao, D., Z. Huang, N. Umino, A. Hasegawa, and T. Yoshida, Seismic imaging of the Amur-Okhotsk plate boundary zone in the Japan Sea, 82–95, Copyright 2011, with permission from Elsevier.)

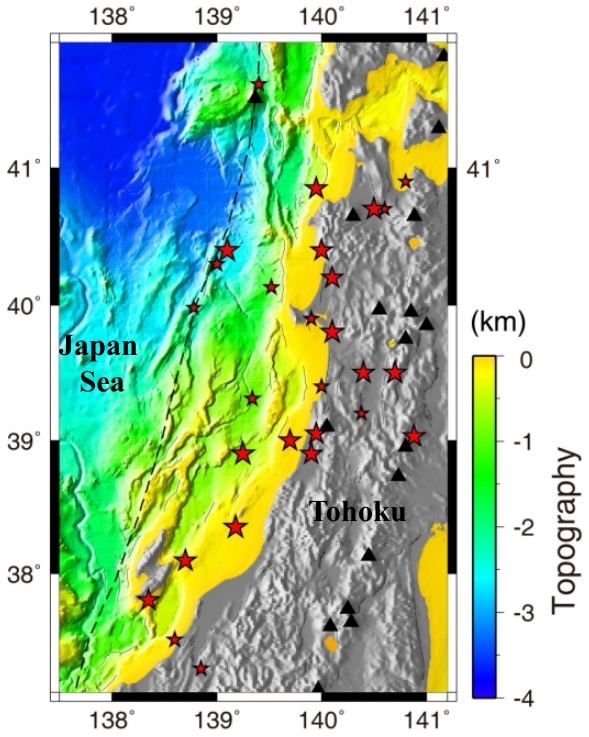

Fig. 33. Surface topography of NE Japan and the eastern margin of the Japan Sea. Blue and yellow denote the deeper and shallower seafloors, respectively. The color scale is shown on the right. Black triangles denote the active arc volcanoes. The dashed line indicates the estimated border of the Amur plate. Red stars denote the large historic earthquakes (the same as those in Fig. 31). (Reprinted from *Phys. Earth Planet. Inter.*, *188*, Zhao, D., Z. Huang, N. Umino, A. Hasegawa, and T. Yoshida, Seismic imaging of the Amur-Okhotsk plate boundary zone in the Japan Sea, 82–95, Copyright 2011, with permission from Elsevier.)

doi:10.5047/meep.2012.00101.0001

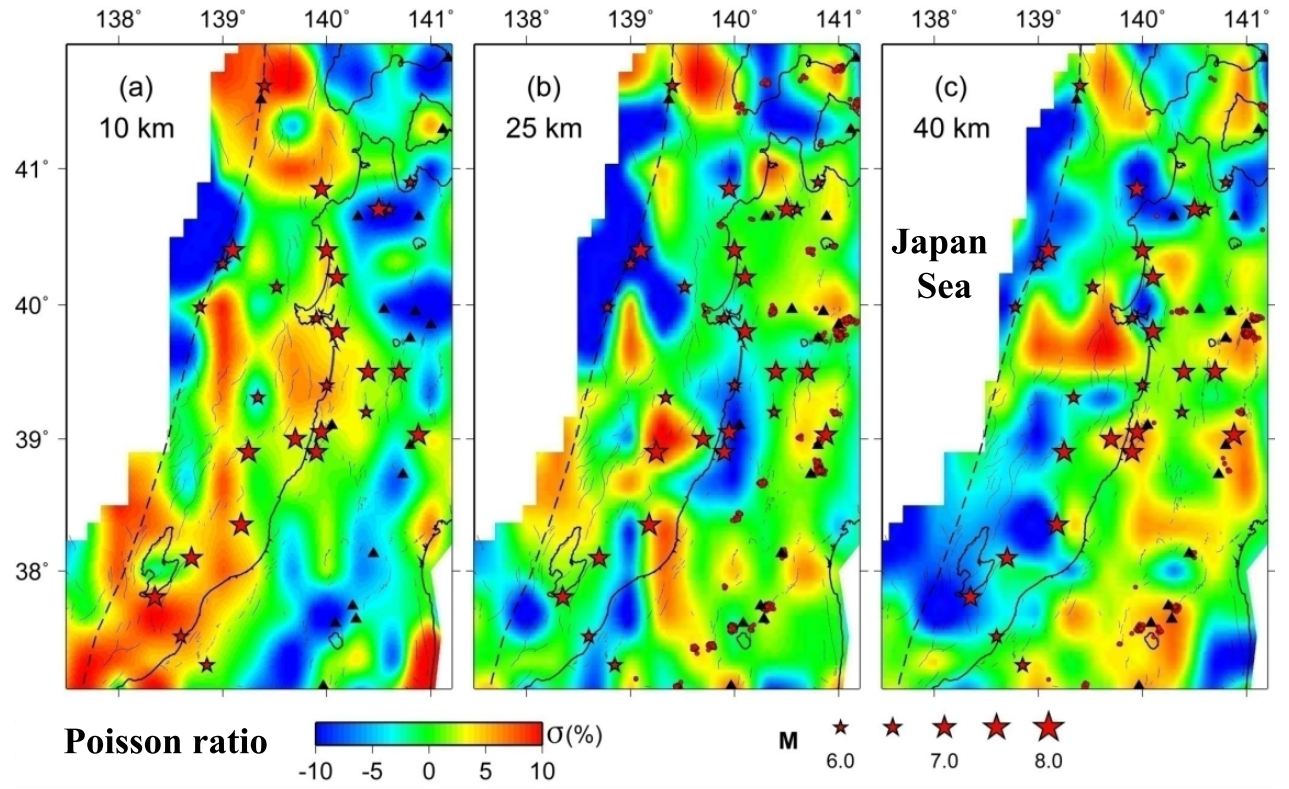

Fig. 34. The same as Fig. 31 but for Poisson's ratio images. (Reprinted from *Phys. Earth Planet. Inter.*, *188*, Zhao, D., Z. Huang, N. Umino, A. Hasegawa, and T. Yoshida, Seismic imaging of the Amur-Okhotsk plate boundary zone in the Japan Sea, 82–95, Copyright 2011, with permission from Elsevier.)

we can exploit the 3-D velocity model to understand the seismogenesis in the interplate megathrust zone.

The most recent and striking example of large subduction-zone earthquakes is the great Tohoku-oki earthquake (M_w 9.0) that occurred at 14:46 local time (05:46 UTC) on 11 March, 2011, under the NE Japan forearc (Figs. 22, 23). A large foreshock of this earthquake took place at 11:45 local time on 9 March, 2011, with a magnitude (M_{JMA}) of 7.3, as determined by JMA (www.jma.go.jp). Following the Tohoku-oki mainshock, and on the same day, three aftershocks occurred with $M_{JMA} \geq 7.4$, and many smaller aftershocks were recorded and located by the dense seismic network installed on the Japan Islands (Fig. 23). Soon after the occurrence of these earthquakes, JMA, the United States Geological Survey (USGS) (earthquake.usgs.gov), and several other research agencies, published hypocentral parameters for these earthquakes. The locations were similar, but significant differences were apparent. For example, with respect to the Tohoku-oki mainshock, the JMA location was: (38.103N, 142.861E, 24 km), whereas the USGS location was: (38.322N, 142.369E, 32.0 km). The difference between them is over 50 km and was caused by several factors, such as the differences in the arrival-time data sets and the velocity models used for the earthquake location. The JMA hypocenters are determined using the seismic stations on the Japan Islands and the JMA one-dimensional (1-D) velocity model (Ueno *et al.*, 2002), whereas the USGS hypocenters are determined with globally-distributed seismic stations and a global 1-D velocity model (Kennett and Engdahl, 1991). The hypocentral distribution of earthquakes in the NE Japan forearc under the Pacific Ocean has been investigated by deploying ocean-bottom-seismometer (OBS) stations (e.g., Hino *et al.*, 2000, 2006; Miura *et al.*, 2003), and using *sP* depth phases (Fig. 12) (e.g., Umino *et al.*, 1995; Mishra *et al.*, 2003; Wang and Zhao, 2005; Gamage *et al.*, 2009; Zhao *et al.*, 2009a).

Zhao *et al.* (2011b) relocated the great Tohoku-oki earthquake and its 339 foreshocks and 5,609 aftershocks during 9–27 March, 2011, using the 3-D *P* and *S* wave velocity model of Huang *et al.* (2011a) and the high-quality arrival-time data recorded by the seismic stations (Okada *et al.*, 2004) in NE Japan (Fig. 23). Note that six OBS stations located in the Pacific Ocean were used, which provided valuable constraints on the locations of the suboceanic events. The hypocentral parameters were determined for each earthquake by inverting the *P* and *S* wave arrival-time data iteratively using a least-squares method (Zhao *et al.*, 1992b, 2009a). A 3-D ray-tracing technique (Zhao *et al.*, 1992b) was used to calculate accurate travel times and ray paths in the 3-D velocity model (Huang *et al.*, 2011a). The changes in the hypocenters before and after relocation are smaller (<5 km) for events beneath land, whereas the changes become larger for events under the Pacific Ocean, being 5–30 km, in particular, for events near the Japan Trench (Zhao *et al.*, 2011b). The relocated hypocenters of the 4 biggest events ($M_{JMA} \geq 7.3$) are all located at, or very close to, the upper boundary of the subducting Pacific slab (Fig. 24(b–e)), which is consistent with their thrust focal mechanism (JMA,

doi:10.5047/meep.2012.00101.0001

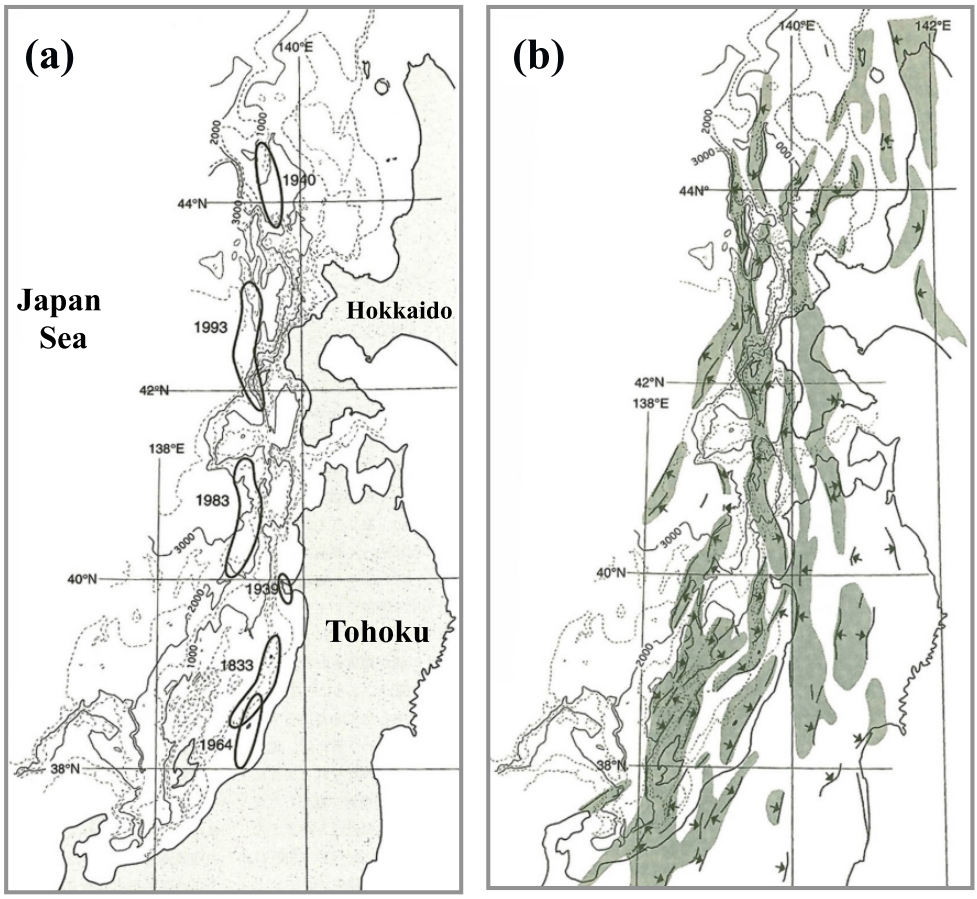

Fig. 35. (a) The solid contour lines show the rupture areas of large earthquakes that occurred in the eastern margin of the Japan Sea. The thin dotted lines show the bathymetry of the Japan Sea. (b) Distribution of the zones with high strain rates (grey colors) in the eastern margin of the Japan Sea estimated from the anticline structures. The solid lines show the active reverse faults. The arrows show the moving direction of the hanging wall of an active fault. (From Okamura, 2002.)

www.jma.go.jp; Koper *et al*., 2011; Lay *et al*., 2011; Shao *et al*., 2011). For the 5 biggest events (Fig. 24), their seismograms, recorded by the High-Sensitivity Seismic Network, were examined and an effort was made to search for *sP* depth phases, but this was unsuccessful because the seismograms were very complicated, possibly due to the complex rupture processes (Zhao *et al*., 2011b).

Significant velocity variations are noticeable in the megathrust zone under the NE Japan forearc (Huang *et al*., 2011a; Zhao *et al*., 2011b) (Fig. 24(a)). Three low-V anomalies exist off Sanriku, off Fukushima and off Ibaraki (Fig. 24(a)). Detailed resolution tests indicate that the main features of the tomographic image are reliable (Huang *et al*., 2011a) (e.g., Fig. 25). There is a correlation between the velocity variation and the distribution of large earthquakes ($M_{\rm JMA} \geq 6.0$) that have occurred from 1900 to 2008, most of which are considered to be interplate thrust-type earthquakes (Umino *et al*., 1990; Usami, 2003; Yamanaka and Kikuchi, 2004; Zhao *et al*., 2009a). These large earthquakes were located using the seismic network on the Japan Islands, and their epicentral locations are accurate to 10 km (Umino *et al*., 1990; Usami, 2003; Yamanaka and Kikuchi, 2004). Most of the large earthquakes are located in the high-V patches or at the boundary between the low-V and high-V zones, with only a few situated in the low-V patches (Fig. 24(a)).

The 2011 Tohoku-oki mainshock and its foreshock ($M_{\rm JMA}$ 7.3) on 9 March, 2011, are located in a significant high-V zone off Miyagi (Fig. 24(a)). The northern aftershock ($M_{\rm JMA}$ 7.4) that occurred at 15:08, 11 March, 2011, is located at the boundary between the off-Sanriku low-V zone and a high-V zone in the north. The southern aftershock ($M_{\rm JMA}$ 7.7) that took place at 15:15, 11 March, 2011, is located at the northern edge of the off-Ibaraki low-V zone. Such a pattern of hypocenter distribution for the 2011 Tohoku-oki earthquakes is quite consistent with that of the large earthquakes from 1900 to 2008 (Fig. 24(a)). The aftershock ($M_{\rm JMA}$ 7.5) that took place at 15:25, 11 March, 2011, is located east of the Japan Trench and so is considered to be an outer-rise earthquake (JMA, www.jma.go.jp; Kanamori, 1971; Lay *et al*., 2011) beyond the range of the 3-D velocity model.

The low-V patches in the megathrust zone (Fig. 24(a)) may contain subducted sediments and fluids associated with slab dehydration (Mishra *et al*., 2003; Huang *et al*., 2011a; Zhao *et al*., 2011b). Thus, the subducting Pacific plate and the over-riding continental plate may become weakly coupled, or even decoupled, in the low-V areas. Large-amplitude reflected waves from the slab boundary were de-

doi:10.5047/meep.2012.00101.0001

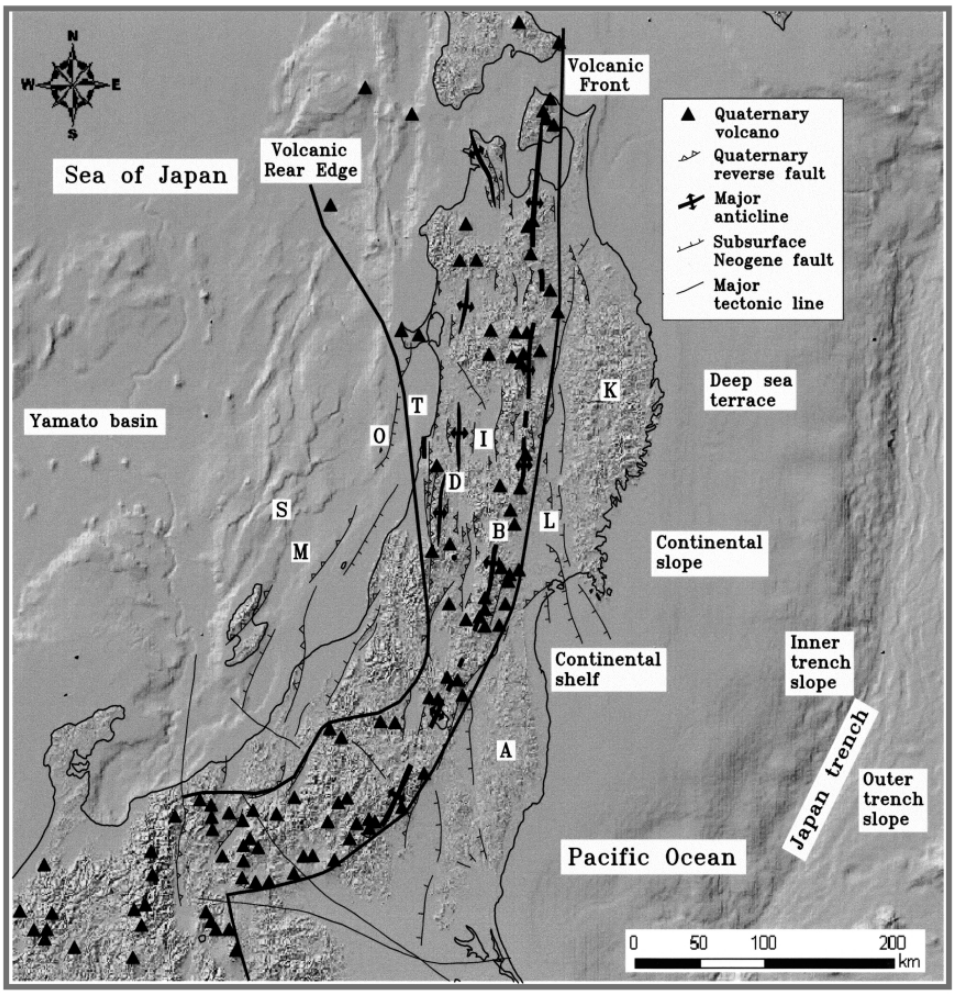

Fig. 36. Distribution of Quaternary volcanoes (triangles) and surface topography and tectonics in the NE Japan arc (Sato, 1994; Yoshida *et al*., 2005). The two solid bold lines show the western and eastern edges of the Quaternary volcanoes; the eastern edge is the present volcanic front, whereas the western edge is called the volcanic rear edge. Legends for the other symbols are shown in the upper-right box. A: Abukuma Mountains; B: Ou Backbone Range; D: Dewa Hills; I: Intermountain Basins; K: Kitakami Mountains; L: Kitakami River Valley; M: Mogami Trough; O: Oga-Awashima fault zone (also Tobishima-Funakawa uplift zone); S: Sado Ridges; T: Tobishima Basin (also Akita-Niigata Basin). (Reprinted from Yoshida *et al*., 2005, ©JAQUA.)

tected in a low-seismicity area under the forearc region off Sanriku (Fujie *et al*., 2002), as were some slow and ultra-slow thrust earthquakes (Heki *et al*., 1997; Kawasaki *et al*., 2001). Both the seismic reflectors and the slow thrust earthquakes are thought to be caused by fluids at the slab boundary (Kawasaki *et al*., 2001; Fujie *et al*., 2002), and they are all located in the off-Sanriku low-V zone (Fig. 24(a)).

In contrast, the high-V patches in the megathrust zone (Fig. 24(a)) may result from subducted oceanic ridges, seamounts, and other topographic highs, as well as compositional variations in the seafloor of the Pacific plate that become asperities (Kanamori, 1981; Yamanaka and Kikuchi, 2004) where the subducting Pacific plate and the over-riding continental plate are strongly coupled (Zhao *et al*., 2011b). Thus, tectonic stress tends to accumulate in these areas for a relatively long time during subduction, leading to the nucleation of large and great earthquakes in those high-V areas (Fig. 24(a)). The off-Miyagi high-V zone, where the Tohoku-oki mainshock and its largest foreshock occurred (Fig. 24(a)), corresponds to the area with large coseismic slip ($>$25 m) during the Tohoku-oki mainshock (e.g., Iinuma *et al*., 2011; Koper *et al*., 2011; Lay *et al*., 2011; Shao *et al*., 2011) (Fig. 26(b)). This indicates that the off-Miyagi high-V zone is a large asperity (or a cluster of asperities) in the megathrust zone that ruptured during the 2011 Tohoku-oki mainshock.

The distribution of structural heterogeneities in the megathrust zone, and its correlation with the distribution of large thrust earthquakes (Fig. 24(a)), suggest varying degrees of interplate seismic coupling from north to south in the NE Japan forearc, possibly controlling the nucleation of the large interplate earthquakes. The great 2011 Tohoku-oki earthquake sequence may be related to such a process. Differences in interplate seismic coupling could result from variations in the frictional behavior of materials (Pacheco *et al*., 1993; Heki *et al*., 1997; Kato and Hirasawa, 1997; Miura *et al*., 2003). The velocity variations revealed by the tomography of the megathrust zone (Fig. 24(a)) may be a manifestation of such variations in the frictional behavior. The tomographic result (Fig. 24(a)) is also in general agreement

doi:10.5047/meep.2012.00101.0001

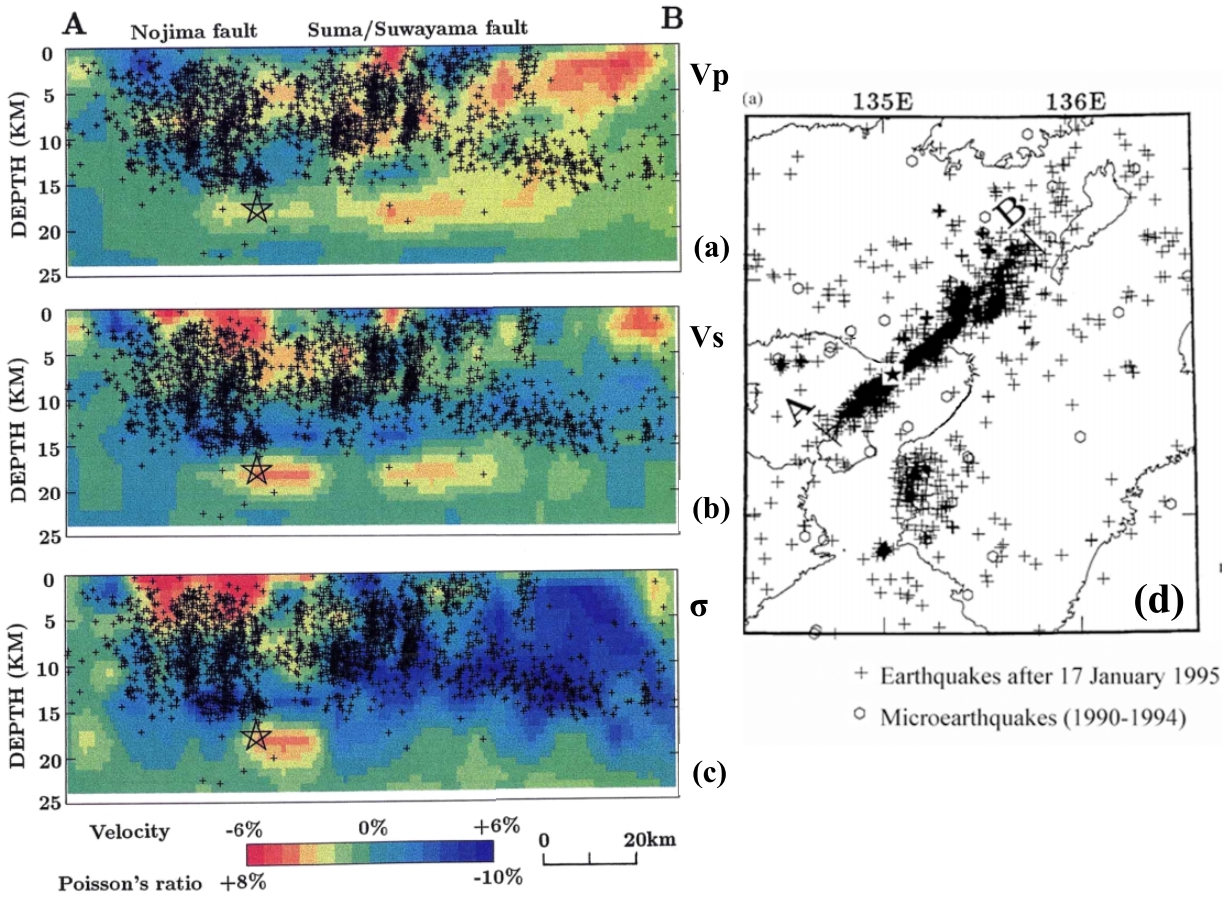

Fig. 37. Vertical cross-sections of (a) *P* and (b) *S* wave velocity and (c) Poisson's ratio images along profile A–B as shown in (d). Red color denotes low velocity and high Poisson's ratio, while blue color denotes high velocity and low Poisson's ratio. The color scale is shown below (c). The average value of Poisson's ratio is 0.25. The star symbol and crosses in (a–d) denote the mainshock and aftershocks of the Kobe earthquake (*M* 7.2) that occurred on January 17, 1995. The vertical exaggeration is 2:1. Circles and crosses in (d) denote the local crustal earthquakes that occurred during the period 1990 to 1994 and those that occurred after January 17, 1995, respectively. (Reprinted from *Science*, *274*, Zhao, D., H. Kanamori, H. Negishi, and D. Wiens, Tomography of the source area of the 1995 Kobe earthquake: Evidence for fluids at the hypocenter? 1891–1894, Copyright 1996, with permission from AAAS.)

with the results of multichannel seismic surveys which revealed along-arc variations of interplate sedimentary units at the Japan Trench (Tsuru *et al*., 2002).

Wang and Zhao (2006b) used *sP* depth phases to relocate the suboceanic events precisely, and then determined a high-resolution 3-D *P* and *S* wave velocity model under the forearc region (Hyuga-nada) of the Kyushu subduction zone (Fig. 27). Their result revealed the same pattern as that in the NE Japan forearc, viz., almost all the large interplate earthquakes are located in the high-V patches, or at the boundary between the low-V and high-V zones (Fig. 27), indicating that the nucleation of large interplate earthquakes is controlled by the structural heterogeneity in the megathrust zone.

6. Back-arc: Eastern Margin of Japan Sea

The Japan Sea is one of the marginal seas in the Northwest Pacific, and it formed as a back-arc basin due to subduction of the Pacific plate beneath the Japanese island arc (Nishizawa and Asada, 1999). The Japan Sea has a complex bathymetry and heterogeneous crustal structures (e.g., Nishisaka *et al*., 2001; Ohtake *et al*., 2002; Iwasaki and Sato, 2009) (Figs. 3, 28). The eastern margin of the Japan Sea (EMJS) has been subject to convergent tectonics since the Pliocene (Tamaki and Honza, 1985; Sato, 1994; Yoshida *et al*., 2005). The relative motion of 9–17 mm/year between the Amur and Okhotsk plates is accommodated in the EMJS as revealed by GPS observations (Heki *et al*., 1999; Jin *et al*., 2007; DeMets *et al*., 2010). Many small and large earthquakes occurred in the EMJS (Fig. 4), and the rupture zones of large earthquakes are generally oriented in the north-south direction (e.g., Satake, 1986; Sato *et al*., 1986; Tanioka *et al*., 1995), which are considered to be associated with the formation of a nascent plate boundary (Kobayashi, 1983; Nakamura, 1983) separating the Amur plate from the Okhotsk plate. This nascent plate-boundary proposal has been demonstrated by many geological and geophysical studies, including GPS observations (e.g., Heki *et al*., 1999; Miyazaki and Heki, 2001; Bird, 2003; Jin *et al*., 2007; Barth and Wenzel, 2010; DeMets *et al*., 2010). The EMJS has a much larger strain rate and higher seismic potential than the surrounding areas (Sagiya *et al*., 2000; Okamura, 2002).

doi:10.5047/meep.2012.00101.0001

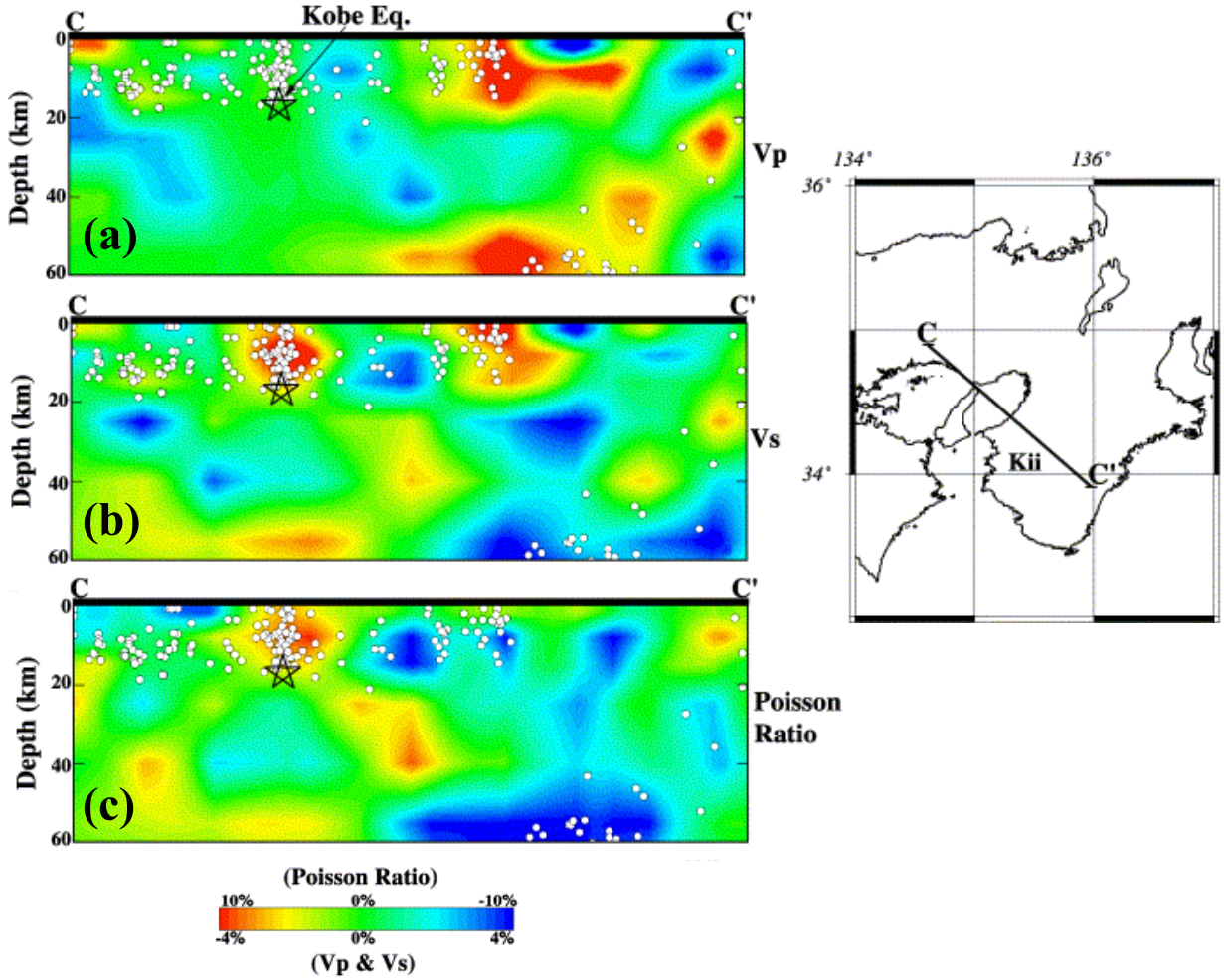

Fig. 38. Vertical cross-sections of (a) P and (b) S wave velocity and (c) Poisson's ratio images along the profile C–C′ as shown on the inset map. Red color denotes low velocity and high Poisson's ratio, while blue color denotes high velocity and low Poisson's ratio. The color scale is shown below (c). The average value of Poisson's ratio is 0.25. The star symbol denotes the hypocenter of the Kobe earthquake (M 7.2) that occurred on 17 January, 1995. White dots show the background seismicity within 20 km of the profile. (Reprinted from *Tectonophysics*, *364*, Salah, M., and D. Zhao, 3-D seismic structure of Kii Peninsula in Southwest Japan: Evidence for slab dehydration in the forearc, 191–213, Copyright 2003, with permission from Elsevier.)

To understand the Amur-Okhotsk plate boundary zone and the back-arc magmatism and seismotectonics, Zhao *et al.* (2011c) determined high-resolution images of V_p, V_s and Poisson's ratio (PR) under the EMJS using a large number of P and S wave arrival-time data from local shallow, and intermediate-depth, earthquakes. To determine the seismic structure under the Japan Sea, they used arrival times from many suboceanic earthquakes that are relocated precisely using sP depth phases detected from 3-component seismograms recorded by the seismic network on Honshu Island (Figs. 29, 30). They conducted extensive resolution tests to examine the resolution scale of the tomographic images, and the test results show that their tomographic model has a resolution of 30–50 km in the horizontal direction and 10–30 km in depth under the EMJS.

Figures 31, 32 and 34 show the obtained V_p, V_s and PR tomographic images at 10-, 25- and 40-km depths together with the distribution of large crustal earthquakes ($M \geq 6.0$) that occurred during the period 830 to 2010 (Utsu, 1982; Usami, 2003, and JMA catalogue). Distributions of active faults and active volcanoes are also shown. The results show that the V_p and V_s images are quite similar to each other, and strong lateral heterogeneities exist in the crust and uppermost mantle under the EMJS. Both high-V and low-V anomalies are visible. Although the correlation between the tomography and the distribution of large crustal earthquakes is not very obvious, many large earthquakes seem to be located in, or around, the low-V zones. However, some large earthquakes are located in, or around, the high-V zones (Figs. 31, 32). Note that the hypocenter locations of the large earthquakes that occurred after 1900 represent the initial points of earthquake ruptures because these earthquakes were located by the modern seismic network in Japan, and they may be accurate to about 10 km or less. In contrast, the hypocenters of large historic earthquakes before 1900 represent the centroid locations of the rupture zones because they were estimated from the macroscopic damage resulting from the earthquakes, and so they have larger uncertainties (Usami, 2003).

The V_p, V_s and PR variations revealed by seismic tomog-

doi:10.5047/meep.2012.00101.0001

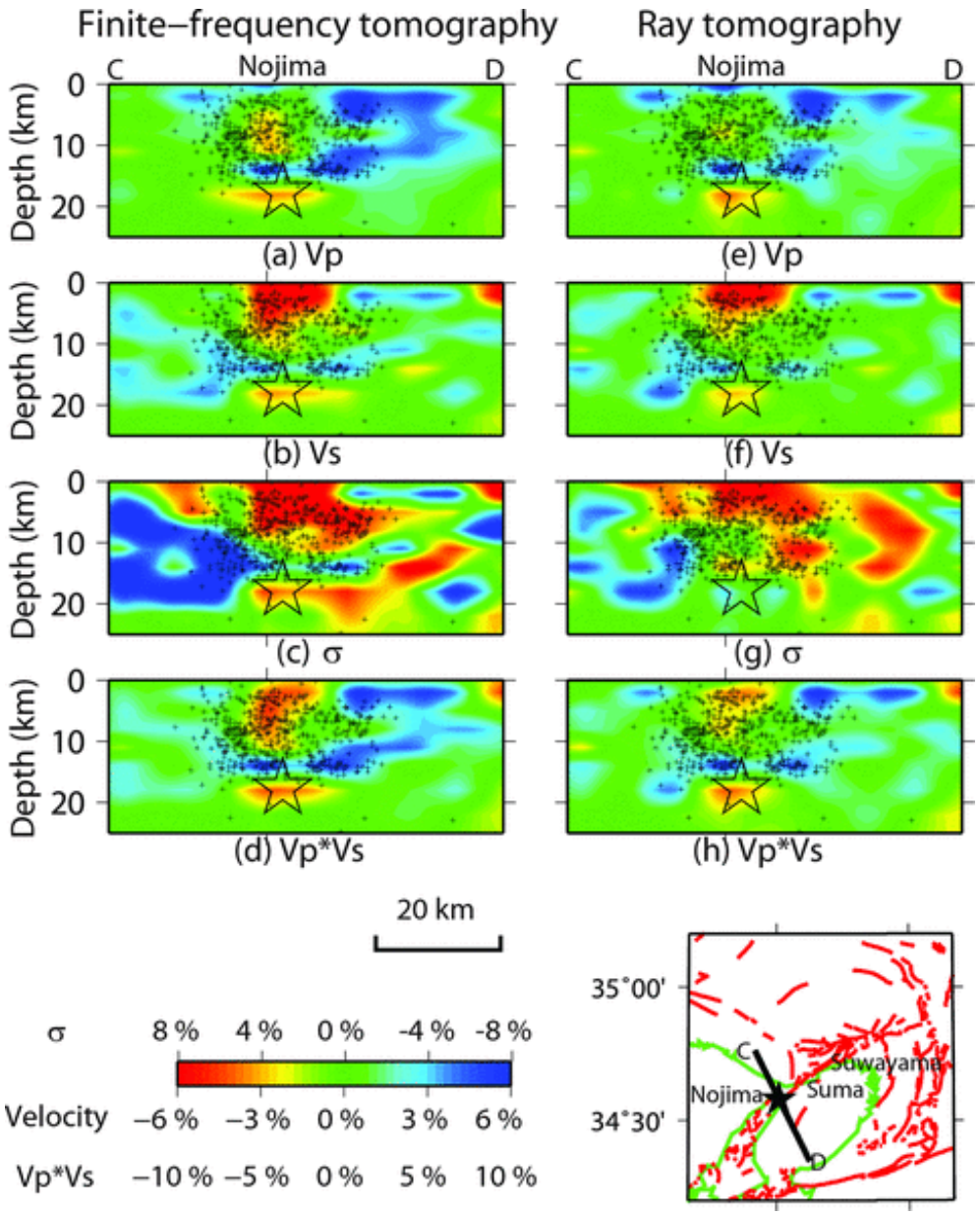

Fig. 39. Vertical cross-sections of P-velocity (a, e), S-velocity (b, f), Poisson's ratio (c, g), and $V_P * V_S$ (d, h) images along the line C–D as shown on the inset map. (a–d) Results obtained with finite-frequency tomography. (e–h) Results obtained with ray tomography. The vertical exaggeration is 1:1. Small crosses denote the Kobe aftershocks during the period 17 January, 1995, to 8 May, 1995, which are located within a 10-km width along the line C–D. The star symbol denotes the hypocenter of the Kobe mainshock (M 7.2), its focal depth is 17.7 km. (Reprinted from *Geophys. J. Int.*, *187*, Tong, P., D. Zhao, and D. Yang, Tomography of the 1995 Kobe earthquake area: Comparison of finite-frequency and ray approaches, 278–302, Copyright 2011, with permission from John Wiley & Sons.)

raphy may be caused by several factors, such as temperature, composition, and the presence of melt or fluids (see, e.g., Zhao *et al*., 2002). To explain the tomographic images obtained, it is necessary to understand the tectonic history and geological structures in the EMJS. Japan was part of the Asian continental margin until the early Miocene (Sato, 1994; Ohtake *et al*., 2002). The NE Honshu arc was constructed by back-arc spreading during 21–18 Ma, when the Yamato basin was formed, and by subsequent rifting during 19–13.5 Ma (when the Northern Honshu rift system formed) and island-arc uplifting up to the present time (Ohtake *et al*., 2002; Yamada and Yoshida, 2004; Yoshida *et al*., 2005). The EMJS region has been subject to convergent tectonics, since the Pliocene, under an E-W compressional stress regime caused by the collision of the Amur plate with the Okhotsk plate (Tamaki and Honza, 1985; Okamura, 2002). Many normal faults and fault-related rifts and grabens developed in the Early to Middle Miocene, simultaneous with back-arc spreading of the Japan Sea (Okamura *et al*., 1995). The normal faults reactivated as reverse faults during an inversion stage, due to an increase in compressional stress since 1–2 Ma ago (Tamaki and Honza, 1985). As a result, complex geologic structures exist in the EMJS, such as alternate rift zones, ridges, basins, horsts, grabens, reverse

doi:10.5047/meep.2012.00101.0001

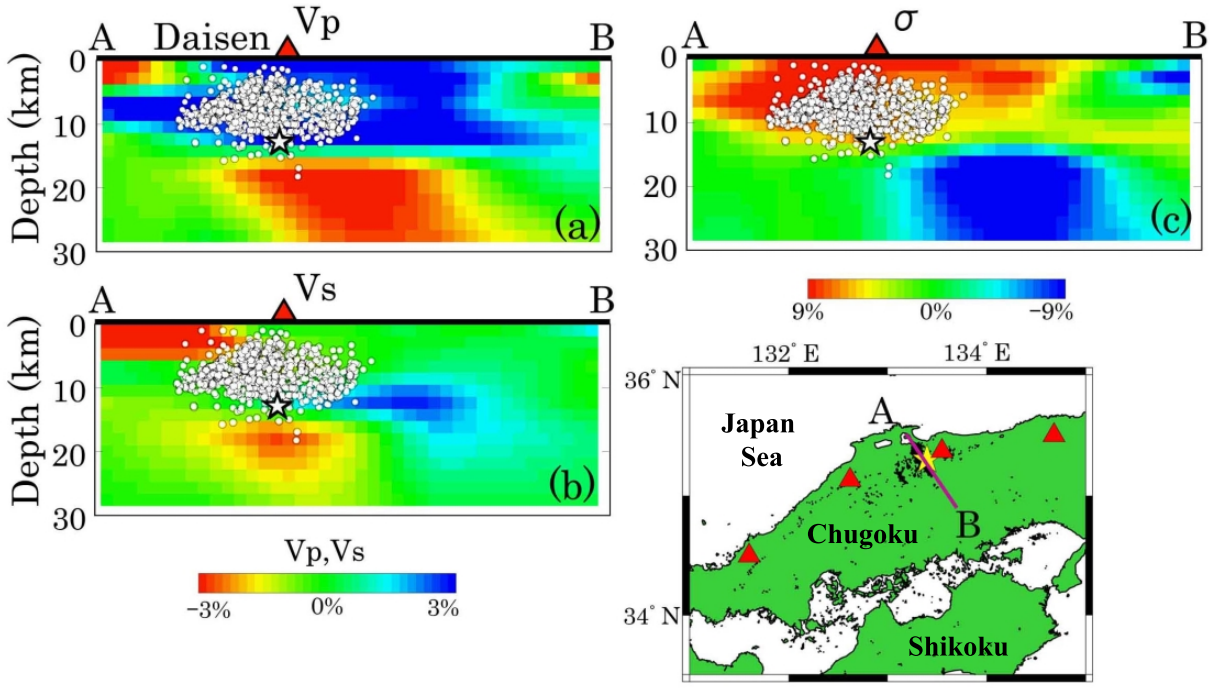

Fig. 40. Vertical cross-sections of (a) P and (b) S wave velocity and (c) Poisson's ratio images along the profile A–B as shown on the inset map. Red color denotes low velocity and high Poisson's ratio, while blue color denotes high velocity and low Poisson's ratio. The scales for velocity and Poisson's ratio are shown below (b) and (c), respectively. The average value of Poisson's ratio is 0.25. The star symbol and white dots denote the mainshock and aftershocks of the Western Tottori earthquake (M 7.3) that occurred on October 6, 2000. The red triangles and yellow star on the inset map show the Quaternary volcanoes and epicenter of the Western Tottori earthquake, respectively. (Reprinted from *Phys. Earth Planet. Inter.*, *145*, Zhao, D., H. Tani, and O. P. Mishra, Crustal heterogeneity in the 2000 western Tottori earthquake region: effect of fluids from slab dehydration, 161–177, Copyright 2004, with permission from Elsevier.)

faults, anticlines, magmatic intrusions, and continental fragments (Ohtake *et al*., 2002; Yoshida *et al*., 2005) (Figs. 35(b), 36). The strong velocity variations in the crust and uppermost mantle in the EMJS revealed by seismic tomography may reflect these complex geological features. Nishimoto *et al*. (2008) made a mineral-physics study of the lower-crust mafic xenoliths sampled in the EMJS and this showed that the high-V anomalies in the lower crust under the EMJS represent cooled igneous rocks formed in the back-arc igneous period (21–13.5 Ma). In contrast, the low-V anomalies in the crust and uppermost mantle under the EMJS may reflect continental fragments and/or more recent magmatic and fluid activities in the back-arc region.

In the uppermost mantle, significant high-V anomalies (∼4–6%) are imaged under the Japan Sea side, while low-V zones are revealed under the Honshu inland area (Figs. 31(c), 32(c)). This feature is well consistent with the results of seismic explosion experiments carried out across the EMJS, which show a higher sub-Moho V_p under the Japan Sea (∼8.0 km/s) than that under the Honshu Island (∼7.5–7.7 km/s) (Nishisaka *et al*., 2001; Iwasaki and Sato, 2009). Significant high-V anomalies are visible in the northern part of the EMJS (Figs. 31, 32), which correspond to the lower seafloor topography (Fig. 33), suggesting that that part of the EMJS has an oceanic crust, whereas the southern part has a continental crust (Nishizawa and Asada, 1999; Iwasaki and Sato, 2009).

The EMJS region is seismically very active (Fig. 4). The large crustal earthquakes in the EMJS are generally caused by thrust-faulting with fault planes striking in the N-S direction and dipping eastward, which are considered to represent the subduction of the Amur plate beneath the Okhotsk plate (Satake, 1986; Sato *et al*., 1986) (Fig. 35(a)). The tomographic results show strong structural heterogeneities in the EMJS, but a sharp and clear boundary between the Amur and Okhotsk plates is not visible in the tomographic images, perhaps because the plate boundary is still nascent (Kobayashi, 1983; Nakamura, 1983).

In the NE Japan arc, seismic and volcanic activities are mainly caused by the subduction of the Pacific plate under the Okhotsk and Amur plates. The low-V zones in the uppermost mantle represent mantle diapirs associated with the ascending flow of subduction-induced convection in the mantle wedge, and dehydration reactions in the subducting slab (Zhao *et al*., 2002; Hasegawa *et al*., 2005). Magmas rising further from the mantle diapirs to the crust can cause low-frequency microearthquakes at levels of the lower crust and uppermost mantle (Figs. 15–17), and make their appearance as S-wave reflectors at mid-crustal levels (Hasegawa and Yamamoto, 1994; Matsumoto and Hasegawa, 1996; Horiuchi *et al*., 1997). Their upward intrusion raises the temperature and reduces the seismic velocity of crustal materials there, causing the brittle seismogenic layer above them to become locally thinner and weaker, thus large crustal earth-

doi:10.5047/meep.2012.00101.0001

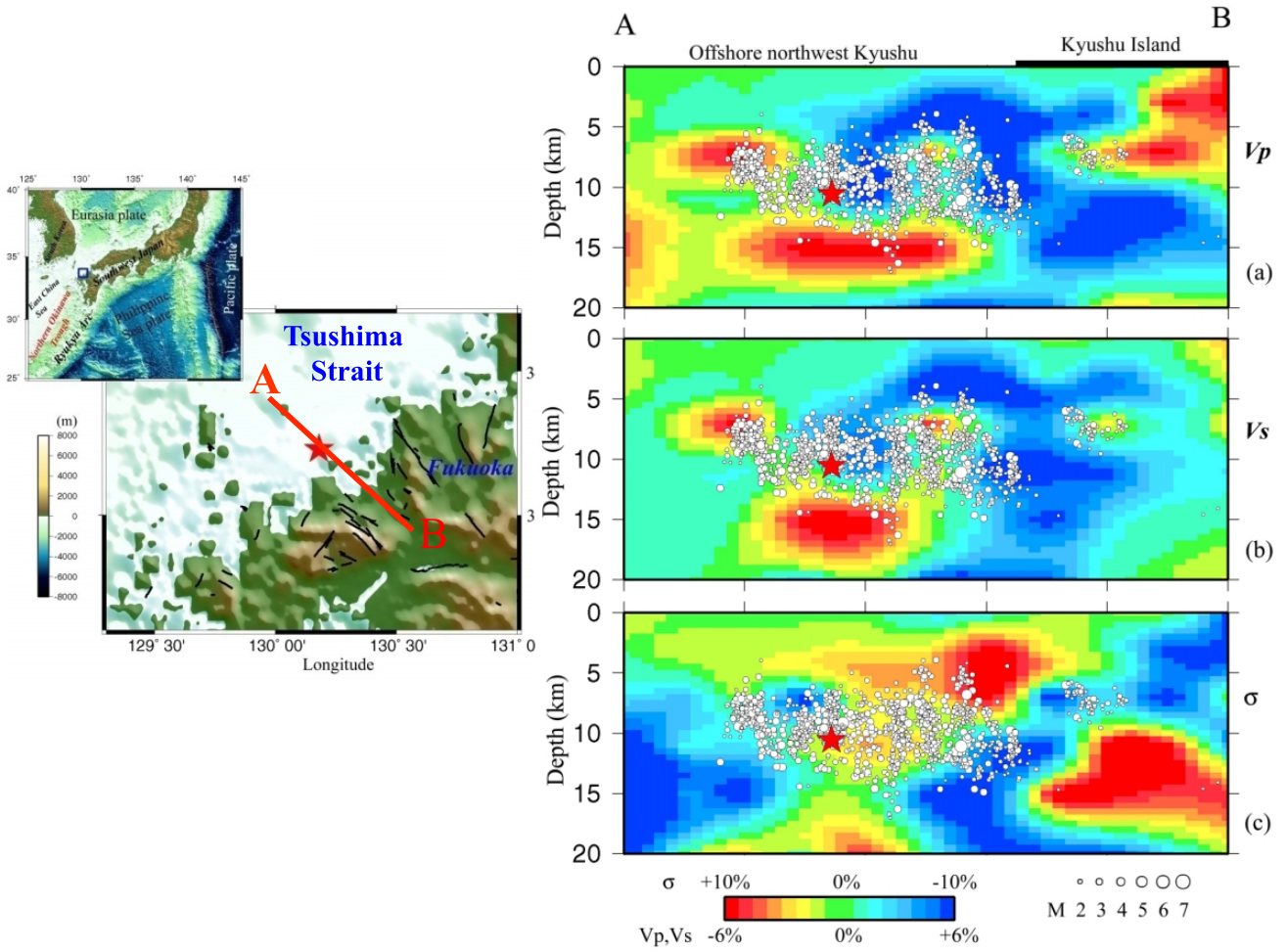

Fig. 41. Vertical cross sections of (a) *P* and (b) *S* wave velocity and (c) Poisson's ratio images along the profile A–B as shown on the inset map. Red color denotes low velocity and high Poisson's ratio, while blue color denotes high velocity and low Poisson's ratio. The color scale is shown at the bottom. The average value of Poisson's ratio is 0.25. The red star and white dots denote the mainshock and aftershocks of the West off-Fukuoka earthquake (*M* 7.0) that occurred on March 20, 2005. (Reprinted from *Phys. Earth Planet. Inter.*, *155*, Wang, Z., and D. Zhao, Seismic evidence for the influence of fluids on the 2005 west off Fukuoka prefecture earthquake in southwest Japan, 313–324, Copyright 2006, with permission from Elsevier.)

quakes are apt to take place in those areas under the E-W compressional stress field (Hasegawa *et al*., 2005; Zhao *et al*., 2010a).

High-resolution tomographic images were determined for the source areas of the 2004 and 2007 Niigata earthquakes (*M* 6.8) in the southwestern part of NE Japan (see Fig. 2) (e.g., Xia *et al*., 2008b; Kato *et al*., 2010). An anomaly with low-*V* and high-*PR* in the lower crust and uppermost mantle was revealed under the Niigata source areas, which also exhibits high conductivity and a high He^3/He^4 ratio (Ogawa and Honkura, 2004; Uyeshima *et al*., 2005; Horiguchi *et al*., 2010), indicating the existence of fluids under the EMJS rising from the upper mantle as a result of slab dehydration and corner flow in the mantle wedge. Some large thrust faults during large earthquakes may cut through the whole crust (Satake, 1986; Tanioka *et al*., 1995). When the fluids enter the active faults, pore pressure will increase and fault friction will decrease, thus a large crustal earthquake can be triggered (Zhao *et al*., 2002; Cheng *et al*., 2011). These geophysical and geochemical results suggest that high-temperature arc and back-arc magmas and fluids rising from the mantle wedge can affect (advance) the rupture nucleation of large crustal earthquakes. This may be one reason for the frequent occurrence of damaging earthquakes in the EMJS and Tohoku (Figs. 4, 22), in addition to the E-W compressional stress regime caused by the strong interactions among the Amur, Okhotsk and Pacific plates.

7. Anatomy of Large Crustal Earthquakes

Since the pioneering work of Reid (1910) on the 1906 San Francisco earthquake (*M* 7.8), seismologists have reached a consensus that an earthquake is caused by the (sudden) rupture of an active fault in the crust or in the subducting slab. So far, seismologists have been quite successful in using seismic waveforms radiated by a large earthquake to estimate the coseismic slip distribution on the fault plane (see the review by Kanamori, 2004). Although seismic tomography has been applied successfully to various tectonic environments on Earth since the late 1970s, the application of seismic tomography to the study of earthquake faults has not

doi:10.5047/meep.2012.00101.0001

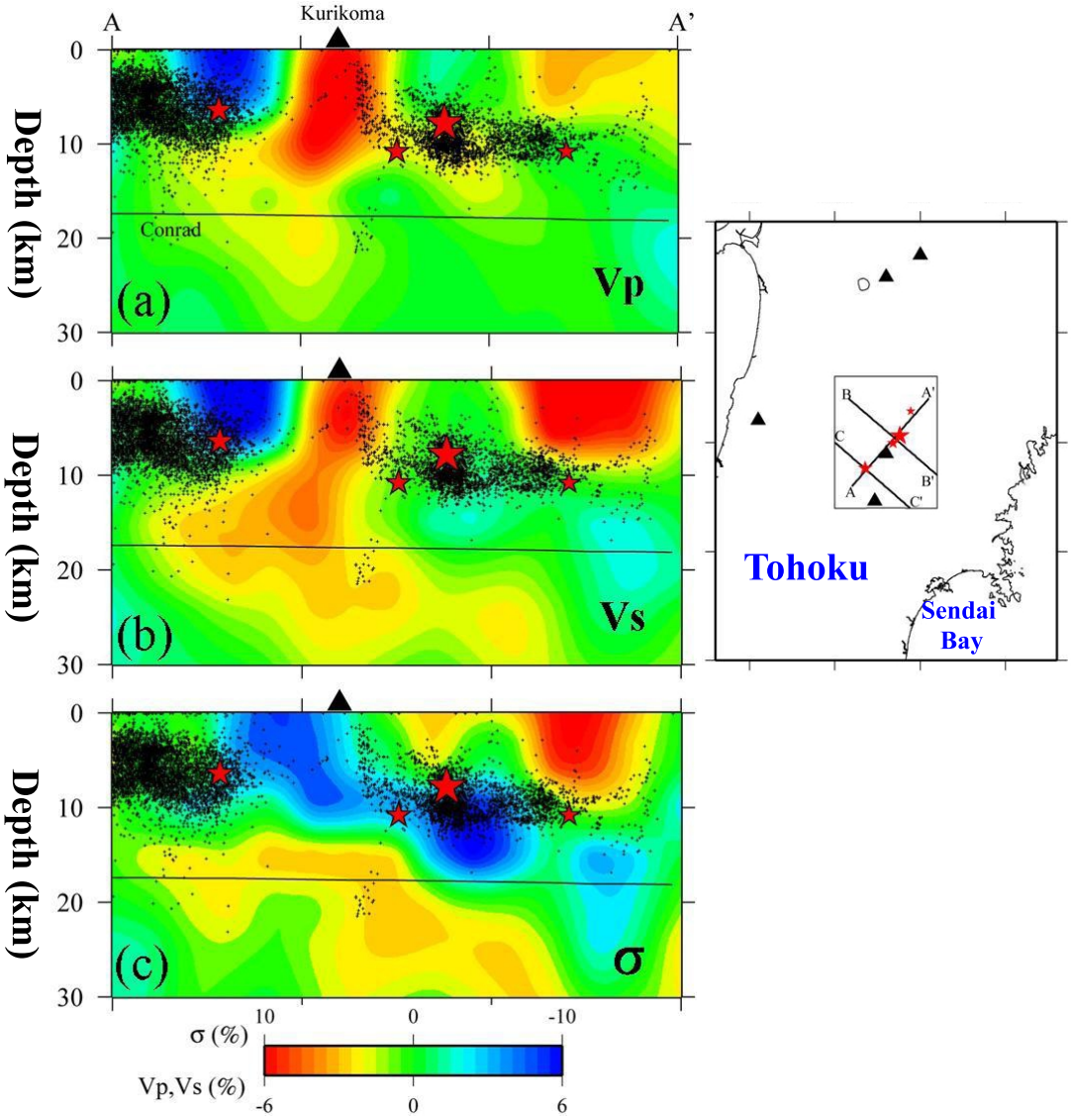

Fig. 42. Vertical cross-sections of (a) *P*-wave velocity, (b) *S*-wave velocity, and (c) Poisson's ratio images along the profile A–A′ as shown on the inset map. Red denotes low velocity and high Poisson's ratio, while blue denotes high velocity and low Poisson's ratio. The color scale is shown at the bottom. Red triangles denote the active Kurikoma volcano. Small black dots show earthquakes which occurred within a 10-km width along the profile A–A′. The thin lines show the Conrad discontinuity. The red stars denote the mainshock and large aftershocks of the 2008 Iwate-Miyagi earthquake (*M* 7.2). (Reprinted from *Phys. Earth Planet. Inter.*, *184*, Cheng, B., D. Zhao, and G. Zhang, Seismic tomography and anisotropy in the source area of the 2008 Iwate-Miyagi earthquake (M 7.2), 172–185, Copyright 2011, with permission from Elsevier.)

been as successful as for the other tectonic environments. This is because the spatial resolution of local-scale tomography is usually tens of kilometers. Even the best resolution of local tomography is of the order of a few kilometers (e.g., Zhao *et al*., 1996; Zhao and Negishi, 1998), which is one to three orders of magnitude greater than the width of an active fault zone. Thus, structural heterogeneity (such as asperities) on a fault plane can hardly be imaged by seismic tomography at this stage. Seismic tomography is suited for imaging three-dimensional voluminal heterogeneity of Earth materials, but not good at detecting two-dimensional heterogeneity on a plane like a fault zone (Zhao, 2001b). Nevertheless, seismic tomography has been applied with some success in studying the cause of large earthquakes. In the source areas of some large earthquakes that are covered by a dense network of permanent or portable seismic stations, tomographic imaging has detected structural heterogeneities that may be related to the nucleation process of large earthquakes.

The application of seismic tomography to earthquake fault zones started relatively late, around the early 1990s (e.g., Lees, 1990; Michael and Eberhart-Phillips, 1991). Since then, however, there has been rapid progress in tomographic studies of large earthquake source areas, thanks to the progress made in seismic instrumentation technology and the deployment of portable and/or permanent seismic arrays in seismically active regions in various parts of the world. Many high-resolution images have been determined for large earthquake source areas, which shed new light on the nucleation process of earthquake faulting.

Six damaging crustal earthquakes with magnitudes greater

doi:10.5047/meep.2012.00101.0001

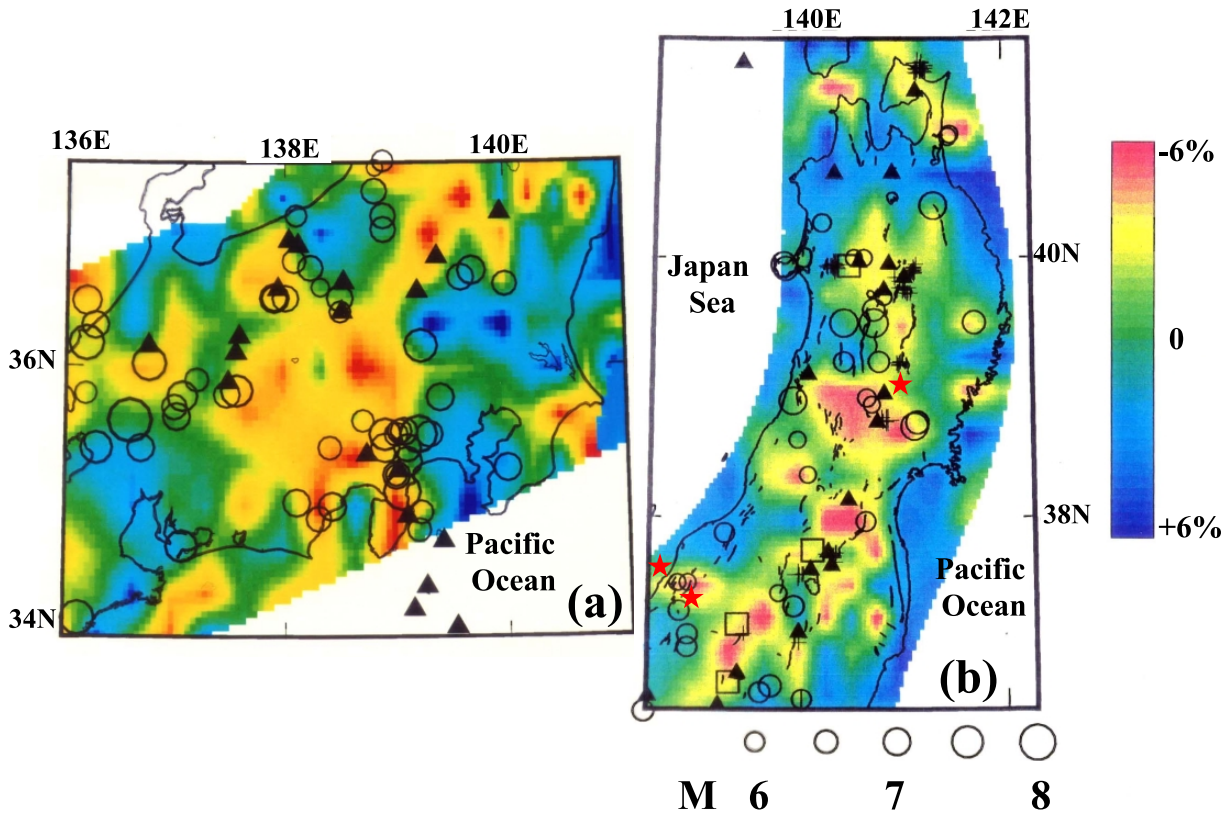

Fig. 43. *P*-wave velocity image at a depth of 40 km beneath (a) central, and (b) northeast, Japan. Red and blue colors denote low and high velocities, respectively. Circles denote earthquakes (M 5.7–8.0, depths 0–20 km) that occurred during a period of 124 years from 1885 through 2008. Solid triangles denote active volcanoes. The velocity perturbation scale and the earthquake magnitude scale are shown on the right and at the bottom, respectively. Crosses and open squares in (b) show low-frequency earthquakes and *S*-wave reflectors in mid-crust, respectively. Short lines and red stars in (b) show the active faults and three large earthquakes (the 2004 and 2007 Niigata, and the 2008 Iwate-Miyagi) discussed in this work. (Reprinted from *Island Arc*, *19*, Zhao, D., M. Santosh, and A. Yamada, Dissecting large earthquakes in Japan: Role of arc magma and fluids, 4–16, Copyright 2010, with permission from John Wiley & Sons.)

than M 6.8 have occurred in the Japan land areas since 1995 (Fig. 2). Because the source zones of these large earthquakes are covered by the dense permanent seismic network (Fig. 5), as well as portable seismic stations deployed soon after the mainshocks, detailed tomographic images in the source areas of these earthquakes were determined with a high resolution, which has enabled the examination of the relationship between crustal heterogeneity and earthquake generation.

The 17 January, 1995, Kobe earthquake (M 7.3) was one of the most damaging earthquakes in Japan in the past 50 years, and accounted for over 6400 fatalities. Soon after the occurrence of the Kobe mainshock, many portable seismic stations were deployed in the epicenter area to record its aftershocks (Hirata *et al*., 1996). These portable stations and permanent network stations formed a dense seismic array covering the Kobe aftershock area, resulting in accurate hypocenter locations of the aftershocks (Fig. 37). A large number of arrival-time data from the well-located aftershocks and other local earthquakes in the Kobe area were used to determine high-resolution (4–5 km), 3-D V_p, V_s and PR images in the Kobe aftershock area (Zhao *et al*., 1996). A prominent low-V and high-PR anomaly was detected at depths of 16–21 km directly beneath the hypocenter of the Kobe mainshock (under the Akashi strait and Osaka Bay) (Fig. 37). Its lateral extension is about 15 km. Because there is no active volcano in the Kobe area and the surface heat flow is not very high there, the anomaly in the Kobe hypocenter was interpreted as a fluid-filled, fractured rock matrix that triggered the 1995 Kobe earthquake (Zhao *et al*., 1996; Zhao and Negishi, 1998).

Later, detailed tomographic images of the crust and upper mantle under SW Japan were determined, which indicate that fluids at the Kobe hypocenter area originated from the dehydration of the subducting PHS slab under SW Japan (Zhao *et al*., 2000a, 2002; Salah and Zhao, 2003b; Salah *et al*., 2005; Ikeda *et al*., 2006; Gupta *et al*., 2009b) (Fig. 38). Zhao and Mizuno (1999) estimated the distribution of crack density and saturation rate in the Kobe source area by applying a crack theory to the values of V_p, V_s and PR determined by seismic tomography. It was suggested that sea water in Osaka Bay may have permeated down to the deep crust through the active faults that may have been ruptured many times during all the earthquake cycles of the past 2 million years after the formation of Osaka Bay and the active faults there (Zhao and Mizuno, 1999). Recently, Tong *et al*. (2011) used a better data set and adopted both finite-frequency and

doi:10.5047/meep.2012.00101.0001

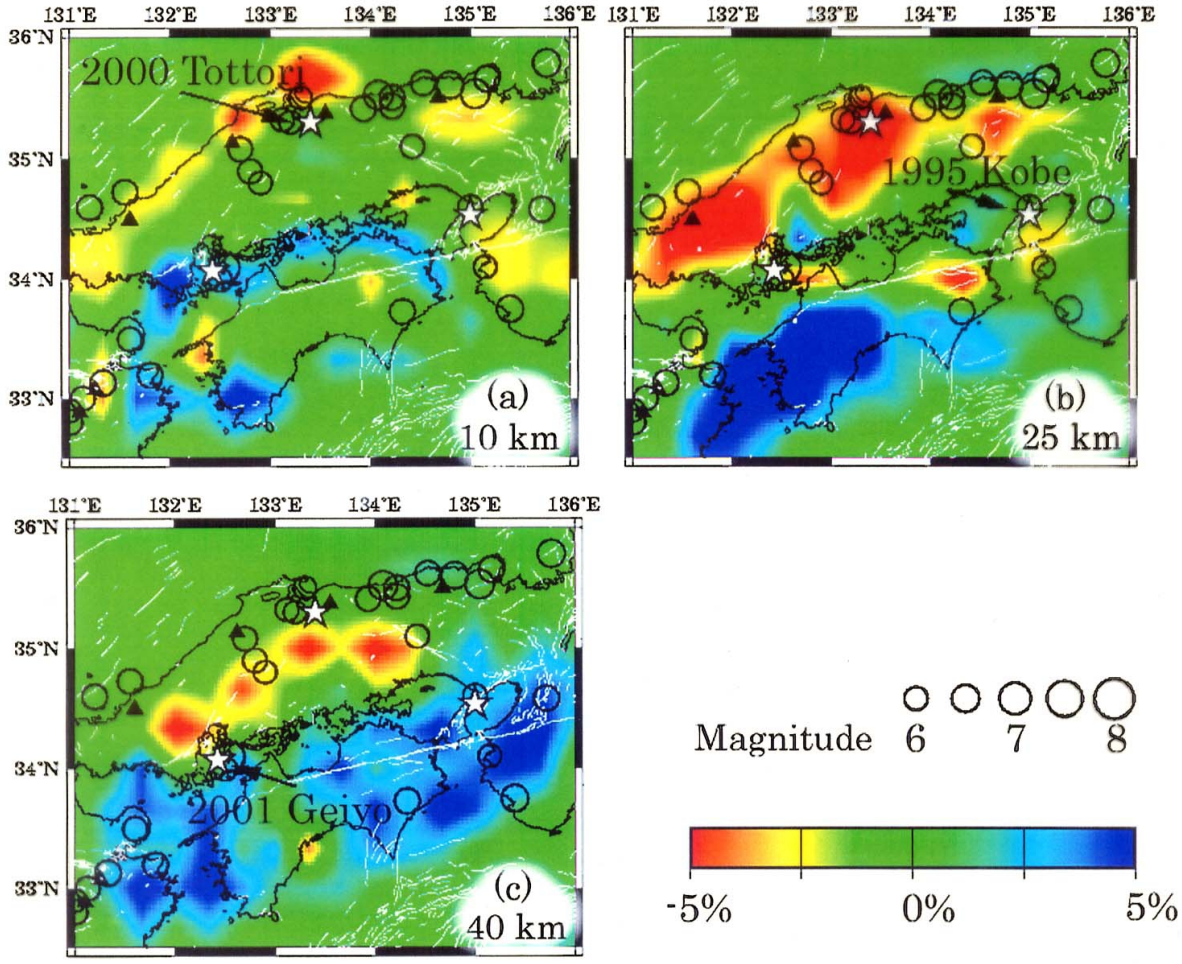

Fig. 44. *P*-wave velocity image at a depth of (a) 10, (b) 25, and (c) 40 km beneath southwest Japan. Solid triangles denote volcanoes. The star symbols denote the epicenters of the 1995 Kobe earthquake (*M* 7.2), the 2000 West Tottori earthquake (*M* 7.3), and the 2001 Geiyo earthquake (*M* 6.8). Other labelings are the same as Fig. 43. (Reprinted from *Island Arc*, *19*, Zhao, D., M. Santosh, and A. Yamada, Dissecting large earthquakes in Japan: Role of arc magma and fluids, 4–16, Copyright 2010, with permission from John Wiley & Sons.)

ray tomography methods to determine a detailed 3-D crustal model of the 1995 Kobe earthquake area (Fig. 39). Their new results confirmed the earlier findings of Zhao *et al.* (1996).

Figure 40 shows V_p, V_s and *PR* images in the source area of the Western-Tottori earthquake (*M* 7.3) that occurred on 6 October, 2000 (Zhao *et al.*, 2004a). The mainshock epicenter is located close to the Daisen volcano, and its hypocenter is located at 12-km depth where the tomographic images change drastically. The upper crust above the mainshock hypocenter exhibits high V_p, slightly low V_s and high *PR*, indicating a brittle seismogenic layer probably containing fluids. The lower crust beneath the mainshock hypocenter exhibits low V_p and low V_s, which may reflect high-temperature materials possibly containing melts under Daisen, which is a potentially active volcano (Zhao *et al.*, 2004a, 2011a; Sun *et al.*, 2008). Later, Shibutani *et al.* (2005) used a better data set and also found significant velocity variations in the Tottori source area.

Near the focal area of the 2000 Western-Tottori earthquake, low-frequency (LF) microearthquakes were detected at depths of around 30 km (Ohmi and Obara, 2002). Five LF events occurred within 3 years before the Tottori mainshock and more than 60 LF events occurred during 13 months after the mainshock. Waveform analyses show that a single-force source mechanism is preferable to the double-couple mechanism for those LF events (Ohmi and Obara, 2002). These results suggest that the LF events were caused by the transport of fluids such as water or magma. A detailed magnetotelluric imaging detected high electric-conductivity anomalies down to a depth of 30 km beneath the western Tottori area, suggesting the existence of fluids in the lower crust, which caused the lower crust to be electrically conductive (Oshiman, 2002). A joint inversion of local and teleseismic data imaged the subducting PHS slab under the Tottori area and offshore under the Japan Sea (see figure 12 in Zhao *et al.*, 2004a). The PHS slab is located at about 55-km depth under the Daisen volcano, and a significant low-V zone is imaged above the PHS slab and beneath the Daisen volcano. The low-V zone may reflect a magma chamber under the Daisen volcano, associated with the dehydration process of the PHS

doi:10.5047/meep.2012.00101.0001

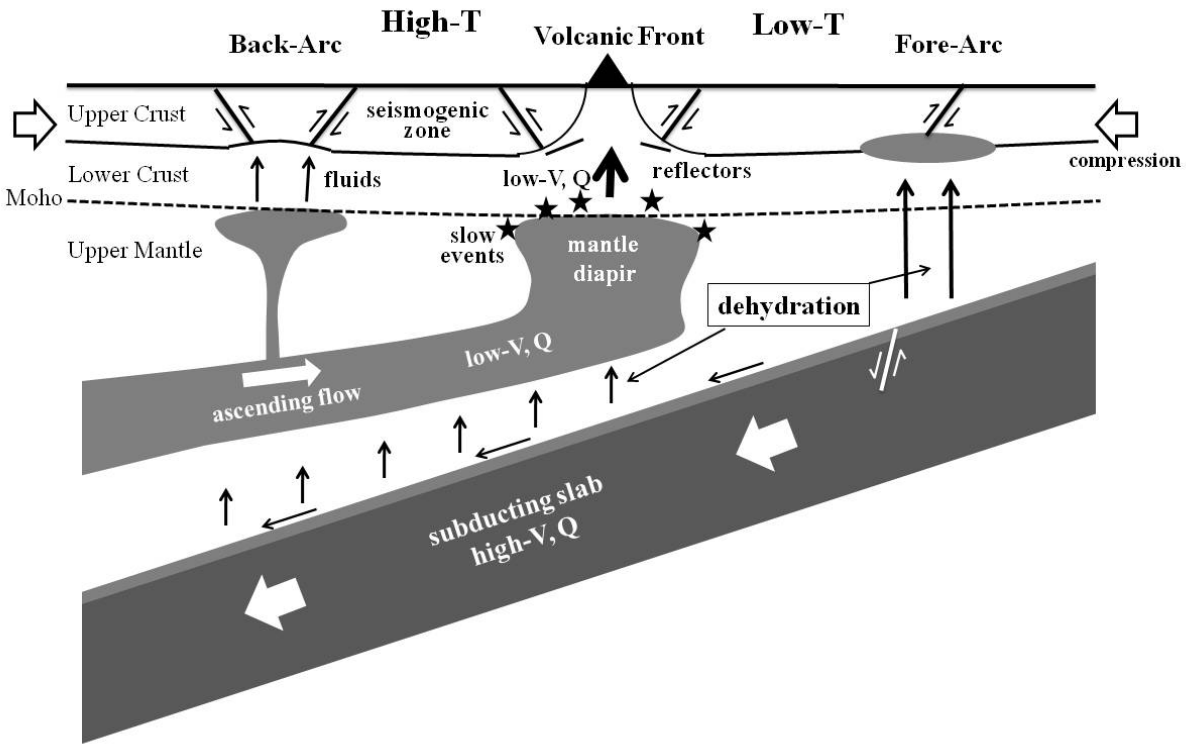

Fig. 45. Schematic illustration of across-arc vertical cross-section of the crust and upper mantle under the Japan subduction zone. The generation of large crustal earthquakes is affected by the tectonic background and structural heterogeneities, in particular, arc magma and fluids (see text for details). (Reprinted from *Island Arc*, *19*, Zhao, D., M. Santosh, and A. Yamada, Dissecting large earthquakes in Japan: Role of arc magma and fluids, 4–16, Copyright 2010, with permission from John Wiley & Sons.)

slab. All these pieces of geophysical evidence suggest the existence of arc magma and fluids in the Tottori area and their influence on the generation of the 2000 Western-Tottori earthquake (Zhao *et al*., 2004a).

On 20 March, 2005, the west off-Fukuoka earthquake (M 7.0) occurred in the northwestern portion of Fukuoka Prefecture, western Japan (Fig. 41). Most of its aftershocks occurred in a NW-SE trending fault offshore under Tsushima Strait, which are outside the seismic network in Kyushu. Wang and Zhao (2006c) collected *sP* depth-phase data, together with the first P and S wave data, to relocate the aftershocks accurately, and then determined high-resolution tomographic images in the source area of the Fukuoka earthquake (Fig. 41). V_p and V_s images exhibit similar features in the source area. The mainshock hypocenter is located in a high-V area, while prominent low-V zones exist in the lower crust under the mainshock hypocenter and at 5–10 km depth northwest of the hypocenter (Fig. 41(a, b)). High *PR* anomalies are visible in, and below, the mainshock hypocenter (Fig. 41(c)). These features are similar to those in the source areas of the 1995 Kobe and 2000 Western-Tottori earthquakes (Figs. 37–40). Hence, it is considered that crustal fluids existed in the source area of the Fukuoka earthquake and affected its nucleation (Wang and Zhao, 2006c).

The fluids in the Fukuoka hypocenter area may be related to a diapiric mantle upwelling off western Kyushu due to the opening of the Okinawa Trough. A regional tomography of East Asia shows that the PHS slab is subducting down to 500-km depth under East Asia, and the opening of the Okinawa Trough is caused by the dehydration of the PHS slab and a convective circulation process in the mantle wedge above the PHS slab (Huang and Zhao, 2006).

Two crustal earthquakes of magnitude 6.8 occurred in Niigata Prefecture, Japan: one on 23 October, 2004, the other on 16 July, 2007. Detailed tomographic images were determined in the source area of the Niigata earthquakes (e.g., Kato *et al*., 2005; Wang and Zhao, 2006d; Xia *et al*., 2008b). Similar to the 1995 Kobe, 2000 Western-Tottori, and the 2005 west off Fukuoka, earthquakes (Figs. 37–41), significant low-V and high-*PR* anomalies were detected in the Niigata source areas, and the anomalies in the crust seem to be connected with the low-V zone in the upper mantle wedge. Hence, arc magma and fluids are considered to play an important role in the nucleation of the two Niigata earthquakes (Wang and Zhao, 2006d; Xia *et al*., 2008b).

Close to the Niigata source area, a large crustal earthquake ($M_{\rm JMA}$ 6.9) occurred in the Noto Peninsula on 25 March, 2007, which caused significant damage. Detailed crustal tomography revealed prominent low-V and high-*PR* anomalies in the Noto earthquake area (Padhy *et al*., 2011), indicating the effect of back-arc magma and fluids on the generation of the earthquake, very similar to those in the Niigata earthquake areas.

The 2008 Iwate-Miyagi earthquake (M 7.2) occurred in

doi:10.5047/meep.2012.00101.0001

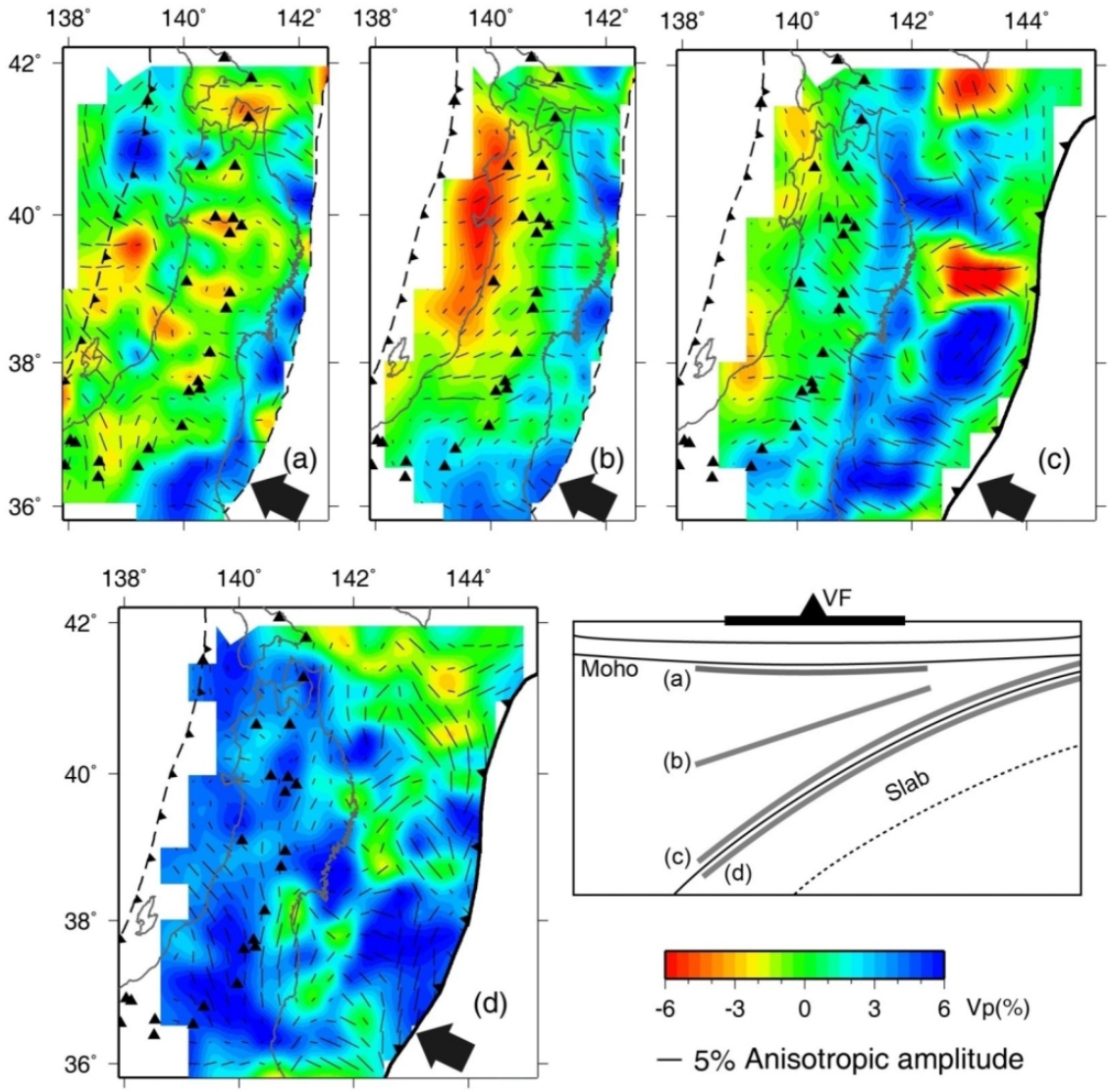

Fig. 46. *P*-wave anisotropic tomography along four slices (a) in the uppermost mantle, (b) in the middle mantle wedge, (c) on the top and (d) in the subducting Pacific slab as shown in the inset sketch below (c). The dashed lines in (a) and (b) denote the upper boundary of the Pacific slab at 40-km depth, while the bold curves in (c) and (d) denote the Japan Trench. The black arrows in (a–d) denote the motion direction of the Pacific plate relative to the Honshu arc. The orientation and length of the short bars represent the fast velocity direction and the anisotropic amplitude with the scale shown at the bottom. Red and blue colors denote slow and fast velocities, respectively. The velocity perturbation scale is shown at the bottom. Black triangles denote active volcanoes. (Reprinted from *Geophys. J. Int.*, *184*, Huang, Z., D. Zhao, and L. Wang, Seismic heterogeneity and anisotropy of the Honshu arc from the Japan Trench to the Japan Sea, 1428–1444, Copyright 2011, with permission from John Wiley & Sons.)

the upper crust under the central portion of Tohoku on 14 June, 2008 (Fig. 42). Its epicenter is located about 10 km east of the volcanic front and the closest volcano is the active Kurikoma volcano. Detailed 3-D V_p, V_s and *PR* images in the Iwate-Miyagi source area were determined (Okada *et al.*, 2010; Cheng *et al.*, 2011) (Fig. 42). The hypocenters of the mainshock, and three large aftershocks, are located in a boundary zone where both seismic velocity and Poisson's ratio change drastically. A zone with pronounced low-V and high-*PR* is revealed in the lower crust and uppermost mantle under the source area, which reflect arc magma and fluids ascending from the upper-mantle wedge. The result indicates that the generation of the 2008 Iwate-Miyagi earthquake was influenced by the ascending magma and fluids from the upper-mantle wedge, similar to the other large crustal earthquakes in NE Japan mentioned above.

Detailed tomographic images have been determined for recent large earthquakes, but not for old, historic large earthquakes because a dense seismic network was not available then. To understand the general relationship between the structural heterogeneity and seismogenesis, Zhao *et al.* (2010a) compared the tomographic images with the distribution of 164 crustal earthquakes (M 5.7 to 8.0) in Japan that occurred during 1885 to 2008. The tomographic image at 40-km depth (Figs. 43, 44(c)) was best resolved because of the crisscrossing of horizontal P_n rays from crustal earthquakes and vertical rays from intermediate-depth earthquakes in the subducting slab, and the image also reflects

doi:10.5047/meep.2012.00101.0001

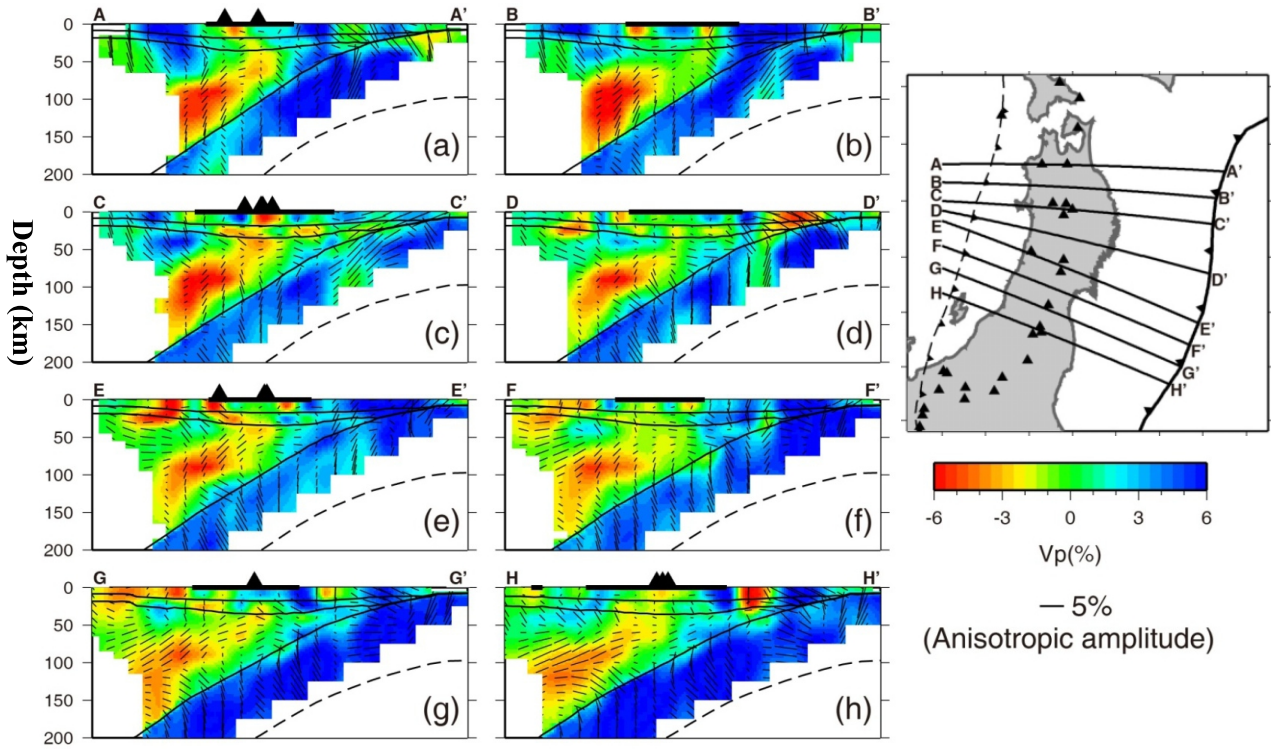

Fig. 47. Vertical cross-sections of P-wave anisotropic tomography along the eight profiles shown on the inset map. Red and blue colors denote slow and fast velocities, respectively. The velocity perturbation scale is shown at the bottom. The orientation and length of the short bars represent the fast velocity direction (azimuth) and the anisotropic amplitude with the scale shown at the bottom. The horizontal bold line at the top of each cross-section shows the land area where seismic stations are deployed. Solid triangles denote active volcanoes within a 30-km width along each profile. The three curved lines denote the Conrad and Moho discontinuities and the upper boundary of the subducting Pacific slab, while the dashed lines denote the inferred lower boundary of the Pacific slab. The triangles and curved line on the inset map denote active volcanoes and the Japan Trench, respectively. (Reprinted from *Geophys. J. Int.*, *184*, Huang, Z., D. Zhao, and L. Wang, Seismic heterogeneity and anisotropy of the Honshu arc from the Japan Trench to the Japan Sea, 1428–1444, Copyright 2011, with permission from John Wiley & Sons.)

well the fluids and magma arising from the mantle wedge. Hypocenter locations, and the magnitudes, of large earthquakes are taken from Utsu (1982), Usami (2003), and the JMA catalogue for recent events. Because all the large historic earthquakes considered in this study occurred beneath inland areas, their locations and magnitudes were relatively well determined. Zhao *et al*. (2010a) calculated P-velocity perturbations (dV/V) in the crust and uppermost mantle at the hypocenters of the 164 large earthquakes and they found that for 71% of the earthquakes, $-3\% < dV/V < 0\%$, and 12% of them had a $dV/V < -3\%$. For the remaining 17% of the large earthquakes, $0 < dV/V < 1.5\%$. These results indicate that the large earthquakes generally occurred at the edge portion of low-V zones or along the boundary between low-V and high-V bodies (Figs. 43, 44). Only some smaller events (M 5.7–5.8) are located in the central part of the low-V zones. A few earthquakes are located in high-V areas, but they are generally smaller than M 6.0. Note that the resolution of the tomographic images is 25 to 33 km in the horizontal direction and 10–15 km at depth in the crust and uppermost mantle. It is possible that some low-V and high-V zones smaller than the resolution scale were not detected in the tomographic maps.

Figure 45 shows a qualitative model to explain the seismogenesis of large crustal earthquakes in Japan, referring to the previous studies (Hasegawa and Zhao, 1994; Zhao *et al*., 2000a, 2002; Hasegawa *et al*., 2005). Two processes are considered to be the most important in a subduction zone. One is corner flow in the mantle wedge that can bring heat to the mantle wedge from the deeper mantle through convection because of the temperature gradient in the mantle. The other is the dehydration reactions of the subducting oceanic slab. In the forearc region, the temperature is lower, and hence magma cannot be produced, and the fluids from slab dehydration may migrate up to the crust. If the fluids enter an active fault in the crust, pore pressure will increase and fault zone friction will decrease, which may trigger large crustal earthquakes such as the 1995 Kobe earthquake (M 7.2). Under the volcanic front and back-arc areas, arc magma can be produced because of the high temperature in the mantle wedge and fluids from the slab dehydration. Migration of magma up to the crust produces arc volcanoes and causes lateral heterogeneities and a weakening of the seismogenic upper crust, which can lead to large crustal earthquakes, such as the 2000 Western-Tottori, 2004 and 2007 Niigata, 2005 west off Fukuoka, and the 2008 Iwate-Miyagi, earthquakes, as mentioned above. Dehydration reactions of the subducting slab may also trigger large intraplate earthquakes, such as the 24 March, 2001, Geiyo earthquake (M 6.8) that occurred within the subducting Philippine Sea slab under the

doi:10.5047/meep.2012.00101.0001

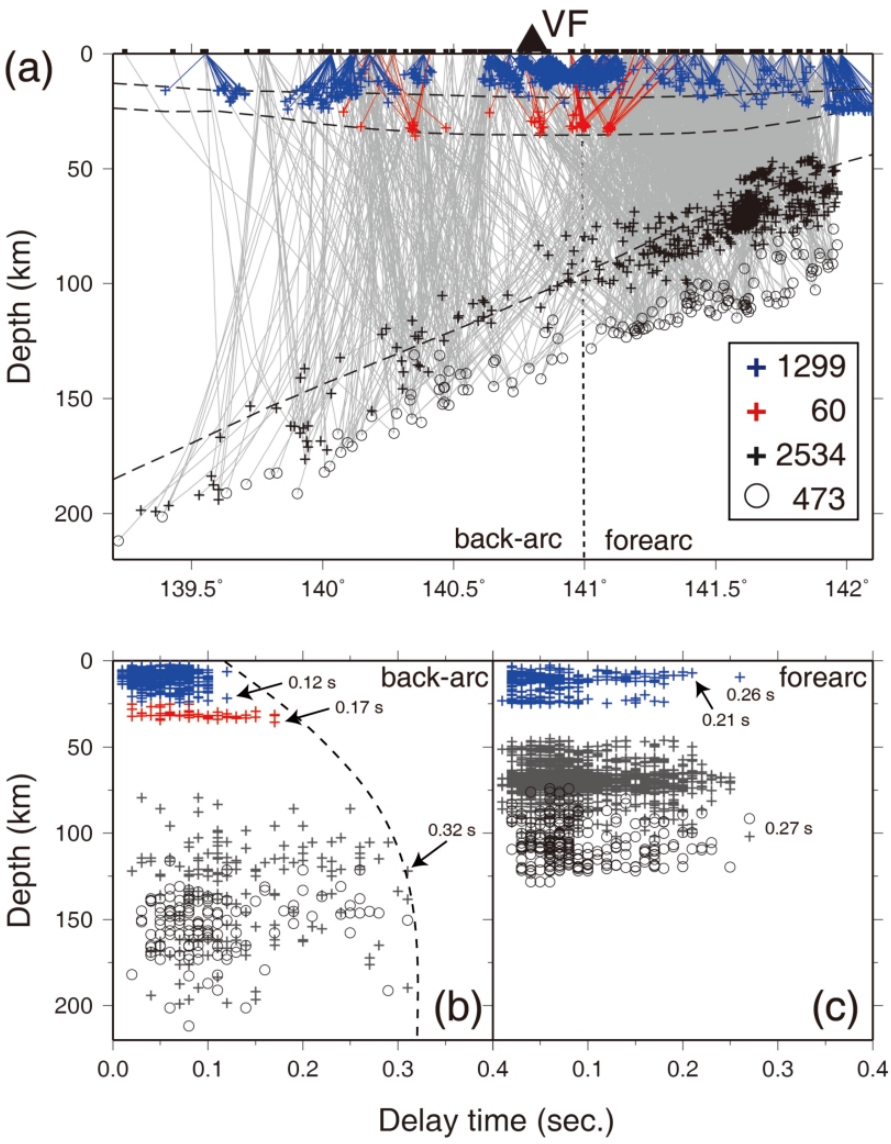

Fig. 48. (a) Ray paths from shallow earthquakes (blue crosses), low-frequency earthquakes (red crosses), upper-plane earthquakes (gray crosses) and lower-plane earthquakes (open circles) in the subducting slab used in the shear-wave splitting analysis. Solid squares at the top denote the seismic stations, while the triangle indicates the position of the volcanic front (VF). The dashed lines denote the Conrad and the Moho discontinuities and the upper boundary of the subducting Pacific slab at the latitude of 40°N. (b) The delay time for the earthquakes whose ray paths only pass through the back-arc shown in (a). The dashed line indicates the envelope of the maximum delay time. The maximum delay times for the earthquakes in different layers are marked. (c) The same as (b) but for earthquakes in the forearc. (From Huang *et al*., 2011b.)

Seto Inland Sea in SW Japan (Zhao *et al*., 2002), and the 26 May, 2003, Miyagi-oki earthquake that occurred within the subducting Pacific slab under the Pacific coast in NE Japan (Mishra and Zhao, 2004).

The low-V zones in the uppermost mantle (Figs. 43, 44(c)) are the manifestation of mantle diapirs associated with an ascending flow of subduction-induced convection in the mantle wedge, and dehydration reactions in the subducting slab (Zhao *et al*., 1992b, 2009a; Hasegawa and Zhao, 1994; Hasegawa *et al*., 2005). As mentioned above, magma rising further from the mantle diapirs to the crust causes LF events in the lower crust and uppermost mantle, which make their appearance as S-wave reflectors. Their upward intrusion raises the temperature and reduces the seismic velocity of crustal materials around them, causing the brittle seismogenic layer above them to become locally thinner and weaker (Fig. 45). Subject to the horizontally-compressional stress field in the plate-convergence direction, contractive deformations will take place mainly in the low-V areas because of the thinning of the brittle seismogenic layer and a weakening of the crust and uppermost mantle there, due to the higher temperature and the existence of magma- or fluid-filled, thin, inclined reflectors that are incapable of sustaining the applied shear stress (Hasegawa *et al*., 2005). The deformation proceeds partially in small earthquakes but mainly as a plastic deformation, causing crustal shortening, upheaval and mountain building. Large crustal earthquakes cannot occur within the weak low-V zones but in their edge portions,

doi:10.5047/meep.2012.00101.0001

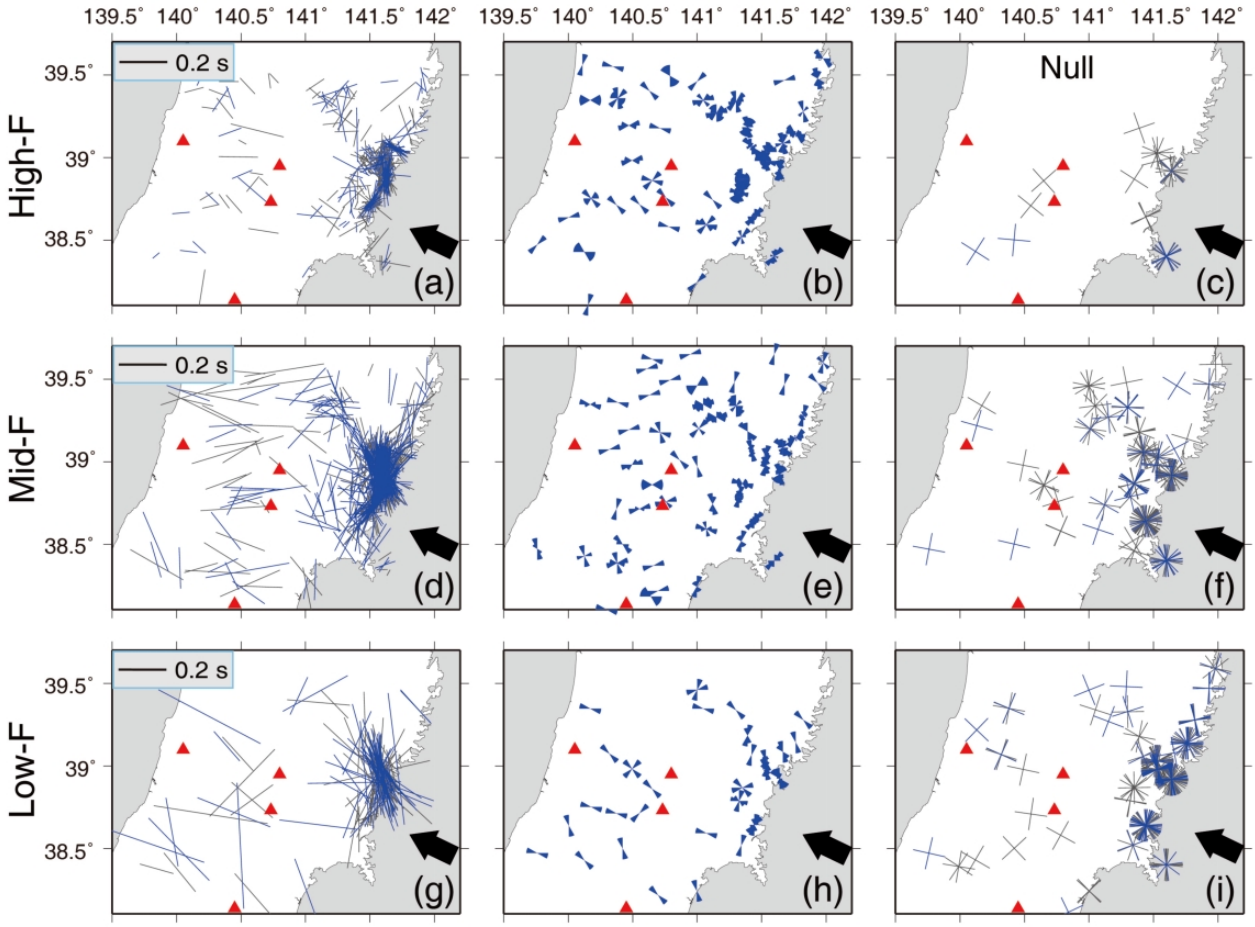

Fig. 49. (a, d, g) The individual shear-wave splitting measurements are plotted at the middle of each ray path for the (a) high, (d) middle and (g) low frequency bands. The blue and black bars denote the best and good measurements, respectively. The splitting parameters (φ, δt) obtained are indicated by the orientation and length of each short bar. The δt scale is shown in the upper-left inset. The red triangles denote the active volcanoes, while the bold arrow indicates the motion direction of the Pacific plate relative to NE Japan. (b, e, h) The weighted rose diagrams for φ plotted at the stations for the (b) high, (e) middle and (h) low frequency bands. The weight for the best and good measurements is 1.0 and 0.5, respectively. (c, f, i) The measured nulls plotted at the stations with the bars orientated in the initial polarization of the waveform and its orthogonal direction for the (c) high, (f) middle and (i) low frequency bands. The blue and black crosses denote the good and fair nulls, respectively. (From Huang *et al*., 2011c.)

where the mechanical strength of materials is stronger than that of the low-V zones but still weaker than the normal sections of the seismogenic layer. Thus, the edge portion of the low-V areas becomes the ideal location to generate large crustal earthquakes that produce faults reaching the Earth's surface or blind faults within the brittle upper crust. Although the tomographic results are complex and details of the image change in different earthquake areas (Figs. 37–44), low-V and/or high-PR anomalies are generally visible below or around the mainshock hypocenters. This suggests one common feature: the significant influence of fluids and magma on the rupture nucleation of large crustal earthquakes.

Significant structural heterogeneities, and their effects on the seismogenesis, are also revealed in the source areas of many large earthquakes in the continental regions (e.g., Lees, 1990; Michael and Eberhart-Phillips, 1991; Zhao and Kanamori, 1992, 1993, 1995; Kayal *et al*., 2002; Mishra and Zhao, 2003; Huang and Zhao, 2004, 2009; Zhao *et al*., 2005; Mukhopadhyay *et al*., 2006; Qi *et al*., 2006; Tian *et al*., 2007a, b; Lei and Zhao, 2009; Tian and Zhao, 2011). The occurrence of deep moonquakes seems also to be affected by structural heterogeneities in the lunar mantle, in addition to tidal forces (Zhao *et al*., 2008; Sakamaki *et al*., 2010; Zhao and Arai, 2011).

8. Seismic Anisotropy Tomography

Seismic anisotropy is the direction-dependent nature of the propagation velocity of seismic waves. Natural minerals usually have some crystallographic structure. Under the physical conditions of high temperature and high pressure in the Earth's deep interior, rocks undergo slow plastic deformation (e.g., Zhang *et al*., 2006, 2007). Through the deformation process, crystallographic axes of minerals are realigned to a particular direction due to uniaxial tectonic stress. Rocks may thus exhibit petrofabic structure, which in turn will produce seismic anisotropy on a macroscopic scale (e.g., Zhang *et al*., 2005; Shiraishi *et al*., 2008). Anisotropy can also form due to the presence of aligned cracks. It is found that seismic anisotropy exists in almost every portion

doi:10.5047/meep.2012.00101.0001

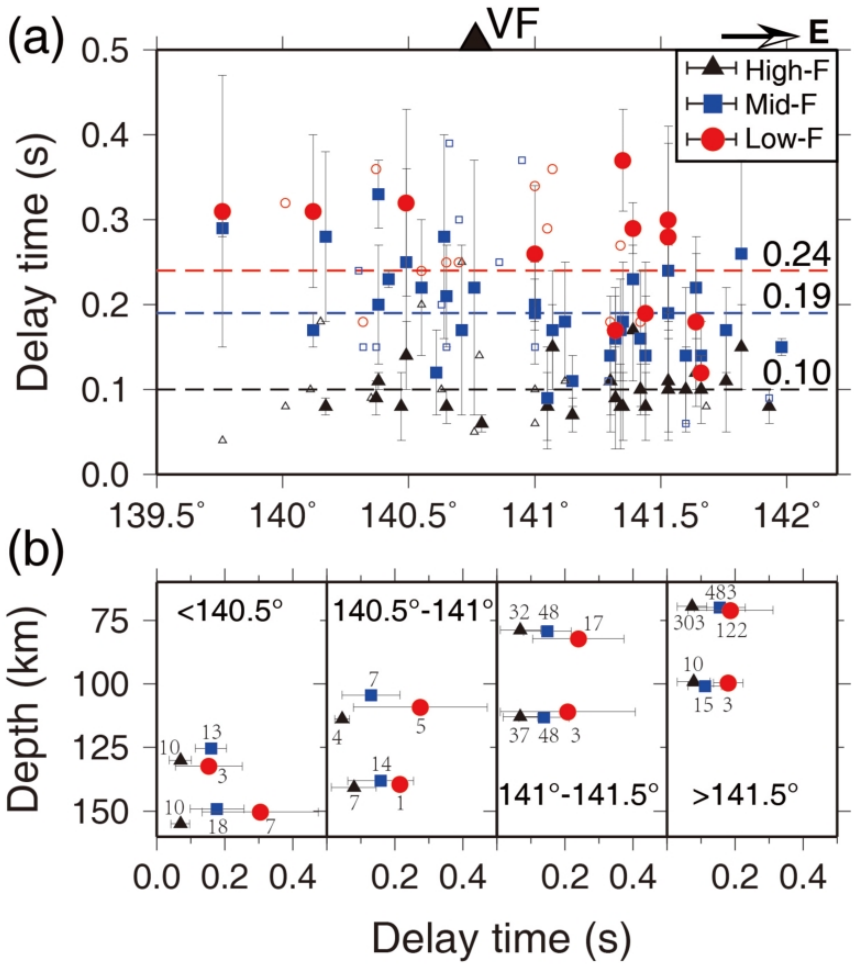

Fig. 50. (a) The mean delay time (δt) and its standard deviation at each station are plotted against the longitude. The larger solid symbols denote the stations where more than two reliable measurements were made, while the smaller open symbols denote the stations with only one measurement. The weighted averages of the δt values for the high, middle and low frequency bands are shown as black triangles, blue squares and red circles, respectively, with the corresponding standard deviations indicated by short bars. The weight for the best and good measurements is 1.0 and 0.5, respectively. The three horizontal dashed lines show the overall mean δt values for the three frequency bands. The black triangle on the top denotes the volcanic front (VF). (b) The weighted averages of the δt values for the upper-plane and lower-plane earthquakes (Fig. 48(a)) in four sub-areas from the west to east (the longitude range is shown for each sub-area). The number of splitting measurements is shown beside each symbol. (From Huang *et al*., 2011c.)

of the Earth, from the crust, mantle, to the inner core.

The above-mentioned tomographic studies in Japan determined only 3-D isotropic velocity models. Shear-wave splitting studies, however, have revealed significant anisotropic anomalies in the upper-mantle wedge and the subducting Pacific slab under Japan (e.g., Ando *et al*., 1980; Okada *et al*., 1995; Hiramatsu *et al*., 1997; Nakajima and Hasegawa, 2004). Studying seismic anisotropy is very important for understanding dynamical processes in the Earth. The anisotropy in the upper mantle is caused mainly by the strain-induced crystallographic preferred orientation (CPO) of olivine, which is generally considered to be associated with the mantle flow (Karato *et al*., 2008). Thus, seismic anisotropy can provide direct information on dynamical processes in a subduction zone. Shear-wave splitting could detect seismic anisotropy under a region, but it has a poor depth resolution and cannot clarify in what depth range the anisotropy exists.

Several researchers have tried to determine *P*-wave anisotropic tomography in the Japan and New Zealand subduction zones, and the results show that complex anisotropic anomalies exist in wide areas of the crust, mantle wedge and the subducting Pacific slab (e.g., Hirahara and Ishikawa, 1984; Eberhart-Phillips and Henderson, 2004; Ishise and Oda, 2005; Wang and Zhao, 2008, 2009, 2010; Cheng *et al*., 2011). Huang *et al*. (2011a) used a large number of arrival-time data from local earthquakes in the crust and the subducting Pacific slab to determine a detailed *P*-wave anisotropic tomography of the NE Japan arc from the Japan Trench to the Japan Sea (Figs. 46, 47). Their results show that the fast velocity direction (FVD) in the uppermost mantle and right above the slab ranges from E-W to NW-SE, which agrees well with the motion direction of the Pacific plate relative to NE Japan. The trench-normal FVD can be explained by the deformation and alignment of A-type fabric olivine caused by the subduction of the Pacific plate and induced mantle wedge convection (Karato *et al*., 2008). The FVD in the middle of the mantle wedge ranges from E-W to NE-SW,

doi:10.5047/meep.2012.00101.0001

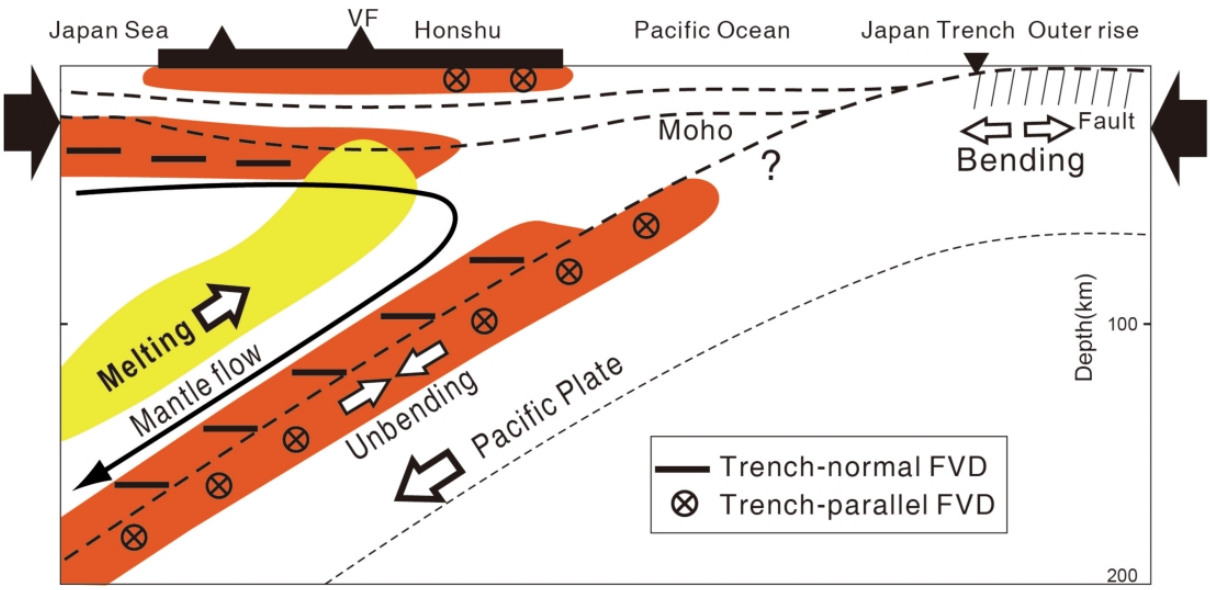

Fig. 51. A schematic diagram showing the anisotropic structures under NE Japan. Anisotropy is considered to exist in the color hatched areas. The orange and yellow colors indicate strong and weak anisotropy, respectively. The horizontal bars and circled crosses denote the trench-normal and trench-parallel fast polarization directions, respectively. The curve with a downward-pointing arrow denotes the mantle flow in the mantle wedge driven by the subduction of the Pacific slab, while the upward-pointing arrow indicates the secondary mantle flow containing partial melts. The thick horizontal bar at the top denotes the land area. The triangles indicate the active volcanoes. The inverted triangle denotes the Japan Trench. Horizontal solid arrows denote the horizontally-compressional regime in NE Japan while double blank arrows denote the bending and unbending in the subducting Pacific slab. Dipping lines in the outer rise part of the Pacific plate denote the normal faults. The dashed lines denote the Conrad and the Moho discontinuities and the upper and lower boundaries of the subducting Pacific slab, respectively. (Modified from Huang *et al*., 2011b.)

arguing for a 3-D mantle flow or an alignment of olivine's A-axis 90° to the shear direction in the partially molten mantle.

The FVD is found to be N-S in the subducting Pacific slab, which reflects either the original fossil anisotropy when the Pacific plate was produced, or the trench-parallel CPO and shaped preferred orientation (SPO) of the faults and cracks developed in the subducting slab due to slab bending and unbending (Faccenda *et al*., 2008). Hiramatsu *et al*. (1997) found that the subducting slab shows a strong anisotropy resulting from phase changes in the slab from shear-wave splitting analyses of *ScS* waves that travel from the events in the slab down to the deep mantle and are bounced back from the core-mantle boundary.

Huang *et al*. (2011b) further studied the anisotropic structure under NE Japan by analyzing shear-wave splitting of earthquakes that occurred in the upper crust, lower crust and in the double seismic zone within the subducting Pacific slab (Fig. 48). The 4366 measurements they made provide important new information on the anisotropic structures in the crust, Pacific slab, and especially the mantle wedge. In the upper crust, the anisotropy is mainly caused by the stress-aligned fluid-saturated microcracks. The measured delay time increases to 0.10 s at 10–11 km depth while the FVD is parallel to either the tectonic stress or the strike of active faults. The maximum delay time for the low-frequency earthquakes near the Moho is 0.15–0.17 s, suggesting strong anisotropy at the base of the lower crust that is caused by the preferred orientation of minerals. The splitting parameters of the intermediate-depth earthquakes in the Pacific slab show a dominant E-W (trench-normal) FVD in the back-arc and an N-S (trench-parallel) FVD in the forearc. In the back-arc, the trench-normal FVD can be explained by the corner flow in the mantle wedge driven by subduction of the Pacific plate. The maximum delay time can reach as large as 0.30–0.32 s for the events at 100-km depth, but only about half of the total delay time is produced in the mantle wedge (Fig. 48). The apparent weak anisotropy may be explained by an isotropic or weak anisotropic zone in the middle of the mantle wedge. In the forearc, the dominant trench-parallel FVD is consistent with that in the upper crust where ∼80% of the total delay time can be accounted for, suggesting that the shear-wave splitting in the forearc is mainly caused by the anisotropy in the crust.

To clarify the cause of the complex features of *S*-wave anisotropy in NE Japan, Huang *et al*. (2011c) analyzed carefully shear-wave splitting on 320 intermediate-depth earthquakes occurring in the subducting Pacific slab in different frequency bands (Figs. 49, 50). Their results show that the delay time is definitely smaller (<0.2 s) in the high-frequency band than that (0.3–0.4 s) in the low-frequency band, and so the splitting parameters, especially the delay time, are strongly frequency-dependent. Although the delay time is indubitably smaller under NE Japan than in the other subduction zones regardless of the frequency band, nine large delay time values (0.5–0.7 s) were detected, which indicates that the anisotropy is potentially strong in NE Japan (Huang *et al*., 2011c).

Both the *P* and *S* wave anisotropy results in NE Japan are consistent with a model of subduction-driven back-

doi:10.5047/meep.2012.00101.0001

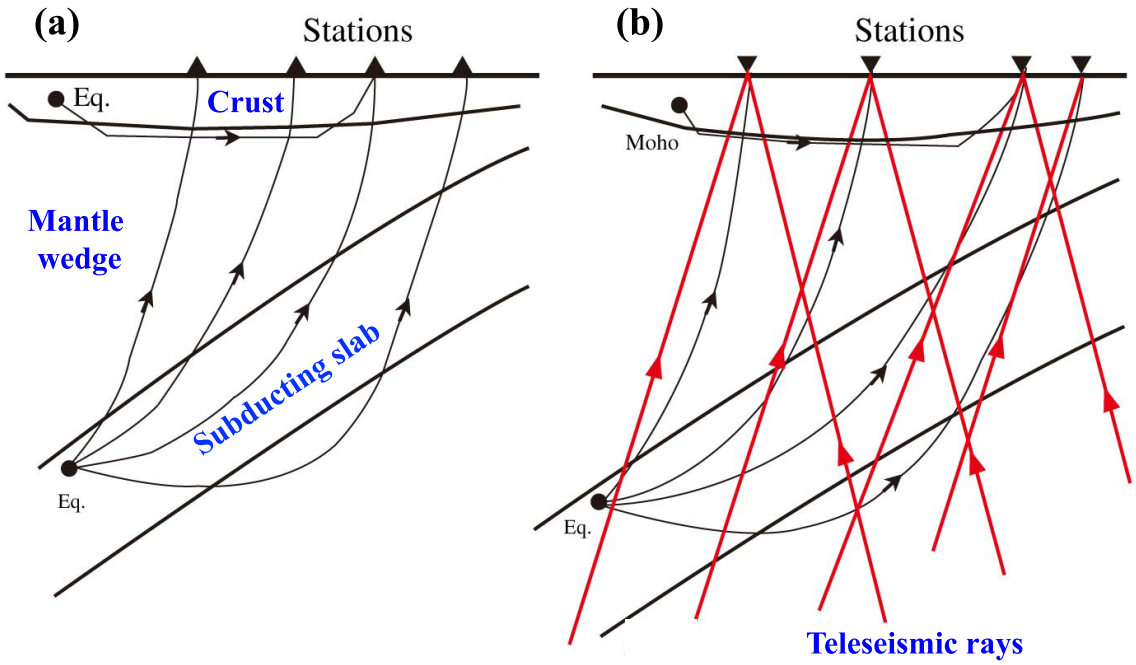

Fig. 52. (a) Local earthquake tomography for a subduction zone. (b) Local and teleseismic joint inversion for the tomography of a subduction zone. (Reprinted from *Gondwana Res.*, *15*, Zhao, D., Multiscale seismic tomography and mantle dynamics, 297–323, Copyright 2009, with permission from Elsevier.)

arc spreading and convection in the mantle wedge causing trench-normal fast orientations in the wedge, and aligned faults and cracks in the subducting Pacific slab causing trench-parallel fast orientations in the slab (Fig. 51). When an *S* wave travels through an area having multilayer orthogonal anisotropies, some of its splitting would be cancelled and thus a small delay time is observed. The trench-parallel FVD under the land area of the forearc revealed by shear-wave splitting of local earthquakes can be explained by the anisotropy in the crust and the subducting slab. The B-type fabric olivine in the mantle wedge under the forearc (Karato *et al.*, 2008) is unnecessary and not supported by the new results of Wang and Zhao (2008, 2010) and Huang *et al.* (2011a, b, c).

9. Deep Structure of Japan Subduction Zone

Beneath the Japan Islands, earthquakes occur mainly in the upper crust and in the subducting Pacific and Philippine Sea slabs, which enable us to determine the 3-D velocity model of the crust, mantle wedge and the upper portion of the subducting slab, but we cannot study the mantle structure below the slab using only the local event data (Fig. 52(a)). Zhao *et al.* (1994) proposed to make joint use of local-earthquake arrival times and teleseismic residuals in tomographic inversion (Fig. 52(b)). This joint inversion approach preserves the advantages of the separate approaches of local-earthquake tomography and teleseismic tomography and overcomes their drawbacks. Moreover, the horizontally-propagating local rays and vertically-traveling teleseismic rays crisscross well in the shallow portion of the model, which can improve the resolution there (Fig. 52(b)).

The deep structure of the Japan subduction zone is determined by using a large number of high-quality arrival-time data from local, regional and distant earthquakes recorded by the dense seismic networks on the Japan Islands (Zhao *et al.*, 1994; Zhao and Hasegawa, 1994; Abdelwahed and Zhao, 2007; Yanada *et al.*, 2010). Figures 53 and 54 show five vertical cross-sections of *P*-wave tomography down to 700-km depth under Japan. Beneath NE Japan, the mantle-wedge low-V zone is found to extend westward beneath the Japan Sea, and is not just confined to beneath the Honshu land (Fig. 53(b)). Earthquakes occur within the PHS slab down to a depth of ∼50 km under Chugoku and ∼200 km under Kyushu, whereas a high-V zone is revealed below the seismic zone in the PHS slab, which represents the aseismic portion of the PHS slab that extends down to ∼300-km depth with a dipping angle of ∼45 degrees under the Japan Sea (Fig. 53(c)) and down to ∼400-km depth under western Kyushu (Fig. 53(d)). It is not clear whether the PHS slab has subducted to a greater depth or not under the Japan Sea. Even if it has, the slab may not be detected because there are still no seismic stations installed in the Japan Sea. The PHS slab bends suddenly right beneath the Daisen volcano that is located on the Japan Sea coast (Fig. 53(c)). A prominent low-V anomaly is visible at depths of 20–50 km beneath the Daisen volcano and right above the subducting PHS slab, which may represent the arc magma under the volcano associated with the dehydration of the PHS slab (Zhao *et al.*, 2004a; Sun *et al.*, 2008).

Beneath northern Kyushu, a significant low-V zone is visible in the crust and upper-mantle wedge above the PHS slab (Fig. 53(d), 54). The low-V zone extends down to 400-km depth dipping toward the west, which is considered to be associated with the shallow and deep dehydration of the

doi:10.5047/meep.2012.00101.0001

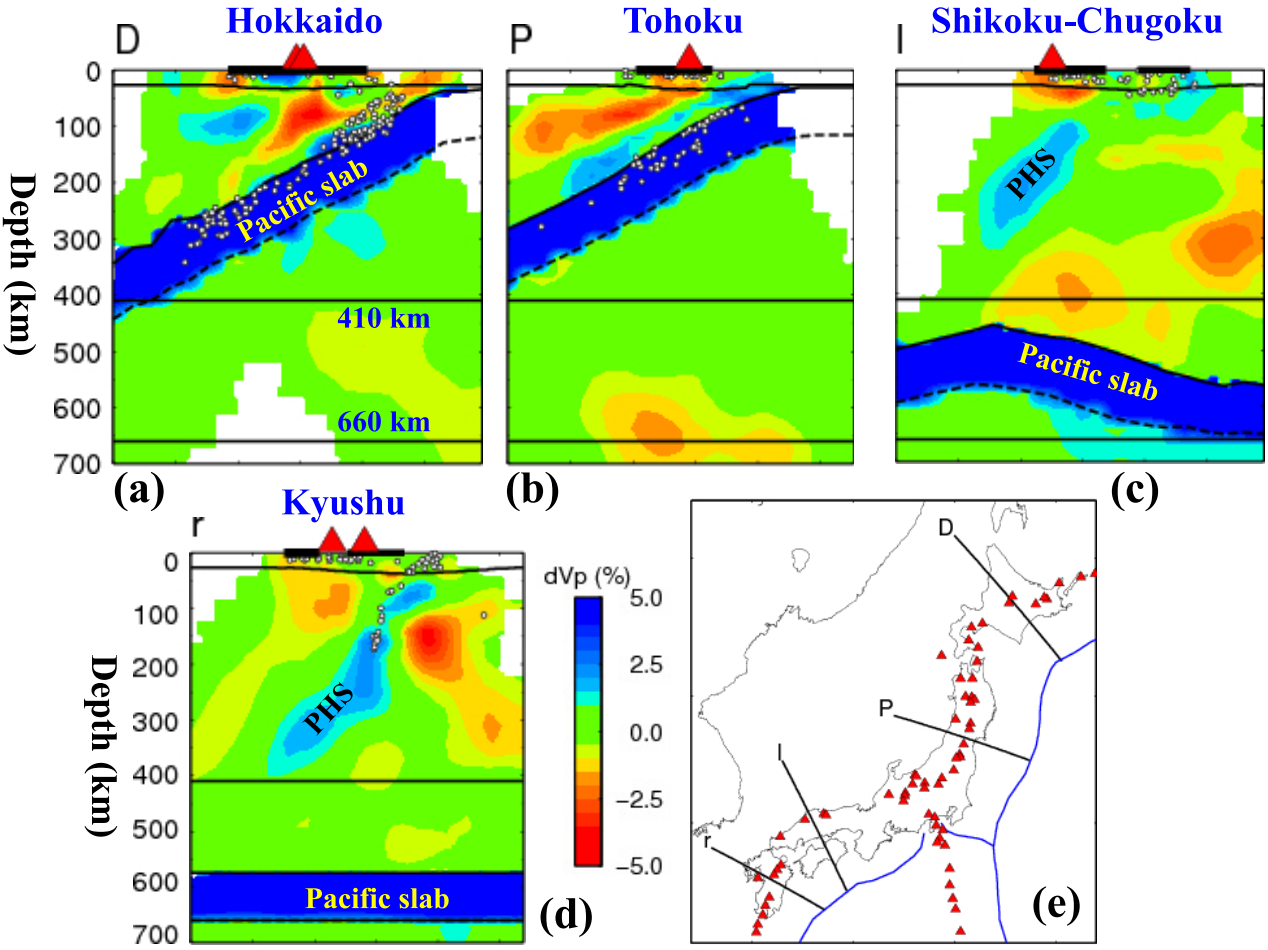

Fig. 53. Vertical cross-sections of *P*-wave tomography from 0- to 700-km depth beneath Japan (Yanada *et al.*, 2010). Location of the cross-section is shown on the inset map. Red and blue colors denote slow and fast velocities, respectively. The velocity perturbation scale is shown at the bottom. The red triangles and the thick line on the top denote active volcanoes and the land area, respectively. Earthquakes within a 30-km width from the cross-section are shown in open circles.

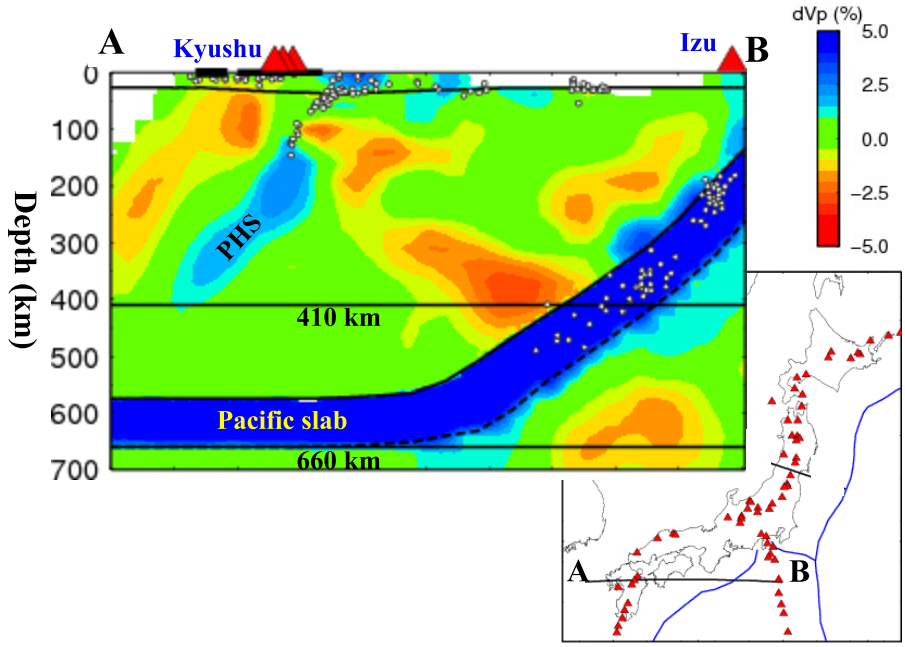

Fig. 54. The same as Fig. 53 but an east-west vertical cross-section of *P*-wave tomography from 0- to 700-km depth.

doi:10.5047/meep.2012.00101.0001

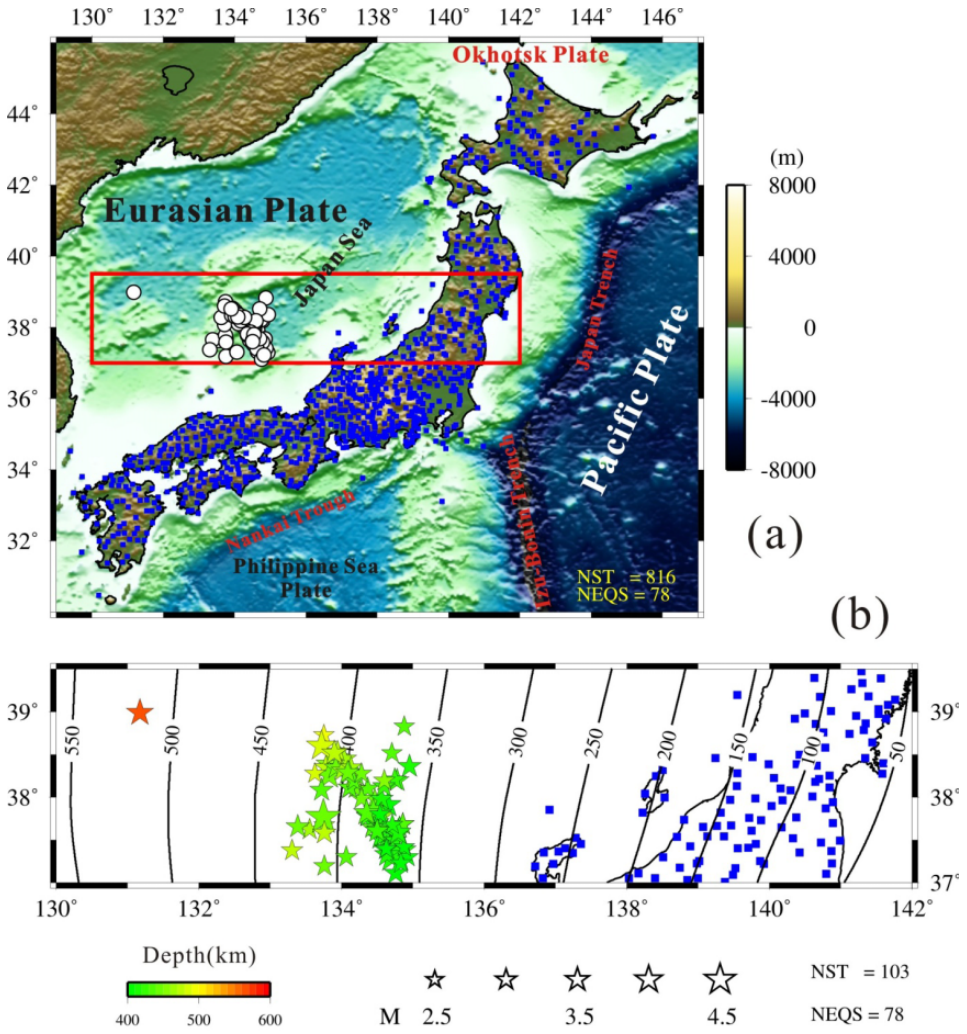

Fig. 55. (a) Tectonic background in and around the Japan Islands. The color scale shows the topography. The box outlined by the red lines represents the region shown in (b). The white circles and blue squares denote the deep earthquakes and seismic stations used, respectively. (b) Distribution of earthquakes (stars) and seismic stations (blue squares) used to calculate the RMS travel-time residuals for slab models including the metastable olivine wedge. The contour lines indicate the depth distribution of the upper boundary of the subducting Pacific plate (after Zhao *et al*., 1994, 1997b). Magnitude and depth scales of the earthquakes are shown at the bottom. NST and NEQS are abbreviations for Number of Stations and Number of Earthquakes, respectively. (Reprinted from *J. Asian Earth Sci*., *42*, Jiang, G., and D. Zhao, Metastable olivine wedge in the subducting Pacific slab and its relation to deep earthquakes, 1411–1423, Copyright 2011, with permission from Elsevier.)

PHS slab and a convective circulation process in the mantle wedge, similar to the processes occurring in the mantle wedge above the Pacific slab. These processes may have led to the formation and opening of the Okinawa Trough with its northern end at the Unzen volcano in western Kyushu.

The deep subduction of the PHS slab is also imaged by the regional tomography of East Asia (Huang and Zhao, 2006). The PHS slab is visible down to the mantle transition zone (MTZ) depths (Fig. 65). Detailed resolution analyses and synthetic tests have been conducted (Huang and Zhao, 2006; Abdelwahed and Zhao, 2007; Yanada *et al*., 2010), which have confirmed that the deep subduction of the PHS slab down to MTZ is a reliable feature.

Significant low-V anomalies are imaged between the subducting PHS slab and the Pacific slab at depths of 100 to 500 km under SW Japan (Figs. 53(c, d), 54). The low-V zones are connected with the Pacific slab, which may be caused by fluids from the deep dehydration of the Pacific slab, as well as a convective circulation process in the mantle wedge. The Pacific slab has a large subduction rate of 7–10 cm/yr at the Japan Trench, and so the slab has a lower temperature, which allows deep slab dehydration at 400–500 km depth, similar to that occurring in the subducting Pacific slab under the Tonga arc and the Lau back-arc spreading center (Zhao *et al*., 1997b; Conder and Wiens, 2006). Water transported to the deep upper mantle and the MTZ is stored in some hydrous minerals such as phase A, phase E, superhydrous phase B, phase D, and nominally anhydrous minerals such as wadsleyite and ringwoodite (Inoue *et al*., 2004; Komabayashi *et al*., 2004; Ohtani *et al*., 2004; Zhao and Ohtani, 2009). Dehydration reactions proceed by decomposition of the hydrous minerals due to the temperature increase of the stagnant slab. The decrease of the maximum water solubility in wadsleyite and ringwood-

doi:10.5047/meep.2012.00101.0001

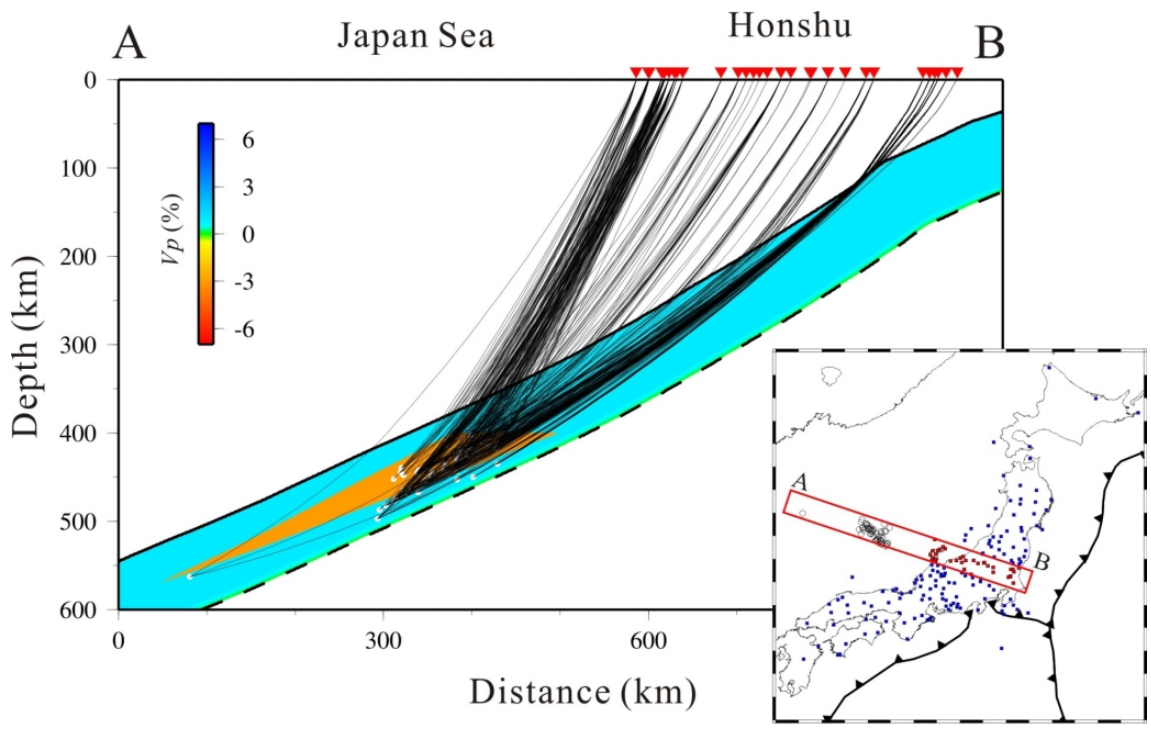

Fig. 56. *P*-wave ray paths from deep earthquakes (white dots) to seismic stations (red triangles) within the red box on the inset map. The thick black line and dashed line indicate the upper and lower boundaries of the subducting Pacific slab, respectively. The color shows *P*-wave velocity perturbations in the slab relative to an average 1-D velocity model. (Reprinted from *J. Asian Earth Sci.*, *42*, Jiang, G., and D. Zhao, Metastable olivine wedge in the subducting Pacific slab and its relation to deep earthquakes, 1411–1423, Copyright 2011, with permission from Elsevier.)

ite may also cause slab dehydration (Inoue *et al.*, 2004; Komabayashi *et al.*, 2004; Ohtani *et al.*, 2004; Zhao *et al.*, 2007b; Ohtani and Zhao, 2009).

The deep low-V zones at depths of 100–500 km between the Pacific and PHS slabs should have a higher temperature due to the corner flow in the mantle wedge above the Pacific slab. Thus, the PHS slab can be heated from below and so its brittleness is lost at a shallower depth, and so intermediate-depth earthquakes do not occur within the slab below 80-km depth under Chugoku and below 200 km under Kyushu. The heating by the hot low-V zones from below may also reduce the stiffness of the PHS slab so that the slab suddenly bends where the intraslab seismicity stops (Fig. 53(c)). The arc magma under the Daisen volcano and the PHS slab dehydration may also contribute to the softening of the slab because the bending occurs right beneath the Daisen volcano (Zhao *et al.*, 2004a; Fig. 53(c)).

A dipping low-V zone is visible at depths of 80–300 km above the Pacific slab and beneath the active volcanoes in the Izu-Bonin arc (Fig. 54), which represents the upwelling flow in the central part of the mantle wedge, similar to that under Hokkaido and NE Japan (Fig. 53(a, b)). Another low-V anomaly is visible at 80–250 km depth directly beneath the PHS slab (Figs. 53(d), 54), which may reflect an upwelling flow from the deep part of the mantle wedge bumping the PHS slab from below, which may have changed the PHS slab geometry and affected the cut-off depth of seismicity in the PHS slab.

10. Metastable Olivine Wedge and Deep Earthquakes

Although deep earthquakes constitute only a few percent of global seismic activity, estimated from either the number of earthquakes or seismic moments, they can provide direct information on the thermal, thermodynamic, and mechanical properties inside the subducting slab (Kirby *et al.*, 1996). However, the mechanism of deep earthquakes is a subject of debate, and several models have been proposed, including dehydration embrittlement (Raleigh and Paterson, 1965), transformational faulting of olivine (Green and Burnley, 1989; Green and Houston, 1995; Green, 2003), and adiabatic shear instability (Hobbs and Ord, 1988; Karato *et al.*, 2001). The second model (i.e., transformational faulting of olivine) seems more popular than the other hypotheses because it was recognized early on that the deepest earthquakes occur in the mantle transition zone (Green and Houston, 1995).

Using travel-time residuals from deep earthquakes, Iidaka and Suetsugu (1992) showed the presence of a metastable olivine wedge (MOW) with a depth of about 550 km inside the subducting Pacific slab beneath the Izu-Bonin region, and they suggested that the occurrence of deep earthquakes is related to the MOW in the Pacific slab. Koper *et al.* (1998) investigated this issue for the subducting slab in the Tonga region, but they failed to detect a MOW in the Tonga slab. Kaneshima *et al.* (2007) and Kubo *et al.* (2009) revealed a MOW of 5% low-velocity relative to the iasp91 Earth model (Kennett and Engdahl, 1991) inside the subducting Mariana slab.

doi:10.5047/meep.2012.00101.0001

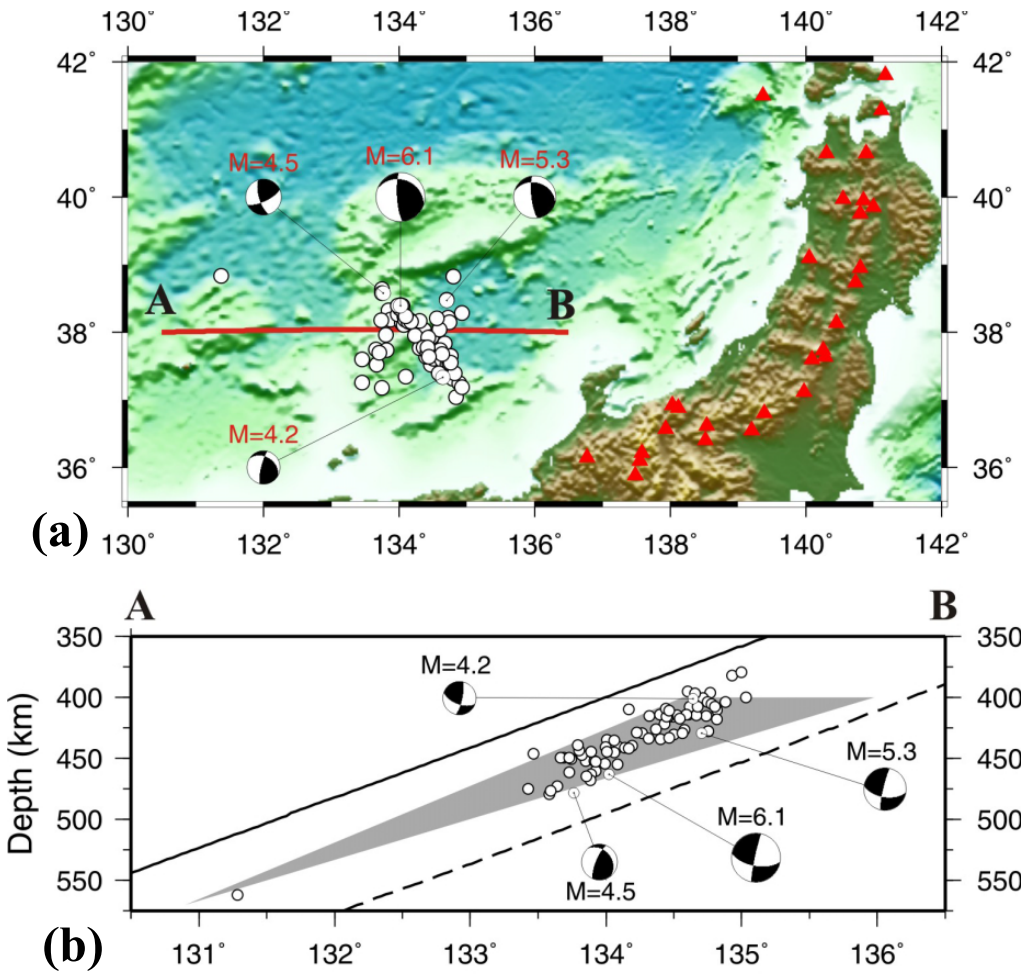

Fig. 57. (a) Epicenter locations of the 78 deep earthquakes used. Focal mechanism solutions (lower-hemisphere projection) of four earthquakes are also shown, whose sizes are proportional to their magnitudes shown above each beach ball. The black portions in each beach ball denote the compressional area. The red triangles represent the active volcanoes. (b) Vertical cross-section of the relocated 78 earthquakes and the focal mechanism solutions of four earthquakes in the optimal slab model along the line A–B. The solid and dashed lines denote the upper and lower boundaries of the Pacific slab. The grey triangle in the slab represents the optimal MOW model. (Reprinted from *J. Asian Earth Sci.*, *42*, Jiang, G., and D. Zhao, Metastable olivine wedge in the subducting Pacific slab and its relation to deep earthquakes, 1411–1423, Copyright 2011, with permission from Elsevier.)

Jiang *et al*. (2008) and Jiang and Zhao (2011) studied the fine structure of the subducting Pacific slab under the Japan Sea using a large number of high-quality arrival-time data from deep earthquakes under the Japan Sea and the East Asian margin recorded by the dense seismic network of the Japan Islands (Fig. 55). They detected a low-V finger within the subducting Pacific slab in the MTZ depth under the Japan Sea, which is interpreted to be a MOW (Fig. 56). They carefully relocated the deep earthquakes using the final slab model and found that all the deep earthquakes are located within the MOW or along its edges (Fig. 57), suggesting that the occurrence of deep earthquakes is related to the fine structural heterogeneity and phase changes in the subducting slab, as suggested by earlier studies (e.g., Kirby, 1991; Green and Houston, 1995).

The MOW is a tiny feature in the subducting slab, and the resolution of current tomography under the Japan Sea is still too low to image such a small feature because of the lack of seismic stations in the Japan Sea (e.g., Abdelwahed and Zhao, 2007; Yanada *et al*., 2010). Hence, so far seismologists have adopted forward-modeling approaches to investigate the MOW structure. In future studies, it would be ideal to detect the MOW by tomographic imaging when a dense OBS network is installed in the marginal sea (e.g., the Japan Sea) above the deep earthquakes.

11. The Pacific Slab Edge under Kamchatka

The Kamchatka peninsula is located at the northwestern edge of the Pacific Ocean (Fig. 58(a)). The Pacific plate, of Cretaceous age, is subducting beneath the Kamchatka arc and moving along the strike-slip Bering fault at 7.7 cm/yr at 55°N to 8.3 cm/yr at 47°N (DeMets *et al*., 1990; Steblov *et al*., 2003). Geological studies showed that the volcanism and convergence in Kamchatka ceased about 55 Ma ago, but resumed about 30 Ma ago (Watson and Fujita, 1985). About 10 Ma ago, island-arc magmatism extended to the north of the Aleutian-Kamchatka junction along the mid-Kamchatka volcanic belt, but it is now extinct (Honthaas *et al*., 1995). A chain of active volcanoes, Holocene in age, along the eastern coast of Kamchatka are underlain by about a 100-

doi:10.5047/meep.2012.00101.0001

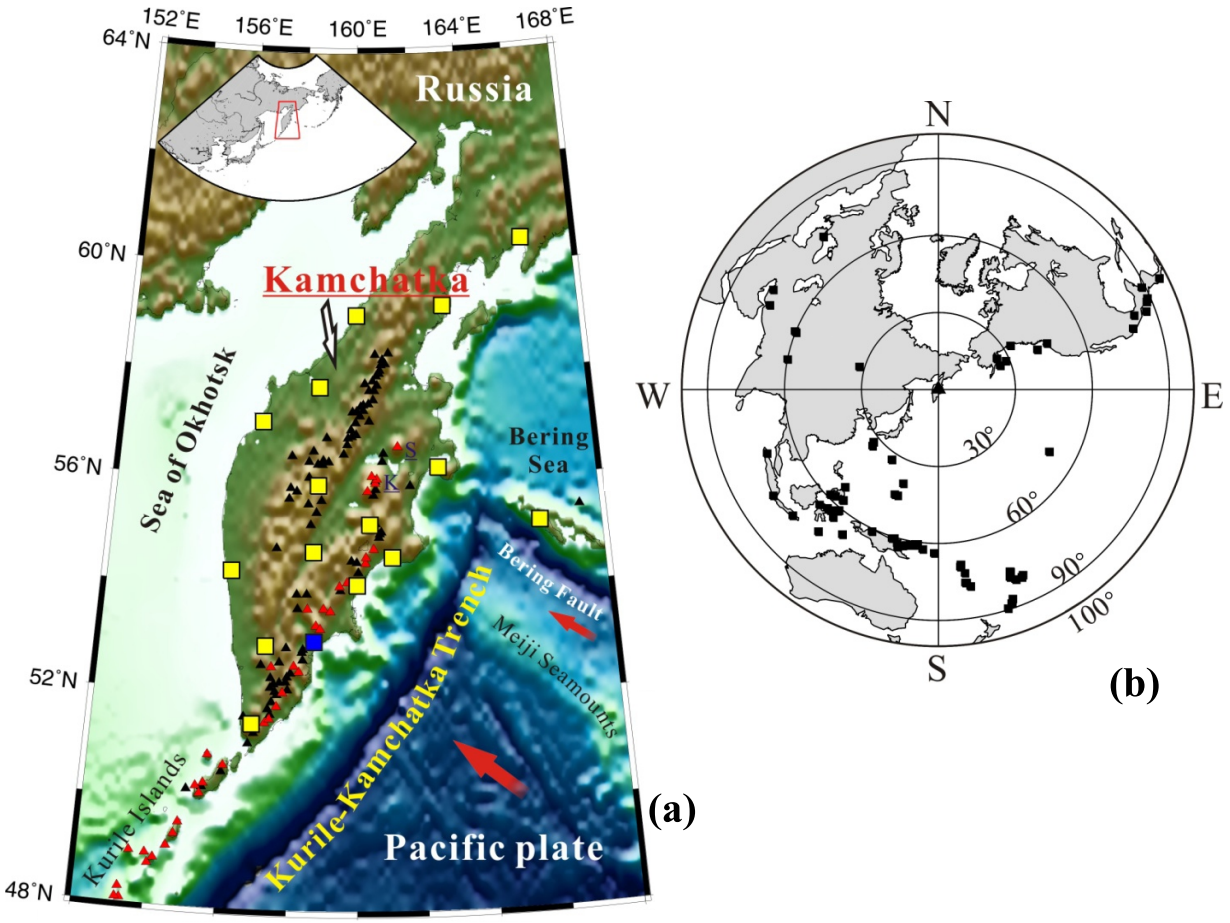

Fig. 58. (a) Map of the Kamchatka region with surface topography shown in colors. Yellow squares show the locations of 15 portable seismic stations. The blue square denotes a permanent seismic station. Red arrows denote the direction of motion of the Pacific plate subducting along the Kurile-Kamchatka trench and transcurrent motion along the Bering Fault. Red and black triangles represent the active and inactive volcanoes, respectively. S, Sheveluch volcano; K, Klyuchevskoy volcano. The inset map shows the location of the tomographic study area. (b) Epicentral locations of 75 teleseismic events (squares) used in the tomographic imaging. The triangle denotes the center of Kamchatka. (Reprinted from *Tectonophysics*, *465*, Jiang, G., D. Zhao, and G. Zhang, Seismic tomography of the Pacific slab edge under Kamchatka, 190–203, Copyright 2009, with permission from Elsevier.)

km depth-contour of the subducting Pacific slab (Gorbatov *et al*., 1997). The Sheveluch and Klyuchevskoy volcanoes have shifted northwestward from the volcanic front. Between 54°N and 55°N, the Meiji seamounts, the northernmost segment of the Hawaii-Emperor seamount chain, enter the Kamchatka trench (Fig. 58(a)). The configuration of the Pacific slab under the Kamchatka region was studied using the distribution of intermediate-depth and deep earthquakes occurring in the slab, which shows that the dipping angle of the slab decreases northward from about 55° to 35° (Gorbatov *et al*., 1997). The maximum depth of earthquakes becomes shallower along the subduction zone from ~600 km beneath southern Kamchatka to ~100–200 km near the junction (Davaille and Lees, 2004).

The 3-D upper mantle structure under the Kamchatka peninsula has been investigated by several researchers to date. Gorbatov *et al*. (1999) applied the tomographic method of Zhao *et al*. (1992b) to determine a 3-D P-wave velocity model down to a depth of 200 km, and their results showed a prominent low-V anomaly beneath the volcanic front and a high-V zone corresponding to the subducted Pacific slab. But their study region was in the southeastern Kamchatka arc, because of the distribution of seismic stations then available. Levin *et al*. (2002) determined a surface-wave tomography down to 200-km depth, which shows that the subducting Pacific slab terminates at the Aleutian-Kamchatka junction and no relict slab underlies the extinct northern Kamchatka volcanic arc. Lees *et al*. (2007) determined P-wave teleseismic tomography, revealing that the depth of the subducting slab under Kamchatka shoals toward the north, and they considered thermal ablating related to the asthenosphere as a possible cause for the feature.

Jiang *et al*. (2009) determined a 3-D P-wave velocity model of the mantle down to 700-km depth under the Kamchatka peninsula using arrival-time data collected from digital seismograms of 75 teleseismic events recorded by 15 portable seismic stations and 1 permanent station in Kamchatka (Fig. 58). The data used have a very good ray path coverage under Kamchatka Peninsula (Fig. 59), resulting in a reliable tomographic image under the region (Fig. 60). The subducting Pacific slab is imaged clearly and is visible in the upper mantle and extends down to the 660-

doi:10.5047/meep.2012.00101.0001

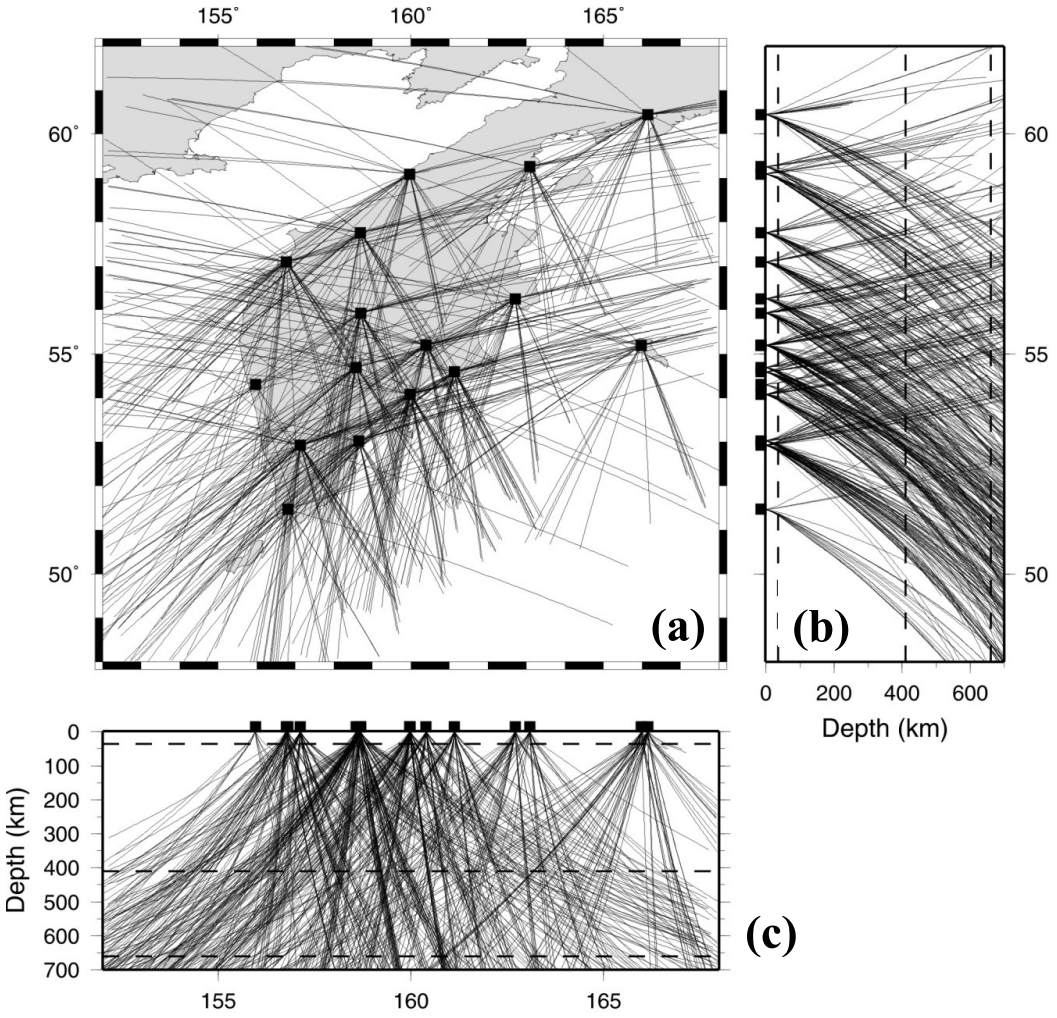

Fig. 59. Distribution of P-wave ray paths in plan view (a) and in north-south (b) and east-west (c) vertical cross-sections. Squares denote the 16 seismic stations used. The dashed lines in panels (b) and (c) denote the Moho, 410-km and 660-km discontinuities, respectively. (Reprinted from *Tectonophysics*, *465*, Jiang, G., D. Zhao, and G. Zhang, Seismic tomography of the Pacific slab edge under Kamchatka, 190–203, Copyright 2009, with permission from Elsevier.)

km discontinuity under southern Kamchatka, while the slab shortens toward the north and terminates near the Aleutian-Kamchatka junction (Figs. 60, 61). Low-V anomalies are visible beneath northern Kamchatka and under the junction (Fig. 60(e–h)), which are interpreted as asthenospheric flow. Beneath the active arc volcanoes in Kamchatka, however, low-V zones are not revealed clearly in the crust and uppermost mantle as are those under the Japan Islands, because only teleseismic data were used in the tomographic imaging and so the shallow structure was not well resolved.

Shear-wave splitting studies suggested that a trench-parallel strain follows the seismogenic Wadati-Benioff zone, but rotates to become trench-normal beyond the slab edge (Peyton *et al*., 2001; Portnyagin *et al*., 2005), indicating that the asthenospheric flow passes through a slab window beneath the junction. In addition, thermal modeling of the reheating of a torn slab shows that the Pacific plate was already thinner well before its entering of the trench due to delayed thickening of the lithosphere below the Meiji-Hawaiian hotspot (Davaille and Lees, 2004).

Figure 61 schematically depicts the main seismological results under Kamchatka. Based on the tomographic image and other geological and geophysical results, it is considered that the slab loss under northern Kamchatka was induced by friction between the slab and the surrounding asthenosphere as the Pacific plate rotated clockwise about 30 Ma ago, and then it was enlarged by the slab-edge pinch-off by the asthenospheric flow and the presence of Meiji seamounts (Jiang *et al*., 2009). As a result, the slab loss and the subducted Meiji seamounts have jointly caused the Pacific plate to subduct under Kamchatka with a smaller dip angle near the junction, which made the Sheveluch and Klyuchevskoy volcanoes shift westward (for details, see Davaille and Lees, 2004; Jiang *et al*., 2009).

12. Subduction and Dehydration of Continental Plates

A high-resolution P-wave tomography of the crust and upper mantle under Taiwan was determined by using a large number of data from local, regional and teleseismic events

doi:10.5047/meep.2012.00101.0001

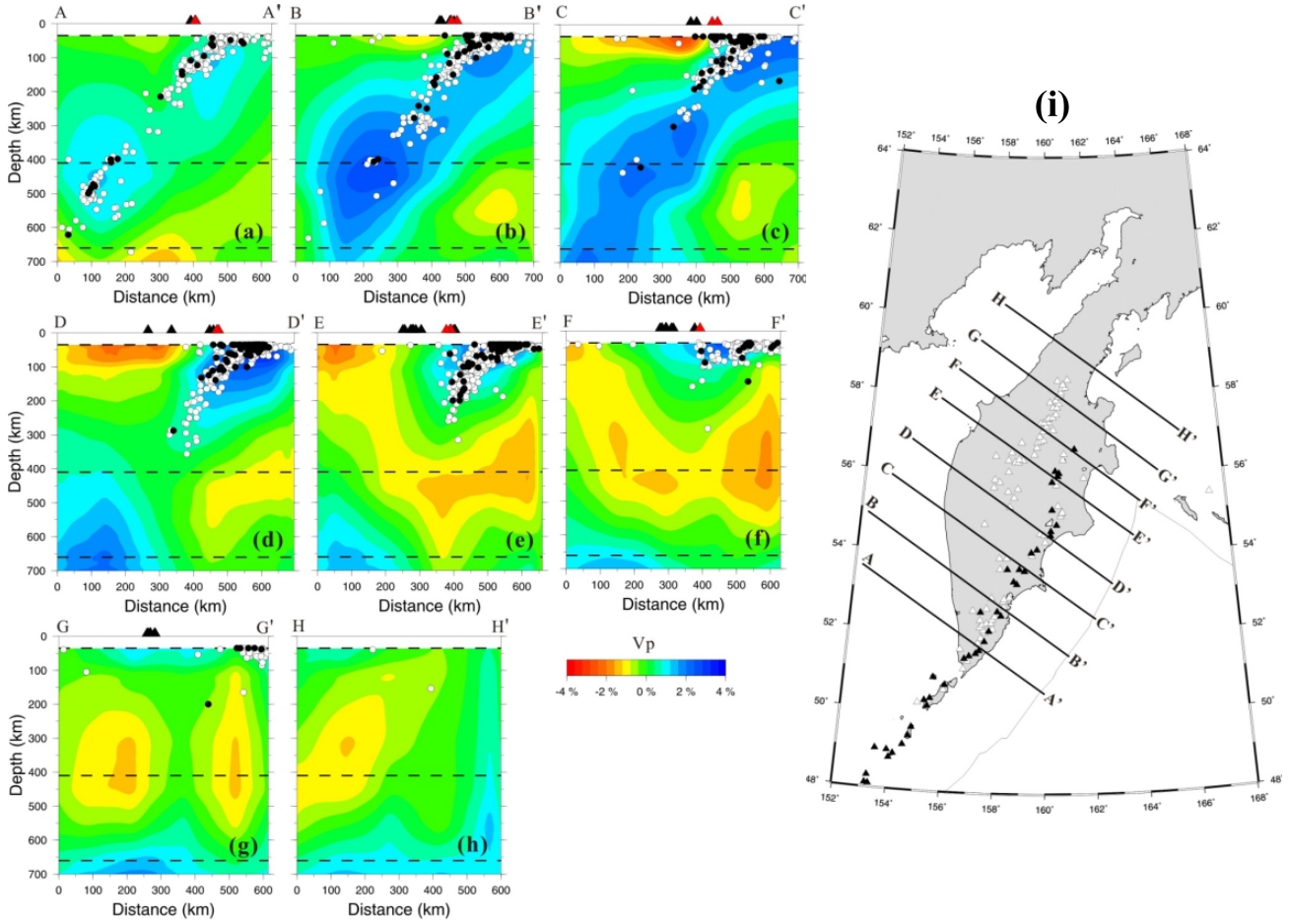

Fig. 60. (a–h) Vertical cross-sections of P-wave velocity images of the Kamchatka subduction zone. The locations of the cross-sections are shown in (i). Red and blue colors denote slow and fast velocities, respectively. The velocity perturbation scale is shown below (f). Black and red triangles denote inactive and active volcanoes within a 30-km width of each profile, respectively. White dots indicate earthquake hypocenters within a 30-km width of each cross-section (the hypocenter parameters are obtained from the IRIS web site), while black dots show the relocated hypocenters which are more accurate. The three dashed lines denote the Moho, 410-km and 660-km discontinuities, respectively. The black and white triangles in (i) denote active and inactive volcanoes, respectively. (Reprinted from *Tectonophysics*, *465*, Jiang, G., D. Zhao, and G. Zhang, Seismic tomography of the Pacific slab edge under Kamchatka, 190–203, Copyright 2009, with permission from Elsevier.)

simultaneously (Wang *et al*., 2006). A high-V zone was revealed from the surface down to a depth of 300 km under South Taiwan, which is interpreted to be the subducted Eurasian lithosphere (Fig. 62). This tomographic result implies that the tectonic framework of Taiwan has changed from subduction in the south to collision in the north, supporting a previous tectonic model proposed by Lallemand *et al*. (2001) (Fig. 62(d)). The subducted Eurasian lithosphere colliding with the subducting PHS slab may have contributed to mountain building, active seismicity, and crustal deformation in and around Taiwan. Significant low-V anomalies are visible above the subducted Eurasian lithosphere (Fig. 62(a)) and between the Eurasian lithosphere and the PHS slab down to ∼230-km depth (Fig. 62(b)). The low-V zones are connected with a volcano on the surface (Fig. 62(b)). We consider that at least part of the low-V anomalies is associated with the dehydration processes of the PHS slab, as well as the subducted Eurasian plate.

The subducting Indian plate is imaged clearly beneath the Tibetan Plateau by inverting teleseismic data recorded by the portable seismic stations deployed to date in the Tibetan Plateau (Zheng *et al*., 2007; He *et al*., 2010) (Fig. 63). Two low-V zones are visible in the crust and mantle wedge above the subducting Indian slab, which may represent high-temperature anomalies or partial melts associated with the corner flow and slab dehydration processes, similar to the formation of arc magmas in Japan, though the slab is a subducting continental (Indian) plate. In the Tibetan Plateau, there is no prominent volcano, but geothermal anomalies exist there extensively (Liu, 1999). The dehydration of the subducting continental plate may not be as much as that of a subducting oceanic plate, and the crust is too thick in Tibet so that melts in the upper mantle wedge cannot reach the surface easily, hence active volcanoes are not produced in the Tibetan Plateau. Recent body-wave and surface-wave tomographic studies show similar results (e.g., Zhou and Murphy, 2005; Chen *et al*., 2009).

Tengchong is an active intraplate volcano located at the boundary between China and Burma (see the inset maps in Figs. 64 and 65 for its location in SW China). A promi-

doi:10.5047/meep.2012.00101.0001

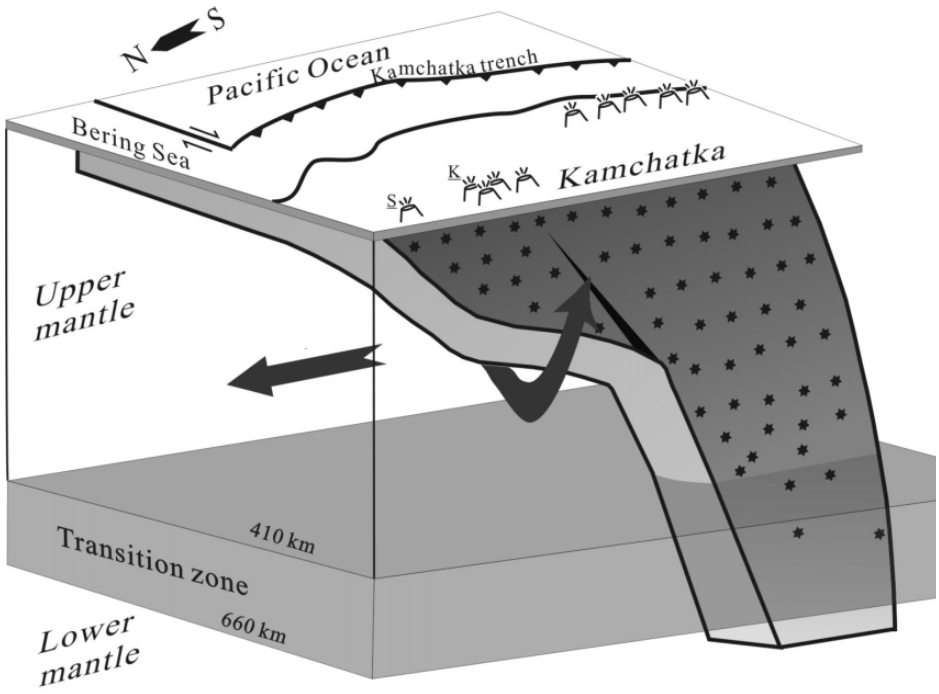

Fig. 61. A perspective image showing the Pacific plate subducting to the west through the mantle transition zone beneath Kamchatka. The uppermost thin board represents the crust. Asterisks indicate the seismicity (schematically) which shoal toward the north beneath Kamchatka. S, Sheveluch volcano; K, Klyuchevskoy volcano. (Reprinted from *Tectonophysics*, *465*, Jiang, G., D. Zhao, and G. Zhang, Seismic tomography of the Pacific slab edge under Kamchatka, 190–203, Copyright 2009, with permission from Elsevier.)

nent low-V zone is revealed down to 300-km depth under the volcano (Fig. 65(b)). The subducting Burma microplate (part of the Indian plate) is clearly imaged as a high-V zone under Tengchong, and intermediate-depth earthquakes occur down to 200-km depth within the high-V zone (Huang and Zhao, 2006). Lei *et al*. (2009) determined a high-resolution P-wave tomography of the crust and upper mantle down to 650-km depth under the Tengchong volcano using a large number of arrival-time data from local and teleseismic events recorded by a new digital seismic network consisting of 35 seismic stations in Yunnan Province, SW China. A clear low-V zone with a width of about 100 km is revealed under the Tengchong volcano down to 410-km depth, and the low-V zone extends toward the east in the depth range of 250–410 km. High-V anomalies are revealed in the MTZ under Tengchong. These local and regional tomographic results suggest that the origin of the Tengchong volcanism is related to the deep subduction and dehydration of the Burma microplate (or the Indian plate) (Huang and Zhao, 2006; Lei *et al*., 2009; Zhao and Liu, 2010).

These tomographic results (Figs. 62, 63, 65) suggest that dehydration may also take place after a continental plate subducts into the upper mantle, which may have contributed to the formation of the active intraplate volcanoes and geothermal anomalies in those continental areas. Water can be transported into the deep upper mantle and the MTZ also by subduction of the continental plate, since there are several minerals that can transport water into the deep mantle (Zhao and Ohtani, 2009). The dehydration of the hydrous minerals in the mafic component of the continental lower crust such as amphibole, chlorite, zoisite, lawsonite and phengite occurs in the upper mantle, whereas the hydrous minerals in the acidic component of the continental upper crust such as phengite, topaz-OH and phase egg dehydrate in the deep upper mantle and the MTZ (e.g., Ono, 1998; Schmidt and Poli, 1998; Ohtani, 2005). Dehydration of these minerals can cause the low-V anomalies in the upper mantle above the subducting continental plate (Zhao and Ohtani, 2009).

13. Stagnant Slab and Big Mantle Wedge

A high-resolution P-wave tomography down to 1300-km depth under the entire East Asia is determined by applying a mantle tomography method (Zhao, 2001c) to about one million arrival-time data of P, pP, PP and PcP waves from 19,361 earthquakes recorded by 1012 seismic stations in the East Asian region (Huang and Zhao, 2006) (Figs. 64, 65). At depths of 15 to 300 km, the most significant features in East Asia are the high-V anomalies corresponding to the subducting Pacific and Philippine Sea slabs. The location of the high-V zones migrates gradually toward the west with increasing depth, generally parallel to the oceanic trenches. Almost all of the intermediate-depth and deep earthquakes are located in the high-V zones. Under the Philippine Sea and between the subducting Pacific and Philippine Sea slabs, clear low-V anomalies are visible from 15- to 900-km depth (Fig. 65). The low-V zone in the upper mantle may represent the hot mantle wedge under the Izu-Mariana arc and back-arc, where fluids from the dehydration of the Pacific slab and corner flow in the mantle wedge result in magma and lead to

doi:10.5047/meep.2012.00101.0001

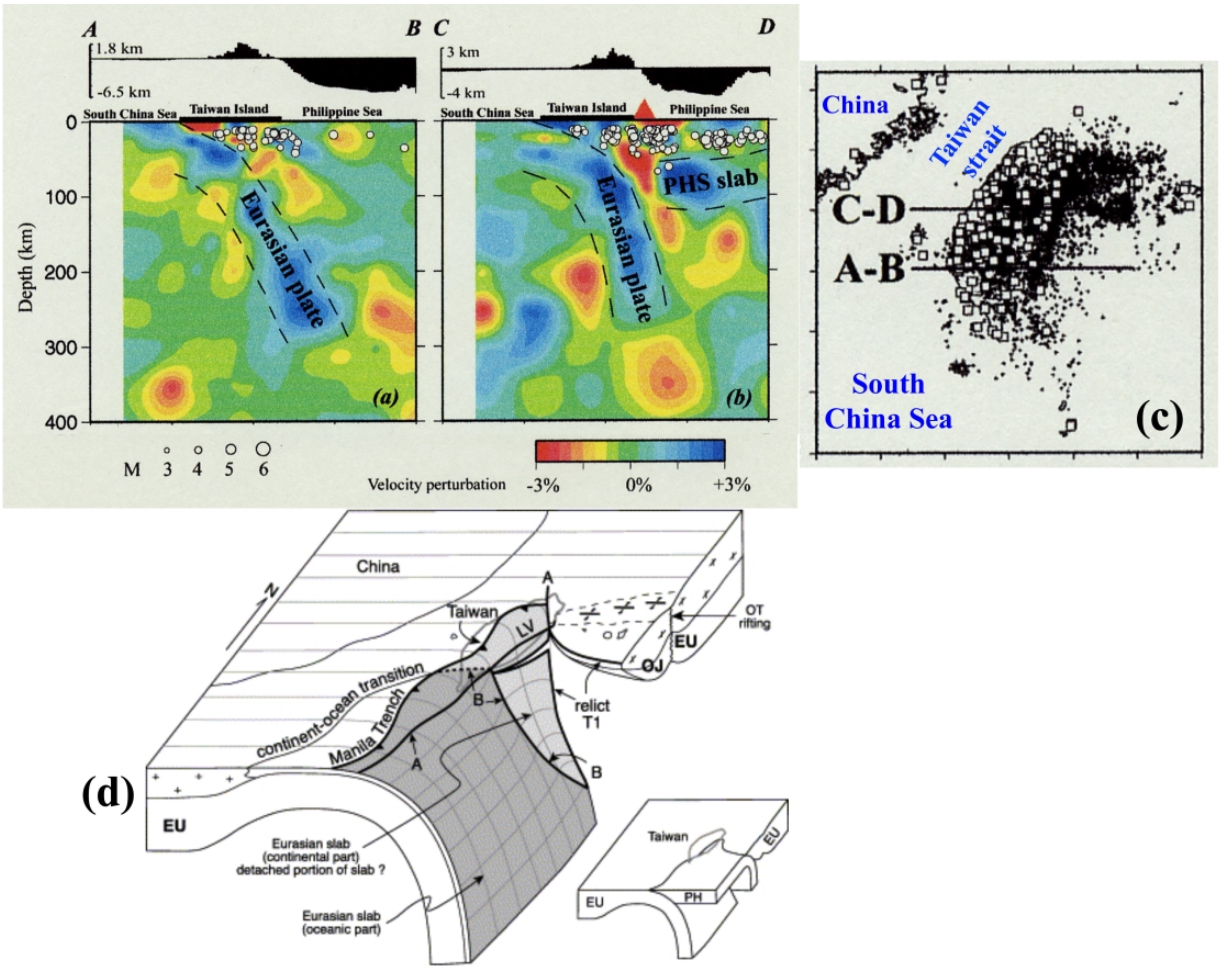

Fig. 62. (a, b) East-west vertical cross-sections of P-wave tomography from 0- to 400-km depth beneath South Taiwan determined by Wang *et al*. (2006). Locations of the cross-sections are shown in (c). Red and blue colors denote slow and fast velocities, respectively. The velocity perturbation scale is shown below (b). The red triangle and the thick lines on the top denote a volcano and the land area, respectively. Earthquakes within a 30-km width from each profile are shown in white dots. (d) Schematic diagram showing the major tectonic features in and around Taiwan. (Reprinted from *Tectonophysics*, *335*, Lallemand, S., Y. Font, H. Bijwaard, and H. Kao, New insights on 3-D plate interaction near Taiwan from tomography and tectonic implications, 229–253, Copyright 2001, with permission from Elsevier.)

the formation of active volcanoes in the Izu-Mariana arc and back-arc, as well as back-arc spreading, similar to the structure and process under the Tonga arc and Lau back-arc basin (Zhao *et al*., 1997b). The low-V zone in the lower mantle under the Philippine Sea may represent the hot upwelling flow associated with the deep subduction of the Pacific slab under Mariana and deep subduction of the Eurasian plate under the Philippine Trench (see figure 6 in Huang and Zhao, 2006).

Under SW China, high-V anomalies corresponding to the subducting Indian plate are visible down to about 300-km depth (Fig. 65). The location of the slab moves gradually toward the north and its northern edge reaches the Qiangtang block (see figure 8(e) in Huang and Zhao, 2006). Some high-V anomalies exist down to 1000-km depth or even deeper under India (Fig. 65), which might be pieces of the old Tethyan slab collapsing down to the lower mantle (Van der Voo *et al*., 1999; Zhou and Murphy, 2005).

Significant low-V anomalies exist in the upper mantle under the Japan Islands, the marginal seas in the Western Pacific, and eastern China, and the low-V zones extend gradually toward the west with increasing depth (Fig. 64). Such a wide extent of the low-V zones under eastern China is consistent with suggestions about the thinning of the lithosphere under eastern China (Menzies *et al*., 2007). Under the intraplate volcanic areas such as Changbai, Datong and Tengchong, low-V zones exist from the surface down to 200–300 km depth.

At the MTZ depths (410–660 km), broad high-V anomalies are visible under eastern China, which show images of the stagnant Pacific slab in the MTZ (Fukao *et al*., 1992; Zhao, 2004; Zhao *et al*., 2009b). In the uppermost lower mantle, the high-V anomalies become less prominent under eastern China, but still visible under Izu-Mariana, the Philippine arc, SW China, and India.

In the Asian continent, there are several prominent active volcanoes, such as the Changbai and Wudalianchi volcanoes in NE China, the Tengchong volcano in SW China, and the Hainan volcano in southernmost China (Hainan Island) (Fig. 64(c)). Recent seismic studies have shed new light on the origin of these intraplate volcanoes (Zhao and Liu, 2010).

doi:10.5047/meep.2012.00101.0001

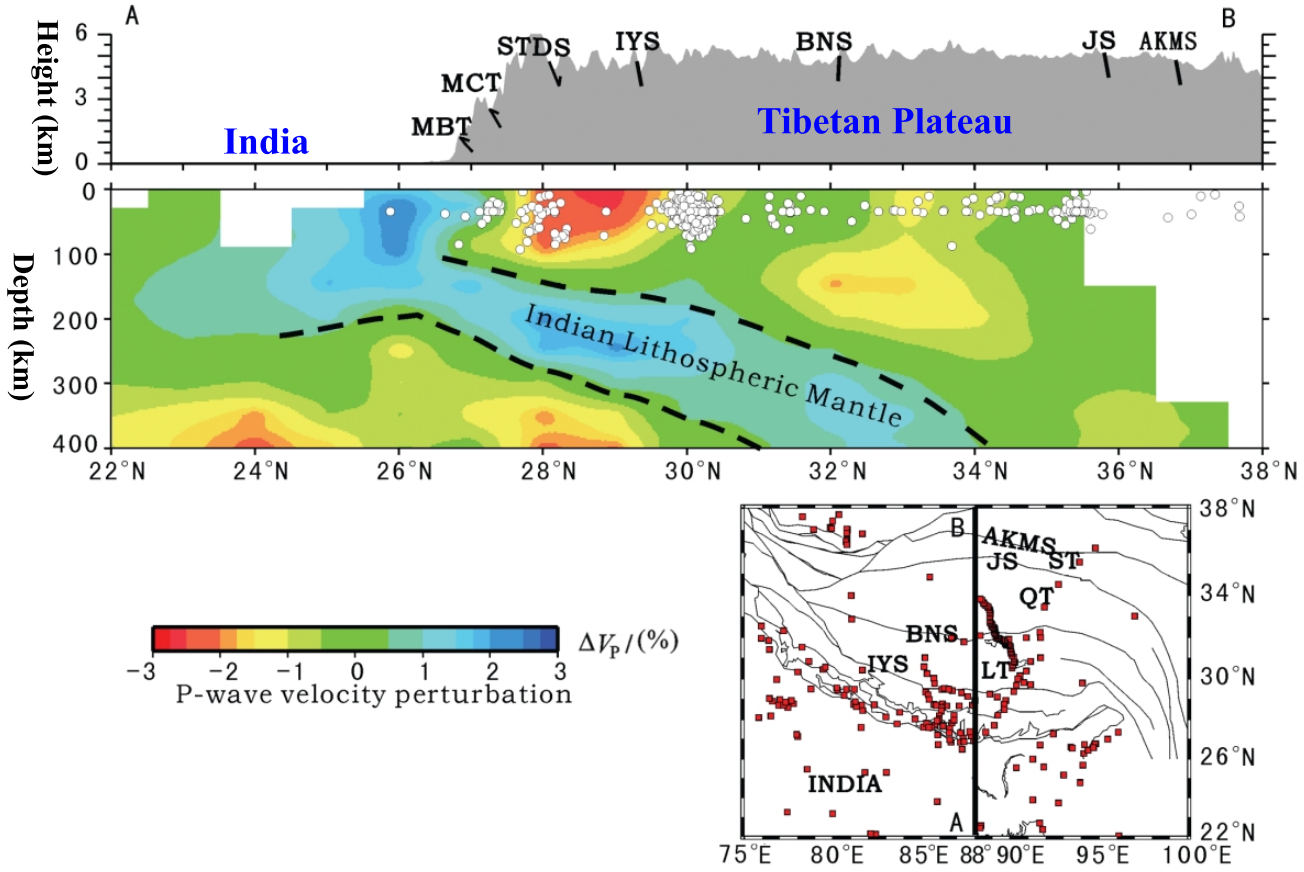

Fig. 63. North-South vertical cross-section of P-wave tomography under the Tibetan Plateau. The location of the cross-section is shown on the inset map. Red and blue colors denote slow and fast velocities, respectively. The velocity perturbation scale is shown at the bottom. White dots denote earthquakes that occurred within 100 km of the profile. The red squares on the map show the portable seismic stations used for the tomographic imaging. (From Zheng *et al*., 2007.)

A detailed 3-D P-wave tomography of the crust and upper mantle beneath the Changbai volcano in NE China was determined by using a large number of arrival-time data from local earthquakes and teleseismic events that were recorded by 645 permanent seismic stations in China and 19 portable stations around the Changbai volcano (Zhao *et al*., 2009b) (Fig. 66). The result shows a clear low-V anomaly extending down to 410-km depth under the Changbai volcano. A high-V anomaly is visible in the MTZ, and deep earthquakes occur at depths of 500–600 km within the high-V zone, suggesting that the stagnant Pacific slab exists under the Changbai region (Fig. 66). This high-resolution tomography under Changbai has greatly improved the previous results for this region (Zhao *et al*., 2004b; Lei and Zhao, 2005). The distribution of seismic stations is very sparse in the Wudalianchi area, hence the tomographic image under Wudalianchi has a lower resolution (e.g., Duan *et al*., 2009). Global tomography (Zhao, 2004, 2009) shows that the overall features of mantle structure under the Wudalianchi volcano are similar to that under the Changbai volcano (No. 25 in Fig. 70), suggesting that the two intraplate volcanoes may have the same origin.

The stress regime in the subducting Pacific slab was investigated by using focal-mechanism solutions of intermediate-depth and deep earthquakes under the Japan Sea and the East Asian margin (Zhao *et al*., 2009b). The result shows that the compressional-stress axes of almost all deep earthquakes are nearly parallel with the down-dip direction of the slab, indicating that the Pacific slab is under a compressional-stress regime in the depth range of 200 to 600 km. It was suggested that such a stress regime in the slab is caused by the slab meeting strong resistance at the 660-km discontinuity, consistent with seismic tomography results (Fig. 64). Ichiki *et al*. (2006) studied the electric-conductivity structure under East Asia, and their results suggest that the asthenosphere under East China is both hot and wet, being associated with the deep dehydration of the stagnant Pacific slab.

A big mantle wedge (BMW) model was proposed to explain the intraplate magmatism and mantle dynamics under East Asia based on the multiscale tomographic images (Zhao *et al*., 2004b, 2007b; Lei and Zhao, 2005) (Fig. 67). It is considered that the upper mantle above the stagnant slab has formed a BMW under East Asia, and corner flow in the BMW, and fluids from deep slab dehydration and/or brought down from the shallow mantle wedge by convection, cause an upwelling of hot asthenospheric materials, resulting in a thinning and fracturing of the lithosphere under Eastern China. The formation of active intraplate volcanism

doi:10.5047/meep.2012.00101.0001

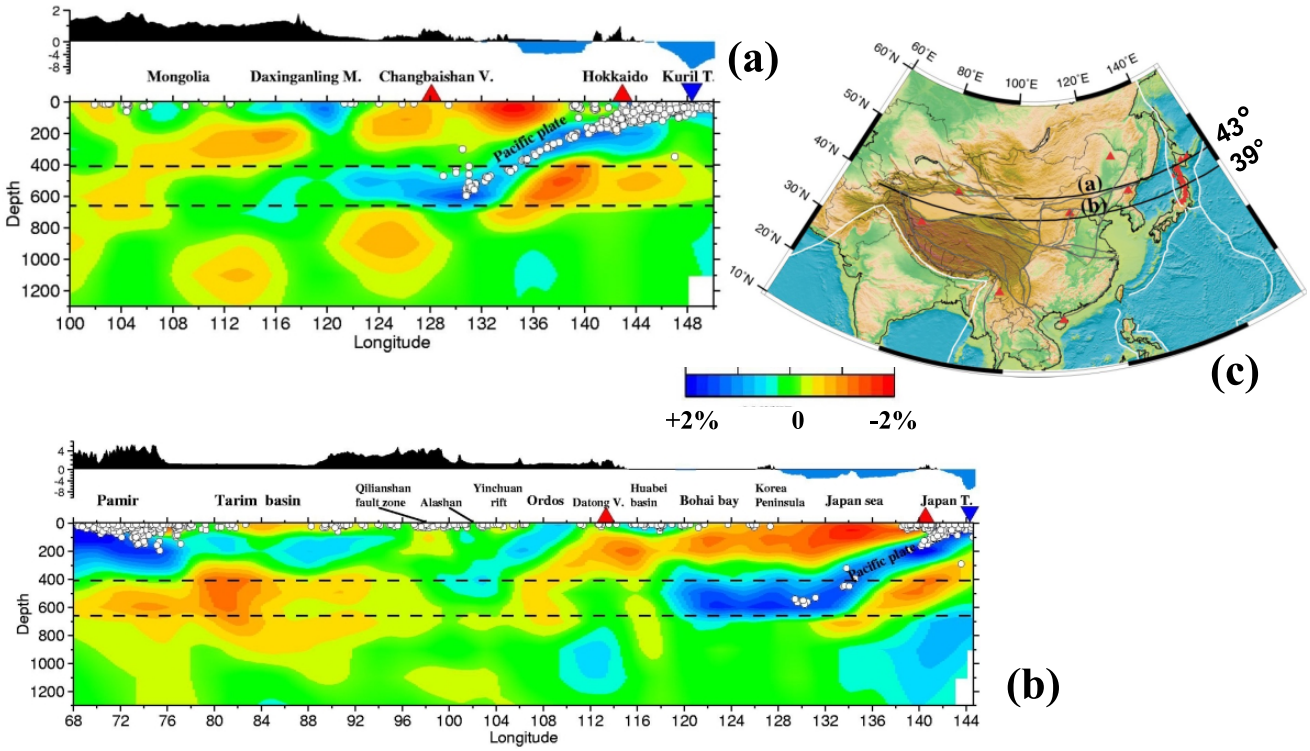

Fig. 64. (a, b) East-west vertical cross-sections of P-wave tomography along the two profiles shown on the inset map (c). Red and blue colors denote low and high velocities, respectively. The velocity perturbation scale is shown above (b). The white dots show earthquakes that occurred within 100 km of each profile. The two dashed lines denote the 410-km and 670-km discontinuities. (Modified from Huang and Zhao, 2006.)

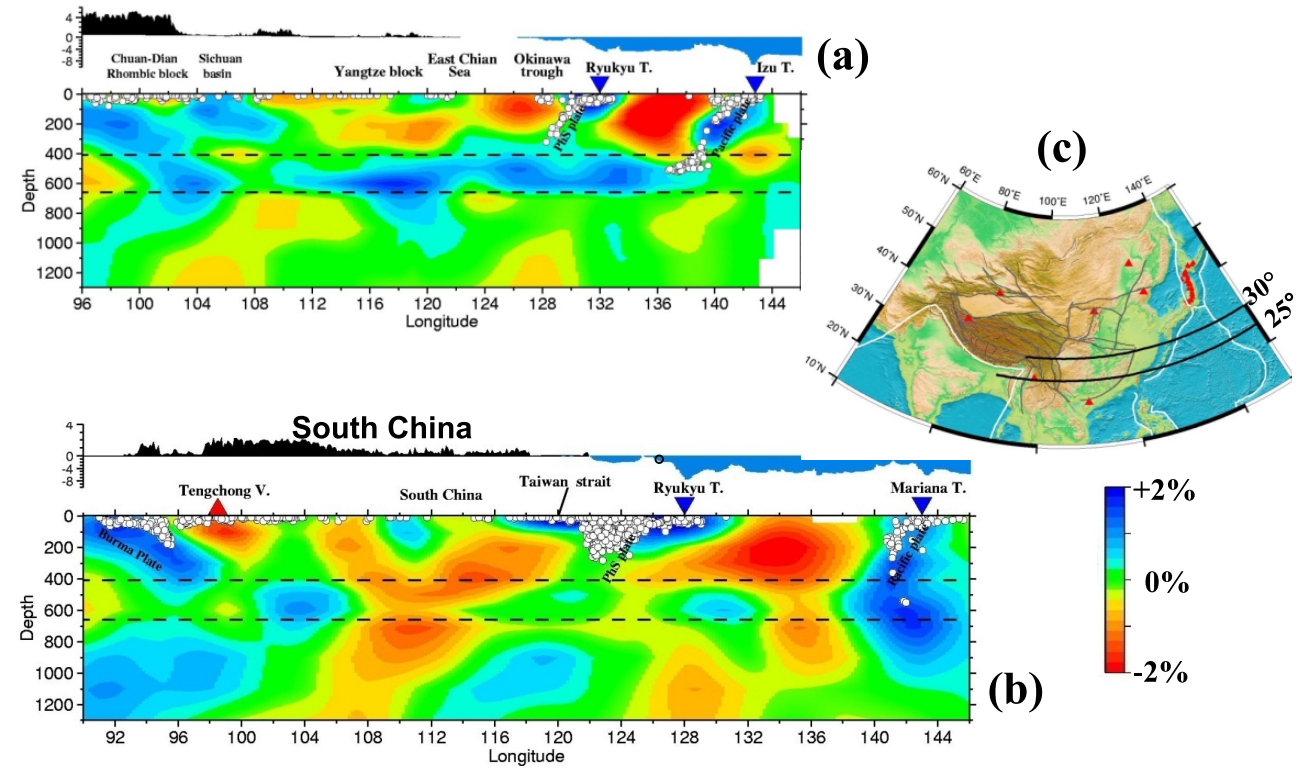

Fig. 65. The same as Fig. 64 but for two other vertical cross-sections. (Modified from Huang and Zhao, 2006.)

doi:10.5047/meep.2012.00101.0001

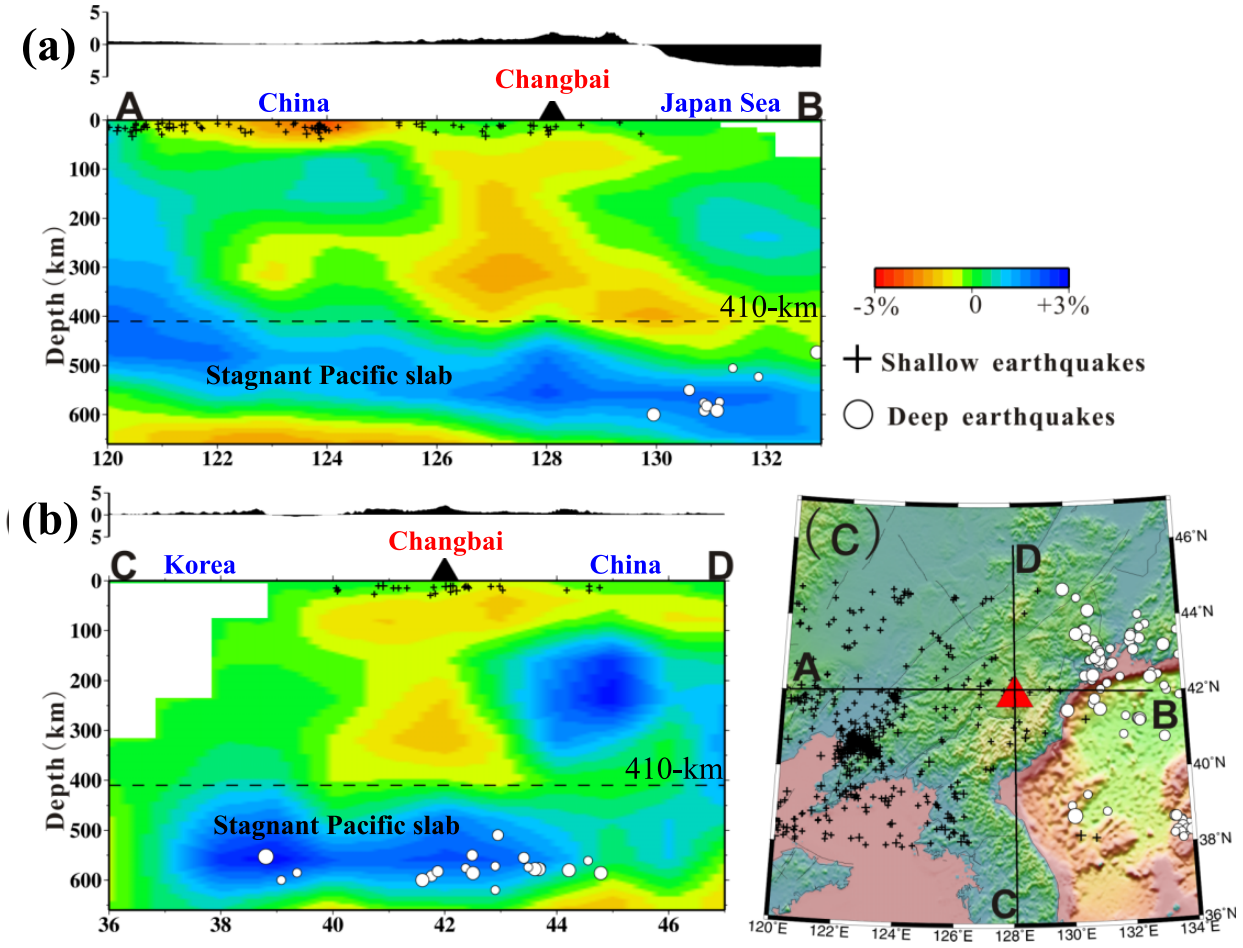

Fig. 66. (a) East-west and (b) north-south vertical cross-sections of P-wave velocity tomography along profiles shown in (c). Red and blue colors denote slow and fast velocity anomalies, respectively. The velocity perturbation scale is shown beside (a). The black triangles denote the active Changbai volcano. The dashed lines show the 410-km discontinuity. (c) Map showing locations of the two cross-sections in (a) and (b). The red triangle denotes the Changbai volcano. Black crosses and white dots show the shallow (0–30 km) and deep (450–600 km) earthquakes. (Reprinted from *Phys. Earth Planet. Inter.*, *173*, Zhao, D., Y. Tian, J. Lei, L. Liu, and S. Zheng, Seismic image and origin of the Changbai intraplate volcano in East Asia: Role of big mantle wedge above the stagnant Pacific slab, 197–206, Copyright 2009, with permission from Elsevier.)

(such as the Changbai and Wudalianchi volcanoes), strong intraplate earthquakes, reactivation of the North China craton, the abundant oil and other natural mineral resources (such as the Daqing oil field), and a boundary in surface topography and gravity anomaly in eastern China are all related to the structure and dynamic processes in the BMW above the stagnant slab in the MTZ under East Asia (Zhao *et al*., 2010b, 2011d). Mineral-physics studies have shown that deep slab dehydration in the MTZ is possible (e.g., Inoue *et al*., 2004; Ohtani *et al*., 2004; Ohtani and Litasov, 2006; Ohtani and Zhao, 2009). Recent results of shear-wave splitting (Liu *et al*., 2008; Huang *et al*., 2011d), electrical conductivity (Ichiki *et al*., 2006), numerical modeling (Faccenna *et al*., 2010; Zhu *et al*., 2010), and geochemical analysis (Chen *et al*., 2007; Zou *et al*., 2008; Kuritani *et al*., 2009), all suggest a hot and wet upper-mantle above the stagnant Pacific slab and their close relationship to the intraplate volcanism and active tectonics in NE China, and so all support this BMW model (Fig. 67).

Figures 68–70 show 36 vertical cross-sections of whole-mantle P-wave tomography under the Northern and Western Pacific, and East Asia, from a new global tomography model (Zhao *et al*., 2010b). Over one million arrival times of first P-wave and later phases (pP, PP, PcP, and $P_{\rm diff}$ waves) were used in the whole-mantle tomographic inversion by adopting a flexible-grid approach (Zhao, 2009). Active volcanoes (Simkin and Siebert, 1994) and seismicity in the vicinity of each cross-section are also shown in the tomographic images. The subducting Pacific slab is clearly imaged as a high-V zone in the upper mantle under southern Alaska and the eastern Aleutian arc, where earthquakes occur down to 200–300 km depths (Fig. 68). Active arc volcanoes are located above the slab. Local high-resolution tomography has revealed that the subducting Pacific slab is 50–70 km thick, and low-V anomalies exist in the upper mantle wedge under the active arc volcanoes (e.g., Zhao *et al*., 1995; Qi *et al*., 2007a, b). The global tomography model has a lower resolution than the local tomography, hence the slab is imaged as a broader dipping zone (Fig. 68).

Some Cenozoic volcanoes exist in western Alaska and the eastern Bering Sea, and a few of them have erupted in the last 10,000 years (Simkin and Siebert, 1994; Mukasa *et al*.,

doi:10.5047/meep.2012.00101.0001

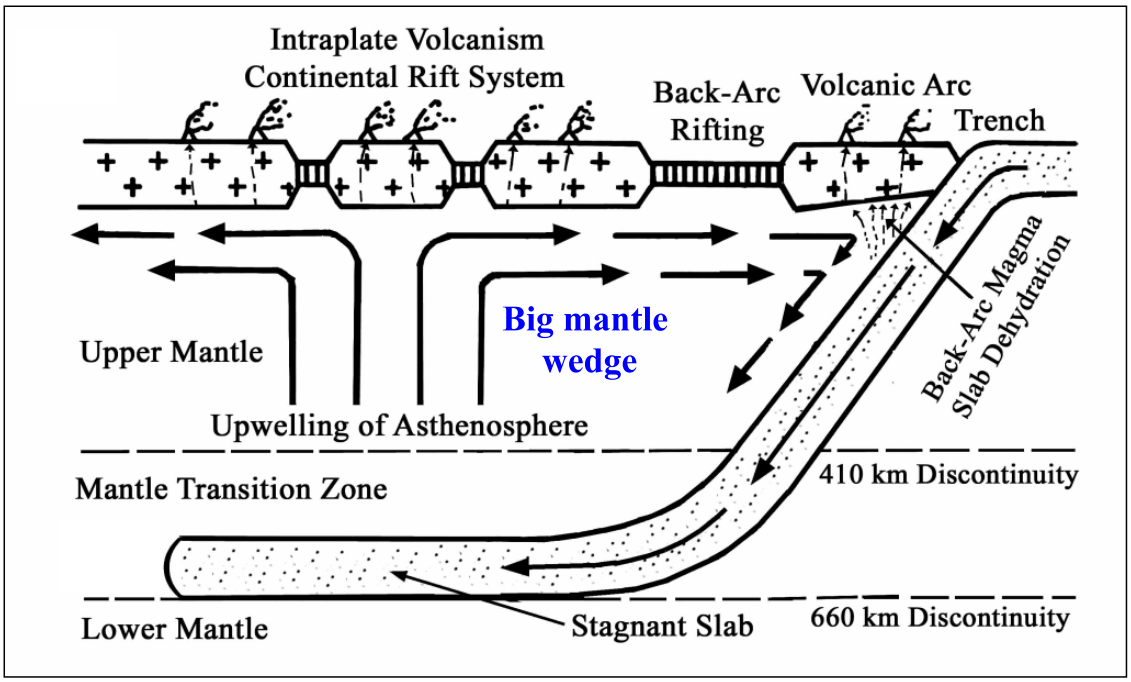

Fig. 67. The big mantle wedge (BMW) model. The subducting Pacific slab becomes stagnant in the mantle transition zone, and a BMW has formed in the upper mantle above the stagnant slab. The convective circulation process in the BMW and the deep dehydration process of the slab cause upwellings of hot and wet asthenospheric materials, leading to the formation of continental rift systems as well as intraplate volcanoes in NE Asia. (With kind permission from Springer Science+Business Media: *Chinese Sci. Bull.*, Origin of the Changbai intraplate volcanism in Northeast China: Evidence from seismic tomography, *49*, 2004, 1401–1408, Zhao, D., J. Lei, and R. Tang, figure 6(b).)

2007). Low-V anomalies exist in the upper mantle under those intraplate volcanoes (Fig. 68). High-V anomalies are visible in the MTZ, which represent the Pacific slab stagnating in the MTZ, similar to the results beneath Eastern China (Fig. 64). Under the western portion of the Aleutian arc, the Pacific plate is not subducting beneath the Bering Sea, and the boundary between the Pacific and North American plates actually becomes a strike-slip transform fault (the Bering fault), hence no intermediate-depth and deep earthquakes occur there and a high-V slab is not visible in the upper mantle there (Fig. 68, a12). However, a high-V zone exists in the MTZ under the western Bering Sea (Fig. 68, a11–12), which may represent the old Pacific slab, or the Farallon slab, stagnating in the MTZ that is detached from the present Pacific plate. These features are also visible in the cross-sections parallel to the Aleutian trench (Fig. 69, a13–17).

In the upper mantle under the Kamchatka Peninsula and the Kuril arc, the subducting Pacific slab is clearly visible and intermediate-depth and deep earthquakes occur actively in the high-V Pacific slab, forming a clear Wadati-Benioff deep seismic zone (Fig. 69, a18–24). Active arc volcanoes are located above the eastern edge of a big low-V zone in the upper mantle. The stagnant slab in the MTZ is visible under the Kuril arc (Fig. 69, a20–24) but not beneath Kamchatka (Fig. 69, a18–19). The bottom depths of the Wadati-Benioff deep seismic zone and the Pacific slab itself become shallower toward the north under Kamchatka Peninsula, and the slab disappears under the northernmost Kamchatka (Figs. 60, 61). High-V anomalies extend continuously to the lower mantle under southern Kamchatka and northern Kuril (Fig. 69, a19–21), suggesting that part of the Pacific slab has subducted down to the lower mantle, whereas the remaining part remains in the MTZ. Under the southern Kuril arc, the entire Pacific slab seems to be stagnating in the MTZ (Fig. 69, a22–24). Note that the dip angle of the Wadati-Benioff zone becomes smaller gradually from north to south beneath the Kuril arc, i.e., it decreases from 45–50 degrees under southern Kamchatka to ∼30 degrees under Hokkaido in northern Japan (Fig. 69, a20–24).

The global tomography model has a better resolution beneath the East Asia region because of a better coverage of seismic stations there. Hence the Pacific slab shows up more clearly in the mantle tomography under East Asia (Fig. 70) than under the northern Pacific regions (Figs. 68, 69). The overall features of the tomographic images in Fig. 70 are quite similar. The Pacific plate subducting from the Japan Trench is clearly visible in the upper mantle with a clear Wadati-Benioff deep seismic zone within the slab. The Pacific slab becomes stagnant in the MTZ under East Asia. The slab and the deep seismic zone have a gentle dip angle of ∼30 degrees under the Japan arc and back-arc (Fig. 70, a25–a33), while they become steep and nearly vertical beneath the Izu-Mariana region (Fig. 70, a34–a36). The subducting Philippine Sea slab is also revealed in the upper mantle beneath the Ryukyu arc and back-arc (Fig. 70, a33–a36).

Many Quaternary intraplate volcanoes exist in East Asia, such as the Wudalianchi, Jingbo, Changbai, Sikhote-Alin, Ulreung, etc. (Simkin and Siebert, 1994). Under these volcanoes, significant low-V anomalies exist in the upper mantle above the stagnant slab in the MTZ (Fig. 70(a)). The

doi:10.5047/meep.2012.00101.0001

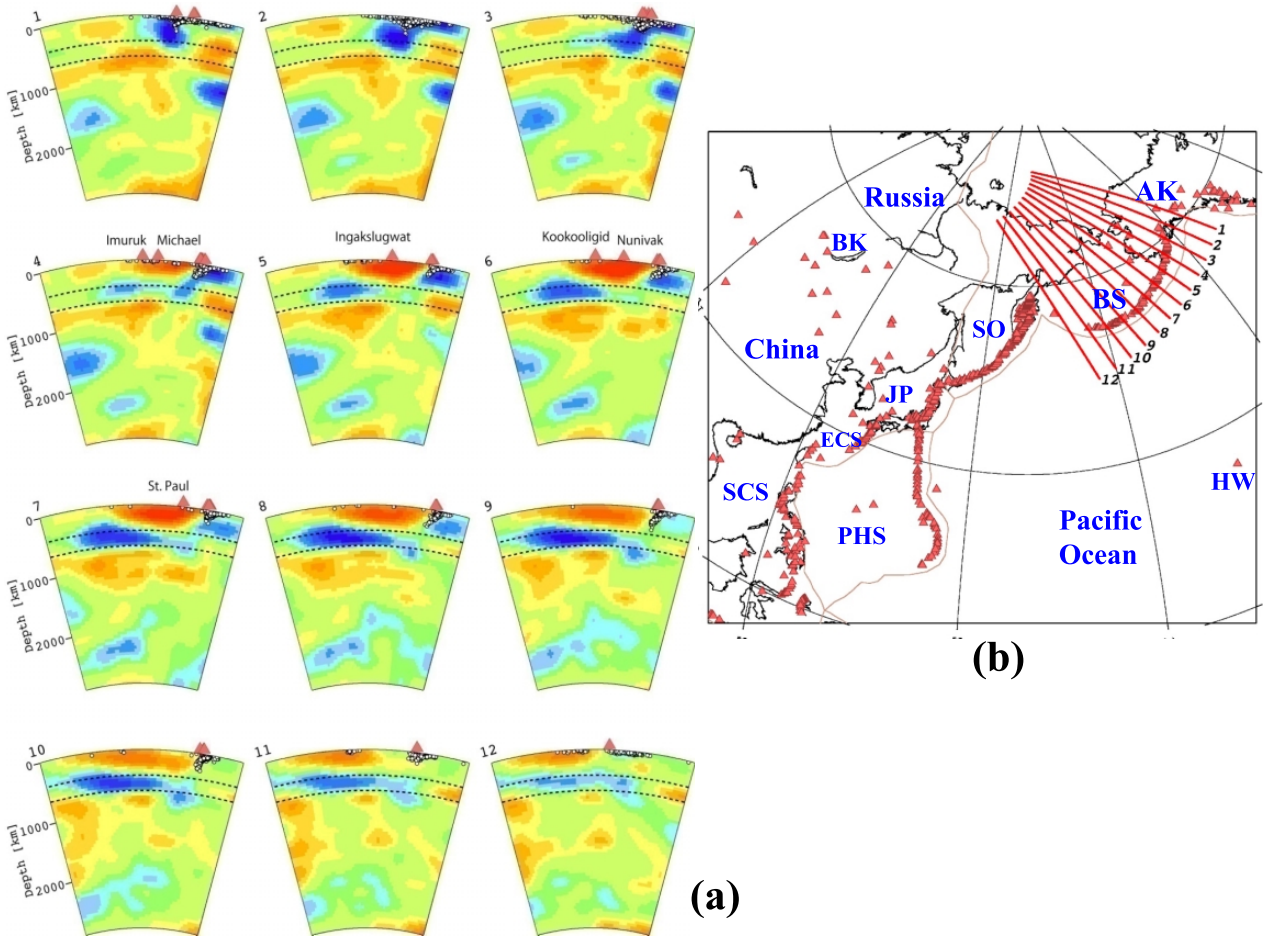

Fig. 68. (a) Vertical cross-sections of whole-mantle P-wave tomography along the profiles shown on the inset map (b). Red and blue colors denote low and high velocities, respectively. The maximum amplitude of the velocity anomalies is 1%. The white dots show earthquakes which occurred within 100 km of the profile. The two dotted lines denote the 410-km and 670-km discontinuities. Red triangles show active volcanoes. The thin red lines on the inset map show the plate boundaries. AK, Alaska; BK, Lake Baikal; BS, Bering Sea; ECS, East China Sea; HW, Hawaii; JP, Japan Sea; PHS, Philippine Sea; SCS, South China Sea; SO, Sea of Okhotsk. (Reprinted from *Russ. Geol. Geophys.*, *51*, Zhao, D., F. Pirajno, N. Dobretsov, and L. Liu, Mantle structure and dynamics under East Russia and adjacent regions, 925–938, Copyright 2010, with permission from Elsevier.)

stagnant slab and upper mantle structure under the intraplate volcanoes in East Asia are better imaged by high-resolution local and regional tomography (Figs. 64–66).

These global tomography results (Figs. 68–70) indicate that the BMW model (Fig. 67) works not only for the East Asia region, but is also applicable to the broad regions in the northern and western Pacific subduction zones. Most, or all, of the intraplate volcanoes in western Alaska, the Aleutian and eastern Eurasian regions, may be explained by the BMW model, and so those intraplate volcanoes may have an origin which is the same as that of the Changbai volcano; hence, they may be called *Changbai-type volcanoes*.

Significant high-V anomalies are visible in the lower mantle down to the core-mantle boundary (CMB) (Figs. 68–70), which represent pieces of slab materials collapsing down to the CMB (Maruyama, 1994; Zhao, 2004, 2009; Idehara *et al.*, 2007; Maruyama *et al.*, 2007). Low-V anomalies are also imaged in the lower mantle, which may represent upwelling return flows caused by the down-welling of the slab materials (Zhao *et al.*, 2011d).

14. Discussion and Future Perspectives

As mentioned above, many studies, using high-resolution crustal tomography, have revealed fluid-related low-V anomalies in the source areas of large crustal earthquakes, but it is hard to clarify exactly where the fluids come from just from tomographic images. The He^3/He^4 ratio is a useful geochemical indicator for the origin of fluids. It is found that the He^3/He^4 ratio is higher in the source areas of the 1995 Kobe earthquake (M 7.2) and the 2004 and 2007 Niigata earthquake areas, suggesting that the fluids originate from the dehydration of subducting Pacific and Philippine Sea slabs (e.g., Umeda *et al.*, 2006; Horiguchi and Matsuda, 2008). Studies using the He^3/He^4 ratio, and/or other geochemical indicators, should be made in the source areas of large crustal earthquakes in China and India to clarify the origin of the fluids in the continental areas. Deep dehydration of the stagnant slab under East Asia may have contributed fluids to the uppermost mantle and the crust to affect the generation of large crustal earthquakes in the reactivated North China Craton, such as the 1679 Sanhe earthquake (M 8.0) and the 1976 Tangshan earthquake (M 7.8), but such a sce-

doi:10.5047/meep.2012.00101.0001

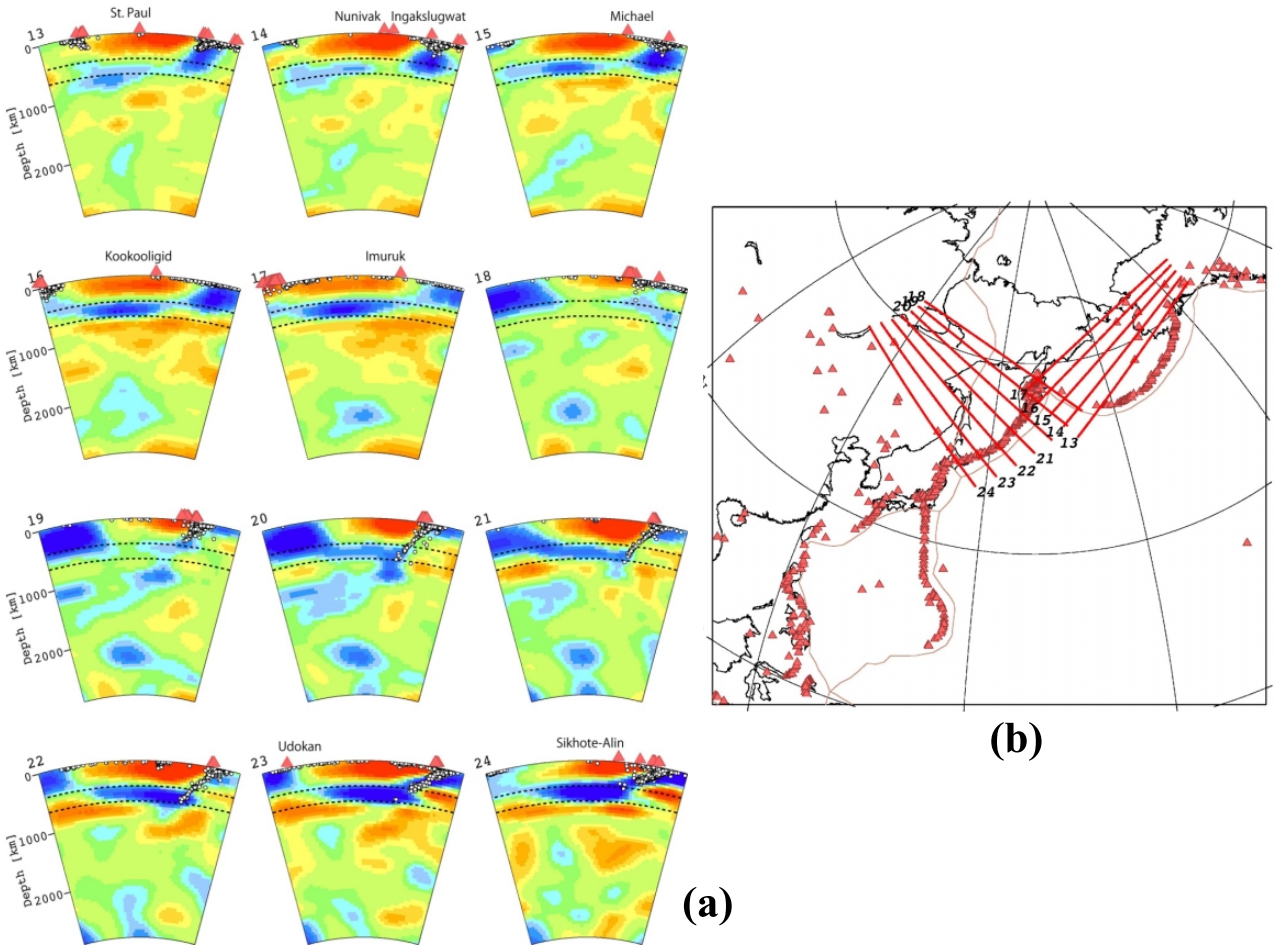

Fig. 69. The same as Fig. 68 but for other cross-sections. Profiles No. 13–17 pass through the Bering Sea, while profiles No. 18–24 pass through Sea of Okhotsk. (Reprinted from *Russ. Geol. Geophys.*, *51*, Zhao, D., F. Pirajno, N. Dobretsov, and L. Liu, Mantle structure and dynamics under East Russia and adjacent regions, 925–938, Copyright 2010, with permission from Elsevier.)

nario should be confirmed, or refuted, by using geochemical or other methods (Zhao *et al*., 2011d).

The existence of fluids in the crust and uppermost mantle can affect the long-term structural and compositional evolution of fault zones, change the strength of a fault zone, and alter the local stress regime (Sibson, 1992; Hickman *et al*., 1995). These factors can enhance the stress concentration in the seismogenic layer leading to mechanical failure. Spatial and temporal variations in the crustal stress field have been reported for the source areas of some large earthquakes (e.g., Katao *et al*., 1997; Zhao *et al*., 1997c; Huang *et al*., 2011e), which have been associated with fluids in the fault zones.

These many pieces of geophysical and geochemical evidence, as mentioned above, suggest that the generation of a large earthquake is not entirely a mechanical process, but is also closely related to the physical and chemical properties of the materials in the crust and upper mantle, such as magma, fluids, etc. (Zhao *et al*., 2002, 2010a). The rupture nucleation zone should have a three-dimensional spatial extent, not just limited to the two-dimensional surface of a fault, as suggested earlier by Tsuboi (1956) on the concept of earthquake volume. Complex physical and chemical reactions take place in the source zone of future earthquakes, causing heterogeneities in the material properties and stress field, which can be detected using seismic tomography and other geophysical methods. The source zone of an M 6 to 9 earthquake extends from about 10 km to 500 km (Kanamori, 2004). The spatial resolution of recent tomographic images is close to that scale, which has enabled us to image earthquake-related heterogeneities (e.g., earthquake volume) in the crust and uppermost mantle. These results indicate that large earthquakes do not strike anywhere randomly, but only in anomalous areas that may be detected using geophysical methods (Zhao *et al*., 2002, 2010a).

It should be noted that the tomographic images shown in this monograph have different resolution scales and different amplitudes of velocity anomalies. The resolution scale of a tomographic image is determined by the density of ray path coverage and the degree of ray crisscrossing, which are determined by the distribution of seismic stations and the earthquakes considered. The amplitude of velocity anomalies retrieved by seismic tomography is affected by damping and smoothing regularizations that are required for stabilizing tomographic inversions, because of the uneven distribution of seismic rays in the crust and mantle under a study area (Zhao, 2009). Thus, the amplitude of velocity anomalies in

doi:10.5047/meep.2012.00101.0001

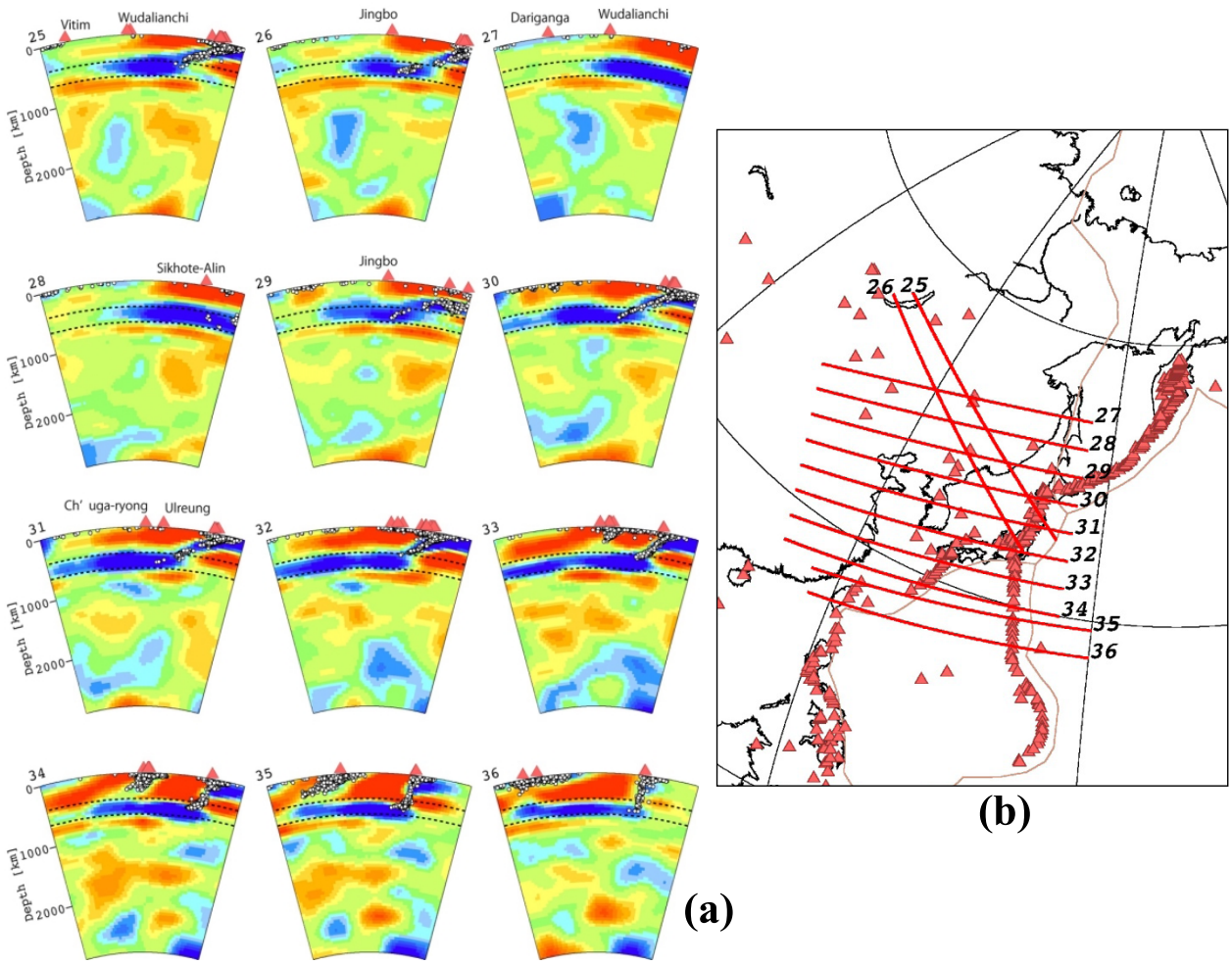

Fig. 70. The same as Fig. 68 but for cross-sections passing through the Japan Islands, Japan Sea and East Asia. (Reprinted from *Russ. Geol. Geophys.*, *51*, Zhao, D., F. Pirajno, N. Dobretsov, and L. Liu, Mantle structure and dynamics under East Russia and adjacent regions, 925–938, Copyright 2010, with permission from Elsevier.)

the real Earth is difficult to recover fully, and the degree of recovery depends on the scale of the study area, as well as the density and homogeneity of the ray path coverage. In local-scale tomography (e.g., Figs. 11, 14–21), seismic stations and earthquakes have a relatively uniform distribution, and so weak damping and smoothing are applied, leading to a better recovering of the amplitude of velocity anomalies, which can be up to 6–10%. In contrast, strong damping and smoothing have to be applied in global and large-scale regional tomography because of the very uneven distribution of seismic stations and earthquakes, which lead to a smaller amplitude of velocity anomalies (1–2%) (e.g., Figs. 64, 65, 68–70). Therefore, the amplitudes of velocity anomalies in a tomographic image should be interpreted carefully by considering the strength of damping and smoothing applied in the inversion as well as the scale of the tomographic model.

The future development of seismic tomography depends on the progress of both seismic instrumentation and methodology. The data coverage determines the first-order features of a tomographic result. At present, most of the seismic stations are installed in land areas, whereas few are in broad oceanic regions. The gradual deployment of many seismometers on the seafloor, and in less-instrumented land areas, will be a most important task for seismologists in the future. Installing a dense permanent or portable network of ocean-bottom seismometers in the marginal seas (e.g., East China Sea, Japan Sea, Sea of Okhotsk, and Bering Sea, etc.) will be necessary to resolve several important geodynamic issues in subduction zones, such as the fate of subducting slabs, the detailed structure and processes in the big mantle wedge, the mechanism of deep earthquakes, and the back-arc and intraplate magmatism, etc.

At the same time, new technologies and more efforts are needed to extract useful data from the seismograms. Many different converted and reflected waves have been identified in subduction zones because of the complex structures there, in particular, seismic discontinuities associated with subducting slabs. These later phases of converted and reflected waves, collected from local and regional seismograms, have been demonstrated to be very useful for body-wave tomography. The discovery of every new later phase, and its use in tomography, may open a new window for us to reveal novel features of the Earth's structure. For example, the detection of *sP* depth-phases at a short epicentral distance (<300 km)

doi:10.5047/meep.2012.00101.0001

from suboceanic earthquakes (Umino *et al*., 1995), and its application in tomography, enables us to determine a 3-D velocity model outside a seismic network (Zhao *et al*., 2002, 2007a). The use of multiple reflected waves in the crust (*SmS*, *sSmS*) results in a high-resolution crustal tomography with only two stations (Zhao *et al*., 2005). The use of Moho reflected waves (*PmP*) in tomography leads to a better mapping of the lower crustal structure and the crustal thickness (e.g., Salah and Zhao, 2004; Xia *et al*., 2007; Sun *et al*., 2008; Gupta *et al*., 2009b; Lei *et al*., 2011). The addition of various types of later phases in the mantle and core in global tomography enables a better imaging of deep mantle plumes (Zhao, 2001c, 2007, 2009). Advanced waveform-modeling techniques make it possible to identify and collect many later-phase data from high-frequency seismograms (e.g., Helmberger *et al*., 2001; Abdelwahed and Zhao, 2005).

Continuous efforts are also needed to improve the theoretical aspects of seismic imaging. The limitation of the ray theory is recognized, and more advanced seismic wave-propagation theories are needed. A finite-frequency wave-propagation theory (the so-called Banana-Doughnut theory) was proposed for body-wave and surface-wave tomography (Dahlen *et al*., 2000), and has been applied to study the 3-D Earth structure at both local and global scales (e.g., Montelli *et al*., 2004; Hung *et al*., 2004). However, the effectiveness of this Banana-Doughnut theory in tomography is still debatable (e.g., van der Hilst and de Hoop, 2005; Nolet *et al*., 2007; Tong *et al*., 2011). Tomographic images obtained with the Banana-Doughnut theory are very similar to those obtained with ray theory; the obtained velocity pattern is exactly the same, and there is only a minor difference in the amplitude of velocity anomalies (Montelli *et al*., 2004; Boschi *et al*., 2006; Tong *et al*., 2011). It seems that the inhomogeneous data coverage, as well as the damping and smoothing regularizations in tomographic inversion, have a much greater effect than the difference in the wave-propagation theory adopted (van der Hilst and de Hoop, 2005; Boschi *et al*., 2006). That is to say, the ray theory is still robust enough for tomographic imaging of the Earth's structure for a long time to come; in particular, for local and regional tomography which uses high-frequency seismic waves. Figure 39 shows a comparison of local crustal-tomography models determined with ray theory and finite-frequency theory (Tong *et al*., 2011). The two models are very similar to each other; the only difference between them is in the amplitude of velocity anomalies. The finite-frequency images exhibit stronger velocity anomalies than those revealed by the ray tomography, which conclusion was also drawn by previous studies (e.g., Hung *et al*., 2004; Montelli *et al*., 2004).

Recently, waveform tomography has become feasible for both regional and local scale tomography (e.g., Friedrich, 2003; Pollitz and Fletcher, 2005; Fichtner *et al*., 2009). Ambient-noise tomography has also been proposed to study the crust and uppermost mantle structure (e.g., Shapiro *et al*., 2005). These studies demonstrate that seismograms can be further exploited to better image the 3-D Earth structure. Some researchers have tried to determine temporal variations in structure (i.e., 4-D tomography). Examples are the study of geothermal reservoir changes at The Geysers, CA (Gunasekera *et al*., 2003), the investigation of temporal changes at Mammoth Mountain, CA, related to CO_2 outgassing (Foulger *et al*., 2003; Julian and Foulger, 2010), and the source area of a large earthquake (e.g., Lei *et al*., 2011). But one should be very careful in 4-D tomography studies that the data sets used for the different time periods should be the same in order to detect the temporal variations in the 3-D structure. Of course, a tomographic detection of any temporal variations in the 3-D structure is expected only for small local areas with rapid crustal deformations, such as volcanic eruptions and large earthquakes.

Acknowledgments. This work was partially supported by Grant-in-aid for Scientific Research (Kiban-B 11440134, Kiban-A 17204037) from Japan Society for the Promotion of Science as well as by the Global-COE program of the Earth and Planetary Sciences of Tohoku University. The author is very grateful for effective collaborations and helpful discussions with many colleagues and coworkers, including A. Hasegawa, H. Kanamori, N. Umino, S. Horiuchi, E. Ohtani, T. Matsuzawa, R. Hino, T. Okada, J. Nakajima, K. Asamori, S. Maruyama, A. Yamada, M. Ikeda, Y. Nishizono, H. Inakura, O. P. Mishra, M. Salah, M. Abdelwahed, I. Serrano, J. Huang, J. Lei, Z. Wang, S. Gupta, J. Wang, C. Qi, A. Sun, Y. Tian, X. Tian, G. Jiang, S. Xia, S. Padhy, B. Cheng, W. Wei, Z. Huang, and P. Tong. Figure 22 was provided by Dr. Z. Huang. Professors H. Kanamori (the editor), K. Hirahara and A. Hasemi provided very thoughtful review comments and suggestions that have improved the manuscript. The author would also like to thank K. Oshida and M. Tagawa for their kind help during the preparation of this monograph.

References

Abdelwahed, M., and D. Zhao (2005), Waveform modelling of local earthquakes in southwest Japan, *Earth Planets Space*, *57*, 1039–1054.

Abdelwahed, M., and D. Zhao (2007), Deep structure of the Japan subduction zone, *Phys. Earth Planet. Inter.*, *162*, 32–52.

Ai, Y., D. Zhao, X. Gao, and W. Xu (2005), The crust and upper mantle discontinuity structure beneath Alaska inferred from receiver functions, *Phys. Earth Planet. Inter.*, *150*, 339–350.

Aki, K., and W. Lee (1976), Determination of three-dimensional velocity anomalies under a seismic array using first P arrival times from local earthquakes, 1. A homogeneous initial model, *J. Geophys. Res.*, *81*, 4381–4399.

Aki, K., A. Christoffersson, and E. Husebye (1977), Determination of the three-dimensional seismic structure of the lithosphere, *J. Geophys. Res.*, *82*, 277–296.

Ando, M., Y. Ishikawa, and H. Wada (1980), S-wave anisotropy in the upper mantle under a volcanic area in Japan, *Nature*, *268*, 43–46.

Ballard, S., J. Hipp, and C. Young (2009), Efficient and accurate calculation of ray theory seismic travel time through variable resolution 3D Earth models, *Seismol. Res. Lett.*, *86*, 989–999.

Barth, A., and F. Wenzel (2010), New constraints on the intraplate stress field of the Amurian plate deduced from light earthquake focal mechanisms, *Tectonophysics*, *482*, 160–169.

Bird, P. (2003), An updated digital model of plate boundaries, *Geochem. Geophys. Geosyst.*, *4*, 1027.

Boschi, L., T. Becker, G. Soldati, and A. Dziewonski (2006), On the relevance of Born theory in global seismic tomography, *Geophys. Res. Lett.*, *33*, L06302.

Chen, Y., Y. Zhang, D. Graham, S. Su, and J. Deng (2007), Geochemistry of Cenozoic basalts and mantle xenoliths in Northeast China, *Lithos*, *96*, 108–126.

Chen, Y., J. Badal, and Z. Zhang (2009), Radial anisotropy in the crust and upper mantle beneath the Qinghai-Tibet Plateau and surrounding regions, *J. Asian Earth Sci.*, *36*, 289–302.

Cheng, B., D. Zhao, and G. Zhang (2011), Seismic tomography and anisotropy in the source area of the 2008 Iwate-Miyagi earthquake (M

doi:10.5047/meep.2012.00101.0001

7.2), *Phys. Earth Planet. Inter.*, *184*, 172–185.
Chou, H., B. Kuo, S. Hung, L. Chiao, D. Zhao, and Y. Wu (2006), The Taiwan-Ryukyu subduction-collision complex: Folding of a viscoelastic slab and the double seismic zone, *J. Geophys. Res.*, *111*, B04410.
Chou, H., B. Kuo, L. Chiao, D. Zhao, and S. Hung (2009), Tomography of the westernmost Ryukyu subduction zone and the serpentinization of the forearc mantle, *J. Geophys. Res.*, *114*, B12301.
Conder, J., and D. Wiens (2006), Seismic structure beneath the Tonga arc and Lau back-arc basin determined from joint Vp, Vp/Vs tomography, *Geochem. Geophys. Geosyst.*, *7*, Q03018.
Dahlen, F., S. Hung, and G. Nolet (2000), Frechet kernels for finite-frequency traveltimes. I. Theory, *Geophys. J. Int.*, *141*, 157–174.
Davaille, A., and M. Lees (2004), Thermal modeling of subducted plates: tear and hotspot at the Kamchatka corner, *Earth Planet. Sci. Lett.*, *226*, 293–304.
DeMets, C., R. Gordon, D. Argus, and S. Stein (1990), Current plate motions, *Geophys. J. Int.*, *101*, 425–478.
DeMets, C., R. Gordon, and D. Argus (2010), Geologically current plate motions, *Geophys. J. Int.*, *181*, 1–80.
Duan, Y., D. Zhao, X. Zhang, and S. Xia (2009), Seismic structure and origin of active intraplate volcanoes in Northeast Asia, *Tectonophysics*, *470*, 257–266.
Dziewonski, A., and D. Anderson (1984), Seismic tomography of the Earth's interior, *Am. Sci.*, *72*, 483–494.
Dziewonski, A., B. Hager, and R. O'Connell (1977), Large-scale heterogeneities in the lower mantle, *J. Geophys. Res.*, *82*, 239–255.
Eberhart-Phillips, D., and C. Henderson (2004), Including anisotropy in 3-D velocity inversion and application to Marlborough, New Zealand, *Geophys. J. Int.*, *156*, 237–254.
Engdahl, E., and S. Billington (1986), Focal depth determination of central Aleutian earthquakes, *Bull. Seismol. Soc. Am.*, *76*, 77–93.
Faccenda, M., L. Burlini, T. Gerya, and D. Mainprice (2008), Fault-induced seismic anisotropy by hydration in subducting oceanic plates, *Nature*, *455*, 1097–1100.
Faccenna, C., T. Becker, S. Lallemand, Y. Lagabrielle, F. Funiciello, and C. Piromallo (2010), Subduction-triggered magmatic pulses: A new class of plumes? *Earth Planet. Sci. Lett.*, *299*, 54–68.
Fan, G., T. Wallace, and D. Zhao (1998), Tomographic imaging of deep velocity structure beneath the eastern and southern Carpathians, Romania: Implications for continental collision, *J. Geophys. Res.*, *103*, 2705–2723.
Fichtner, A., B. Kennett, H. Igel, and H. Bunge (2009), Full seismic waveform tomography for upper-mantle structure in the Australian region using adjoint methods, *Geophys. J. Int.*, *179*, 1703–1725.
Forsyth, D. (1982), Determination of focal depths of earthquakes associated with the bending of oceanic plates at trenches, *Phys. Earth Planet. Inter.*, *28*, 141–160.
Foulger, G., B. Julian, A. Pitt, D. Hill, P. Malin, and E. Shalev (2003), Three-dimensional crustal structure of Long Valley caldera, California, and evidence for the migration of CO_2 under Mammoth Mountain, *J. Geophys. Res.*, *108*, JB000041.
Friederich, W. (2003), The S-velocity structure of the east Asian mantle from inversion of shear and surface waveforms, *Geophys. J. Int.*, *153*, 88–102.
Fujie, G., J. Kasahara, R. Hino, T. Sato, M. Shinohara, and K. Suyehiro (2002), A significant relation between seismic activities and reflection intensities in the Japan Trench region, *Geophys. Res. Lett.*, *29*, GL013764.
Fukao, Y., M. Obayashi, H. Inoue, and M. Nenbai (1992), Subducting slabs stagnant in the mantle transition zone, *J. Geophys. Res.*, *97*, 4809–4822.
Furumura, T., and T. Moriya (1990), Three-dimensional Q structure in and around the Hidaka mountains, Hokkaido, Japan, *J. Seismol. Soc. Jpn.*, *43*, 121–132.
Gamage, S., N. Umino, A. Hasegawa, and S. Kirby (2009), Offshore double-planed shallow seismic zone in the NE Japan forearc region revealed by sP depth phases recorded by regional networks, *Geophys. J. Int.*, *178*, 195–214.
Gerya, T. (2011), Future directions in subduction modeling, *J. Geodyn.*, *52*, 344–378.
Gerya, T., and D. Yuen (2003), Rayleigh-Taylor instabilities from hydration and melting propel "cold plumes" at subduction zones, *Earth Planet. Sci. Lett.*, *212*, 47–62.
Gerya, T., J. Connolly, D. Yuen, W. Gorczyk, and A. Capel (2006), Seismic implications of mantle wedge plumes, *Phys. Earth Planet. Inter.*, *156*, 59–74.
Gorbatov, A., V. Kostoglodov, and G. Suárez (1997), Seismicity and structure of the Kamchatka subduction zone, *J. Geophys. Res.*, *102*, 17,883–17,898.
Gorbatov, A., J. Domínguez, G. Suárez, V. Kostoglodov, and D. Zhao (1999), Tomographic imaging of the P-wave velocity structure beneath the Kamchatka peninsula, *Geophys. J. Int.*, *137*, 269–279.
Gorczyk, W., T. Gerya, J. Connolly, D. Yuen, and M. Rudolph (2006), Large-scale rigid-body rotation in the mantle wedge and its implications for seismic tomography, *Geochem. Geophys. Geosyst.*, *7*, Q05018.
Green, H. (2003), Tiny triggers deep down, *Nature*, *424*, 893–894.
Green, H., and P. Burnley (1989), A new self-organizing mechanism for deep-focus earthquakes, *Nature*, *341*, 733–737.
Green, H., and H. Houston (1995), The mechanisms of deep earthquakes, *Ann. Rev. Earth Planet. Sci.*, *23*, 169–213.
Gunasekera, R., G. Foulger, and B. Julian (2003), Three-dimensional tomographic images of progressive pore-fluid depletion at the Geysers geothermal area, California, *J. Geophys. Res.*, *108*, JB000638.
Gupta, S., D. Zhao, and S. Rai (2009a), Seismic imaging of the upper mantle under the Erebus hotspot in Antarctica, *Gondwana Res.*, *16*, 109–118.
Gupta, S., D. Zhao, M. Ikeda, S. Ueki, and S. Rai (2009b), Crustal tomography under the Median Tectonic Line in Southwest Japan using P and PmP data, *J. Asian Earth Sci.*, *35*, 377–390.
Hall, P., and C. Kincaid (2001), Diapiric flow at subduction zones: a recipe for rapid transport, *Science*, *292*, 2472–2475.
Hasegawa, A., and A. Yamamoto (1994), Deep, low-frequency microearthquakes in or around seismic low-velocity zones beneath active volcanoes in northeastern Japan, *Tectonophysics*, *233*, 233–252.
Hasegawa, A., and D. Zhao (1994), Deep structure of island arc magmatic regions as inferred from seismic observations, in *Magmatic Systems*, edited by M. P. Ryan, Academic Press, pp. 179–195.
Hasegawa, A., N. Umino, and A. Takagi (1978), Double-planed deep seismic zone and upper-mantle structure in the northeastern Japan arc, *Geophys. J. R. Astron. Soc.*, *54*, 281–296.
Hasegawa, A., N. Umino, A. Takagi, S. Suzuki, Y. Motoya, S. Kameya, K. Tanaka, and Y. Sawada (1983), Spatial distribution of earthquakes beneath Hokkaido and northern Honshu, Japan, *J. Seismol. Soc. Jpn.*, *36*, 129–150.
Hasegawa, A., J. Nakajima, N. Umino, and S. Miura (2005), Deep structure of the northeastern Japan arc and its implications for crustal deformation and shallow seismicity, *Tectonophysics*, *403*, 59–75.
Hasemi, A., H. Ishii, and A. Takagi (1984), Fine structure beneath the Tohoku District, northeastern Japan arc, as derived by an inversion of P-wave arrival times from local earthquakes, *Tectonophysics*, *101*, 245–265.
Hashida, T. (1989), Three-dimensional seismic attenuation structure beneath the Japanese Islands and its tectonic and thermal implications, *Tectonophysics*, *159*, 163–180.
He, R., D. Zhao, R. Gao, and H. Zheng (2010), Tracing the Indian lithospheric mantle beneath central Tibetan Plateau using teleseismic tomography, *Tectonophysics*, *491*, 230–243.
Heki, K., S. Miyazaki, and H. Tsuji (1997), Silent fault slip following an interplate thrust earthquake at the Japan trench, *Nature*, *386*, 592–597.
Heki, K., S. Miyazaki, H. Takahashi, and M. Kasahara (1999), The Amurian plate motion and current plate kinematics, *J. Geophys. Res.*, *104*, 29,147–29,155.
Helmberger, D., X. J. Song, and L. Zhu (2001), Crustal complexity from regional waveform tomography: aftershocks of the 1992 Landers earthquake, *J. Geophys. Res.*, *106*, 609–620.
Herrmann, R. (1976), Focal depth determination from the signal character of long-period P waves, *Bull. Seismol. Soc. Am.*, *66*, 1221–1232.
Hickman, S., R. Sibson, and R. Bruhn (1995), Introduction to special section: Mechanical involvement of fluids in faulting, *J. Geophys. Res.*, *100*, 12831–12840.
Hino, R., S. Ito, H. Shiobara, H. Shimamura, T. Sato, T. Kanazawa, J. Kasahara, and A. Hasegawa (2000), Aftershock distribution of the 1994 Sanriku-oki earthquake (Mw 7.7) revealed by ocean bottom seismographic observation, *J. Geophys. Res.*, *105*, 21,697–21,710.
Hino, R., Y. Yamamoto, and A. Kuwano (2006), Hypocenter distribution of the main- and aftershocks of the 2005 Off Miyagi Prefecture earthquake located by ocean bottom seismographic data, *Earth Planets Space*, *58*, 1543–1548.
Hirahara, K. (1977), A large-scale three-dimensional seismic structure under the Japan Islands and the Sea of Japan, *J. Phys. Earth*, *25*, 393–417.

doi:10.5047/meep.2012.00101.0001

Hirahara, K. (1981), Three-dimensional seismic structure beneath southwest Japan: The subducting Philippine Sea plate, *Tectonophysics*, *79*, 1–44.

Hirahara, K. (2006), Toward receiver function tomography, *Fall Meet. AGU*, Abstract #S54B-07.

Hirahara, K., and Y. Ishikawa (1984), Travel-time inversion for three-dimensional P-wave velocity anisotropy, *J. Phys. Earth*, *32*, 197–218.

Hiramatsu, Y., M. Ando, and Y. Ishikawa (1997), ScS wave splitting of deep earthquakes around Japan, *Geophys. J. Int.*, *128*, 400–424.

Hirata, N. *et al.* (1996), Urgent joint observation of aftershocks of the 1995 Hyogo-ken Nanbu earthquake, *J. Phys. Earth*, *44*, 317–328.

Hobbs, B., and A. Ord (1988), Plastic instabilities: implication for the origin of intermediate and deep focus earthquakes, *J. Geophys. Res.*, *93*, 10,521–10,540.

Honda, S., and M. Saito (2003), Small-scale convection under the back-arc occurring in the low viscosity wedge, *Earth Planet. Sci. Lett.*, *216*, 703–715.

Honda, S., M. Saito, and T. Nakakuki (2002), Possible existence of small-scale convection under the back-arc, *Geophys. Res. Lett.*, *29*, 2043.

Honthaas, C., H. Bellon, P. Kepezhinskas, and R. Maury (1995), New ^{40}K-^{40}Ar dates for the Cretaceous-Quaternary magmatism of Northern Kamchatka (Russia), *C. R. Acad. Sci. Paris Series II*, *320*, 197–204.

Horie, A., and K. Aki (1982), Three-dimensional velocity structure beneath the Kanto District, Japan, *J. Phys. Earth*, *30*, 255–281.

Horiguchi, K., and J. Matsuda (2008), On the change of ^{3}He/^{4}He ratios in hot spring gases after the Iwate-Miyagi Nairiku Earthquake in 2008, *Geochem. J.*, *42*, e1–e4.

Horiguchi, K., S. Ueki, and Y. Sano (2010), Geographic distribution of helium isotope ratios in northeastern Japan, *Island Arc*, *19*, 60–70.

Horiuchi, S., H. Ishii, and A. Takagi (1982a), Two-dimensional depth structure of the crust beneath the Tohoku district, the northeastern Japan arc, I. Method and Conrad discontinuity, *J. Phys. Earth*, *30*, 47–69.

Horiuchi, S., A. Yamamoto, and S. Ueki (1982b), Two-dimensional depth structure of the crust beneath the Tohoku district, the northeastern Japan arc, II. Moho discontinuity and P-wave velocity, *J. Phys. Earth*, *30*, 71–86.

Horiuchi, S., N. Tsumura, and A. Hasegawa (1997), Mapping of a magma reservoir beneath Nikko-Shirane volcano in northern Kanto, Japan, from travel time and seismogram shape anomalies, *J. Geophys. Res.*, *102*, 18,071–18,090.

Huang, J., and D. Zhao (2004), Crustal heterogeneity and seismotectonics of the region around Beijing, China, *Tectonophysics*, *385*, 159–180.

Huang, J., and D. Zhao (2006), High-resolution mantle tomography of China and surrounding regions, *J. Geophys. Res.*, *111*, B09305.

Huang, J., and D. Zhao (2009), Seismic imaging of the crust and upper mantle under Beijing and surrounding regions, *Phys. Earth Planet. Inter.*, *173*, 330–348.

Huang, Z., D. Zhao, N. Umino, L. Wang, T. Matsuzawa, A. Hasegawa, and T. Yoshida (2010), P-wave tomography, anisotropy and seismotectonics in the eastern margin of Japan Sea, *Tectonophysics*, *489*, 177–188.

Huang, Z., D. Zhao, and L. Wang (2011a), Seismic heterogeneity and anisotropy of the Honshu arc from the Japan Trench to the Japan Sea, *Geophys. J. Int.*, *184*, 1428–1444.

Huang, Z., D. Zhao, and L. Wang (2011b), Shear-wave anisotropy in the crust, mantle wedge and the subducting Pacific slab under Northeast Japan, *Geochem. Geophys. Geosyst.*, *12*, Q01002.

Huang, Z., D. Zhao, and L. Wang (2011c) Frequency-dependent shear-wave splitting and multilayer anisotropy in Northeast Japan, *Geophys. Res. Lett.*, *38*, L08302.

Huang, Z., L. Wang, D. Zhao, N. Mi, and M. Xu (2011d), Seismic anisotropy and mantle dynamics beneath China, *Earth Planet. Sci. Lett.*, *306*, 105–117.

Huang, Z., D. Zhao, and L. Wang (2011e), Stress field in the 2008 Iwate-Miyagi earthquake (M 7.2) area, *Geochem. Geophys. Geosyst.*, *12*, Q06006.

Hung, S., Y. Shen, and L. Chiao (2004), Imaging seismic velocity structure beneath the Iceland hotspot: A finite frequency approach, *J. Geophys. Res.*, *109*, B08305.

Ichiki, M., K. Baba, M. Obayashi, and H. Utada (2006), Water content and geotherm in the upper mantle above the stagnant slab: Interpretation of electrical conductivity and seismic P-wave velocity models, *Phys. Earth Planet. Inter.*, *155*, 1–15.

Ide, S., K. Shiomi, K. Mochizuki, T. Tonegawa, and G. Kimura (2010), Split Philippine Sea plate beneath Japan, *Geophys. Res. Lett.*, *37*, L21304.

Idehara, K., A. Yamada, and D. Zhao (2007), Seismological constraints on the ultralow velocity zones in the lowermost mantle from core-reflected waves, *Phys. Earth Planet. Inter.*, *165*, 25–46.

Iidaka, T., and D. Suetsugu (1992), Seismological evidence for metastable olivine inside a subducting slab, *Nature*, *356*, 593–595.

Iinuma, T., M. Ohzono, Y. Ohta, and S. Miura (2011), Coseismic slip distribution of the 2011 off the Pacific coast of Tohoku Earthquake (*M* 9.0) estimated based on GPS data—Was the asperity in Miyagi-oki ruptured? *Earth Planets Space*, *63*, 643–648.

Ikeda, M., D. Zhao, and Y. Ohno (2006), Crustal structure, fault segmentation and activity of the Median Tectonic Line in Shikoku, Japan, *Tectonophysics*, *412*, 49–60.

Inoue, T., Y. Tanimoto, T. Irifune, T. Suzuki, H. Fukui, and O. Ohtaka (2004), Thermal expansion of wadsleyite, ringwoodite, hydrous wadsleyite and hydrous ringwoodite, *Phys. Earth Planet. Inter.*, *143*, 279–290.

Ishida, M. (1992), Geometry and relative motion of the Philippine Sea plate and Pacific plate beneath the Kanto-Tokai district, Japan, *J. Geophys. Res.*, *97*, 489–513.

Ishida, M., and A. Hasemi (1988), The three-dimensional fine velocity structure and hypocentral distribution of earthquakes beneath the Kanto-Tokai District, Japan, *J. Geophys. Res.*, *93*, 2076–2094.

Ishise, M., and H. Oda (2005), Three-dimensional structure of P-wave anisotropy beneath the Tohoku district, northeast Japan, *J. Geophys. Res.*, *110*, B07304.

Ito, K. (1993), Cutoff depth of seismicity and large earthquakes near active volcanoes in Japan, *Tectonophysics*, *217*, 11–21.

Iwamori, H. (2000), Deep subduction of H_2O and deflection of volcanic chain towards backarc near triple junction due to lower temperature, *Earth Planet. Sci. Lett.*, *181*, 41–46.

Iwamori, H., and D. Zhao (2000), Melting and seismic structure beneath the northeast Japan arc, *Geophys. Res. Lett.*, *27*, 425–428.

Iwasaki, T., and H. Sato (2009), Crust and upper mantle structure of island arc being elucidated from seismic profiling with controlled sources in Japan, *J. Seismol. Soc. Jpn.*, *61*, S165–S176.

Iwasaki, T., W. Kato, T. Moriya, A. Hasemi, N. Umino, T. Okada, K. Miyashita, T. Mizogami, T. Takeda, S. Sekine, T. Matsushima, K. Tashiro, and H. Miyamachi (2001), Extensional structure in northern Honshu arc as inferred from seismic refraction/wide angle reflection profiling, *Geophys. Res. Lett.*, *28*, 2329–2332.

Jiang, G., and D. Zhao (2011), Metastable olivine wedge in the subducting Pacific slab and its relation to deep earthquakes, *J. Asian Earth Sci.*, *42*, 1411–1423.

Jiang, G., D. Zhao, and G. Zhang (2008), Seismic evidence for a metastable olivine wedge in the subducting Pacific slab under Japan Sea, *Earth Planet. Sci. Lett.*, *270*, 300–307.

Jiang, G., D. Zhao, and G. Zhang (2009), Seismic tomography of the Pacific slab edge under Kamchatka, *Tectonophysics*, *465*, 190–203.

Jin, S., P. Park, and W. Zhu (2007), Micro-plate tectonics and kinematics in Northeast Asia inferred from a dense set of GPS observations, *Earth Planet. Sci. Lett.*, *257*, 486–496.

Julian, B., and G. Foulger (2010), Time-dependent seismic tomography, *Geophys. J. Int.*, *182*, 1327–1338.

Kanamori, H. (1971), Great earthquakes at island arcs and the lithosphere, *Tectonophysics*, *12*, 187–198.

Kanamori, H. (1981), The nature of seismicity patterns before large earthquakes, in *Earthquake Prediction: An International Review*, edited by D. Simpson and P. Richards, Maurice Ewing Ser., Vol. 4, AGU, Washington, D.C., pp. 1–19.

Kanamori, H. (2004), The diversity of the physics of earthquakes, *Proc. Jpn. Acad. Ser. B*, *80*, 297–316.

Kaneshima, S., T. Okamoto, and H. Takenaka (2007), Evidence for a metastable olivine wedge inside the subducted Mariana slab, *Earth Planet. Sci. Lett.*, *258*, 219–227.

Karato, S., M. Riedel, and D. Yuen (2001), Rheological structure and deformation of subducted slabs in the mantle transition zone: implications for mantle circulation and deep earthquakes, *Phys. Earth Planet. Inter.*, *127*, 83–108.

Karato, S., H. Jung, I. Katayama, and P. Skemer (2008), Geodynamic significance of seismic anisotropy of the upper mantle: New insights from laboratory studies, *Ann. Rev. Earth Planet. Sci.*, *36*, 59–95.

Katao, H., N. Maeda, Y. Hiramatsu, Y. Iio, and S. Nakao (1997), Detailed mapping of focal mechanisms in and around the 1995 Hyogo-Ken Nanbu earthquake rupture zone, *J. Phys. Earth*, *45*, 105–119.

doi:10.5047/meep.2012.00101.0001

Kato, A., E. Kurashimo, N. Hirata, T. Iwasaki, and T. Kanazawa (2005), Imaging the source region of the 2004 Mid-Niigata prefecture earthquake and the evolution of the seismogenic thrust related fold, *Geophys. Res. Lett.*, *32*, L07307.

Kato, A., T. Miyatake, and N. Hirata (2010), Asperity and barriers of the 2004 Mid-Niigata Prefecture earthquake revealed by highly dense seismic observations, *Bull. Seismol. Soc. Am.*, *100*, 298–306.

Kato, N., and T. Hirasawa (1997), A numerical study on seismic coupling along subduction zones using a laboratory-derived friction law, *Phys. Earth Planet. Inter.*, *102*, 51–68.

Kawakatsu, H., and S. Watada (2007), Seismic evidence for deep water transportation in the mantle, *Science*, *316*, 1468–1471.

Kawasaki, I., Y. Asai, and Y. Tamura (2001), Space-time distribution of interplate moment release including slow earthquakes and the seismogeodetic coupling in the Sanriku-oki region along the Japan trench, *Tectonophysics*, *330*, 267–283.

Kayal, J., D. Zhao, O. Mishra, D. Reena, and O. Singh (2002), The 2001 Bhuj earthquake: Tomographic evidence for fluids at the hypocenter and its implications for rupture nucleation, *Geophys Res. Lett.*, *29*, GL015177.

Kennett, B., and E. Engdahl (1991), Travel times for global earthquake location and phase identification, *Geophys. J. Int.*, *105*, 426–465.

Kirby, S. (1991), Mantle phase changes and deep-earthquake faulting in subducting lithosphere, *Science*, *252*, 216–224.

Kirby, S., S. Stein, E. Okal, and D. Rubie (1996), Metastable mantle transformations and deep earthquakes in subducting oceanic lithosphere, *Rev. Geophys.*, *34*, 261–306.

Kiyosugi, K., C. Connor, D. Zhao, L. Connor, and K. Tanaka (2010), Relationships between volcano distribution, crustal structure, and P-wave tomography: An example from the Abu monogenetic volcano group, SW Japan, *Bull. Volcanol.*, *72*, 331–340.

Kobayashi, Y. (1983), On the initiation of plate subduction, *Earth Mon.*, *5*, 510–518.

Kobayashi, R., and D. Zhao (2004), Rayleigh wave group velocity distribution in the Antarctic region, *Phys. Earth Planet. Inter.*, *141*, 167–181.

Komabayashi, T., S. Omori, and S. Maruyama (2004), Petrogenetic grid in the system MgO-SiO_2-H_2O up to 30 GPa, 1600 C: Applications to hydrous peridotite subducting into the Earth's deep interior, *J. Geophys. Res.*, *109*, B03206.

Koper, K., D. Wiens, L. Dorman, J. Hildebrand, and S. Webb (1998), Modeling the Tonga slab: can travel time data resolve a metastable olivine wedge? *J. Geophys. Res.*, *103*, 30,079–30,100.

Koper, K., A. R. Hutko, T. Lay, C. J. Ammon, and H. Kanamori (2011), Frequency-dependent rupture process of the 2011 M_w 9.0 Tohoku Earthquake: Comparison of short-period *P* wave back-projection images and broadband seismic rupture models, *Earth Planets Space*, *63*, 599–602.

Kubo, T., S. Kaneshima, Y. Torii, and S. Yoshioka (2009), Seismological and experimental constraints on metastable phase transformations and rheology of the Mariana slab, *Earth Planet. Sci. Lett.*, *287*, 12–23.

Kuritani, T., J. Kimura, T. Miyamoto, H. Wei, T. Shimano, F. Maeno, X. Jin, and H. Taniguchi (2009), Intraplate magmatism related to deceleration of upwelling asthenospheric mantle: Implications from the Changbaishan shield basalts, northeast China, *Lithos*, *112*, 247–258.

Lallemand, S., Y. Font, H. Bijwaard, and H. Kao (2001), New insights on 3-D plate interaction near Taiwan from tomography and tectonic implications, *Tectonophysics*, *335*, 229–253.

Lay, T., C. J. Ammon, H. Kanamori, M. J. Kim, and L. Xue (2011), Outer trench-slope faulting and the 2011 M_w 9.0 off the Pacific coast of Tohoku Earthquake, *Earth Planets Space*, *63*, 713–718.

Lees, J. (1990), Tomographic P-wave velocity images of the Loma Prieta earthquake asperity, *Geophys. Res. Lett.*, *17*, 1433–1436.

Lees, J., J. VanDecar, E. Gordeev, A. Ozerov, M. Brandon, J. Park, and V. Levin (2007), Three-dimensional images of the Kamchatka-Pacific plate cusp, in *Volcanism and Subduction: The Kamchatka Region*, edited by J. Eichedlberger, E. Gordeev, M. Kasahara, P. Izbekov, and J. Lees, AGU, Washington, D.C., pp. 65–75.

Lei, J., and D. Zhao (2005), P-wave tomography and origin of the Changbai intraplate volcano in Northeast Asia, *Tectonophysics*, *397*, 281–295.

Lei, J., and D. Zhao (2009), Structural heterogeneity of the Longmenshan fault zone and the mechanism of the 2008 Wenchuan earthquake (Ms 8.0), *Geochem. Geophys. Geosyst.*, *10*, Q10010.

Lei, J., D. Zhao, and Y. Su (2009), Insight into the origin of the Tengchong intraplate volcano and seismotectonics in southwest China from local and teleseismic data, *J. Geophys. Res.*, *114*, B05302.

Lei, J., D. Zhao, F. Xie, and J. Liu (2011), An attempt to detect temporal variations of crustal structure in the source area of the 2006 Wen-An earthquake in North China, *J. Asian Earth Sci.*, *40*, 978–996.

Levin, V., N. Shapiro, J. Park, and M. Ritzwoller (2002), Seismic evidence for catastrophic slab loss beneath Kamchatka, *Nature*, *418*, 763–767.

Liu, J. (1999), *Volcanoes in China*, Science Press, Beijing, 219 pp.

Liu, K., S. Gao, Y. Gao, and J. Wu (2008), Shear wave splitting and mantle flow associated with the deflected Pacific slab beneath northeast Asia, *J. Geophys. Res.*, *113*, B01305.

Ma, K., J. Wang, and D. Zhao (1996), Three-dimensional seismic velocity structure of the crust and uppermost mantle beneath Taiwan, *J. Phys. Earth*, *44*, 85–105.

Maruyama, S. (1994), Plume tectonics, *J. Geol. Soc. Jpn.*, *100*, 24–49.

Maruyama, S., and M. Santosh (2007), Island arcs: past and present, *Gondwana Res.*, *11*, 3–6.

Maruyama, S., M. Santosh, and D. Zhao (2007), Superplume, supercontinent, and post-perovskite: Mantle dynamics and anti-plate tectonics on the core-mantle boundary, *Gondwana Res.*, *11*, 7–37.

Matsubara, M., K. Obara, and K. Kasahara (2008), Three-dimensional P- and S-wave velocity structures beneath the Japan Islands obtained by high-density seismic stations by seismic tomography, *Tectonophysics*, *454*, 86–103.

Matsumoto, S., and A. Hasegawa (1996), Distinct S wave reflector in the midcrust beneath Nikko-Shirane volcano in the northeastern Japan arc, *J. Geophys. Res.*, *101*, 3067–3086.

Matsuzawa, T., N. Umino, A. Hasegawa, and A. Takagi (1986), Upper mantle velocity structure estimated from PS-converted wave beneath the northeastern Japan arc, *Geophys. J. R. Astron. Soc.*, *86*, 767–787.

Matsuzawa, T., T. Kono, A. Hasegawa, and A. Takagi (1990), Subducting plate boundary beneath northeastern Japan arc estimated from SP converted waves, *Tectonophysics*, *181*, 123–133.

Menzies, M., Y. Xu, H. Zhang, and W. Fan (2007), Integration of geology, geophysics and geochemistry: A key to understanding the North China Craton, *Lithos*, *96*, 1–21.

Michael, A., and D. Eberhart-Phillips (1991), Relations among fault behavior, subsurface geology, and three-dimensional velocity models, *Science*, *253*, 651–654.

Mishra, O. P., and D. Zhao (2003), Crack density, saturation rate and porosity at the 2001 Bhuj, India, earthquake hypocenter: A fluid driven earthquake? *Earth Planet. Sci. Lett.*, *212*, 393–405.

Mishra, O. P., and D. Zhao (2004), Seismic evidence for dehydration embrittlement of the subducting Pacific slab, *Geophys. Res. Lett.*, *31*, L09610.

Mishra, O. P., D. Zhao, N. Umino, and A. Hasegawa (2003), Tomography of Northeast Japan forearc and its implications for interplate seismic coupling, *Geophys. Res. Lett.*, *30(16)*, GL017736.

Miura, S., S. Kodaira, A. Nakanishi, and T. Tsuru (2003), Structural characteristics controlling the seismicity of southern Japan Trench fore-arc region, revealed by ocean bottom seismographic data, *Tectonophysics*, *363*, 79–102.

Miyamachi, H., and T. Moriya (1984), Velocity structure beneath the Hidaka Mountains in Hokkaido, Japan, *J. Phys. Earth*, *32*, 13–42.

Miyazaki, S., and K. Heki (2001), Crustal velocity field of southwest Japan: Subduction and arc-arc collision, *J. Geophys. Res.*, *106*, 4305–4326.

Montelli, R., G. Nolet, G. Master, F. Dahlen, and H. Hung (2004), Global P and PP traveltime tomography: Rays versus waves, *Geophys. J. Int.*, *158*, 637–654.

Mukasa, S., A. Andronikov, and C. Hall (2007), The $^{40}Ar/^{39}Ar$ chronology and eruption rates of Cenozoic volcanism in the eastern Bering Sea Volcanic Province, Alaska, *J. Geophys. Res.*, *112*, B06207.

Mukhopadhyay, S., O. P. Mishra, D. Zhao, and J. Kayal (2006), 3-D seismic structure of the source area of the 1993 Latur, India, earthquake and its implications for rupture nucleations, *Tectonophysics*, *415*, 1–16.

Myers, S., S. Beck, G. Zandt, and T. Wallace (1998), Lithospheric-scale structure across the Bolivian Andes from tomographic images of velocity and attenuation for P and S waves, *J. Geophys. Res.*, *103*, 21,233–21,252.

Nakajima, J., and A. Hasegawa (2004), Shear-wave polarization anisotropy and subduction-induced flow in the mantle wedge of northeastern Japan, *Earth Planet. Sci. Lett.*, *225*, 365–377.

Nakajima, J., T. Matsuzawa, A. Hasegawa, and D. Zhao (2001), Three-dimensional structure of Vp, Vs, and Vp/Vs beneath northeastern Japan: Implications for arc magmatism and fluids, *J. Geophys. Res.*, *106*, 21,843–21,858.

doi:10.5047/meep.2012.00101.0001

Nakajima, J., T. Matsuzawa, and A. Hasegawa (2002), Moho depth variation in the central part of northeastern Japan estimated from reflected and converted waves, *Phys. Earth Planet. Inter.*, *130*, 31–47.

Nakamura, K. (1983), Possible nascent trench along the eastern Japan Sea as convergent boundary between the Eurasian and North American plates, *Bull. Earthq. Res. Inst. Univ. Tokyo*, *58*, 711–722.

Nakanishi, I. (1980), Precursors to ScS phases and dipping interface in the upper mantle beneath southwestern Japan, *Tectonophysics*, *69*, 1–35.

Nakanishi, I. (1985), Three-dimensional structure beneath the Hokkaido-Tohoku region as derived from a tomographic inversion of arrival times, *J. Phys. Earth*, *33*, 241–256.

Nakanishi, I., and D. Anderson (1982), World-wide distribution of group velocity of mantle Rayleigh waves as determined by spherical harmonic inversion, *Bull. Seismol. Soc. Am.*, *72*, 1185–1194.

Nishimoto, S., M. Ishikawa, M. Arima, T. Yoshida, and J. Nakajima (2008), Simultaneous high P-T measurements of ultrasonic compressional and shear wave velocities in Ichino-megata mafic xenoliths: Their bearings on seismic velocity perturbations in lower crust of northeast Japan arc, *J. Geophys. Res.*, *113*, B12212.

Nishisaka, H., M. Shinohara, T. Sato, R. Hino, K. Mochizuki, and J. Kasahara (2001), Crustal structure of the Yamato basin and the margin of the northeastern Japan Sea using ocean bottom seismographs and controlled sources, *J. Seismol. Soc. Jpn.*, *54*, 365–379.

Nishizawa, A., and A. Asada (1999), Deep crustal structure off Akita, eastern margin of the Japan Sea, deduced from ocean bottom seismographic measurements, *Tectonophysics*, *306*, 199–216.

Nolet, G. (1987), *Seismic Tomography*, Reidel, Hingham, MA, pp. 1–234.

Nolet, G., R. Allen, and D. Zhao (2007), Mantle plume tomography, *Chem. Geol.*, *241*, 248–263.

Obara, K. (1989), Regional extent of the S wave reflector beneath the Kanto district, Japan, *Geophys. Res. Lett.*, *16*, 839–842.

Obara, K., A. Hasegawa, and A. Takagi (1986), Three-dimensional P and S wave velocity structure beneath the northeastern Japan arc, *J. Seismol. Soc. Jpn.*, *39*, 201–215.

Ogawa, Y., and Y. Honkura (2004), Mid-crustal electrical conductors and their correlations to seismicity and deformation at Itoigawa-Shizuoka Tectonic Line, central Japan, *Earth Planets Space*, *56*, 1285–1291.

Ohmi, S., and K. Obara (2002), Deep low-frequency earthquakes beneath the focal region of the Mw 6.7 2000 Western Tottori earthquake, *Geophys. Res. Lett.*, *29*, GL014469.

Ohtake, M., A. Taira, and Y. Ohta, Y. (2002), *Active Faults and Seismo-Tectonics of the Eastern Margin of the Japan Sea*, Univ. Tokyo Press, Tokyo, pp. 201.

Ohtani, E. (2005), Water in the mantle, *Elements*, *1*, 25–30.

Ohtani, E., and K. Litasov (2006), Effect of water on mantle phase transitions, *Rev. Mineral. Geochem.*, *62*, 397–420.

Ohtani, E., and D. Zhao (2009), The role of water in the deep upper mantle and transition zone: dehydration of stagnant slabs and its effects on the big mantle wedge, *Russ. Geol. Geophys.*, *50*, 1073–1078.

Ohtani, E., K. Litasov, T. Hosoya, T. Kubo, and T. Kondo (2004), Water transport into the deep mantle and formation of a hydrous transition zone, *Phys. Earth Planet. Inter.*, *143*, 255–269.

Okada, H. (1971), Forerunners of ScS waves from nearby deep earthquakes and upper mantle structure in Hokkaido, *J. Seismol. Soc. Jpn.*, *24*, 228–239.

Okada, H. (1979), New evidence of the discontinuous structure of the descending lithosphere as revealed by ScSp phase, *J. Phys. Earth*, *27*, S53–S64.

Okada, T., T. Matsuzawa, and A. Hasegawa (1995), Shear-wave polarization anisotropy beneath the north-eastern part of Honshu, Japan, *Geophys. J. Int.*, *123*, 781–797.

Okada, T., N. Umino, and A. Hasegawa (2010), Deep structure of the Ou mountain range strain concentration zone and the focal area of the 2008 Iwate-Miyagi Nairiku earthquake, NE Japan—Seismogenesis related with magma and crustal fluid, *Earth Planets Space*, *62*, 347–352.

Okada, Y., K. Kasahara, S. Hori, and K. Obara (2004), Recent progress of seismic observation networks in Japan—Hi-net, F-net, K-NET and KiK-net, *Earth Planets Space*, *56*, xv–xxviii.

Okamura, Y. (2002), The geological high strain-rate zone after the Neogene, in *Active Faults and Seismo-Tectonics of the Eastern Margin of the Japan Sea*, edited by Ohtake, M., A. Taira, and Y. Ohta, Univ. Tokyo Press, pp. 111–121.

Okamura, Y., M. Watanabe, R. Morijiri, and M. Satoh (1995), Rifting and basin inversion in the eastern margin of the Japan Sea, *Island Arc*, *4*, 166–181.

Ono, S. (1998), Stability of hydrous minerals in sediment and mid-oceanic ridge basalt compositions: Implications for water transport in subduction zones, *J. Geophys. Res.*, *103*, 18,353–18,264.

Oshiman, N. (2002), Electric conductivity structure of western Japan, *Earth Mon.*, *38*, 82–90.

Pacheco, J., L. Sykes, and C. Scholz (1993), Nature of seismic coupling along simple plate boundaries of the subduction type, *J. Geophys. Res.*, *98*, 14,133–14,159.

Padhy, S., O. P. Mishra, D. Zhao, and W. Wei (2011), Crustal heterogeneity in the 2007 Noto-Hanto earthquake area and its geodynamical implications, *Tectonophysics*, *42*, 1381–1393.

Peacock, S. (1990), Fluid processes in subduction zones, *Science*, *248*, 329–345.

Peyton, V., V. Levin, J. Park, M. Brandon, and J. Lees (2001), Mantle flow at a slab edge: seismic anisotropy in the Kamchatka region, *Geophys. Res. Lett.*, *28*, 379–382.

Pollitz, F., and J. Fletcher (2005), Waveform tomography of crustal structure in the south San Francisco Bay region, *J. Geophys. Res.*, *110*, B08308.

Portnyagin, M., K. Hoernle, G. Avdeiko, F. Hauff, R. Werner, I. Bindeman, V. Uspensky, and D. Garbe-Schönberg (2005), Transition from arc to oceanic magmatism at the Kamchatka-Aleutian junction, *Geology*, *33*, 25–28.

Qi, C., D. Zhao, and Y. Chen (2006), 3-D P and S wave velocity structures and their relationship to strong earthquakes in the Chinese capital region, *Chinese J. Geophys.*, *49*, 805–815.

Qi, C., D. Zhao, and Y. Chen (2007a), Search for deep slab segments under Alaska, *Phys. Earth Planet. Inter.*, *165*, 68–82.

Qi, C., D. Zhao, Y. Chen, and N. Ruppert (2007b), New insight into the crust and upper mantle structure under Alaska, *Polar Sci.*, *1*, 85–100.

Raleigh, C., and M. Paterson (1965), Experimental deformation of serpentinite and its tectonic implications, *J. Geophys. Res.*, *70*, 3965–3985.

Rawlinson, N., S. Pozgay, and S. Fishwick (2010), Seismic tomography: A window into deep Earth, *Phys. Earth Planet. Inter.*, *178*, 101–135.

Reid, H. (1910), The mechanics of the earthquake: the California Earthquake of April 18, 1906, in *Report of the State Investigation Commission*, Vol. 2, Carnegie Institution of Washington, Washington, D.C, pp. 16–28.

Roth, E., D. Wiens, and D. Zhao (2000), An empirical relationship between seismic attenuation and velocity anomalies in the upper mantle, *Geophys. Res. Lett.*, *27*, 601–604.

Sagiya, T., S. Miyazaki, and T. Tada (2000), Continuous GPS array and present-day crustal deformation of Japan, *Pure Appl. Geophys.*, *157*, 2303–2322.

Sakamaki, T., E. Ohtani, S. Urakawa, A. Suzuki, Y. Katayama, and D. Zhao (2010), Density of high-Ti basalt magma at high pressure and origin of heterogeneities in the lunar mantle, *Earth Planet. Sci. Lett.*, *299*, 285–289.

Salah, M., and D. Zhao (2003a), Three-dimensional attenuation structure of Southwest Japan estimated from spectra of microearthquakes, *Phys. Earth Planet. Inter.*, *136*, 215–231.

Salah, M., and D. Zhao (2003b), 3-D seismic structure of Kii Peninsula in Southwest Japan: Evidence for slab dehydration in the forearc, *Tectonophysics*, *364*, 191–213.

Salah, M., and D. Zhao (2004), Mapping the crustal thickness in southwest Japan using Moho reflected waves, *Phys. Earth Planet. Inter.*, *141*, 79–94.

Salah, M., D. Zhao, J. Lei, and M. Farouk (2005), Crustal heterogeneity beneath southwest Japan estimated from direct and Moho-reflected waves, *Tectonophysics*, *395*, 1–17.

Satake, K. (1986), Re-examination of the 1940 Shakotan-oki earthquake and the fault parameters of the earthquakes along the eastern margin of the Japan Sea, *Phys. Earth Planet. Inter.*, *43*, 137–147.

Sato, H. (1994), The relationship between late Cenozoic tectonic events and stress field and basin development in northeast Japan, *J. Geophys. Res.*, *99*, 22,261–22,274.

Sato, T., M. Kosuga, K. Tanaka, and H. Sato (1986), Aftershock distribution of the 1983 Nihonkai-Chubu (Japan Sea) earthquake determined from relocated hypocenters, *J. Phys. Earth*, *34*, 203–223.

Scambelluri, M., and P. Philippot, (2001), Deep fluids in subduction zones, *Lithos*, *55*, 213–227.

Schmidt, M., and S. Poli (1998), Experimental base water budgets for dehydrating slabs and consequences for arc magma generation, *Earth Planet.*

doi:10.5047/meep.2012.00101.0001

Sci. Lett., *163*, 361–379.
Schmincke, H. (2004), *Volcanism*, Springer-Verlag, Heidelberg, 324 pp.
Sekiguchi, S. (1991), Three-dimensional Q structure beneath the Kanto-Tokai district, Japan, *Tectonophysics*, *195*, 83–104.
Seno, T., S. Stein, and A. Gripp (1993), A model for the motion of the Philippine Sea plate consistent with NUVEL-1 and geological data, *J. Geophys. Res.*, *98*, 17,941–17,948.
Seno, T., D. Zhao, Y. Kobayashi, and M. Nakamura (2001), Dehydration of serpentinized slab mantle: Seismic evidence from southwest Japan, *Earth Planets Space*, *53*, 861–871.
Shao, G., C. Ji, and D. Zhao (2011), Rupture process of the 9 March, 2011 Mw 7.4 Sanriku-Oki, Japan earthquake constrained by jointly inverting teleseismic waveforms, strong motion data and GPS observations, *Geophys. Res. Lett.*, *38*, L00G20, doi:10.1029/2011GL049164.
Shapiro, N., M. Campillo, L. Stehly, and M. Ritzwoller (2005), High-resolution surface-wave tomography from ambient seismic noise, *Science*, *307*, 1615–1618.
Shibutani, T., H. Katao *et al.* (2005), High-resolution 3-D velocity structure in the source region of the 2000 Western Tottori earthquake in southwestern Honshu, Japan using very dense aftershock observations, *Earth Planets Space*, *57*, 825–838.
Shiomi, K., K. Obara, and H. Sato (2006), Moho depth variation beneath southwestern Japan revealed from the velocity structure based on receiver function inversion, *Tectonophysics*, *420*, 205–221.
Shiraishi, R., E. Ohtani, K. Kanagawa, A. Shimojuku, and D. Zhao (2008), Crystallographic preferred orientation of Akimotoite and seismic anisotropy of the Tonga slab, *Nature*, *455*, 657–660.
Sibson, R. (1992), Implications of fault-valve behavior for rupture nucleation and recurrence, *Tectonophysics*, *211*, 283–293.
Simkin, T., and L. Siebert (1994), *Volcanoes of the World*, Geoscience Press, pp. 1–368.
Simmons, N., S. Myers, and G. Johannesson (2011), Global-scale P wave tomography optimized for prediction of teleseismic and regional travel times for Middle East events: 2. Tomographic inversion, *J. Geophys. Res.*, *116*, B04305.
Steblov, G., M. Kogan, R. King, C. Scholz, R. Bürgmann, and D. Frolov (2003), Imprint of the North American plate in Siberia revealed by GPS, *Geophys. Res. Lett.*, *30*, 1924.
Stern, R. (2002), Subduction zones, *Rev. Geophys.*, *40(4)*, RG000108.
Sun, A., D. Zhao, M. Ikeda, Y. Chen, and Q. Chen (2008), Seismic imaging of southwest Japan using P and PmP data: Implications for arc magmatism and seismotectonics, *Gondwana Res.*, *14*, 535–542.
Takanami, T. (1982), Three-dimensional seismic structure of the crust and upper mantle beneath the orogenic belts in southern Hokkaido, Japan, *J. Phys. Earth*, *30*, 87–104.
Tamaki, K., and E. Honza (1985), Incipient subduction and deduction along the eastern margin of the Japan Sea, *Tectonophysics*, *119*, 381–406.
Tamura, Y., Y. Tatsumi, D. Zhao, Y. Kido, and H. Shukuno (2002), Hot fingers in the mantle wedge: new insight into magma genesis in subduction zones, *Earth Planet. Sci. Lett.*, *197*, 105–116.
Tanimoto, T., and D. Anderson (1985), Lateral heterogeneity and azimuthal anisotropy of the upper mantle: Love and Rayleigh waves: 100–250 s, *J. Geophys. Res.*, *90*, 1842–1858.
Tanioka, Y., K. Satake, and L. Ruff (1995), Total analysis of the 1993 Hokkaido Nansei-oki earthquake using seismic wave, tsunami, and geodetic data, *Geophys. Res. Lett.*, *22*, 9–12.
Tatsumi, Y. (1989), Migration of fluid phases and genesis of basalt magmas in subduction zones, *J. Geophys. Res.*, *94*, 4697–4707.
Thurber, C. (1983), Earthquake locations and three-dimensional crustal structure in the Coyote Lake area, central California, *J. Geophys. Res.*, *88*, 8226–8236.
Tian, X., D. Zhao, H. Zhang, Y. Tian, and Z. Zhang (2010), Mantle transition zone topography and structure beneath the central Tien Shan orogenic belt, *J. Geophys. Res.*, *115*, B10308.
Tian, Y., and D. Zhao (2011), Destruction mechanism of the North China craton: Insight from P and S wave mantle tomography, *J. Asian Earth Sci.*, *42*, 1132–1145.
Tian, Y., D. Zhao, R. Sun, and J. Teng (2007a), The 1992 Landers earthquake: Effect of crustal heterogeneity on earthquake generation, *Chinese J. Geophys.*, *50*, 1488–1496.
Tian, Y., D. Zhao, and J. Teng (2007b), Deep structure of southern California, *Phys. Earth Planet. Inter.*, *165*, 93–113.
Tonegawa, T., K. Hirahara, T. Shibutani, H. Iwamori, H. Kanamori, and K. Shiomi (2008), Water flow to the mantle transition zone inferred from a receiver function image of the Pacific slab, *Earth Planet. Sci. Lett.*, *274*, 346–354.
Tong, P., D. Zhao, and D. Yang (2011), Tomography of the 1995 Kobe earthquake area: Comparison of finite-frequency and ray approaches, *Geophys. J. Int.*, *187*, 278–302.
Tsuboi, C. (1956), Earthquake energy, earthquake volume, aftershock area, and strength of the Earth's crust, *J. Phys. Earth*, *4*, 63–66.
Tsumura, N., S. Matsumoto, S. Horiuchi, and A. Hasegawa (2000), Three-dimensional attenuation structure beneath the northeastern Japan arc estimated from spectra of small earthquakes, *Tectonophysics*, *319*, 241–260.
Tsuru, T., J. Park, S. Miura, S. Kodaira, Y. Kido, and T. Hayashi (2002), Along-arc structural variation of the plate boundary at the Japan Trench margin: Implications of interplate coupling, *J. Geophys. Res.*, *107*, 2357, doi:10.1029/2001JB001664.
Ueno, H., S. Hatakeyama, T. Aketagawa, J. Funasaki, and N. Hamada (2002), Improvement of hypocenter determination procedures in the Japan Meteorological Agency, *Q. J. Seismol.*, *65*, 123–134.
Um, J., and C. Thurber (1987), A fast algorithm for two-point seismic ray tracing, *Bull. Seismol. Soc. Am.*, *77*, 972–986.
Umeda, K., Y. Ogawa, K. Asamori, and T. Oikawa (2006), Aqueous fluids derived from a subducting slab: Observed high ^{3}He emanation and conductive anomaly in a non-volcanic region, Kii Peninsula southwest Japan, *J. Volcanol. Geotherm. Res.*, *149*, 47–61.
Umino, N., and A. Hasegawa (1975), On the two-layered structure of deep seismic plane in northeastern Japan arc, *J. Seismol. Soc. Jpn.*, *27*, 125–139.
Umino, N., and A. Hasegawa (1984), Three-dimensional Qs structure in the northeastern Japan arc, *J. Seismol. Soc. Jpn.*, *37*, 217–228.
Umino, N., and A. Hasegawa (1994), Aftershock focal depths of the 1993 Hokkaido- Nansei-Oki earthquake estimated from sP depth phase at small epicentral distances, *J. Phys. Earth*, *42*, 321–329.
Umino, N., A. Hasegawa, and A. Takagi (1990), The relationship between seismicity patterns and fracture zones beneath northeastern Japan, *Tohoku Geophys. J.*, *33*, 149–162.
Umino, N., A. Hasegawa, and T. Matsuzawa (1995), sP depth phase at small epicentral distances and estimated subducting plate boundary, *Geophys. J. Int.*, *120*, 356–366.
Usami, T. (2003), *Materials for Comprehensive List of Destructive Earthquakes in Japan*, Univ. Tokyo Press, Tokyo.
Utsu, T. (1982), Catalog of large earthquakes in the region of Japan from 1885 through 1980, *Bull. Earthq. Res. Inst. Univ. Tokyo*, *57*, 401–463.
Uyeshima, M., Y. Ogawa, and Y. Honkura (2005), Resistivity imaging across the source region of the 2004 mid-Niigata prefecture earthquake (M6.8), central Japan, *Earth Planets Space*, *57*, 441–446.
van der Hilst, R., and M. de Hoop (2005), Banana-doughnut kernels and mantle tomography, *Geophys. J. Int.*, *163*, 956–961.
Van der Voo, R., W. Spakman, and H. Bijwaard (1999), Tethyan subducted slabs under India, *Earth Planet. Sci. Lett.*, *171*, 7–20.
van Keken, P., B. Hacker, E. Syracuse, and G. Abers (2011), Subduction factory: 4. Depth-dependent flux H2O from subducting slabs worldwide, *J. Geophys. Res.*, *116*, B01401.
Wada, I., C. Rychert, and K. Wang (2011), Sharp thermal transition in the forearc mantle wedge as a consequence of nonlinear mantle wedge flow, *Geophys. Res. Lett.*, *38*, L13308.
Wagner, L., S. Beck, and G. Zandt (2005), Upper mantle structure in the south central Chilean subduction zone (30° to 36°S), *J. Geophys. Res.*, *110*, B01308.
Wang, J., and D. Zhao (2008), P-wave anisotropic tomography beneath Northeast Japan, *Phys. Earth Planet. Inter.*, *170*, 115–133.
Wang, J., and D. Zhao (2009), P-wave anisotropic tomography of the crust and upper mantle under Hokkaido, Japan, *Tectonophysics*, *469*, 137–149.
Wang, J., and D. Zhao (2010), Mapping P-wave anisotropy of the Honshu arc from Japan Trench to the back-arc, *J. Asian Earth Sci.*, *39*, 396–407.
Wang, Z. (2010), Interplate coupling and seismotectonics under the fore-arc regions of Japan, *Earthq. Sci.*, *23*, 555–565.
Wang, Z., and D. Zhao (2005), Seismic imaging of the entire arc of Tohoku and Hokkaido in Japan using P-wave, S-wave and sP depth-phase data, *Phys. Earth Planet. Inter.*, *152*, 144–162.
Wang, Z., and D. Zhao (2006a), Suboceanic earthquake location and seismic structure in the Kanto district, central Japan, *Earth Planet. Sci. Lett.*, *241*, 789–803.
Wang, Z., and D. Zhao (2006b), Vp and Vs tomography of Kyushu, Japan:

doi:10.5047/meep.2012.00101.0001

New insight into arc magmatism and forearc seismotectonics, *Phys. Earth Planet. Inter.*, *157*, 269–285.

Wang, Z., and D. Zhao (2006c), Seismic evidence for the influence of fluids on the 2005 west off Fukuoka prefecture earthquake in southwest Japan, *Phys. Earth Planet. Inter.*, *155*, 313–324.

Wang, Z., and D. Zhao (2006d), Seismic images of the source area of the 2004 Mid-Niigata prefecture earthquake in Northeast Japan, *Earth Planet. Sci. Lett.*, *244*, 16–31.

Wang, Z., D. Zhao, J. Wang, and H. Kao (2006), Tomographic evidence for the Eurasian lithosphere subducting beneath South Taiwan, *Geophys. Res. Lett.*, *33*, L18306.

Watson, B., and K. Fujita (1985), Tectonic evolution of Kamchatka and Sea of Okhotsk and implication for the Pacific basin, in *Tectonostratigraphic Terranes of the Circum-Pacific Region*, edited by D. Howell, pp. 333–348, Circum-Pacific Council, Houston, TX.

Woodhouse, J., and A. Dziewonski (1984), Mapping the upper mantle: three-dimensional modeling of earth structure by inversion of seismic waveforms, *J. Geophys. Res.*, *89*, 5953–5986.

Xia, S., D. Zhao, X. Qiu, J. Nakajima, T. Matsuzawa, and A. Hasegawa (2007), Mapping the crustal structure under active volcanoes in central Tohoku, Japan using P and PmP data, *Geophys. Res. Lett.*, *34*, L10309.

Xia, S., D. Zhao, and X. Qiu (2008a), Tomographic evidence for the subducting oceanic crust and forearc mantle serpentinization under Kyushu, Japan, *Tectonophysics*, *449*, 85–96.

Xia, S., D. Zhao, and X. Qiu (2008b), The 2007 Niigata earthquake: Effect of arc magma and fluids, *Phys. Earth Planet. Inter.*, *166*, 153–166.

Yamada, R., and T. Yoshida (2004), Volcanic sequences related to Kuroko mineralization in the Hokuroku district, Northeast Japan, *Resource Geol.*, *54*, 399–412.

Yamamoto, F. (2002), Surface topography in and around the Japanese Islands, in *Active Faults and Seismo-Tectonics of the Eastern Margin of the Japan Sea*, edited by Ohtake, M., A. Taira, and Y. Ohta, Univ. Tokyo Press.

Yamanaka, Y., and M. Kikuchi (2004), Asperity map along the subduction zone in northeastern Japan inferred from regional seismic data, *J. Geophys. Res.*, *109*, B07307.

Yanada, T., D. Zhao, and A. Hasegawa (2010), Teleseismic tomography of mantle structure beneath the Japan Islands, *Abstract in Ann. Meet. Seismol. Soc. Jpn., Hiroshima*, Japan.

Yoshida, T., J. Nakajima, A. Hasegawa, H. Sato, Y. Nagahashi, and J. Kimura (2005), Distribution of Quaternary volcanoes and mantle structures in the NE Honshu arc, *Quaternary Res.*, *44*, 195–216.

Yoshizawa, K., K. Miyake, and K. Yomogida (2010), 3D upper mantle structure beneath Japan and its surrounding region from inter-station dispersion measurements of surface waves, *Phys. Earth Planet. Inter.*, *183*, 4–19.

Zhang, Y., D. Zhao, and M. Matsui (2005), Anisotropy of Akimotoite: a molecular dynamics study, *Phys. Earth Planet. Inter.*, *151*, 309–319.

Zhang, Y., D. Zhao, M. Matsui, and G. Guo (2006), Equations of state of $CaSiO_3$ perovskite: A molecular dynamics study, *Phys. Chem. Miner.*, *33*, 126–137.

Zhang, Y., D. Zhao, M. Matsui, and G. Guo (2007), Temperature dependence of the first pressure derivative of isothermal bulk modulus at zero pressure: Implications for the thermodynamic validity of equations of state, *J. Geophys. Res.*, *112*, B11202.

Zhao, D. (1991), A tomographic study of seismic velocity structure in the Japan Islands, Ph.D. thesis, Tohoku University, 301 pp.

Zhao, D. (2001a), Seismological structure of subduction zones and its implications for arc magmatism and dynamics, *Phys. Earth Planet. Inter.*, *127*, 197–214.

Zhao, D. (2001b), New advances of seismic tomography and its applications to subduction zones and earthquake fault zones, *Island Arc*, *10*, 68–84.

Zhao, D. (2001c), Seismic structure and origin of hotspots and mantle plumes, *Earth Planet. Sci. Lett.*, *192*, 251–265.

Zhao, D. (2004), Global tomographic images of mantle plumes and subducting slabs: insight into deep Earth dynamics, *Phys. Earth Planet. Inter.*, *146*, 3–34.

Zhao, D. (2007), Seismic images under 60 hotspots: Search for mantle plumes, *Gondwana Res.*, *12*, 335–355.

Zhao, D. (2009), Multiscale seismic tomography and mantle dynamics, *Gondwana Res.*, *15*, 297–323.

Zhao, D., and T. Arai (2011), Deep structure of the Procellarum KREEP Terrane from lunar seismic tomography, *Planet. People*, *20*, 11–19.

Zhao, D., and A. Hasegawa (1993), P-wave tomographic imaging of the crust and upper mantle beneath the Japan Islands, *J. Geophys. Res.*, *98*, 4333–4353.

Zhao, D., and A. Hasegawa (1994), Teleseismic evidence for lateral heterogeneities in the northeastern Japan arc, *Tectonophysics*, *237*, 189–199.

Zhao, D., and H. Kanamori (1992), P-wave image of the crust and uppermost mantle in southern California, *Geophys. Res. Lett.*, *19*, 2329–2332.

Zhao, D., and H. Kanamori (1993), The 1992 Landers earthquake sequence: Earthquake occurrence and structural heterogeneities, *Geophys. Res. Lett.*, *20*, 1083–1086.

Zhao, D., and H. Kanamori (1995), The 1994 Northridge earthquake: 3-D crustal structure in the rupture zone and its relation to the aftershock locations and mechanisms, *Geophys. Res. Lett.*, *22*, 763–766.

Zhao, D., and J. R. Kayal (2000), Impact of seismic tomography on Earth sciences, *Curr. Sci.*, *79*, 1208–1214.

Zhao, D., and J. Lei (2004), Seismic ray path variations in a 3-D global velocity model, *Phys. Earth Planet. Inter.*, *141*, 153–166.

Zhao, D., and L. Liu (2010), Deep structure and origin of active volcanoes in China, *Geosci. Front.*, *1*, 31–44.

Zhao, D., and T. Mizuno (1999), Crack density and saturation rate in the 1995 Kobe earthquake region, *Geophys. Res. Lett.*, *26*, 3213–3216.

Zhao, D., and H. Negishi (1998), The 1995 Kobe earthquake: Seismic image of the source zone and its implications for the rupture nucleation, *J. Geophys. Res.*, *103*, 9967–9986.

Zhao, D., and E. Ohtani (2009), Deep slab subduction and dehydration and their geodynamic consequences: Evidence from seismology and mineral physics, *Gondwana Res.*, *16*, 401–413.

Zhao, D., S. Horiuchi, and A. Hasegawa (1990), 3-D seismic velocity structure of the crust and uppermost mantle in the northeastern Japan arc, *Tectonophysics*, *181*, 135–149.

Zhao, D., S. Horiuchi, and A. Hasegawa (1992a), Seismic velocity structure of the crust beneath the Japan Islands, *Tectonophysics*, *212*, 289–301.

Zhao, D., A. Hasegawa, and S. Horiuchi (1992b), Tomographic imaging of P and S wave velocity structure beneath northeastern Japan, *J. Geophys. Res.*, *97*, 19,909–19,928.

Zhao, D., A. Hasegawa, and H. Kanamori (1994), Deep structure of Japan subduction zone as derived from local, regional and teleseismic events, *J. Geophys. Res.*, *99*, 22,313–22,329.

Zhao, D., D. Christensen, and H. Pulpan (1995), Tomographic imaging of the Alaska subduction zone, *J. Geophys. Res.*, *100*, 6487–6504.

Zhao, D., H. Kanamori, H. Negishi, and D. Wiens (1996), Tomography of the source area of the 1995 Kobe earthquake: Evidence for fluids at the hypocenter? *Science*, *274*, 1891–1894.

Zhao, D., T. Matsuzawa, and A. Hasegawa (1997a), Morphology of the subducting slab boundary in the northeastern Japan arc, *Phys. Earth Planet. Inter.*, *102*, 89–104.

Zhao, D., Y. Xu, D. Wiens, L. Dorman, J. Hildebrand, and S. Webb (1997b), Depth extent of the Lau back-arc spreading center and its relation to subduction processes, *Science*, *278*, 254–257.

Zhao, D., H. Kanamori, and D. Wiens (1997c), State of stress before and after the 1994 Northridge earthquake, *Geophys. Res. Lett.*, *24*, 519–522.

Zhao, D., F. Ochi, A. Hasegawa, and A. Yamamoto (2000a), Evidence for the location and cause of large crustal earthquakes in Japan, *J. Geophys. Res.*, *105*, 13,579–13,594.

Zhao, D., K. Asamori, and H. Iwamori (2000b), Seismic structure and magmatism of the young Kyushu subduction zone, *Geophys. Res. Lett.*, *27*, 2057–2060.

Zhao, D., O. P. Mishra, and R. Sanda (2002), Influence of fluids and magma on earthquakes: seismological evidence, *Phys. Earth Planet. Inter.*, *132*, 249–267.

Zhao, D., H. Tani, and O. P. Mishra (2004a), Crustal heterogeneity in the 2000 western Tottori earthquake region: effect of fluids from slab dehydration, *Phys. Earth Planet. Inter.*, *145*, 161–177.

Zhao, D., J. Lei, and R. Tang (2004b), Origin of the Changbai intraplate volcanism in Northeast China: Evidence from seismic tomography, *Chinese Sci. Bull.*, *49*, 1401–1408.

Zhao, D., S. Todo, and J. Lei (2005), Local earthquake reflection tomography of the Landers aftershock area, *Earth Planet. Sci. Lett.*, *235*, 623–631.

Zhao, D., J. Lei, T. Inoue, A. Yamada, and S. Gao (2006), Deep structure and origin of the Baikal rift zone, *Earth Planet. Sci. Lett.*, *243*, 681–691.

Zhao, D., Z. Wang, N. Umino, and A. Hasegawa (2007a), Tomographic imaging outside a seismic network: Application to the northeast Japan

doi:10.5047/meep.2012.00101.0001

arc, *Bull. Seismol. Soc. Am.*, *97*, 1121–1132.
Zhao, D., S. Maruyama, and S. Omori (2007b), Mantle dynamics of western Pacific to East Asia: New insight from seismic tomography and mineral physics, *Gondwana Res.*, *11*, 120–131.
Zhao, D., J. Lei, and L. Liu (2008), Seismic tomography of the Moon, *Chinese Sci. Bull.*, *53*, 3897–3907.
Zhao, D., Z. Wang, N. Umino, and A. Hasegawa (2009a), Mapping the mantle wedge and interplate thrust zone of the northeast Japan arc, *Tectonophysics*, *467*, 89–106.
Zhao, D., Y. Tian, J. Lei, L. Liu, and S. Zheng (2009b), Seismic image and origin of the Changbai intraplate volcano in East Asia: Role of big mantle wedge above the stagnant Pacific slab, *Phys. Earth Planet. Inter.*, *173*, 197–206.
Zhao, D., M. Santosh, and A. Yamada (2010a), Dissecting large earthquakes in Japan: Role of arc magma and fluids, *Island Arc*, *19*, 4–16.
Zhao, D., F. Pirajno, N. Dobretsov, and L. Liu (2010b), Mantle structure and dynamics under East Russia and adjacent regions, *Russ. Geol. Geophys.*, *51*, 925–938.
Zhao, D., W. Wei, Y. Nishizono, and H. Inakura (2011a), Low-frequency earthquakes and tomography in western Japan: Insight into fluid and magmatic activity, *J. Asian Earth Sci.*, *42*, 1381–1393.
Zhao, D., Z. Huang, N. Umino, A. Hasegawa, and H. Kanamori (2011b), Structural heterogeneity in the megathrust zone and mechanism of the 2011 Tohoku-oki earthquake (Mw 9.0), *Geophys. Res. Lett.*, *38*, L17308.
Zhao, D., Z. Huang, N. Umino, A. Hasegawa, and T. Yoshida (2011c), Seismic imaging of the Amur-Okhotsk plate boundary zone in the Japan Sea, *Phys. Earth Planet. Inter.*, *188*, 82–95.
Zhao, D., S. Yu, and E. Ohtani (2011d), East Asia: Seismotectonics, magmatism and mantle dynamics, *J. Asian Earth Sci.*, *40*, 689–709.
Zheng, H., T. Li, R. Gao, D. Zhao, and R. He (2007), Teleseismic P-wave tomography evidence for the Indian lithospheric mantle subducting northward beneath the Qiangtang terrane, *Chinese J. Geophys.*, *50*, 1418–1426.
Zhou, H., and M. Murphy (2005), Tomographic evidence for wholesale underthrusting of India beneath the entire Tibetan plateau, *J. Asian Earth Sci.*, *25*, 445–457.
Zhu, G., Y. Shi, and P. Tackley (2010), Subduction of the western Pacific plate underneath Northeast China: Implications of numerical studies, *Phys. Earth Planet. Inter.*, *178*, 92–99.
Zou, H., Q. Fan, and Y. Yao (2008), U-Th systematics of dispersed young volcanoes in NE China: Asthenosphere upwelling caused by piling up and upward thickening of stagnant Pacific slab, *Chem. Geol.*, *255*, 134–142.

doi:10.5047/meep.2012.00101.0001